



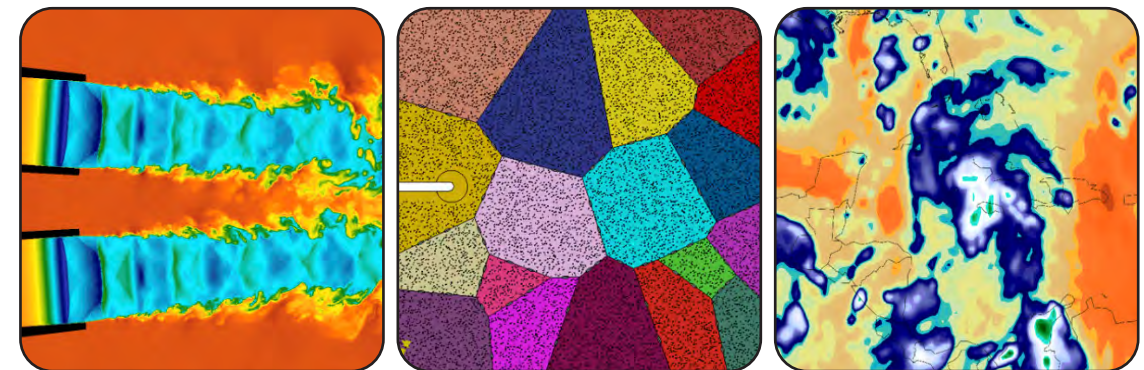
FY23 NRL DoD High Performance Computing Modernization Program Annual Reports

EDITED BY
BONNIE J. ASSAD

PREPARED BY
BETH A. HOWELL

*Center for Computational Science
Information Technology Division*

August 1, 2024



REVIEWED AND APPROVED
NRL/PU/5594--24-678
IR-5594-24-1-U
August 2024

Center for Computational Science
Information Technology Division

Introduction

This book is a compilation of reports on all the work accomplished by NRL scientists and engineers and their collaborators using the DoD High Performance Computing Modernization Program's (HPCMP) resources for fiscal year 2023. The reports encompass work performed by researchers at all three NRL sites: Washington, DC, Stennis Space Center, Mississippi, and Monterey, California.

These reports are categorized according to the primary Computational Technology Area (CTA) as specified by the HPCMP and include resources at the DOD Supercomputing Resource Centers (DSRC) as well as the Affiliated Resource Centers (ARC). This volume includes three indices for ease of reference: an author index, a site index, and an NRL hierarchical index of reports from the branches and divisions in the Laboratory.

THIS PAGE INTENTIONALLY LEFT BLANK

Table of Contents

Computational Structural Mechanics (CSM)

Stochastic Methods for Uncertainty Quantification in Computational Mechanics.....2

K. Teferra,¹ L.P. Kuna,² and R.N. Saunders¹

¹ U.S. Naval Research Laboratory, Washington, DC

² National Research Council Postdoctoral Research Associate, U.S. Naval Research Laboratory, Washington, DC

Atomistic Simulations of Structural Materials4

E. Antillon

U.S. Naval Research Laboratory, Washington, DC

Computational Analysis of Warfighter Brain Injury and Protective Equipment.....6

X.G. Tan and A.E. Moser

U.S. Naval Research Laboratory, Washington, DC

Geometric, Constitutive and Loading Complexities in Structural Materials8

S.A. Wimmer,¹ N. Wade,² A. Arcari,¹ L.P. Kuna,³ T. McCoy,¹ and J.G. Michopoulos¹

¹ U.S. Naval Research Laboratory, Washington, DC

² American Society of Engineering Education, Washington, DC

³ National Academies of Sciences, Engineering, and Medicine, Washington, DC

Computational Fluid Dynamics (CFD)

Applications of FEFLO Incompressible Flow Solver12

R. Ramamurti

U.S. Naval Research Laboratory, Washington, DC

Airbreathing Combustion for Hypersonics14

G.B. Goodwin and C.J. Rising

U.S. Naval Research Laboratory, Washington, DC

Predicting Fluid-Structure Interaction for Military Applications.....16

D.R. Mott and Y. Khine

U.S. Naval Research Laboratory, Washington, DC

Multidimensional Chemically Reacting Fluid Dynamics with Application to Flameless Combustors18

R.F. Johnson

U.S. Naval Research Laboratory, Washington, DC

Numerical Simulations of Turbulence Impact on Optical Signal Transmission and Near-Surface Turbulence.....20

S. Matt

U.S. Naval Research Laboratory, Stennis Space Center, MS

High-Fidelity CFD Simulations of High-Speed Flows in Realistic Atmospheric Conditions.....22

D.A. Kessler, T.K. Patel, R.F. Johnson, A.M. Hess and B.T. Bojko

U.S. Naval Research Laboratory, Washington, DC

Modeling of Detonations in Jet Fuel Sprays.....24

V.N. Gamezo¹ and A.Y. Poludnenko²

¹*U.S. Naval Research Laboratory, Washington, DC*

²*University of Connecticut, Storrs, CT*

Numerical Investigation of Advanced Military Aircraft Noise Reduction Concepts.....26

J. Liu

U.S. Naval Research Laboratory, Washington, DC

Detonations with Multi-Phase Flows for Propulsion.....28

D.A. Schwer

U.S. Naval Research Laboratory, Washington, DC

Numerical Simulations of Noise Generated by Non-Circular Advanced Military Aircraft Nozzles.....30

K. Viswanath and R. Ramamurti

U.S. Naval Research Laboratory, Washington, DC

Direct Numerical Simulation of Fluid-Sediment Wave Bottom Boundary Layer.....32

J. Simeonov,¹ I. Adams,² A. Penko,¹ S. Schoenauer,¹ S. Bateman,¹ K. Edwards,¹ R. Phillip,¹ and J. Veeramony¹

¹*U. S. Naval Research Laboratory, Stennis Space Center, MS*

²*National Research Council Postdoctoral Fellow, Stennis Space Center, MS*

Computational Biology, Chemistry, and Materials Science (CCM)

Materials for Energy Storage and Generation.....36

M. Johannes

U.S. Naval Research Laboratory, Washington, DC

Calculation of Materials Properties Via Density Functional Theory and Its Extensions38

J.L. Lyons and M.W. Swift

U.S. Naval Research Laboratory, Washington, DC

The Impact of Foam and Aerosol Dynamics on Fire, Explosion Safety, and Suppression (Mechanisms of Water Mist Suppression of a Burning Solid Surface)	40
J.A. Cramer, ¹ P.E. Sudol, ² and R. Ananth ¹	
¹ <i>U.S. Naval Research Laboratory, Washington, DC</i>	
² <i>National Research Council Postdoctoral Research Associate, U.S. Naval Research Laboratory, Washington, DC</i>	
Point Defects and Interfaces in Two-Dimensional Materials	42
D. Wickramaratne	
<i>U.S. Naval Research Laboratory, Washington, DC</i>	
Numerical Studies of Semiconductor Nanostructures.....	44
T.L. Reinecke ¹ and I. Welland ²	
¹ <i>U.S. Naval Research Laboratory, Washington DC</i>	
² <i>National Research Council Postdoctoral Research Associate, U.S. Naval Research Laboratory, Washington DC</i>	
Multiple Length and Time Scale Simulations of Material Properties	46
N. Bernstein	
<i>U.S. Naval Research Laboratory, Washington, DC</i>	
Surfaces and Interfaces in Oxides and Semiconductors	48
C.S. Hellberg	
<i>U.S. Naval Research Laboratory, Washington, DC</i>	
Particle-Dynamics Modeling of Autonomous-Agent Clustering	50
S. Lambrakos, A. Shabaev, E. Ward, and D. Chichka	
<i>U.S. Naval Research Laboratory, Washington, DC</i>	
Materials Properties of Surfaces and Two-dimensional Systems.....	52
M. Phillips	
<i>U.S. Naval Research Laboratory, Washington, DC</i>	
First-principles Simulations of Condensed-phase Decomposition of Energetic Materials	54
I.V. Schweigert	
<i>U.S. Naval Research Laboratory, Washington, DC</i>	
Crystal Properties of Explosives from Quantum Molecular Dynamics	56
I.V. Schweigert	
<i>U.S. Naval Research Laboratory, Washington, DC</i>	
Marine Biofilm Metaproteomics	58
W.J. Hervey and G.J. Vora	
<i>U.S. Naval Research Laboratory, Washington, DC</i>	

Synthetic Biology for Military Environments	60
W.J. Hervey and G.J. Vora	
<i>U.S. Naval Research Laboratory, Washington, DC</i>	
Atomistic Simulations of Navy-relevant Materials	62
D. Fragiadakis	
<i>U.S. Naval Research Laboratory, Washington, DC</i>	
 <u>Computational Electromagnetics and Acoustics (CEA)</u>	
Small-Slope Approximation (SSA) Rough-Surface Backscattering Analysis	66
J. Alatishe	
<i>U.S. Naval Research Laboratory, Washington, DC</i>	
Low Grazing Angle Radar Backscatter	68
J.V. Toporkov, M.A. Sletten and J.D. Ouelette	
<i>U.S. Naval Research Laboratory, Washington, DC</i>	
Interactive Scenario Builder	70
B. Dowd ¹ and D. Richie ²	
¹ <i>U.S. Naval Research Laboratory, Washington, DC</i>	
² <i>Brown Deer Scientific, Forest Hill, MD</i>	
Infrared Scattering by Micro-particles.....	72
R. Furstenberg and A. Shabaev	
<i>U.S. Naval Research Laboratory, Washington, DC</i>	
Particle-In-Cell Simulations of Two Cylindrical Reflex Triodes in Parallel.....	74
I.M. Rittersdorf, B.V. Weber, S.B. Swanekamp, and D.D. Hinshelwood	
<i>U.S. Naval Research Laboratory, Washington, DC</i>	
3D Particle-In-Cell Simulations of Electron Beam Plasma: A First Study	76
N.D. Isner, ¹ E.R. Kaiser, ¹ S.B. Swanekamp, ¹ K.L. Cartwright ²	
¹ <i>U.S. Naval Research Laboratory, Washington, DC</i>	
² <i>Sandia National Laboratories, Albuquerque, New Mexico</i>	
Simulation of Passively Mode-locked and Frequency Modulated Interband Cascade Laser Frequency Combs	78
I. Vurgaftman, ¹ J.R. Meyer, ¹ and M. Povolotskyi ²	
¹ <i>U.S. Naval Research Laboratory, Washington DC</i>	
² <i>Jacobs, Hanover MD</i>	
Acoustic Parameter Variability over an Ocean Reanalysis (AVORA).....	80
J.P. Fabre	
<i>U.S. Naval Research Laboratory, Stennis Space Center, MS</i>	

Intense Laser Physics and Advanced Radiation Sources	82
Y.H. Chen, D.F. Gordon, J. Isaacs, and G.M. Petrov	
<i>U.S. Naval Research Laboratory, Washington, DC</i>	
Underwater Electrical Impedance Tomography	84
G.R. Gatling and E.M. Tejero	
<i>U.S. Naval Research Laboratory, Washington, DC</i>	
 <u>Climate Weather Ocean Modeling (CWO)</u>	
COAMPS-TC[®] Tropical Cyclone Rapid Intensification Prediction	88
J.D. Doyle	
<i>U.S. Naval Research Laboratory, Monterey, CA</i>	
Performance Study and Potential Optimization Exploration of an Ocean Modeling Code	90
Y. Khine	
<i>U.S. Naval Research Laboratory, Washington, DC</i>	
Coastal Mesoscale Modeling	92
P.M. Finocchio	
<i>U.S. Naval Research Laboratory, Washington, DC</i>	
Coupled Ocean-Wave-Air-Ice Prediction System.....	94
R. Allard, ¹ T. Campbell, ¹ E. Douglass, ¹ D. Hebert, ¹ T. Jensen, ¹ G. Pantelev, ¹ M. Phelps, ² and T. Smith ¹	
¹ <i>Naval Research Laboratory, Washington, DC</i>	
² <i>Peraton, Inc., Stennis Space Center, MS</i>	
Dynamics of Coupled Models	96
I. Shulman, A. Thombs, S. Matt, and S. Cayula	
<i>U.S. Naval Research Laboratory, Stennis Space Center, MS</i>	
Rogue Wave Probability Estimator for WAVEWATCH III[®]	98
M. Orzech	
<i>U.S. Naval Research Laboratory, Stennis Space Center, MS</i>	
Eddy-Resolving Global/Basin-Scale Ocean Modeling – The Atlantic Ocean’s Deep Water Origins	100
R.W. Helber, G. Pantelev, S.R. Smith, and J.F. Shriver	
<i>U.S. Naval Research Laboratory, Stennis Space Center, MS</i>	
Eddy-Resolving Global/Basin-Scale Ocean Modeling – Navy ESPC Participation in NOAA SubX.....	102
E.J. Metzger	
<i>U.S. Naval Research Laboratory, Stennis Space Center, MS</i>	

Eddy-Resolving Global/Basin-Scale Ocean Modeling – Winter-mixing Intermittency in the Northern Arabian Sea	104
P.G. Thoppil	
<i>U.S. Naval Research Laboratory, Stennis Space Center, MS</i>	
Eddy-Resolving Global/Basin-Scale Ocean Modeling – Enabling Operations Across Ocean Fronts/Eddies	106
E.J. Metzger and C. Trott	
<i>U.S. Naval Research Laboratory, Stennis Space Center, MS</i>	
Eddy-Resolving Global/Basin-Scale Ocean Modeling – An Evaluation of the Uncertainty of Internal Tides using HYCOM Ensembles: Implications for Predictability and Future Improvements	108
J.F. Shriver and E.J. Metzger	
<i>U.S. Naval Research Laboratory, Stennis Space Center, MS</i>	
Eddy-Resolving Global/Basin-Scale Ocean Modeling – Accelerating Ocean Forecasts Through Mixed Precision Data Representation	110
C. Rowley, ¹ P. Thoppil, ¹ K. Obenschain, ² J. Boris, ² Y. Khine, ² R. Rosenberg, ² G. Patnaik, ³ and T. Jensen ¹	
¹ <i>U.S. Naval Research Laboratory, Stennis Space Center, MS</i>	
² <i>U.S. Naval Research Laboratory, Washington, DC</i>	
³ <i>Alion Science and Technology Corporation, Hanover, MD</i>	
Eddy-Resolving Global/Basin-Scale Ocean Modeling – Sea Bottom Warfare.....	112
C.A. Blain, ¹ Z. Yu, ² T. Jensen, ² and T. Campbell ²	
¹ <i>U.S. Naval Research Laboratory, Washington, DC</i>	
² <i>U.S. Naval Research Laboratory, Stennis Space Center, MS</i>	
Atmospheric Process Studies	114
T.R. Whitcomb, J. Ridout, and J. McLay	
<i>U.S. Naval Research Laboratory, Monterey, CA</i>	
Multi-scale Characterization and Prediction of the Global Atmosphere from Ground to the Edge of Space using Next-Generation Navy Modeling Systems.....	116
C.A. Barton, S.D. Eckermann, J.F. Kelly, M.A. Herrera, K.W. Hoppel, D.D. Kuhl, D.R. Allen, J. Ma, and T. Rhodes	
<i>U.S. Naval Research Laboratory, Washington DC</i>	
Ocean Data Assimilation – Ocean State Estimation and Forecasting using SWOT Observations.....	118
J.M. D’Addezio, G.A. Jacobs, and S.R. Smith	
<i>U.S. Naval Research Laboratory, Stennis Space Center, MS</i>	
Ocean Data Assimilation – Results of Year-Long NCOM Simulation of the Northeast Atlantic Domain using the 4DVAR Method	120
M. Carrier, H. Ngodock, and S.R. Smith	
<i>U. S. Naval Research Laboratory, Stennis Space Center, MS</i>	

Ocean Data Assimilation – Deterministic and Statistical Predictability of Mid-Frequency Acoustic Ducts	122
J. Osborne, ¹ C. Amos, ² and G.A. Jacobs ¹	
¹ <i>U.S. Naval Research Laboratory, Stennis Space Center, MS</i>	
² <i>American Society for Engineering Education, Stennis Space Center, MS</i>	
Ocean Data Assimilation – Hybrid NCODA	124
T. Townsend and S.R. Smith	
<i>U.S. Naval Research Laboratory, Stennis Space Center, MS</i>	
Ocean Data Assimilation – Stability of Freshwater Runoff in East Greenland Currents	126
S.R. Smith and R.W. Helber	
<i>U. S. Naval Research Laboratory, Stennis Space Center, MS</i>	
Ocean Data Assimilation	128
S.R. Smith, ¹ J.M. D’Addezio, ¹ C. Amos, ³ M. Carrier, ¹ C. DeHaan, ⁴ S. deRada, ¹ R.W. Helber, ¹ A. Iversen, ⁴ A. Lawrence, ⁴ J. May, ¹ V. Montiforte, ³ H. Ngodock, ¹ , J. Osborne, ¹ M. Phelps, ⁴ C. Rowley, ¹ W. Stevens, ⁵ T. Townsend, ¹ and K. Tremblay ⁴	
¹ <i>U.S. Naval Research Laboratory, Stennis Space Center, MS</i>	
² <i>University of New Orleans, Stennis Space Center, MS</i>	
³ <i>American Society for Engineering Education, Stennis Space Center, MS</i>	
⁴ <i>Peraton Inc., Stennis Space Center, MS</i>	
⁵ <i>Portland State University, OR</i>	
Coupled Ocean-Wave-Air-Ice Prediction System.....	130
T. Jensen, ¹ J. Yu, ¹ D. Flagg, ² R.W. Helber, ¹ G.A. Jacobs, ¹ A. Rydbeck, ¹ J. Christophersen, ² H. Wijesekera, ¹ and T. Campbell ¹	
¹ <i>U.S. Naval Research Laboratory, Stennis Space Center, MS</i>	
² <i>U.S. Naval Research Laboratory, Monterey, CA</i>	
Turbulent Mixing in NCOM and HYCOM.....	132
Y. Fan	
<i>U.S. Naval Research Laboratory, Stennis Space Center, MS</i>	
Improving Tropical Convective Storm Prediction by Bridging the Gap between Large-Scale Moisture and Convective Dynamics	134
Q. Zhao, N. Baker, Y. Jin, and D. Tyndall	
<i>U.S. Naval Research Laboratory, Monterey, CA</i>	
Bio-Optical Modeling and Forecasting	136
J.K. Jolliff, S. Ladner, and T. Smith	
<i>U.S. Naval Research Laboratory, Stennis Space Center, MS</i>	
Data Assimilation Studies Project	138
J. Tsu and W.F. Campbell	
<i>U.S. Naval Research Laboratory, Monterey, CA</i>	

Signal Image Processing (SIP)

Retrieving Surface Soil Moisture from CyGNSS Reflectivity Measurements142

J.D. Ouellette, E.M. Twarog, L. Li, and S.M. Grossman

U.S. Naval Research Laboratory, Washington, DC

Application of Physics-based Machine Learning to Navy Problems144

L.N. Smith

U.S. Naval Research Laboratory, Washington, DC

Space and Astrophysical Science (SAS)

Modeling Propagation of Ionospheric Disturbances Initiated by Magnetospheric Substorms148

J. Haiducek and J. Helmboldt

U.S. Naval Research Laboratory, Washington, DC

Electromagnetic Pulses from Hypervelocity Impacts on Spacecraft150

A. Fletcher

U.S. Naval Research Laboratory, Washington, DC

Global Kinetic Simulations of Space Plasma Waves and Turbulence152

A. Fletcher

U.S. Naval Research Laboratory, Washington, DC

Searches for Millisecond Pulsars and Pulsar Emission Modeling.....154

P.S. Ray¹ and J. Deneva²

¹*U.S. Naval Research Laboratory, Washington, DC*

²*George Mason University, Fairfax, VA, resident at U.S. Naval Research Laboratory, Washington, DC*

Particle-in-Cell Simulations of Plasma Waves and Turbulence.....156

A.R. Soto-Chavez and J.D. Huba

U.S. Naval Research Laboratory, Washington, DC

Thermosphere & Ionosphere Numerical Models and Ensemble Methods.....158

D.P. Drob, M. Jones, and J. Emmert

U.S. Naval Research Laboratory, Washington, DC

Navy Ionosphere Model for Operations160
 S.E. McDonald,¹ M.R. Burleigh,¹ C.A. Metzler,¹ J.L. Tate,² D. Hodyss,¹ R. Schaefer,³
 G. Romeo³
¹*U.S. Naval Research Laboratory, Washington, DC*
²*Computational Physics, Inc., Springfield, VA*
³*Johns Hopkins University Applied Physics Laboratory, Laurel, MD*

Other (OTH)

Simulation of High Energy-Radiation Environments164
 J. Finke and W. Duvall
U.S. Naval Research Laboratory, Washington, DC

Author Index167

Division Index.....170

Site Index173

THIS PAGE INTENTIONALLY LEFT BLANK



Computational Structural Mechanics

CSM covers the high-resolution multidimensional modeling of materials and structures subjected to a broad range of loading conditions including quasistatic, dynamic, electromagnetic, shock, penetration, and blast. It also includes the highly interdisciplinary research area of materials design, where multiscale modeling from atomistic scale to macroscale is essential. CSM encompasses a wide range of engineering problems in solid mechanics, such as material or structural response to time- and history-dependent loading, large deformations, fracture propagation, shock wave propagation, isotropic and anisotropic plasticity, frequency response, and nonlinear and heterogeneous material behaviors. High-performance computing for CSM addresses the accurate numerical solution of conservation equations, equations of motion, equations of state, and constitutive relationships to model simple or complex geometries and material properties, subject to external boundary conditions and loads. CSM is used for basic studies in continuum mechanics, stress analysis for engineering design studies, predicting structural and material response to impulsive loads, and modeling response of heterogeneous embedded sensors/devices. DoD application areas include conventional underwater explosion and ship response, structural acoustics, coupled field problems, space debris, propulsion systems, structural analysis, total weapon simulation, weapon systems' lethality/survivability (e.g., aircraft, ships, submarines, and tanks), theater missile defense lethality analyses, optimization techniques, and real-time, large-scale soldier- and hardware-in-the-loop ground vehicle dynamic simulation.

Title: Stochastic Methods for Uncertainty Quantification in Computational Mechanics

Author(s): K. Teferra,¹ L.P. Kuna,² and R.N. Saunders¹

Affiliation(s): ¹U.S. Naval Research Laboratory, Washington, DC; ²National Research Council Postdoctoral Associate, U.S. Naval Research Laboratory, Washington, DC

CTA: CSM

Computer Resources: Cray XC40/50 [ERDC, MS]; HPE SGI 8600 [NAVY, MS]

Research Objectives: The research objective for the work in FY23 is to be able to compute residual stresses and strains in additively manufactured (AM) 316L stainless steel at the microstructure-resolved length scale and to identify correlations among processing parameters, microstructural features, and mechanical response. Such analysis provides the capability to quantify the heterogeneous distribution of residual mechanical response due to microstructural heterogeneity, which leads to the accumulation and localization of plastic strain. This information is indicative of weak points in the material from which failure initiates. Further, quantifying the residual stress in as-built parts is an essential prerequisite to understanding as-built material mechanical performance, particularly the tension-compression asymmetry associated with accumulated back stress. The approach taken in this study specifically aims to consider microstructural effects on these mechanical responses and properties.

Methodology: This work primarily utilizes a crystal plasticity finite-element method (CPFEM) application built on the Multiphysics Object Oriented Simulation Environment (MOOSE) developed and maintained by Idaho National Lab. Thermomechanical simulations of the solidification process are performed by coupling a cellular automata finite-element (CAFE) solidification model with the CPFEM model. A validation study is performed that compares the distribution of intragrain rotations between simulation and experimental crystallographic characterization data. Then, multiple cases of thin-wall parts with varying processing parameters are simulated. With a voxel size of 4 μm and a part length of almost 1 mm, such large-scale simulations enable a detailed investigation of the correlations between processing parameters and the mechanical properties at both the local intragranular scale and the global part scale.

Results: Processing simulations of 316L AM thin-wall parts manufactured through laser powder bed fusion were performed. They included processing-specific polycrystalline microstructures and residual stresses and strains. Figure 1 shows the overall workflow conceptually of the methodology. Figure 2 provides scan direction cross section cuts of the von Mises stress as well as the grain morphology and crystallographic orientation of the microstructure. These results are compared with a hypothetical isotropic homogeneous model in order to illustrate the role that microstructural heterogeneity plays in residual mechanical response. In this case, the presence of grains leads to conditions where elastic response is confined, resulting in much larger residual stress than what would be predicted without microstructural considerations. The four microstructures correspond to different processing conditions. These results indicate that slower scan speeds, lower power, and bidirectional raster patterns produce lower residual stress than higher power, higher scan speeds, and unidirectional raster patterns.

DoD Impact/Significance: The enhanced structural material performance in terms of durability, strength-to-weight ratio, and manufacturability are essential ingredients toward transforming fleet capabilities. Understanding the nuances of processing parameters is increasingly important as additive manufacturing becomes a more commonplace manufacturing technique not only for military applications, but also for civilian applications. Understanding the influence of additive manufacturing processing parameters on resulting parts is integral to providing guidance to material designers to achieve manufacturing of materials with not only desired properties, but also maximally optimized properties.

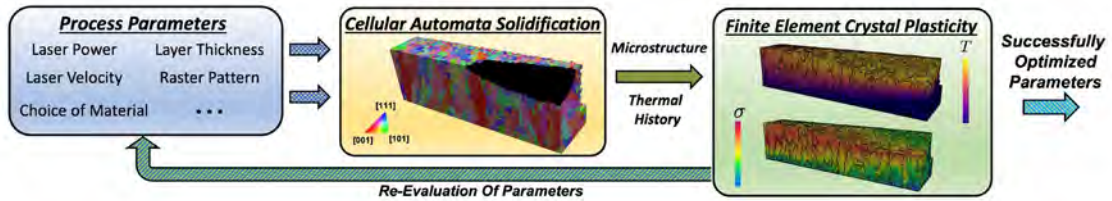


Figure 1. Workflow of developed methodology: process parameters are input to the cellular automata finite-element (CAFE) model to simulate solidified representative volume elements. The produced microstructures are subjected to thermomechanical loading conditions associated with the solidification process using the crystal plasticity finite-element method (CPFEM) to compute microstructure-resolved residual mechanical response.

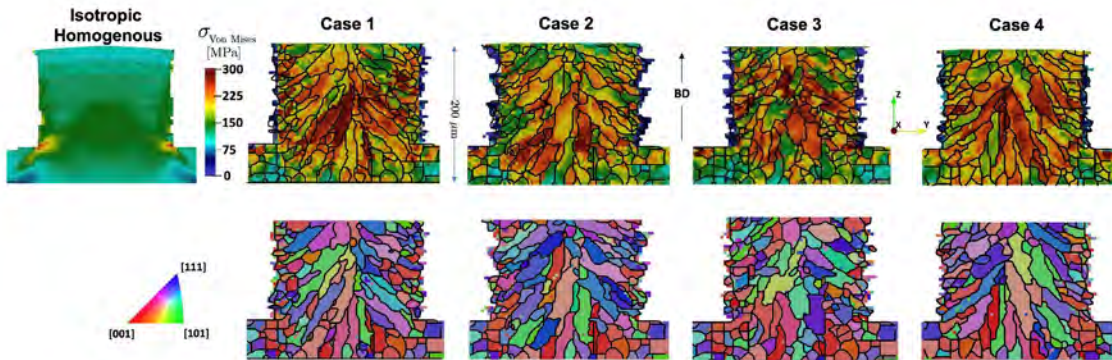


Figure 2. Scan direction cross-sectional cuts comparing the residual von Mises stress in four simulated microstructures using different processing conditions as well as an analogous simulation treating the material as isotropic and homogeneous (top row). The second row shows the grain morphology and crystallographic orientations for these cross sections for the four simulations.

Title: Atomistic Simulations of Structural Materials

Author: E. Antillon

Affiliation: U.S. Naval Research Laboratory, Washington, DC

CTA: CSM

Computer Resources: HPE SGI 8600 [AFRL, OH]; Cray XC40/50 [ERDC, MS]

Research Objectives: The objective is to understand atomistic processes that are responsible for mechanical strength and phase stability in structural materials, specifically steel alloys.

Methodology: We implement atomistic simulations using empirical interatomic potentials that have been fitted to reproduce material properties of stainless-steel alloys (elastic constants, stacking fault energies, etc.). To better understand the interplay between local chemical ordering and material strength, we sample for the most stable configurations using Monte-Carlo annealing approach at various annealing temperatures, and probe microscopic plasticity by monitoring the flow of dislocation movement under various stress and temperature conditions. All calculations in this work have been done using the Large-scale Atomic/Molecular Massively Parallel Simulator (LAMMPS) with interatomic potentials developed by Bonny et al. (2011), Zhou et al. (2018).

Results: We quantify the amount of chemical short-range order (CSRO) for various annealing temperatures on a ternary Fe-12Ni-18Cr (at.%) alloy that is related to the 316L stainless steel often used in naval applications. Moreover, mechanical strength is measured directly with molecular dynamics with various degrees of shear stress using two commonly used interatomic potentials for austenitic stainless steel alloys. A strengthening model that incorporates local ordering is proposed based on a family of analytical models due to Varvenne et al. (2016), which takes into account dislocation-solute misfit interaction, and a more recent extension due to Nag and Curtin (2020), which incorporates the role of solute-solute interactions during dislocation slip. We find that the critical stress needed to initiate plastic flow can be separated into two competing effects: a softening effect due to chemical species' redistributing into more compact atomic configurations, and a strengthening effect due to the formation of stronger chemical bonds after annealing, which result in higher shearing stresses needed to initiate microscopic motion of dislocations. Our results suggest that, while significant CSRO is predicted in the simulations, there is little experimental evidence in cast and annealed alloys analyzed by atom-probe tomography.

DoD Impact/Significance: Understanding the impact of processing conditions on local microstructure and how the microstructure, in turn, influences material properties is essential for designing advanced alloys tailored to withstand extreme conditions. Ordering or phase segregation at the atomic level can introduce substantial variations in material strength and stability. Therefore, it is important to assess how current strengthening predictive models can deviate under such circumstances in order to improve material performance.

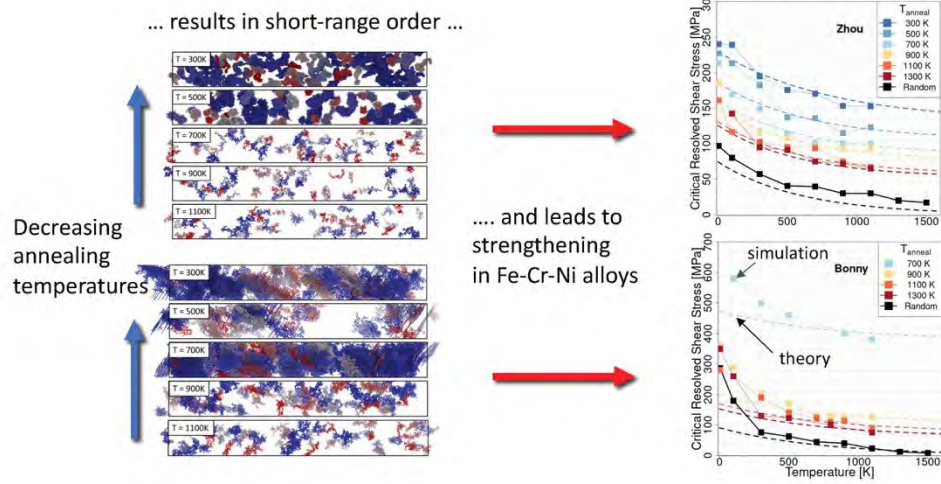


Figure 1. Annealing can result in significant chemical short-range order that influences dislocation mobility.

Title: Computational Analysis of Warfighter Brain Injury and Protective Equipment

Author(s): X.G. Tan and A.E. Moser

Affiliation(s): U.S. Naval Research Laboratory, Washington, DC

CTA: CSM

Computer Resources: HPE Cray EX [NAVY, MS]

Research Objectives: The research objective of this project is developing methods to prevent and mitigate injuries to warfighters. This involves computational analysis of ballistic/blunt impacts on personal protective equipment (PPE) and blast-induced traumatic brain injuries (TBI). Computational methods such as finite-element analysis are used to conduct the simulation analysis. The use of HPC resources is vitally important to this project due to the high fidelity of the models of interest. A typical model to analyze traumatic brain injury requires approximately 24 hours on 216 CPUs. One of the primary outcomes of this research will be the accumulation of a significant number of simulations that will be used to construct the correspondence relationship between humans and animals and to optimize the design of protective equipment.

Methodology: The project uses finite-element methods extensively, but the work is not restricted to finite-element methodologies. Nonlinear material mechanical constitutive response features are highlighted in much of the work performed. Implicit and explicit solutions methods are used as appropriate. The primary finite-element codes used are Abaqus, CoBi and CTH. User subroutines are used for specialized material constitutive response when applicable. Multiphysics analysis is used to capture the fluid/acoustic-structure interaction, thermomechanical, and electromagneto-mechanical effects. Typically, Abaqus/Viewer, ParaView, VisIt, IDL, Matlab are used for visualization of results in formats such as VTU and HDF5, including animation. For model development, the project typically uses CUBIT, ABAQUS/CAE, Simpleware, IDL, and in-house code. Large run times and large model size are often required for the multiphysics/multistep nonlinear finite-element/volume analysis jobs.

Results: This project involves work in several topical areas. Work has been performed in the numerical investigation of auditory injury risk resulting from impulse noises in military high-risk environments. We compared various auditory pathways, including air conduction (via the ear canal) and bone conduction, and examined the response of the inner ear due to the bone conduction. We illustrated the effect of temporal bone protection and explored multilayered structures for sound attenuation. Shown in Fig. 1, a computational model of the human head, incorporating a simplified ear structure, was utilized to simulate the transmission of sound pressure in the spotter's head caused by the muzzle blast noise. A ConWep loading condition with an equivalent sound pressure level (SPL) of 174 dB was applied to the head model. The sound pressure level in the inner ear, considering both air conduction and bone conduction pathways, is 173 dB. The pressure by the bone conduction reaches the inner ear earlier than the air conduction. The sound pressure level in the inner ear from bone conduction alone is 148 dB. Exposure to noise levels exceeding 140 dB SPL can lead to damaging effects. Consequently, bone conduction may pose a risk, even when ear canal protection is utilized. Interestingly, a comparable trend in sound transmission was observed in the cadaver head experiment. This work presents a computational method for separating multiple transmission modes and addressing the effects of impulse noise on sensitive inner ear organs.

DoD Impact/Significance: Insights gained from this project are necessary for the advancement from concept to application. Navy/DoD expected results are an improved understanding of traumatic brain injury for Navy/DoD applications. New insights will be gained through quantifying the effects of anatomical and material property differences on the mechanical response of quantities correlated with traumatic brain injury and hearing loss, which will affect warfighter health in terms of improved protective gear and improved understanding of the correlation between mechanical response thresholds and traumatic brain injuries. The development of techniques to model population-wide anatomical variability will provide insight into the importance of the fit of protective gear.

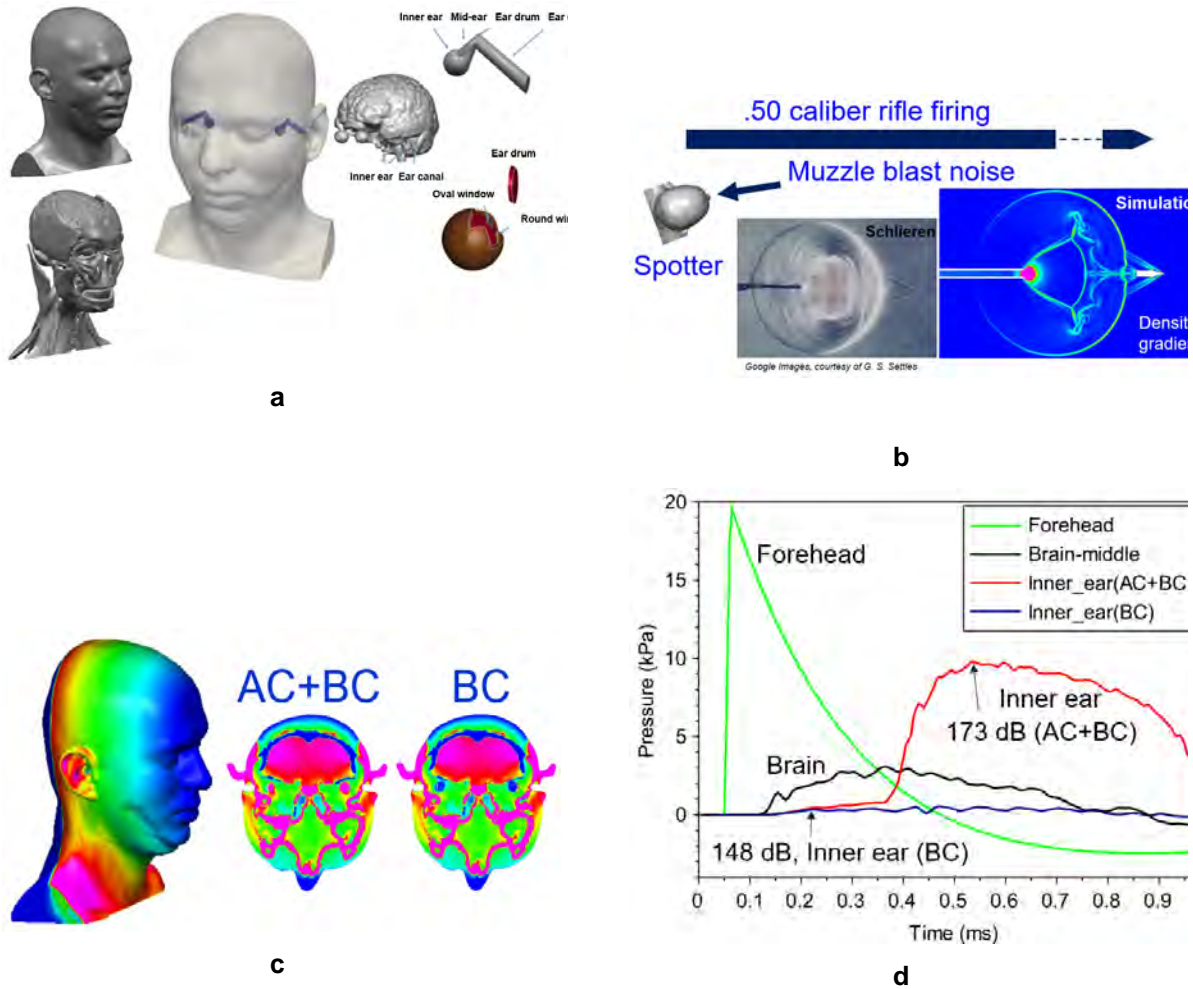


Figure 1. Simulation of impulse noise effects: a) head finite-element (FE) model with a simplified ear structure, b) CFD simulation of muzzle blast noise of .50-caliber rifle firing, c) snapshot of pressures on head surface and on the transverse plane for air conduction (AC) and bone conduction (BC) pathways, d) comparison of pressure transmission between different auditory pathways.

Title: Geometric, Constitutive and Loading Complexities in Structural Materials

Author(s): S.A. Wimmer,¹ N. Wade,² A. Arcari,¹ L.P. Kuna,³ T. McCoy,¹ and J.G. Michopoulos¹

Affiliation(s): ¹U.S. Naval Research Laboratory, Washington, DC; ²American Society of Engineering Education, Washington, DC; ³National Academies of Sciences, Engineering, and Medicine, Washington, DC

CTA: CSM

Computer Resources: HPE SGI 8600 [AFRL, OH], [NAVY, MS]

Research Objectives: The research strives to develop rational bases and mathematical descriptions of complex material responses for structural and novel evolving materials. Structural integrity and life cycle evaluations require an understanding of material responses. Analytical models and techniques cannot describe complex materials and often do not account for interactions, complex geometries, or multiphysics loading. Finite-element methods are used to develop models involving multifunctional materials, novel evolving materials, and multiphysics. In order to accurately model the nonlinear response of conventional structural materials, rate dependence, large deformation, and damage accumulation mechanisms must be understood and accurately represented. The performance of the overall structure or system is also examined via parameters such as kinematics, geometric complexities, loading path dependencies, and interaction between loading types.

Methodology: The project uses finite-element methods extensively. Nonlinear material constitutive response features are highlighted in much of the work. Implicit and explicit solutions methods are used as appropriate. The primary finite-element code used is ABAQUS. Coupled material responses, such as electric-thermal or electrical-mechanical-thermal, are exercised for evaluation of these effects. Model development is done with CUBIT, ABAQUS/CAE, ScanIP, or in-house software. Large run times and large model size are often required for the multistep nonlinear finite-element analysis jobs.

Results: This project involves work in several topical areas. Work has been performed on creating image-based microstructural models, modeling multi-layer ceramic structures, modeling stress corrosion cracking, modeling biofoulants, and modeling transparent armor delamination. Representative results for the modeling of a nickel alloy microstructure are shown. The simulations carried out in this work consisted of a set of 18 grains in a 100 μm \times 100 μm microstructure with all of the major precipitates explicitly modeled within the material microstructure. The delta phase was modeled at the grain boundaries as an ellipsoidal phase; the gamma phases were modeled at the interior of the grain as round precipitates. Material microstructure influences the resulting mechanical properties (on a macroscale) and it is considered as the driving force for the material environmentally assisted cracking behavior. In particular, precipitation-hardened nickel alloys require careful chemistry, forming, and heat treatment control to achieve high-strength while being able to survive a hydrogen-producing seawater environment. Grain shape, grain boundary characteristics, and texture, along with precipitate characteristics, volume fraction, size, shape, and relation to grain boundary characteristics, have all been identified as factors in the alloy environmental behavior. Figure 1 shows the model developed to represent the material microstructure and the resulting accumulated slip and immobile dislocation density distribution in the microstructure as the model is subjected to applied strain. Simulations of hydrogen diffusion from the crack toward the material microstructure are shown in Fig. 2.

DoD Impact/Significance: Environmentally assisted cracking can significantly affect the performance of high-strength alloys. Precipitation-hardened nickel alloys are used in marine service applications and under a variety of conditions. With a better understanding of the influence of the material microstructure on environmentally assisted cracking behavior, materials with higher strength and optimized microstructures with greater environmental resistance can be developed for future-generation Navy assets.

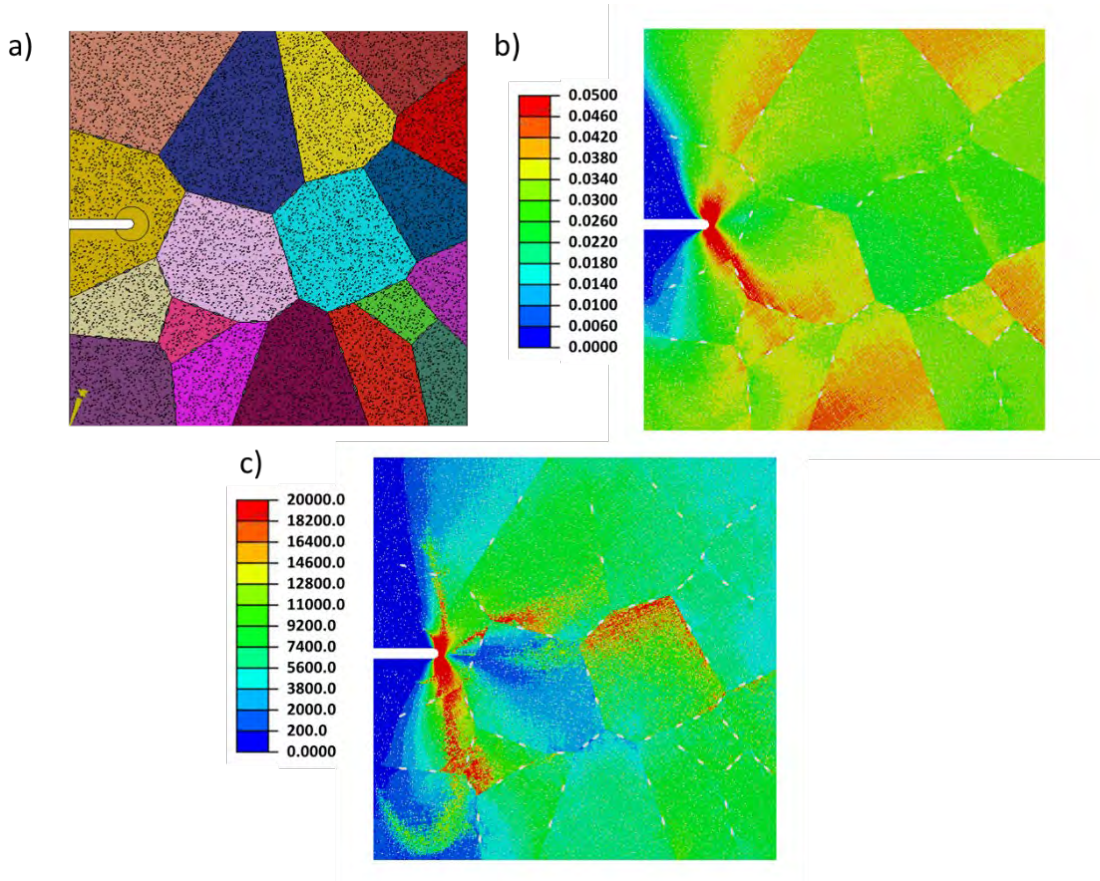


Figure 1. Model of phase-hardened nickel alloy microstructure: a) subjected to constant applied strain representing the mechanical condition at the root of a sharp stress concentrator and resulting accumulated slip, b) immobile dislocation densities distribution, and c) expressed in $1/\mu\text{m}^2$. The model includes a microstructurally small crack with 125 nm root radius to identify the driving forces for hydrogen accumulation and crack propagation.

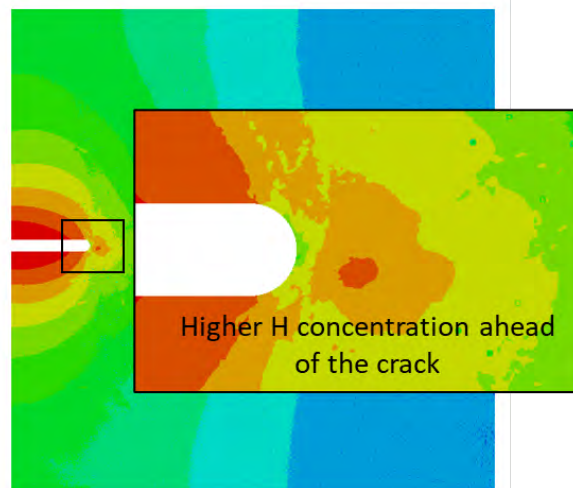


Figure 2. Concentration of hydrogen after weakly coupled simulation of stress- and dislocation density-assisted diffusion. Concentration is highest a small distance away from the crack tip.

THIS PAGE INTENTIONALLY LEFT BLANK

CFD

Computational Fluid Dynamics

CFD covers high-performance computations whose goal is the accurate numerical solution of the equations describing fluid motion and the related use of digital computers in fluid dynamics research. CFD is used for basic studies of fluid dynamics for engineering design of complex flow configurations and for predicting the interactions of chemistry with fluid flow for combustion and propulsion. It is also used to interpret and analyze experimental data and to extrapolate into regimes that are inaccessible or too costly to study. Work in the CFD CTA encompasses all Reynolds number flow regimes and scales of interest to the DoD. Incompressible flows are generally slow (e.g., governing the dynamics of submarines, slow airplanes, pipe flows, and air circulation) while compressible flows are important at higher speeds (e.g., controlling the behavior of transonic and supersonic planes, missiles, and projectiles). Fluid dynamics itself involves some very complex physics, such as boundary-layer flows, transition to turbulence, and turbulence dynamics, that require continued scientific research. CFD also must incorporate complex additional physics to deal with many real-world problems. These effects include additional force fields, coupling to surface atomic physics and microphysics, changes of phase, changes of chemical composition, and interactions among multiple phases in heterogeneous flows. Examples of these physical complexities include direct simulation Monte Carlo and plasma simulation for atmospheric reentry, microelectromechanical systems (MEMS), materials processing, and magnetohydrodynamics (MHD) for advanced power systems and weapons effects. CFD has no restrictions on the geometry and includes motion and deformation of solid boundaries defining the flow.

Title: Applications of FEFLO Incompressible Flow Solver

Author(s): R. Ramamurti

Affiliation(s): U.S. Naval Research Laboratory, Washington, DC

CTA: CFD

Computer Resources: HPE Cray EX [AFRL, OH]

Research Objectives: Perform three-dimensional (3D) numerical simulations of flow past complex configurations. The proposed studies will investigate the use of bioinspired skins for drag reduction for unmanned underwater vehicles and unsteady flow past acoustic sensor enclosures.

Methodology: A finite-element solver, called FEFLO, for 3D incompressible flows based on unstructured grids is used. The flow solver is combined with adaptive remeshing techniques for transient problems with moving grids and is also integrated with the rigid body motion in a self-consistent manner, which allows the simulation of fully coupled fluid-rigid body interaction problems of arbitrary geometric complexity in three dimensions. NRL has developed a coupled fluid structure interaction solver for simulating flapping-fin propulsion for operations. In addition to three-dimensional unsteady flow simulations past a passively deforming flapping pectoral fins in tandem configurations, simulations are performed over a circular cylinder and an Eppler airfoil placed in the hydroacoustic flow channel facility.

Results: The baseline configuration used for simulations is the circular cylinder of 3-in diameter situated in an 8-in \times 8-in test section. The inflow velocity is set to 0.75 m/s. The unsteady forces and the surface pressure distribution are monitored at several locations surrounding the cylinder and are provided to the NRL Acoustics Division for further postprocessing. The cylinder is then replaced by an Eppler airfoil of 3-in thickness and 8.4-in chord. Simulations were performed over this airfoil and the results are shown in Fig. 1. The unsteady surface pressure data and the pressure and velocity at several station points surrounding the airfoil will be postprocessed to measure the acoustic noise that is propagated into the housing. The potential for noise reduction using proper foil shape can then be explored.

DoD Impact/Significance: Simulations have enabled characterization of the unsteady flow behind a circular cylinder and airfoil. This will provide the next steps toward development of low-noise acoustic sensor enclosures in complex environments.

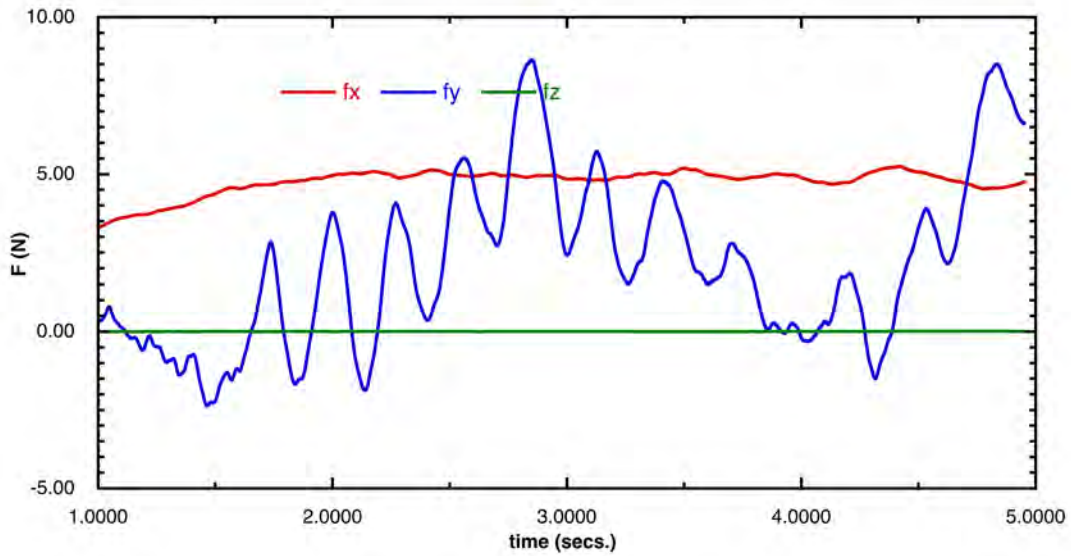


Figure 1. Time history of the unsteady forces over an Eppler airfoil.

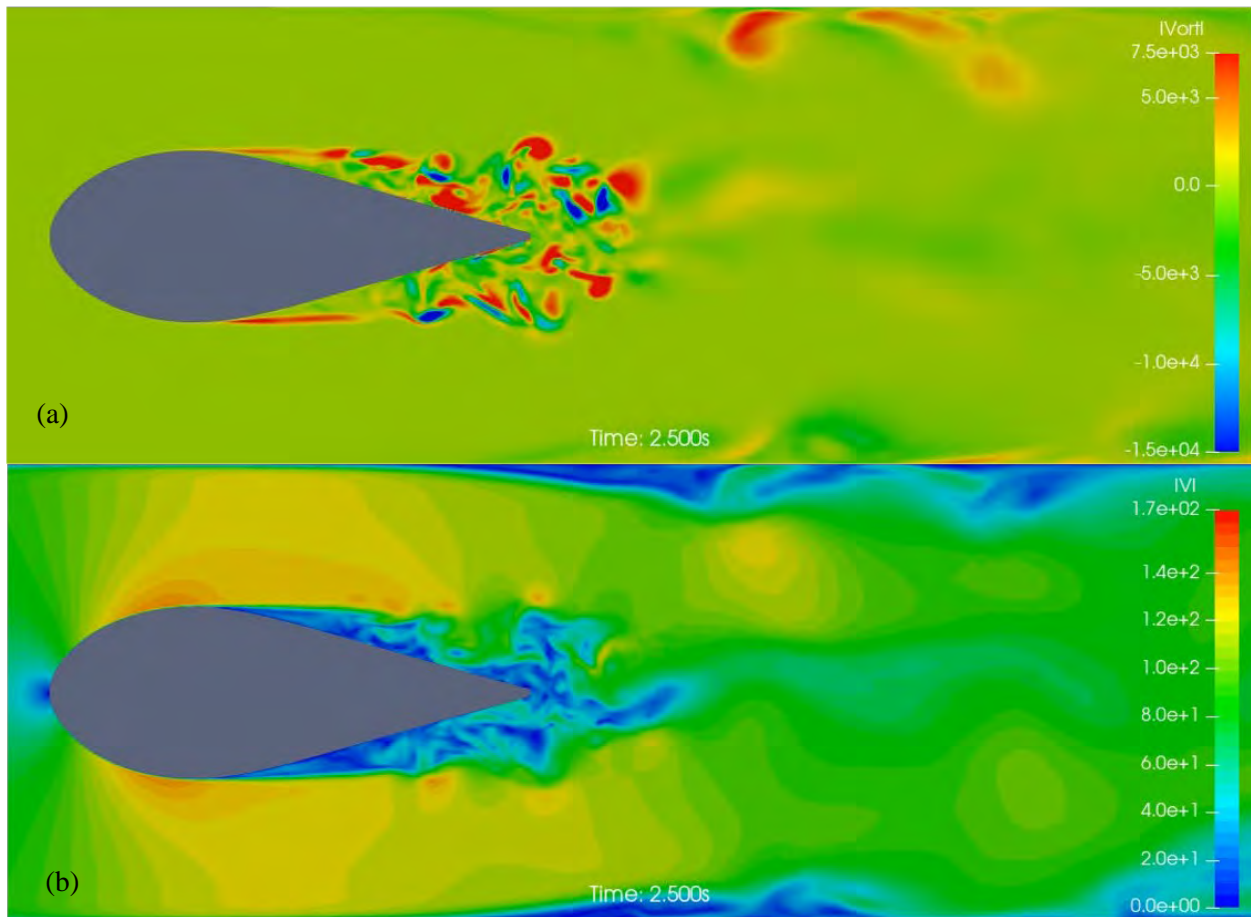


Figure 2. Instantaneous contours of (a) vorticity and (b) magnitude of velocity on the spanwise symmetry plane for the flow past an Eppler airfoil.

Title: Airbreathing Combustion for Hypersonics

Author(s): G.B. Goodwin and C.J. Rising

Affiliation(s): U.S. Naval Research Laboratory, Washington, DC

CTA: CFD

Computer Resources: HPE Cray EX [NAVY, MS]

Research Objectives: The objective of this research is to characterize the effect of freestream turbulence on the flame-vortex interactions within a cavity flameholder. The University of Central Florida's cavity-stabilized combustion facility was simulated in this study using the JENRE[®] multiphysics framework.

Methodology: One of the predominant challenges in using air-breathing engines for hypersonic flight is that the extremely fast flow speeds through the engine present a challenging environment for reliable ignition of the fuel and stable combustion. The methodology for this research is to use high-fidelity computational fluid dynamics (CFD) to simulate the high-speed reactive flow in the combustors of air-breathing hypersonic vehicles. Boundary conditions, fuel chemistry and equivalence ratio, combustor geometry, and turbulence levels are varied to catalog the effect of these phenomena on achieving stable ignition and complete combustion. For the results described in this report, a subsonic cavity combustor with an inflow velocity of 100 m/s at 300 K and 1 atm was used for the problem setup. A turbulent inflow boundary condition was used to apply a freestream turbulence intensity of 10%. The gas composition was premixed ethylene and air at a stoichiometric fuel-equivalence ratio. These computations solved the fully conservative formulation of the multicomponent, chemically reacting Navier Stokes equations. Combustion is modeled using a global three-step, seven-species ethylene-air combustion mechanism.

Results: Figure 1 shows a snapshot of the cavity-stabilized flame. Figure 1(a and b) show CO mass fraction at two different spanwise locations. The increased brightness in the rear of the cavity shows where the bulk of the combustion reactions are occurring. The flame angle is marked in the figure at these locations; the near-constant value between the locations indicates that the flame, as simulated in this particular computational geometry, is predominantly two-dimensional in the near-cavity region. Figure 1(c) shows a three-dimensional view of the flame surface, as visualized by temperature isosurfaces colored by spanwise vorticity. Here, it is evident that three-dimensional structure develops in the flame toward the aft end of the cavity and downstream. Through an analysis of the turbulent spectra and flame-vortex interactions, it was determined that the turbulence intensity influenced the structure of the flow field by creating a more dominant primary vortex within the combustor and decreasing the shear layer reattachment length. The flame-vortex interactions also drove a recurring instability in the combustor.

DoD Impact/Significance: The impact of this research is an improved understanding of the fine-scale combustion and flameholding physics in scramjet engines. Using high-fidelity computational fluid dynamics to simulate scramjet combustion is a critical step in the engine research-and-development process. The simulations are run in tandem with accompanying experiments for validation and comparison.

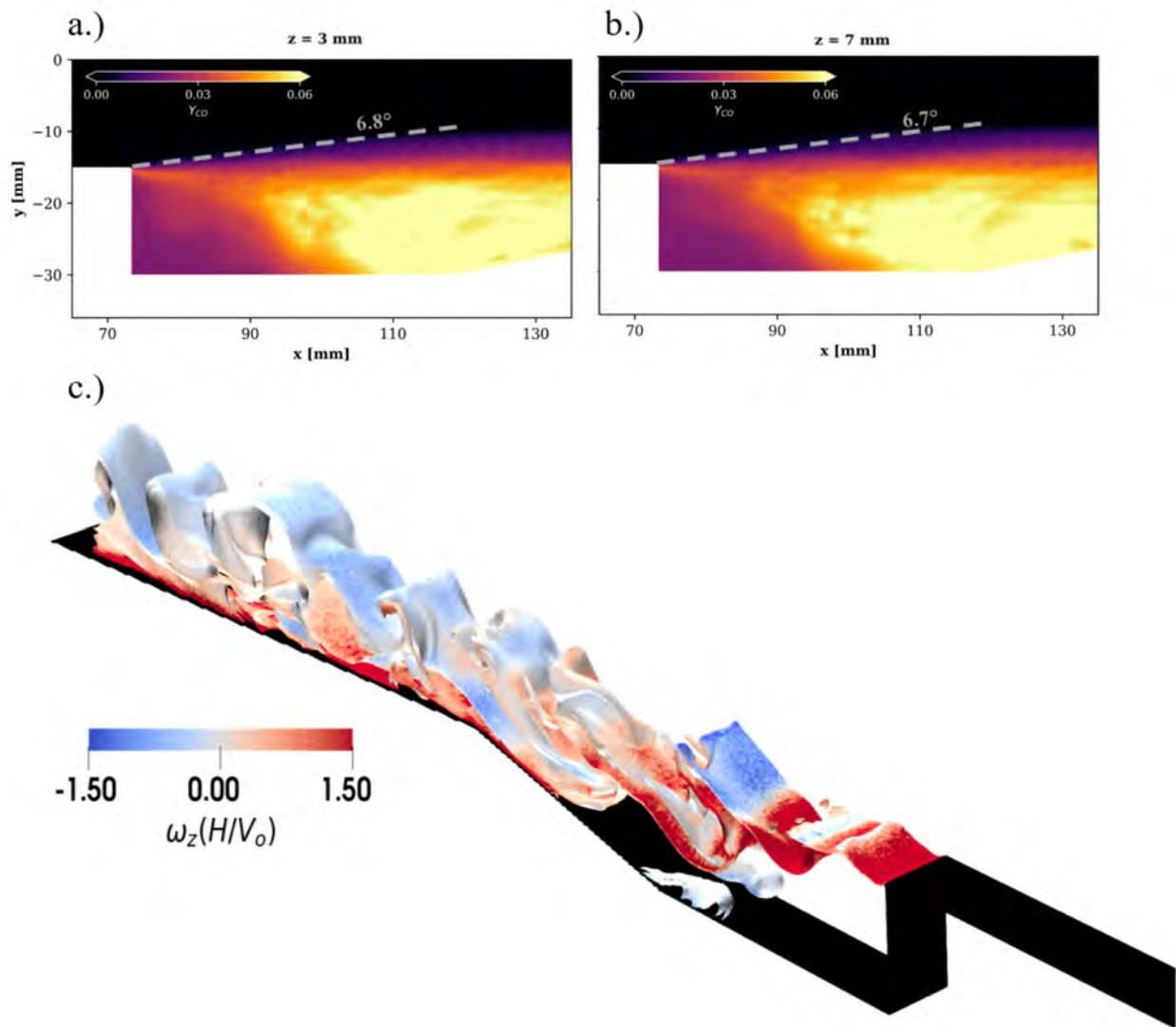


Figure 1. Time averaged CO mass fraction at a) $z = 3$ mm and b) $z = 7$ mm, c) instantaneous isosurfaces of $T = 1500, 1700, 1900$ K colored by normalized spanwise vorticity ($w_z(H/V_o)$).

Title: Predicting Fluid-Structure Interaction for Military Applications

Author(s): D.R. Mott, and Y. Khine

Affiliation(s): U.S. Naval Research Laboratory, Washington, DC

CTA: CFD

Computer Resources: SGI ICE X [ARL, MD]

Research Objectives: Create the computational capability to predict the interaction of fluids with complex structures, and apply these capabilities to solve emerging problems critical to DON and the broader defense community. In FY23, simulations that represent testing transparent armor in environmental chambers are performed for better understanding of the material's response to extreme conditions.

Methodology: In FY23, simulations of transparent armor in extreme temperatures and relative humidity in environmental chambers were performed for single-block and multiple-block cases. Both two-dimensional (2D) and three-dimensional (3D) models were studied using various heating and cooling conditions. Different materials are also considered in the simulations to understand the effects of material properties, such as density, thermal conductivity, and specific heat. Capstone software developed at NRL DC under the Computational Research and Engineering Acquisition Tools and Environments (CREATE) program of the High Performance Computing Modernization Program (HPCMP) is used to generate the geometries and meshes for the simulations. CFD++ Software by Metacomp Technologies, Inc. that is available on DoD HPC resources is used to simulate various scenarios of interest. The simulated results were compared with the measurements performed in the environmental chambers.

Results: In the baseline case presented here with five blocks in the chamber, the inlet is at the top of the back wall with an incoming air for a cooling case with air temperature fixed 20°C and typical flow rate and relative humidity. Air exits at the second slit from the bottom of the chamber. The simulated results at 1500 seconds (25 minutes) from the beginning of the cooling process are presented in Fig. 1. Figure 1(a) presents the slices of temperature variations at midplane and near the front and back walls of the chamber. We can see the air temperature near the back wall close to the incoming air temperature at 20°C , while the air near the front wall has higher temperature. The midplane shows the interaction between the cool air and the blocks at higher temperature, including the temperature variation inside the blocks. Figure 1(b) presents the detail cross section of the blocks in the midplane of the chamber, which is the same as the midplane slice in Fig. 1(a). The air temperature variations within the chamber and between the blocks and the cooling of the blocks can be seen in this figure, especially near the outer surfaces of the blocks. Figure 1(c) presents the isosurface at 296K ($\sim 22.9^{\circ}\text{C}$) in blue in the chamber with streamlines describing the air flow pattern. We can see the air coming out of the top slit of the back wall, traveling over the blocks, some hitting the blocks or going in between the blocks, while some air recirculates before exiting at the lower slit of the back wall. Figure 1(d) presents the slices of velocity in the z-direction where the incoming air is in the +z-direction. We can see the red region near the back wall of the chamber where the incoming air is at fixed velocity, and the air slows down as it travels among the blocks inside the chamber. The z-component velocity is very small near the blocks and at the front wall as expected. The z-velocity is negative near the exit as air is traveling in -z-direction. As air flows among the blocks, the high and low regions of z-component velocity in blue and green are observed near the back wall especially near the exit. The x-component and y-component velocities are very small compared to the z-component velocity in the chamber.

DoD Impact/Significance: Testing materials under various scenarios is very important before requisition for specific military applications in order to avoid material disfunction or failure at extreme conditions. A design approach that accurately emphasizes the relative importance of a variety of design factors and threats, and that can be weighted differently for different scenarios, can produce optimal configuration options for targeted operations.

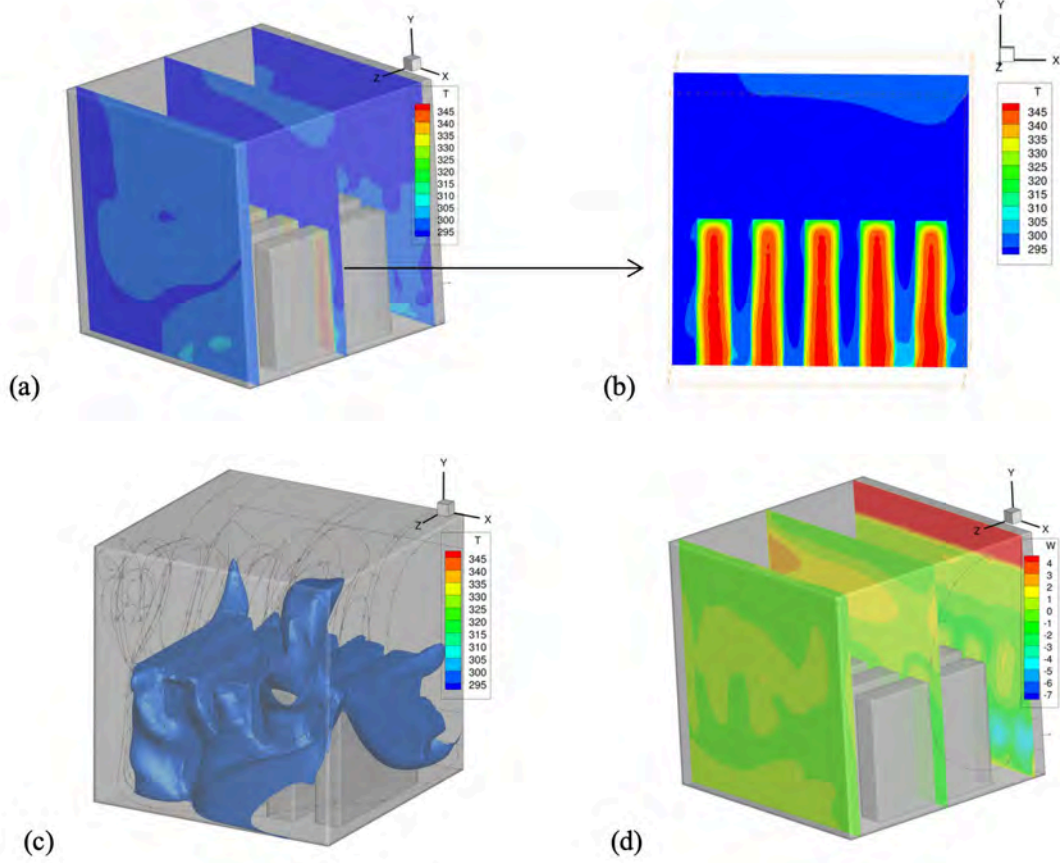


Figure 1. (a) Temperature variations in air and blocks at the midplane, near front, and near back walls of the chamber in the z-direction, (b) temperature variations in air and blocks at the midplane in the z-direction, (c) isosurface of 296K in blue with streamlines describing the air flow inside the chamber, and (d) z-component velocity at midplane and near the front and back walls of the chamber.

Title: Multidimensional Chemically Reacting Fluid Dynamics with Application to Flameless Combustors

Author(s): R.F. Johnson

Affiliation(s): U.S. Naval Research Laboratory, Washington, DC

CTA: CFD

Computer Resources: HPE SGI 8600 [AFRL, OH]

Research Objectives: Conduct computationally intensive simulations of chemically reacting fluid dynamics in diverse multidimensional configurations using HPC resources. The primary goal is to enhance our comprehension of complex, multiscale combustion phenomena.

Methodology: The Laboratories for Computational Physics and Fluid Dynamics employ codes capable of predicting precise flow fields in various configurations. These codes utilize high-order methods that are effective in simulating unsteady flows with strong shocks, chemical reactions, and other intricate features. This work focuses on ongoing developments that facilitate the simulation of high- and low-speed chemically reacting flows using cutting-edge numerical methods. This year, we achieved significant results demonstrating the effectiveness of our methods in simulating chemically reacting flows.

Results: We refined our previously developed methodology, enabling the resolution of multicomponent chemically reacting flows without traditional stabilization methods. Past attempts to simulate the mixing of species like hydrogen and oxygen required costly stabilization methods. Our new simulation method combines the discontinuous Galerkin method (DG) with accurate thermodynamics, allowing us to address propulsion problems with detailed thermodynamics, transport, and chemical kinetics without stability issues. Our goal was not only to increase stability, but also to produce results for larger-scale propulsion demonstration cases.

The DG method's key advantage lies in its ability to resolve structures with high-order accuracy without mesh refinement. Although challenges were encountered in shock capturing, requiring some stabilization near discontinuities, we improved entropy-preserving limiters to prevent oscillations at high order. Three-dimensional results of a chemically reacting hydrogen jet in supersonic cross were successfully generated this year, illustrating our methods work in near-wall applications. These simulations used HPCMP resources, and our methodology with high-order tetrahedral solver provided by the JENRE[®] multiphysics framework. An example of one of our many simulations is shown in Fig. 1, highlighting our codes ability to simulate multidimensional chemically reacting flow features by predicting the complex physics of a hydrogen jet mixing in supersonic air.

DoD Impact/Significance: Advancing numerical techniques for simulating propulsion devices contributes to a greater understanding and improved prediction of Navy/DoD aircraft performance. This year's work specifically showed impressive capabilities of simulating multicomponent chemically reacting flow on fully unstructured grids.

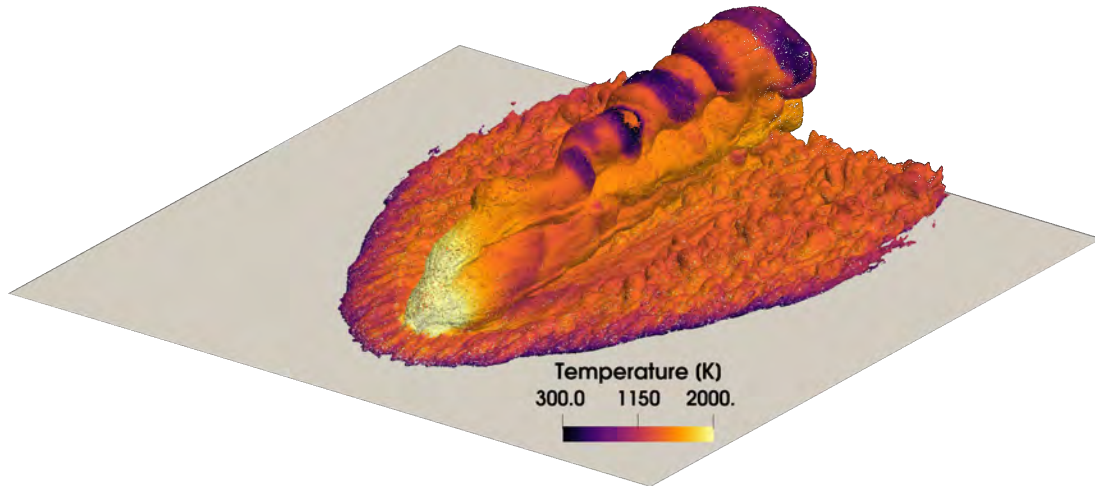


Figure 1. $Y = \text{H}_2\text{O}$ isosurface for JISCF simulation. Hydrogen is injected into supersonic air. The case host three-dimensional chemical reaction zones as well as fine-scale turbulent physics.

Title: Numerical Simulations of Turbulence Impact on Optical Signal Transmission and Near-Surface Turbulence

Author(s): S. Matt

Affiliation(s): U.S. Naval Research Laboratory, Stennis Space Center, MS

CTA: CFD

Computer Resources: HPE SGI 8600 [NAVY, MS]; SGI ICE X, Liquid [ARL, MD]

Research Objectives: The objective is to provide companion numerical experiments to laboratory experiments at various facilities. These laboratories include the large SURge-STRUCTure-Atmosphere INTERaction (SUSTAIN) facility at the University of Miami, the Simulated Turbulence and Turbidity Environment (SiTTE) laboratory at NRL Stennis, and the laminar-to-turbulent-flow channel flow SiTTE (NRLSSC). This work supported base programs to study the dynamics of near-surface turbulence and air-sea interaction processes to improve air-sea flux parameterizations, as well as work on boundary-layer dynamics and drag reduction, the development of new underwater communications approaches based on orbital angular momentum (OAM), and novel fiber-sensor technologies to measure temperature in the ocean.

Methodology: To accurately reproduce the turbulence dynamics, the representation of the numerical tanks is accomplished using large-eddy simulation (LES) and the full physical domain size of the respective tanks. The numerical experiments build on our previous work with OpenFOAM. We expanded our simulations using a compressible multiphase solver with added energy equation to include the effect of heat flux in the wind-wave simulations.

Results: The OpenFOAM code was successfully ported from Centennial to Jean and was updated to the newest available stable version. Code changes required reconfiguring the simulations to reach convergence. Adding heat flux forcing to the more basic wind-wave simulations required extensive tests in the air-water simulations. We used the legacy solver on Centennial to perform simulations of multiphase flow to study air-sea fluxes over waves under varying heat flux conditions. The multiphase model with a volume-of-fluid (VOF) approach to interface tracking is designed to emulate a comprehensive set of laboratory wind-wave experiments at the large SUSTAIN laboratory facility (Fig. 1). Instabilities in the closed model domain emulating the tank pose challenges to model convergence, and a second set of numerical experiments was performed with an open outflow boundary to assess interface dynamics at steady state (Fig. 2). The model allows calculation of turbulent parameters and air-sea momentum flux across the interface with the goal of reproducing phase-dependent dynamics to determine the relationship between near-surface turbulent kinetic energy and wind speed depending on wave and heat flux conditions.

DoD Impact/Significance: CFD simulations of numerical tank environments are critical for the success of research on air-sea interface dynamics to develop physics-based parameterizations for the next generation of coupled models, as well as the continued work on optical communications based on OAM, methodologies for boundary-layer control and drag reduction, and the development of new fiber-optics sensing technologies for oceanographic applications.

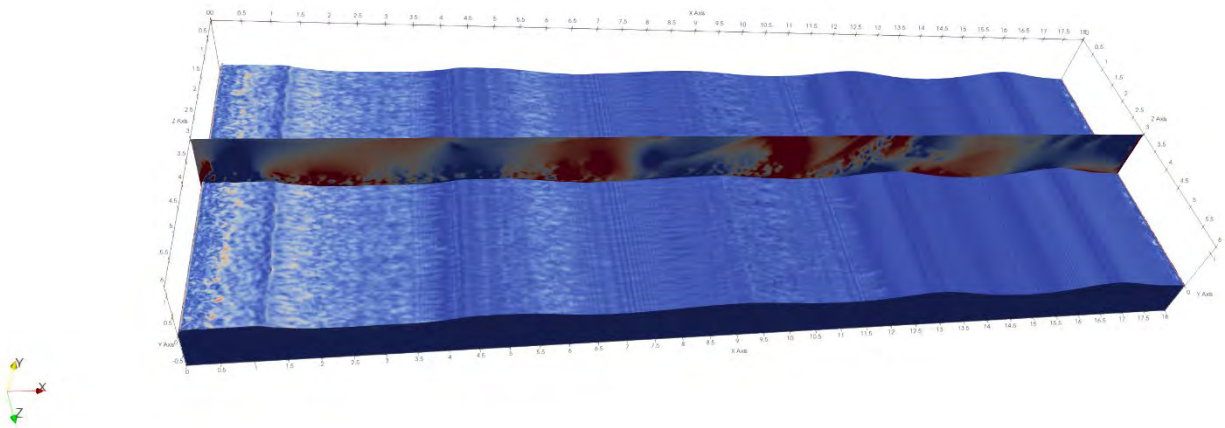


Figure 1. Numerical wind-wave tank in multiphase VOF model in a closed domain emulating the SUSTAIN laboratory. The domain simulates the full size of the lab tank: $x = 18$ m, $y = 2$ m, $z = 6$ m. Here, the water depth (y -direction) is 0.8 m. Vorticity magnitude (s^{-1}) is shown at the water surface at model time $t = 13$ s for simulation with mechanical waves and wind (with speed $U_w = 1.8$ m/s). Cross section shows vertical velocity (m/s). Noise related to model and turbulence implementation is apparent near the air-sea interface.

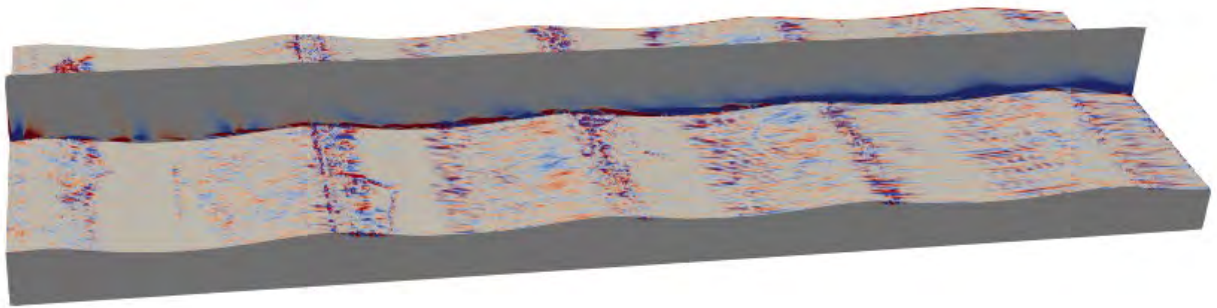


Figure 2. Numerical wind-wave tank in multiphase VOF model in an open domain with mechanical waves, wind ($U_w = 1.8$ m/s), and mean current ($U_c = 2.3$ m/s). Vertical component of vorticity (s^{-1}) is shown (isovolume water and cross section) at model time $t = 195$ s and illustrates the near-surface streaks. Axes as in Fig 1.

Title: High-Fidelity CFD Simulations of High-Speed Flows in Realistic Atmospheric Conditions
Author(s): D.A. Kessler, T.K. Patel, R.F. Johnson, A.M. Hess and B.T. Bojko
Affiliation(s): U.S. Naval Research Laboratory, Washington, DC
CTA: CFD

Computer Resources: HPE Cray EX [AFRL, OH], [NAVY, MS]

Research Objectives: 1) Characterize the optical distortions generated by turbulent supersonic and hypersonic boundary and shear layers. 2) Develop an improved physical understanding of how the aerodynamic performance of hypersonic vehicles changes when encountering multiphase flow environments.

Methodology: We are using the JENRE[®] multiphysics framework to perform high-fidelity and high-resolution simulations of the chemically reacting flows associated with high-Mach-number supersonic and hypersonic flight.

Results: Highly compressible turbulent structures severely distort the propagation of optical signals through the atmosphere. These so-called aero-optical distortions decrease the accuracy of the optical systems used by high-speed weapon platforms for target recognition, course correction, and communication. Density fluctuations in turbulent shear and boundary layers locally alter the effective index of refraction of the atmosphere, causing boresight errors that are characterized by an apparent “shift” in the location of the target. The net effect of these high-frequency aero-optical distortions on optical signal strength and possible boresight errors is not well understood, and fundamental research is required to understand the connection between the formation of the underlying turbulent structures and the development of optical wave aberrations.

During FY23, our team has performed a series of high-resolution large-eddy simulations with the goal of accurately describing the turbulent flow generated by a supersonic shear layer over a recessed optical cavity. The general configuration is shown in Fig. 1, in which a supersonic air stream flows left to right over a sharp wedge. We are concerned primarily with the propagation of optical wavefronts through this flow environment that can be captured on the imaging plane labeled in the figure. The simulations are run long enough for the flow to become statistically stationary. Figures 1a and 1b show instantaneous snapshots for the density and temperature fields obtained for a representative flow condition: Mach 2 flow at nearly atmospheric conditions (free stream pressure and temperatures set to 101.325 kPa and 300 K, respectively). The leading shock from the wedge gives rise to a transonic flow condition over the optical cavity. Various weak shocks emanate from the tip of the cavity that cause the formation of a turbulent shear layer. The net result is a highly variable density field that causes severe distortions of the local index of refraction. Such distortions can be characterized by the optical path difference (OPD), which measures the deviation in the integrated index of refraction field along the path of a light ray from its mean value along that path. Figure 1c gives the instantaneous OPD for the sample density field provided in Fig. 1a. An undistorted wavefront would appear as a horizontal line with OPD of zero. In this example, substantial deviations are evident, with OPD values varying between ± 0.5 across the imaging plane. For reference, the index of refraction of air at standard atmospheric conditions is equal to 1. By mapping these optical distortions to the flow fields that generate them, we can provide methods for performing real-time wavefront correction.

DoD Impact/Significance: Achieving a global prompt-strike capability and countermeasures for similar technologies under development by our adversaries are critical for protecting our fleet and maintaining naval superiority. This work will provide an understanding of how to correct for aero-optical disturbances generated by such systems to improve imaging and seeking capabilities.

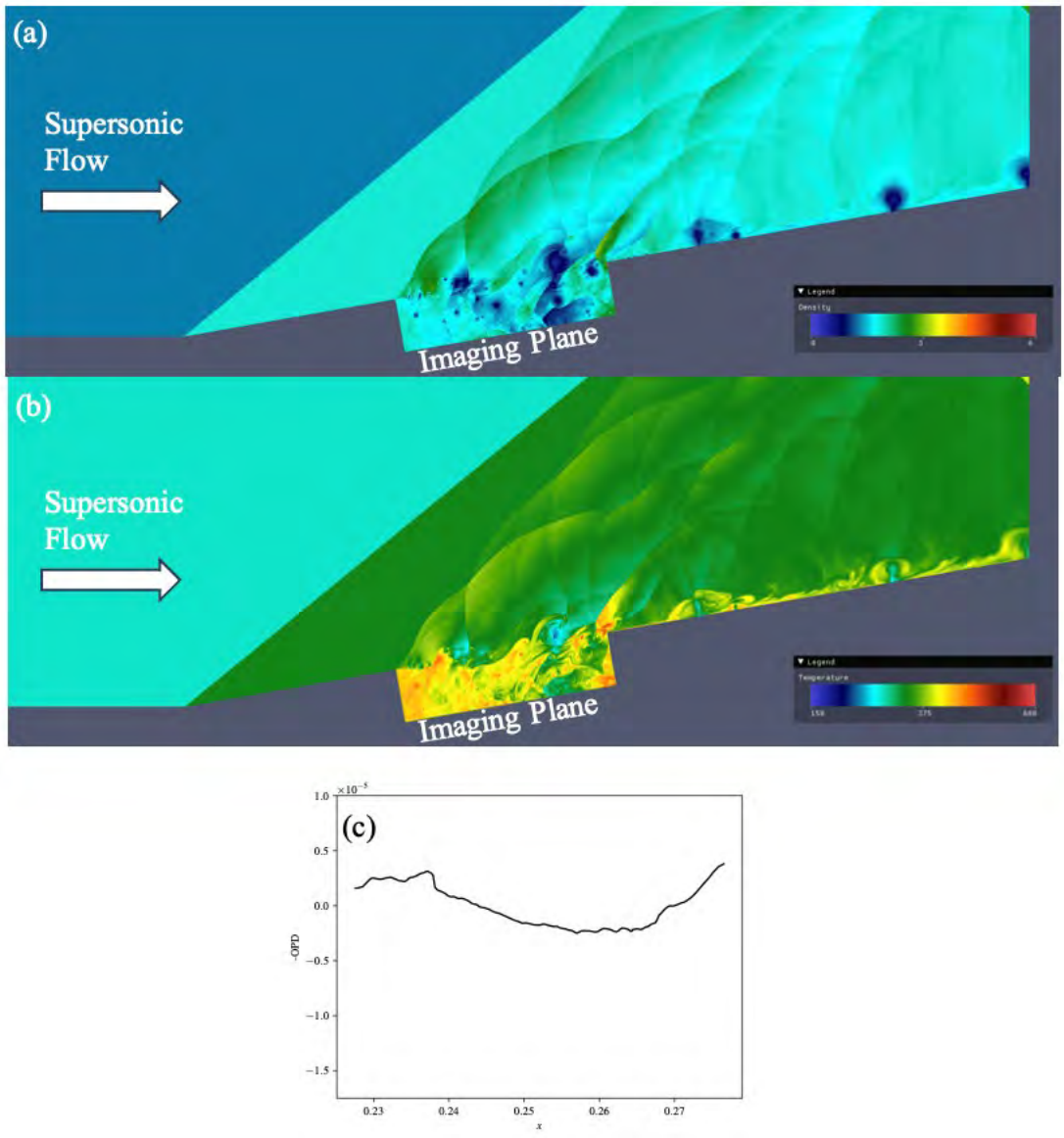


Figure 1. Instantaneous (a) density and (b) temperature contours extracted from a calculation of the supersonic flow over an optical cavity showing the strong local variations in density that create optical distortions over the imaging plane depicted by the optical path difference shown in (c). An undistorted wavefront would appear as a horizontal line with an OPD of zero.

Title: Modeling of Detonations in Jet Fuel Sprays

Author(s): V.N. Gamezo¹ and A.Y. Poludnenko²

Affiliation(s): ¹U.S. Naval Research Laboratory, Washington, DC; ²University of Connecticut, Storrs, CT

CTA: CFD

Computer Resources: HPE Cray EX [AFRL, OH]; [NAVY, MS]; Cray XC40/50 [ERDC, MS]

Research Objectives: High-fidelity numerical modeling of detonations in liquid sprays of hydrocarbon jet fuels is crucial for the design of advanced energy conversion and propulsion systems of direct DoD and Navy relevance. These include novel detonation-based systems, such as rotating detonation engines (RDEs), as well as safe storage and handling of liquid fuels both aboard and ashore. The focus of this effort is on the development of high-fidelity large-scale models in the Eulerian-Lagrangian framework, which fully resolves all dynamically relevant fluid scales while modeling droplets as Lagrangian point particles. To date, study of spray detonations via Eulerian-Lagrangian formulation remains the most widely used method. At the same time, the validity and fidelity of the current state-of-the-art multiphase models employed in such an approach remains unclear. Extreme thermodynamic and hydrodynamic conditions encountered by a spray in a detonation severely limit the accuracy of the underlying spray submodels, which are primarily designed for low-speed flows, and thus the question of such accuracy requires a thorough investigation.

Methodology: In FY23, we extended the work that was started in FY22. In particular, we extended a series of two-dimensional (2D) calculations by initiating work on the first-ever three-dimensional (3D) high-fidelity simulations of liquid n-dodecane spray detonations using an Eulerian-Lagrangian approach with complex chemistry, detailed multispecies transport, and state-of-the-art spray submodels. The physical model represents a coupled gas-particle system that is solved via a Eulerian-Lagrangian approach, in which the gas phase is simulated on a Eulerian grid while the liquid phase is treated as Lagrangian point particles. Simulations are performed on a uniform grid using a fully compressible, reactive flow solver *Athena-RFX*. The particle-gas interaction includes quasisteady drag and forced convective heat transfer, droplet evaporation, and droplet atomization. Liquid spray consists initially of monodisperse 10 μm droplets.

Results: 2D simulations performed by us in FY22 did not include secondary atomization, which is an inherently 3D process. Therefore, in order to develop a more realistic multiphase detonation model, we performed a set of 3D calculations. Given significant uncertainties in the existing atomization models, we considered two models that would result in very fast and also relatively slow atomization processes. The left and right panels of Fig. 1 show significant differences in terms of the thermodynamic conditions experienced by the droplets both between the two 3D calculations as well as between the 3D and 2D (middle panel) cases. In particular, in 3D, droplets undergo atomization and evaporation at high pressures well above the critical pressure. Furthermore, in the case of slow atomization, evaporation occurs virtually exclusively at near- and transcritical conditions, which highlights the essential need to extend the evaporation model to such more extreme regimes. We note that such conditions result in the production of extremely small (submicron) droplets at very high pressures. This results in extremely fast evaporation rates, which in turn, can lead to numerical instabilities.

DoD Impact/Significance: Numerical models of the liquid-fuel detonations obtained in this work represent the state-of-the-art in the field. They constitute a key step toward the development of the realistic 3D models of spray detonations, which do not exist yet and are the focus of the ongoing work in FY24. Such models will provide understanding of the physics of liquid-fuel detonations, which is crucial for the development of advanced propulsion systems by the U.S. Navy. Work carried out in this project is tightly connected with the ongoing efforts at the U.S. Naval Research Laboratory under the 6.1 base program, and more broadly at the Office of Naval Research under the MURI program and at other DoD agencies, such as AFOSR, to study detonations in liquid jet fuel sprays.

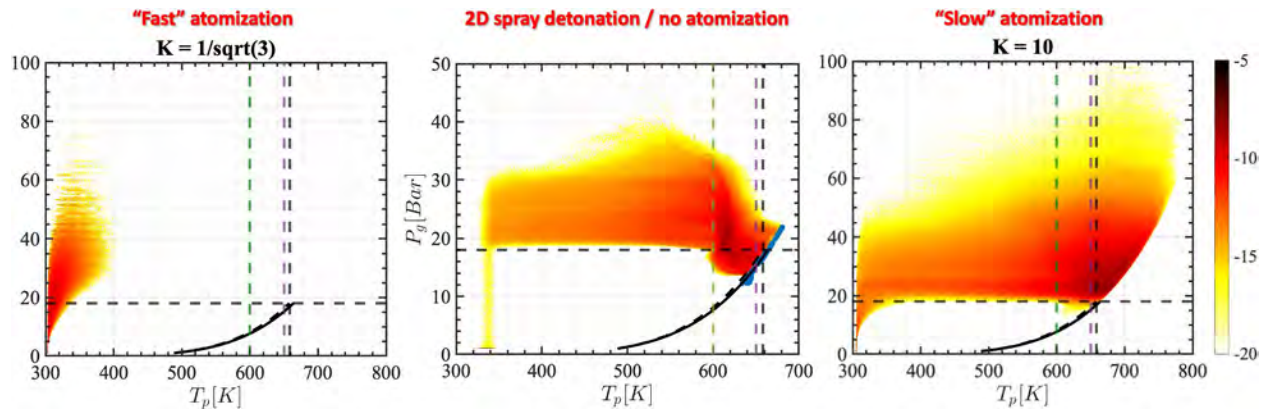


Figure 1. Comparison of the thermodynamic state space in a 2D spray detonation (middle panel) and 3D spray detonations with fast atomization (left panel) and slow atomization (right panel). Shown are the joint probability density functions of the droplet pressure (vertical axis) and temperature (horizontal axis). Solid, black line shows the boiling curve. Horizontal and vertical black, dashed lines mark the critical pressure and temperature, respectively, of n-dodecane. Vertical green and purple lines mark the temperatures at which surface tension of n-dodecane is 10% and 1%, respectively, of that at 300 K.

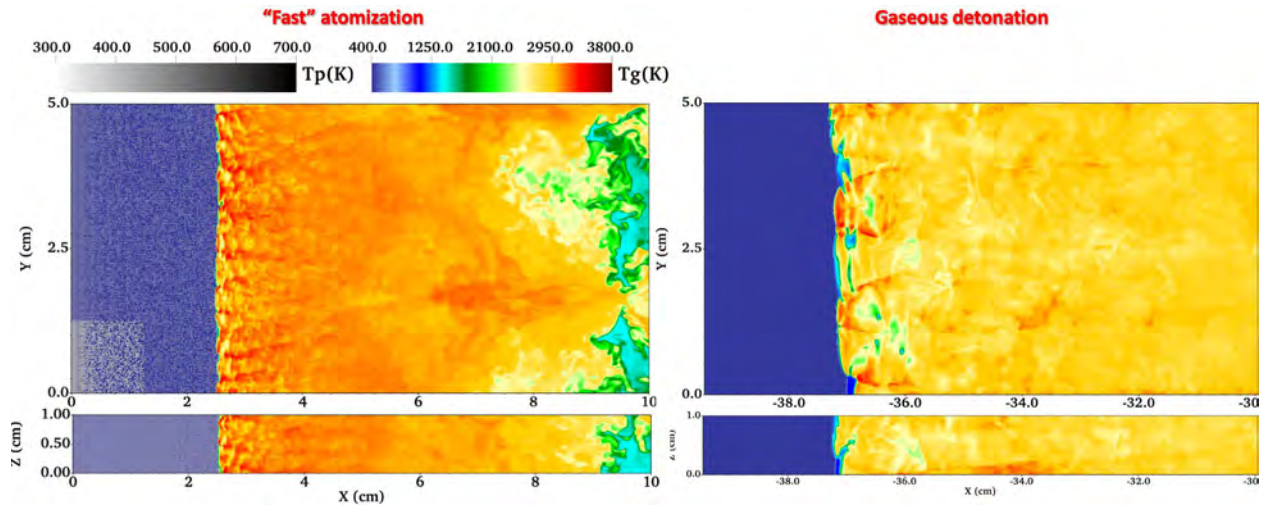


Figure 2. Comparison of the structure of the spray detonation (left panels) and gaseous detonation (right panels) in a rectangular 3D channel. Shown are the temperature fields of the gas phase, T_g (color), and spray droplets, T_p (grayscale, left panels), in the two orthogonal midplane cuts of the computational domain. Spray detonation is shown for the case of “fast” atomization model (cf. left panel in Fig. 1).

Title: Numerical Investigation of Advanced Military Aircraft Noise Reduction Concepts

Author(s): J. Liu

Affiliation(s): U.S. Naval Research Laboratory, Washington, DC

CTA: CFD

Computer Resources: HPE Cray EX [AFRL, OH], [NAVY, MS]; Cray XC40/50 [ERDC, MS]

Research Objectives: Use HPC computational resources to predict details of turbulent flow structures and noise generation in supersonic exhaust jets from representative military aircraft jet engine nozzles and use this information to investigate and assess promising jet noise-reduction concepts in support of the ongoing jet noise-reduction programs.

Methodology: The flow solver is an extended version of the JENRE[®] multiphysics framework. The JENRE[®] multiphysics framework can take structured meshes and unstructured meshes with arbitrary cell types and has multiple levels of parallelism: multicore CPUs or multicore GPUs, and MPI for inter-processor communication. The JENRE[®] multiphysics framework has achieved an exceptional computational performance and scalability. Since using large-eddy simulations (LES) to fully resolve wall-bounded flows at high Reynolds numbers is computationally prohibitive due to the limitations of the available numerical methods and computational resources, the wall-model method is implemented in this extended version to simulate the boundary-layer effect of the wall-bounded flows. The far-field noise prediction is based on the Ffowcs Williams-Hawkings (FW-H) surface integral method. To simulate the high-temperature effect observed in realistic jet engine exhausts, a temperature-dependent function of the specific heat ratio is used.

Results: LES has become an important tool in developing and optimizing the jet noise reduction technologies. In the last year, the noise reduction method of using lower jet Mach numbers has been numerically assessed in mode-scale supersonic jet engine nozzles. Noise reductions have been observed. In addition, some experiments showed that noise reduction can be observed if an exhaust jet presents an inverted velocity profile. In realistic jet engine operations, the combination of using lower jet Mach numbers and inverted velocity profiles can be arranged without compromising the thrust and the mass flow. However, full-scale tests are costly and can be susceptible to structure and design problems. In addition, the jet velocities and temperatures tested in experiments are much lower than those observed in full-scale applications. Thus, it is appropriate to use LES to assess those noise-reduction concepts at comparable jet velocities and temperatures. Figure 1 shows the velocity distributions of the baseline jet and the jet that has a lower jet Mach number and an inverted velocity profile. Figure 2 presents the pressure wave propagations of both jets. It is clear that the jet that has a lower jet Mach number and an inverted velocity profile presents lower pressure intensities in the near-field wave-propagation region. Figure 3 presents far-field noise-intensity distributions. The jet that has a lower jet Mach number and an inverted velocity profile presents more than 3 dB noise reduction in the peak radiation direction. The noise reduction in the upstream direction is up to 5 dB.

DoD Impact/Significance: There is a growing need to significantly reduce the noise generated by high-performance, supersonic military aircraft. The noise generated during takeoffs and landings on aircraft carriers has direct impact on shipboard health and safety issues. It is estimated that the U.S. Veterans Administration pays \$4.2 billion or more for hearing-disability claims each year. The results of our work will provide better understanding of noise production for both industrial and military aircraft and will aid the current effort of noise reduction, especially for supersonic aircraft.

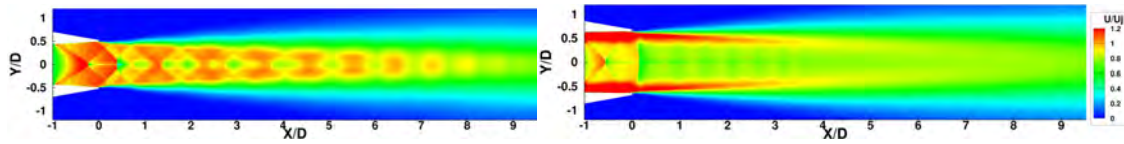


Figure 1. Axial velocity distributions of the baseline jet (left) and the jet that has an inverted velocity profile (right). Both jets have similar thrust and mass flow.

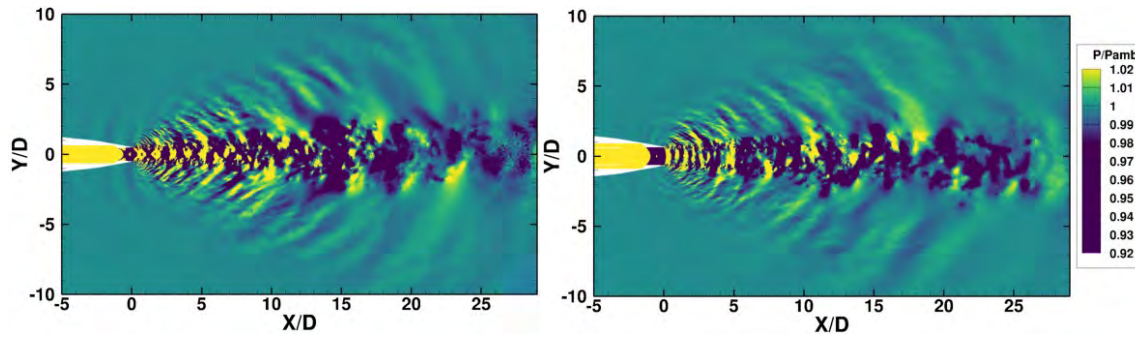


Figure 2. Pressure wave propagations of the baseline jet (left) and the jet that has an inverted velocity profile (right). Both jets have similar thrust and mass flow.

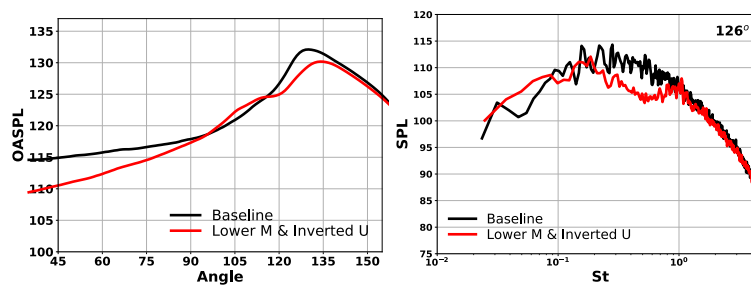


Figure 3. Far-field noise intensity (OASPL) distribution and the sound pressure level at the peak radiation direction.

Title: Detonations with Multi-Phase Flows for Propulsion

Author(s): D.A. Schwer

Affiliation(s): U.S. Naval Research Laboratory, Washington, DC

CTA: CFD

Computer Resources: HPE Cray EX [NAVY, MS]

Research Objectives: The main research goal of the present HPC project is to study high- and low-speed multiphase reacting flows for further understanding of advanced engine concepts, with the specific application for detonation engines.

Methodology: We have used two modeling codes for our research into blast and detonation engine simulations. Simulations are primarily done using the JENRE[®] multiphysics framework. Due to our extensive experience with using the DET3D codes for detonation propulsion, we continue to use them as a benchmark for comparison with the JENRE[®] framework. The framework utilizes unstructured meshes and both continuous- and discontinuous-Galerkin-FEM techniques to solve a wide variety of complex fluid dynamical phenomena. It has been built from the ground up to make efficient use of CUDA, HIP, Thread-Building-Blocks, OpenMP, and MPI through the use of template libraries. By utilizing unstructured meshes, the solver can easily handle complex flow paths from rig assemblies and engine concepts while remaining relatively efficient. Extensive work has gone into improving the JENRE[®] framework for both reacting and multiphase flows during the past several years.

Results: Simulations were conducted for a centerbodyless rotating detonation combustor (RDC) rig from University of Cincinnati. The nonpremixed hollow RDC simulation showed a stable detonation running an ethylene/air mixture with a mass-flow rate of 0.647 kg/s and an equivalence ratio of 1.12. Fuel injection was through discrete axial injectors with a radially inward air slot injection. The injection pattern produced two recirculation zones: a small one near the injectors on the outside wall, and a second recirculation zone farther into the fill region. Three regions of heat release related to the detonation wave were identified: the upper portion of the detonation wave, which was the strongest with heat release extending slightly into the interior of the domain, a corrugated region that hugged the outer wall due to the discrete fuel injection, and a third region near the injectors that lagged behind the other two. The presence of strong heat-release lagging behind the main detonation wave resulted in an additional reflected shock wave running parallel to the oblique shock wave from the top of the detonation, which was consistent with earlier simulations using an ideal injection model. Simulations were also conducted regarding an augmentor concept proposed at the Naval Postgraduate School. This concept proposes separating the core mixture from a fairly standard rotation detonation combustor (RDC) using the inner wall of the RDC. Pilot holes are then cut into the inner wall connecting the RDC to the interior core flow. Penetration of gases through these channels into the core serves as a pilot for the core reactant mixture. Fully coupled simulations initially were run, and then a one-way coupling procedure was developed to enable parametric studies to be accomplished efficiently.

DoD Impact/Significance: The physics involved in RDCs and other detonation engines is substantially different than for gas-turbine engines. Simulations of RDC systems from basic concepts all the way to full propulsion devices are necessary to understand these devices, and they contribute to the design process. The work accomplished this year approaches understanding RDC-piloted augmenters from both ends. More detailed simulations are conducted to investigate the underlying physics, while approximations are made to enable parametric studies of a wide range of conditions and geometries.

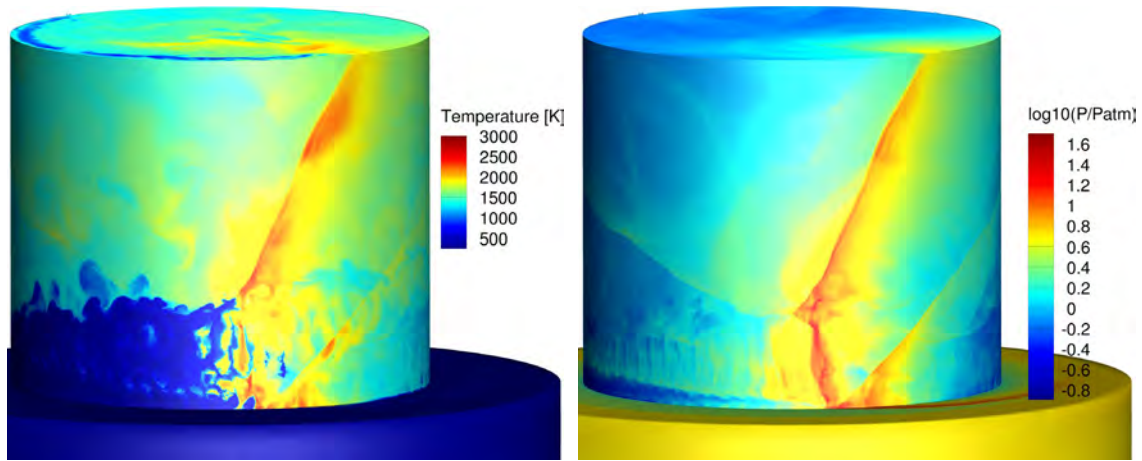


Figure 1. Temperature (left) and \log_{10} (pressure) (right) for the nonpremixed H-RDE simulation based off of a University of Cincinnati rig. $\dot{m} = 0.647$ kg/s, $\phi = 1.16$.

Title: Numerical Simulations of Noise Generated by Non-Circular Advanced Military Aircraft Nozzles

Author(s): K. Viswanath and R. Ramamurti

Affiliation(s): U.S. Naval Research Laboratory, Washington, DC

CTA: CFD

Computer Resources: HPE Cray EX [AFRL, OH], [NAVY, MS]; SGI ICE X [ARL, MD]; Cray XC40/50 [ERDC, MS]

Research Objectives: Use HPC computational resources to predict details of turbulent flow structures and noise generation in supersonic noncircular asymmetric exhaust jets from representative military aircraft jet engine nozzles. This information will be used to investigate and assess promising jet noise-reduction concepts in support of the ongoing testing program.

Methodology: Simulations are performed using the JENRE[®] multiphysics framework, developed by the U.S. Naval Research Laboratory (NRL) with collaborating institutions. This U.S. Government-owned code provides unsteady compressible flow-solver capabilities that support various numerics, as well as cell-centered finite-volume or nodal finite-element methods, while delivering high throughput on calculations. It was developed with an emphasis on raw performance and the ability to exploit emerging massively parallel, high-performance computing (HPC) architectures. It supports different HPC parallel programming paradigms for message passing such as MPI, OpenMP, CUDA, HIP, and hybrid models depending on the HPC cluster architecture. A key bottleneck of HPC throughput is data input-output (IO). The code supports parallel IO via MPI/IO to further complement the multiple levels of parallelism. Taylor-Galerkin finite-element method with second-order spatial accuracy for tetrahedral cells is used with the finite-element flux corrected transport (FEM-FCT) method. The multidimensional FCT flux limiter provides an implicit subgrid stress model, which ensures monotonicity at shocks and sharp gradients with minimal artificial dissipation. We use an extended version of the code that features a wall model that supports high-speed flows and surface roughness effects while significantly reducing grid resolution requirements.

Results: Simulations of a supersonic twin jet at multiple overexpanded operating conditions and nozzle configurations were investigated to understand twin jet interaction and far-field noise behavior. These include canted twin jet configurations as well as multiple separation distances between nozzles. Figure 1 shows an inward-canted, 4-degree cant angle, twin jet nozzle, each of aspect ratio 2, with separation distance of 2.25D (equivalent diameter $D = 0.0076$ m). Results are shown for the nozzle pressure ratio of 3.0 and the temperature ratio of 1.0. Changing the nozzle cant angle and the separation distance informed the impact of twin jet interaction and shielding effects on far-field noise. These simulations analyze potential nozzle configurations where there might be a noise-reduction effect due to the geometrically imposed constraints on jet interaction. Figure 2 (left) shows the difference in far-field noise in the major and minor axis planes. Sideline and upstream of the nozzle, there is approximately a 4dB noise reduction in the major axis plane, with it being consistently lower at all other observer locations. For comparison, Fig. 2 (right) shows the baseline case of a noncanted nozzle, validated with experimental data from the University of Cincinnati (UC), at a higher overexpanded condition of NPR 2.5 that does not show such a difference between the noise profiles in the major and minor axis planes. Figure 3 (top) shows the interaction of the twin jets in the major axis plane and Fig. 3 (bottom) shows the interaction in the symmetry plane, between the jets, in the minor axis. The increased mixing from the inward nozzle cant and the resultant far-field noise change are mainly seen in the minor axis plane results, and this effect can be leveraged for passive noise reduction.

DoD Impact/Significance: The results of our work will provide better understanding of the noise production for both industrial and military aircraft and will aid the current effort of noise reduction, especially for supersonic aircraft, to reduce the impact of the jet noise on shipboard health and safety issues.

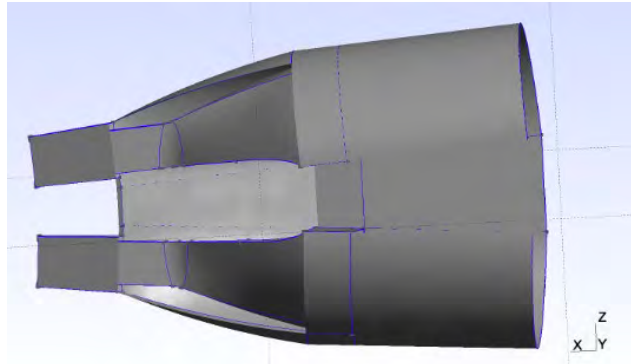


Figure 1. Twin jet nozzle geometry, aspect ratio 2, nozzles with inward cant angle of 4 degrees and separation distance of 2.25D.

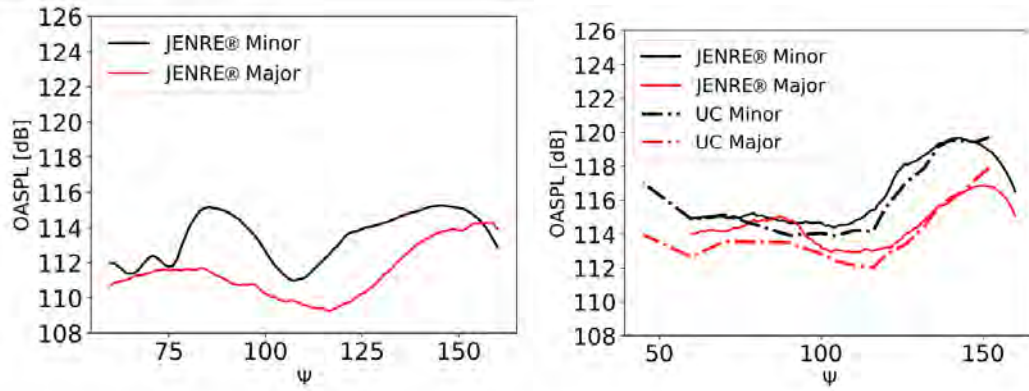


Figure 2. Far-field noise comparison at 100D for the twin jet plume for canted vs. noncanted nozzles. Left shows noise at NPR 3.0 and 4-degree cant and right is at NPR 2.5 with UC data comparison.

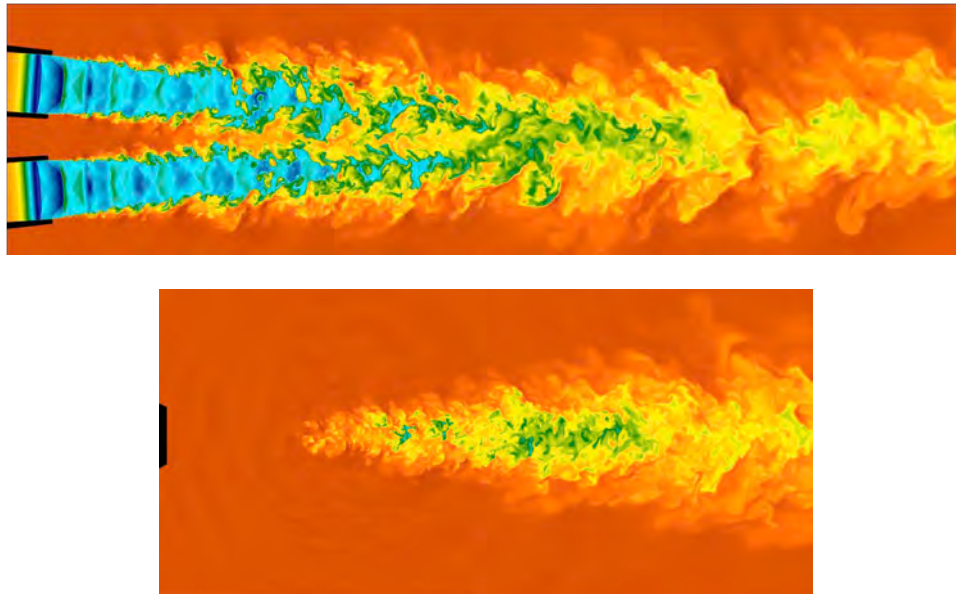


Figure 3. Twin jet interaction for the 2.25D nozzle separation distance case. Top shows the jet interaction in the major axis plane. Bottom shows the interaction in the symmetry plane between the jets.

Title: Direct Numerical Simulation of Fluid-Sediment Wave Bottom Boundary Layer

Author(s): J. Simeonov,¹ I. Adams,² A. Penko,¹ S. Schoenauer,¹ S. Bateman,¹ K. Edwards,¹ R. Phillip,¹ and J. Veeramony¹

Affiliation(s): ¹U. S. Naval Research Laboratory, Stennis Space Center, MS; ²National Research Council Postdoctoral Fellow, Stennis Space Center, MS

CTA: CFD

Computer Resources: HPE SGI 8600, HPE Cray EX [NAVY, MS]; Cray XC40/50 [ERDC, MS]

Research Objectives: Predictive models for nearshore bathymetry and beach topography evolution require a complete understanding of the physics of fluid-sediment interactions in the wave bottom boundary layer (WBBL) and the atmospheric boundary layer. Since such variable three-dimensional (3D) processes are difficult to quantify in situ, we performed coupled fluid-sediment numerical simulations to increase our understanding of the sediment and hydrodynamics in the boundary layer. Fundamental concepts used in describing the phenomena of sediment transport such as particle size and shape, turbulent bottom stress, mixture viscosity and diffusivity, hindered settling, bed failure criterion, and bedforms and their effect of the bottom stress variability are addressed with our models. The models produce high-resolution results necessary to gain insight into the small-scale boundary-layer processes and clarify new directions for measurement techniques needed to improve predictive capabilities.

Methodology: Utilization and development of a suite of discrete and continuum WBBL multiphase models for simulating sediment transport in the nearshore environment from the microscale (cm to m) to the mesoscale (km) is ongoing with HPC resources. At the microscale (<10 cm), the three-dimensional sediment phase is simulated with discrete-element method (DEM) that allows individual grains and their interactions to be uniquely specified. The multiphase models vary in complexity from a simple one-dimensional eddy viscosity with one-way fluid-particle coupling to fully coupled fluid-particle models in three-dimensional direct numerical simulation (DNS). At intermediate scales of tens of meters, we perform OpenFoam CFD numerical simulations of wind flow over real beach topography to determine the connection between bedforms and the distribution of turbulent bed stresses. The topographic surface was measured with lidar and the flow was forced using observations of 10-meter winds. We used the Shear Stress Transport k-omega turbulence model to simulate turbulent kinetic energy and used wall functions in the near bed layers to keep down the cost of resolving the viscous boundary layer.

Results: These simulations produced high-resolution spatially variable estimates (Fig. 1) of wall shear stress τ and bed pressure (not shown) that would allow us to understand the connection between shear velocity and larger scale roughness. The estimated shear velocities will be used to make more accurate predictions of spatially variable sediment transport, and the results will be compared to transport rates from samples collected on site. These results will be used to improve models of aeolian transport to take into account the complex interplay between winds, topographic features, and bed roughness for a more accurate model of changes in beach morphology over time.

DoD Impact/Significance: All process-based models for nearshore bathymetric evolution are limited by shortcomings in fundamental knowledge of the boundary-layer physics. The microscale simulations provide an unprecedented level of detail for the study of fluid-sediment interactions that is impossible to obtain with available measuring technologies in the field or the laboratory. These results are utilized to improve parameterizations of small-scale processes in larger-scale models. At the mesoscale, our models are highly efficient and well suited for coupling to regional operational hydrodynamic models. The computational resources consumed were in direct support of NRL base programs “Observations and modeling of biological cohesion on seafloor evolution time scales,” “Modeling sediment sorting in sand-shell environments,” “Predicting wind driven topographic change in sandy, coastal battlespace environments,” and “Developing a shallow water environmental database for nearshore operations.”

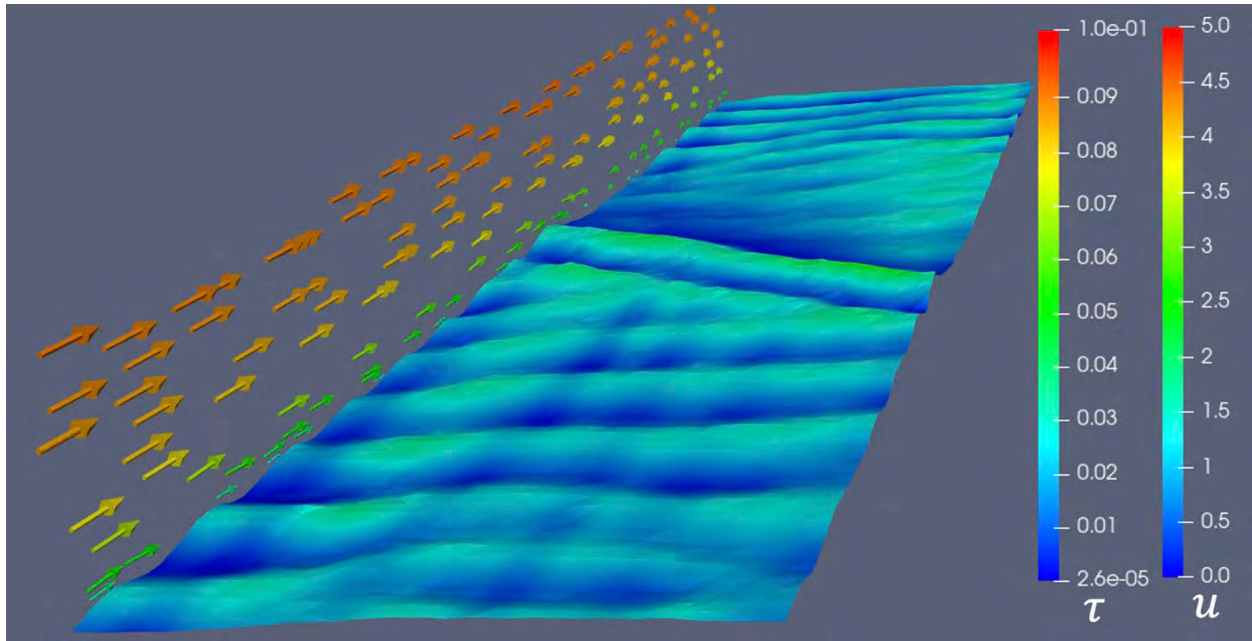


Figure 1. Lidar topographic surface of beach ripples colored by the magnitude of the bottom shear stress τ (in m^2/s^2) normalized by air density. The flow over the rippled bed is illustrated by the quiver plot colored by velocity magnitude μ (in m/s). A steady logarithmic boundary-layer flow is imposed at the inlet corresponding to 10 m velocities of 7 m/s . A small portion of the domain is shown corresponding to a 2-m-long-by-0.5-m-wide section of the beach near the location of the instrument array with sonic anemometers. The full computational domain is 1 m in width, 30 m long, and 5 m tall.

THIS PAGE INTENTIONALLY LEFT BLANK



Computational Biology, Chemistry, and Materials Science

CCM covers computational tools used to predict basic properties of chemicals and materials, including nano- and biomaterials. Properties such as molecular geometries and energies, spectroscopic parameters, intermolecular forces, reaction potential energy surfaces, and mechanical properties are being addressed. Within the DoD, quantum chemistry, molecular dynamics, statistical mechanics, and multiscale methods are used to design new chemical, polymer, nanomolecular, and biomolecular systems for fuel, lubrication, laser protection, explosives, rocket propulsion, catalysis, structural applications, fuel cells, and chemical defense. Solid-state modeling techniques are employed in the development of new high-performance materials for electronics, optical computing, advanced sensors, aircraft engines and structures, semiconductor lasers, advanced rocket engine components, and biomedical applications. Of recent emerging interest in the Computational Biology, Chemistry, and Materials Science (CCM) CTA are methodologies that cover bioinformatics tools, computational biology, and related areas, such as cellular modeling.

Title: Materials for Energy Storage and Generation

Author(s): M. Johannes

Affiliation(s): U.S. Naval Research Laboratory, Washington, DC

CTA: CCM

Computer Resources: HPE SGI 8600 [AFRL, OH]; Liquid [ARL, MD]

Research Objectives: The objectives of this program are to calculate the materials properties with relevance to functionality in materials relevant to energy storage and generation using density functional theory (DFT) and its extensions including molecular dynamics. Materials of particular interest include battery cathode, anode, and electrolyte materials, electrolytes for solid acid fuel cells (SAFCs), and magnetic and superconducting materials.

Methodology: First-principles projector augmented plane-wave (PAW) methods as implemented in the Vienna Ab Initio Software Program (VASP) are employed to solve a self-consistent formulation of the mean-field Schrodinger's equation. A variety of postprocessing analysis and imaging programs are used, primarily developed in house.

Results: In FY23, the project's focus on SAFC electrolytes with superior proton transport at intermediate temperatures continued with an investigation of new so-called "BOB" materials. These are characterized by borate tetrahedra linked at the corners with phosphate tetrahedra that formed the backbone of a structure through which protons can diffuse. The original CsBOB was developed in the Chemistry Department at NRL, and computation from this project identified extrinsic protons as the source of the unusually high ionic conductivity. Further computations identified Rb substitution at the Cs site as a fruitful method of further increasing the conductivity. Additionally, removing protons stimulates a sort of ion "hole" conductivity that may be attainable via Mg^{2+} substitution at intrinsic H sites.

Calculations of the electronic structure of CeO_2 was completed in FY23. Using the Heyd-Scuseria-Ernzerhof (HSE) approximation to the exchange-correlation potential, the full bandgap (O *p* states to Ce *d*-states) was correctly obtained as well as the position of the localized Ce *f* states within this gap. A polaron was created by introducing an electron into these localized states and allowing relaxation of the bonds around it. This was shown to be stable and will be used to calculate the activation energy of photoexcited electrons moving through the system.

Finally, an investigation of an unusual metal-insulator transition in $NaOsO_3$ was undertaken and a heretofore unnoticed change in lattice parameters was uncovered, revealing an electron-lattice coupling that drives the transition.

DoD Impact/Significance: Energy materials are an obvious naval need and our investigation of the SAFC electrolyte has revealed a record-setting conductivity that could enable all-solid-state fuel cells without the necessity for large overpotentials or dangerously high temperatures.

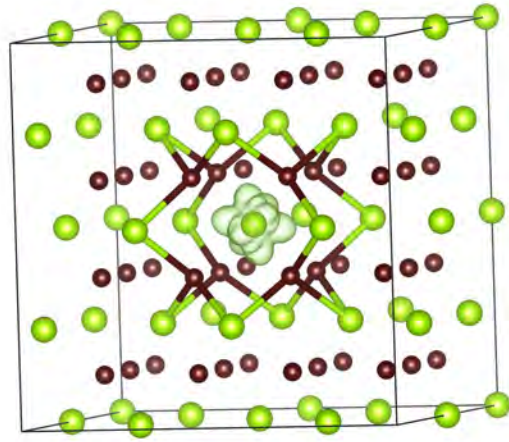


Figure 1. Polaron created at a specific site in CeO_2 imaged along with the lengthened bonds at the second-nearest neighbors of the added electron.

Title: Calculation of Materials Properties Via Density Functional Theory and Its Extensions

Author(s): J.L. Lyons and M.W. Swift

Affiliation(s): U.S. Naval Research Laboratory, Washington, DC

CTA: CCM

Computer Resources: HPE SGI 8600 [AFRL, OH]; Cray XC40/50 [ERDC, MS]; HPE Cray EX [NAVY, MS]

Research Objectives: To determine the electronic structure, as well as the role of defects and dopants, for ultrawide-bandgap semiconductors (UWBGs) such as gallium oxide (Ga_2O_3), and novel materials such as cesium lead bromide (CsPbBr_3), using hybrid density functional theory (DFT).

Methodology: DFT has long been the proven method for deducing semiconductor electronic structure. Although DFT requires no experimental input, when applied to UWBGs, the so-called “bandgap problem” makes difficult the quantitative prediction of defect properties. To overcome this issue, we employ hybrid DFT, which mixes in a fraction of screened Hartree-Fock exchange into the exchange-correlation functional. This approach provides accurate, quantitative prediction of bandgaps and defect transition levels, even for UWBGs. Using hybrid DFT, defect-related charge-state transition levels, formation energies, and optical transitions are calculated. For the lead halide perovskites (e.g., CsPbBr_3), spin-orbit coupling was also required due to the heavy lead atom.

Results: In FY23, we studied Si, Ge, and Sn donors, N acceptors, and native defects in gallium oxide, to compare with experimental studies of high-resistivity, high-mobility Ga_2O_3 that had been implantation-doped with donors. Our calculations indicate that under the expected growth conditions, compensation of incorporated N acceptors should be provided by the implanted donors (as opposed to native defects such as vacancies). This supports the observation that implantation provides a pathway for producing high-quality, selective *n*-type doping of Ga_2O_3 , empowering future gallium-oxide based devices.

We also investigated carbon impurities in gallium nitride (GaN). Infrared absorption (IR) measurements on isotope-enriched, C-doped GaN indicated that complexes containing three carbon species were being unintentionally incorporated during growth. Our hybrid DFT calculations examined what vibrational modes might be produced by such centers and predicted the optical behavior of these complexes. The predicted modes are in excellent agreement with the observed IR modes attributed to the tricarbon complexes, supporting their presence in the material. These results will help optimize heavy C-doping of GaN, which is useful for engineering semi-insulating buffer regions for high-electron-mobility transistors.

Finally, we used DFT to examine trends in acceptor dopants for lead halide perovskites. Though these materials show impressive solar cell efficiencies, optoelectronic applications will require conductivity control via impurity doping. To this end, we examined potential acceptor dopants in a range of halide perovskite materials in order to identify potential trends. Our calculations indicate that sodium is consistently the most promising acceptor dopant, as it incorporates on the correct site to act as a shallow acceptor (see Fig. 1), is free from self-compensation and has a low enough energy not to be compensated by native defect species. Silver is also promising, though is more prone to self-compensation by interstitial donors. These results will help obtain *p*-type perovskites, which are necessary for optoelectronic devices.

DoD Impact/Significance: Along with GaN, UWBGs such as Ga_2O_3 could be utilized in power electronics that play a crucial role in many Navy-relevant applications, and they afford significant SWaP-C when outperforming components based on traditional semiconductor materials. Newer materials such as the halide perovskites are attractive as potentially low-cost, highly efficient energy materials. Controlling electrical conductivity via impurity doping, understanding contaminant species, and characterizing unintentional native defects is crucial for improving such materials and optimizing device designs.

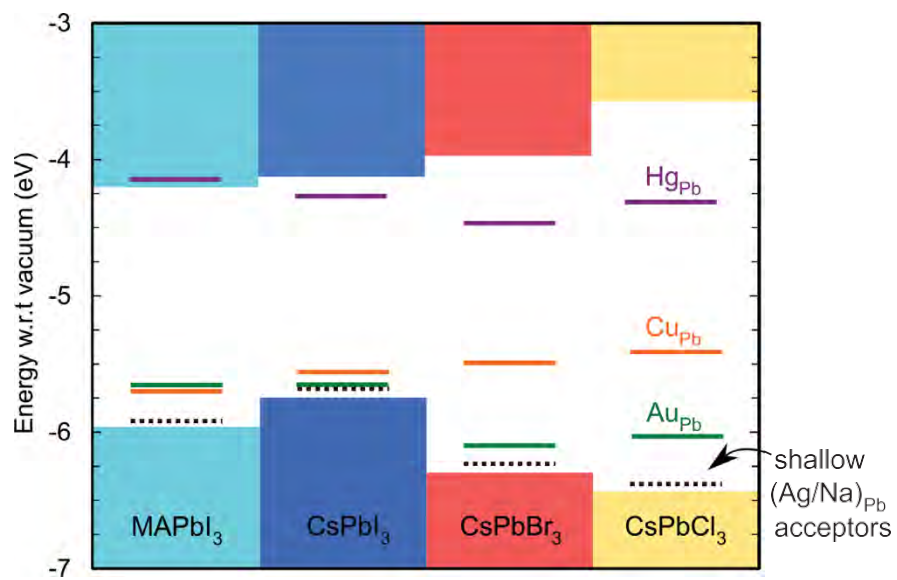


Figure 1. Acceptor dopant levels in the family of halide perovskites.

Title: The Impact of Foam and Aerosol Dynamics on Fire, Explosion Safety, and Suppression (Mechanisms of Water Mist Suppression of a Burning Solid Surface)

Author(s): J.A. Cramer,¹ P.E. Sudol,² and R. Ananth¹

Affiliation(s): ¹U.S. Naval Research Laboratory, Washington DC; ²National Research Council Postdoctoral Research Associate, U.S. Naval Research Laboratory, Washington, DC

CTA: CCM

Computer Resources: HPE SGI 8600 [AFRL, OH]

Research Objectives: To develop machine learning (ML) methods to predict the fire-suppression capabilities of novel nonfluorinated surfactant concepts prior to synthesis, thus both streamlining and otherwise enhancing the development of alternatives to fluorinated fire-suppression materials.

Methodology: In-house firefighting foam performance data collections were collated and reformatted into an expansive database upon which to train future ML models. As a specific application, two ensembles of ten artificial neural networks (ANNs) were trained to correlate area-under-the-curve (AUC) values obtained from 19-cm gasoline pool fire extinction curves to the quantitative molecular descriptors associated with the primary surfactants found in the formulations used to obtain those curves. One ensemble included fluorinated aqueous-film-forming foam (AFFF) fire-suppression agents in its training data, and one was trained only with data obtained from nonfluorinated materials, thus providing parallel validations of all performance predictions. Both ANN model ensembles were used to evaluate proposed surfactant structure concepts to predict their effectiveness in real-world scenarios prior to laboratory synthesis and experimental fire-suppression trials, including the collection of additional 19-cm gasoline pool fire extinction data.

Results: Both of the ANN model ensembles predicted that a novel tetrasiloxane diglycoside surfactant concept would perform better than the two highest-performing non-AFFF surfactants found in the training data, though not as well as reference AFFF materials. The novel surfactant concept might be thought of as a recombination of a head group and a tail group from the two known high-performing materials, a tetrasiloxane sulfobetaine and a trisiloxane diglycoside. However, the high performance of the novel tetrasiloxane diglycoside could not have been taken as a given because a trisiloxane sulfobetaine yielded the second-lowest surfactant performance in the entire original 19-cm gasoline pool fire training data set. It cannot be ignored that the novel tetrasiloxane diglycoside's actual experimental performance (see Fig. 1) did not meet the expectations set forth by the ANN modeling insofar as it performed only as well as the high-performing tetrasiloxane sulfobetaine and trisiloxane diglycoside. However, even the predicted performance would not have been sufficient to meet targeted AFFF formulation performance goals. The fact that the modeling accurately predicted that a presynthesis surfactant concept would yield a high-performing non-AFFF surfactant, and that such a surfactant would not quite perform as well as AFFF, is considered a nontrivial achievement and a successful ML application in the context of fluorine-free firefighting surfactant research and development.

DoD Impact/Significance: Per- and polyfluoroalkyl substances (PFAS) in AFFF firefighting materials pose environmental and health problems. PFAS must be replaced per the National Defense Authorization Act (NDAA, passed by U.S. Congress in 2020). However, while fluorine-free foams can be much more environmentally friendly, these materials do not normally meet the exacting fire-suppression requirements set forth in MIL-PRF-24385F. Research into producing a robust pool of suitable fluorine-free surfactants is ongoing, but trial-and-error empirical development approaches are both inefficient and dependent upon pre-existing expert knowledge. An ML-based capability to accurately screen fire-suppression material concepts prior to synthesis will allow for accelerated development cycles, which, in turn, will allow for a much faster investigation of promising concepts both well-informed by expert knowledge and completely novel in the context of fire suppression.

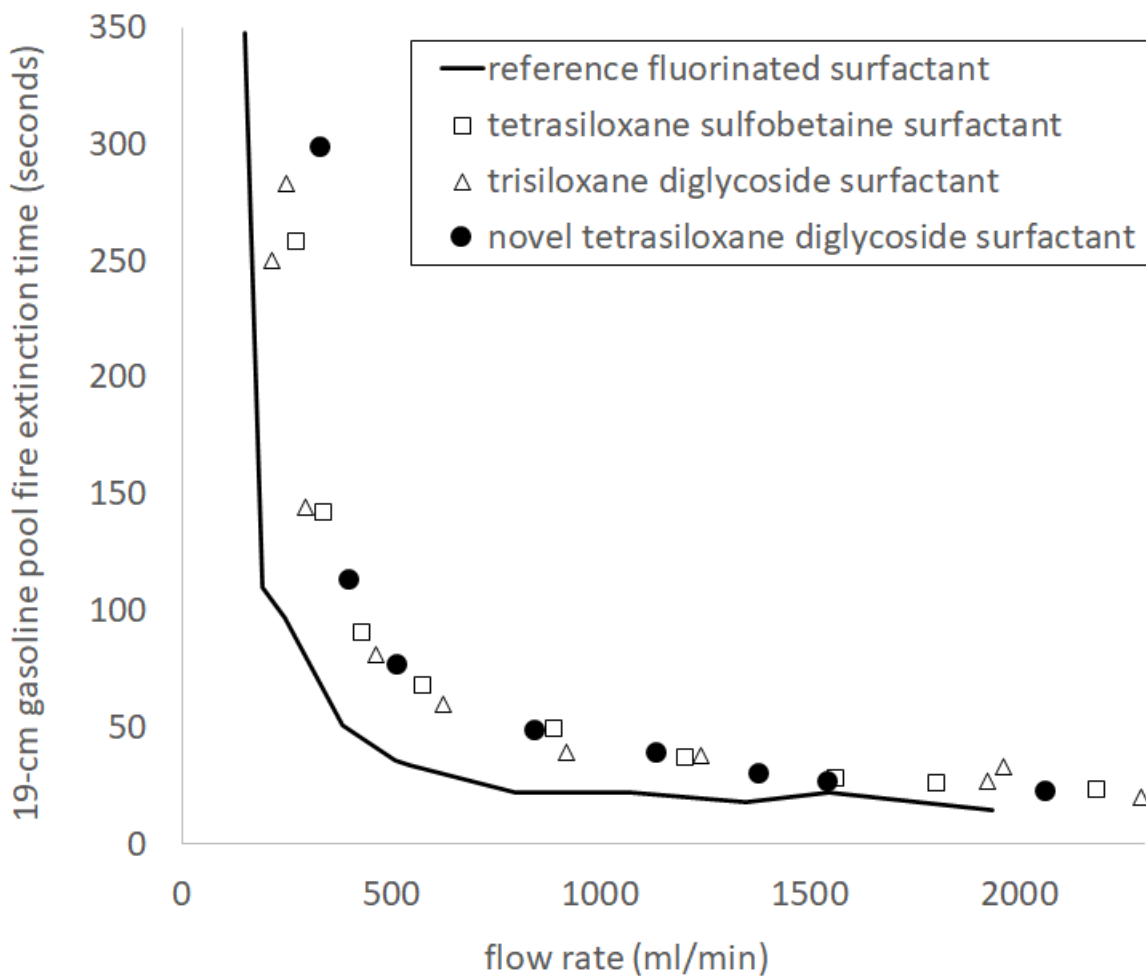


Figure 1. 19-cm gasoline pool fire extinction curve experimental results obtained from firefighting foam formulations comprising a fluorinated surfactant performance target, two high-performing nonfluorinated surfactants, and a novel nonfluorinated surfactant that was predicted to perform well via ML prior to synthesis and pool fire data collections.

Title: Point Defects and Interfaces in Two-Dimensional Materials

Author(s): D. Wickramaratne

Affiliation(s): U.S. Naval Research Laboratory, Washington, DC

CTA: CCM

Computer Resources: HPE SGI 8600 [AFRL, OH]; Cray XC40/50 [ERDC, MS]

Research Objective: To understand and predict the electronic, structural and optical properties of point defects, dopants and interfaces in bulk and low-dimensional semiconductors.

Methodology: We use density functional theory (DFT) and the projector augmented wave (PAW) method as implemented in the Vienna Ab Initio Simulation (VASP) code for our calculations. To accurately describe the bandgap of semiconductors, we use screened hybrid functional calculations. Accurate forces and total energy calculations are required to identify the most stable configurations of point defects in their various charge states. We use this information to determine the formation energies, charge-state transition levels, and optical transitions of various defects.

Results: We systematically compared calculations of deep-level defects and small polarons in semiconductors and insulators using the hybrid functional and the recently developed strongly constrained appropriately normed (SCAN) functional. The SCAN functional leads to an improvement in the description of the bandgap and lattice parameters of semiconductors compared to conventional semi-local functionals such as the generalized gradient approximation (GGA). Since hybrid functional calculations are computationally expensive, the question we wanted to address is whether the SCAN functional can also be applied as a reliable functional to investigate defects in semiconductors. We find that the SCAN functional is not able to reliably describe the properties of deep defects and small polarons in several semiconductors. This is due to a failure to identify large structural distortions and charge localization that accompanies the presence of defects and small polarons.

DoD Impact/Significance: First-principles calculations of defects and doping of semiconductors are crucial in the development and understanding of new materials for electronics and optoelectronic applications. The current state-of-the-art approach for such calculations is to rely on hybrid functionals that are computationally expensive. Evaluation of new functionals, as we have done here, will help to assess whether popular functionals such as SCAN can be used to rapidly investigate the role of defects and doping in new materials that have potential DoD relevance.

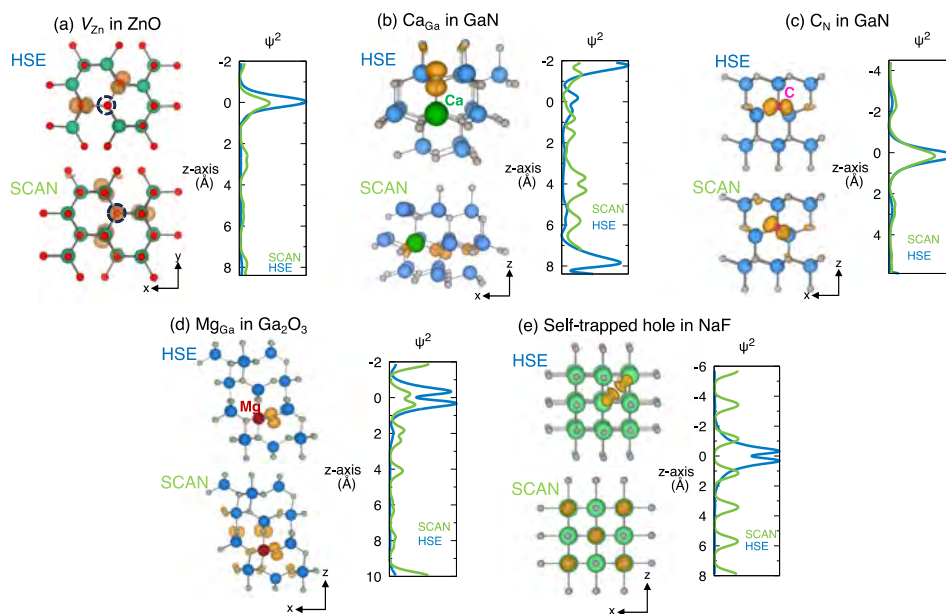


Figure 1. Isosurfaces of the defect spin densities (at 5% of the maximum value) obtained using HSE and SCAN for the following defects and charge states: (a) V_{Zn} in ZnO with the position of the vacancy illustrated with the black, dotted circle, (b) Ca_{Ga} in GaN, (c) C_N in GaN, (d) Mg_{Ga} in Ga_2O_3 , and (e) the self-trapped hole in NaF. A one-dimensional profile of this density obtained by taking a planar average along the z-axis of the supercell is plotted with respect to the defect position at $z = 0 \text{ \AA}$ and is illustrated to the right of the isosurface plots.

Title: Numerical Studies of Semiconductor Nanostructures

Author(s): T.L. Reinecke¹ and I. Welland²

Affiliation(s): ¹U.S. Naval Research Laboratory, Washington DC, ²National Research Council Postdoctoral Research Associate at U.S. Naval Research Laboratory, Washington DC

CTA: CCM

Computer Resources: HPE SGI 8600 [AFRL, OH]; Cray XC40/50 [ERDC, MS]

Research Objectives: To make first-principles calculations of the optical properties of a range of monolayer transition-metal dichalcogenide (TMDC) materials as a basis for determining their deformation potentials and photo-induced stress in them.

Methodology: *Ab initio* density functional methods using Quantum Espresso were used to calculate the electronic properties of a range of natural monolayer transition-metal dichalcogenide materials, including WSe₂, MoS₂, and ReS₂, as functions of applied isotropic, in-plane, and out-of-plane strain. These results were used to obtain the deformation potentials of these materials and were compared to results of photoacoustic experiments at NRL.

Results: Naturally occurring monolayer materials such as WSe₂, MoS₂, and ReS₂ are of considerable interest in widely varying theoretical and experimental research, including for ultrafast optical sensing and solid-state quantum technologies. The present work used density functional techniques to calculate a range of optical properties of these materials. It was found that these properties depend sensitively on the number of layers in the materials, and that different semiconductor valleys experience different deformation potentials as functions of stresses along different crystal directions. This behavior can be of opposite character in different TMDCs, e.g., WSe₂ and ReS₂, which explains the different reflectivity measurements in these materials.

DoD Impact/Significance: It has been demonstrated that accurate theoretical results can be obtained for a wide variety of novel monolayer materials using density functional approaches and that the results can be used to guide experimental research at NRL. Theoretical insights into the experimental observations will inform the development of terahertz photoacoustic devices using with these materials.

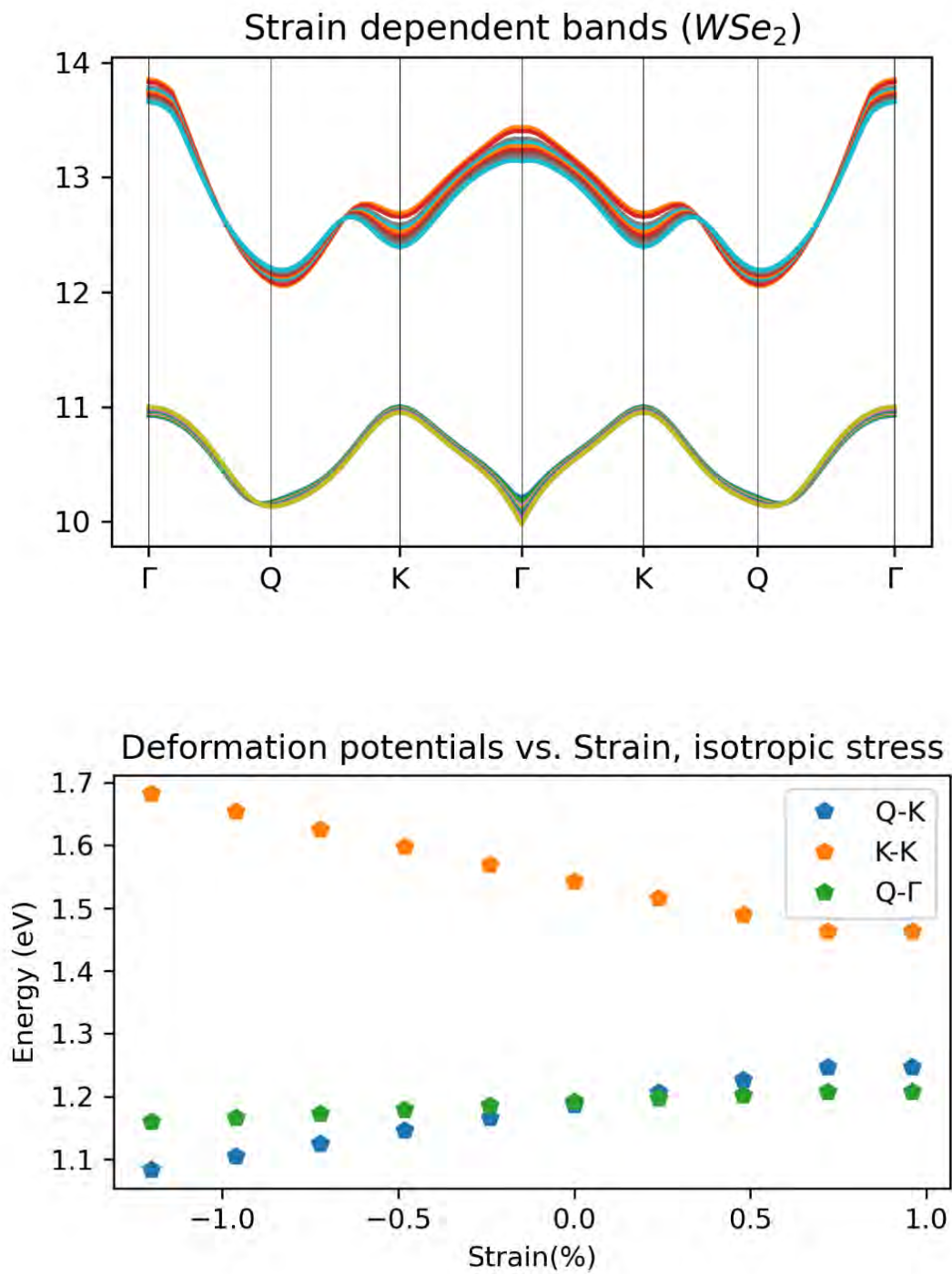


Figure 1. (top) Strain-dependent band structures of WSe_2 . (bottom) The direct transition K-K has an oppositely signed deformation potential to either indirect transitions Q- Γ and Q-K.

Title: Multiple Length and Time Scale Simulations of Material Properties

Author(s): N. Bernstein

Affiliation(s): U.S. Naval Research Laboratory, Washington, DC

CTA: CCM

Computer Resources: HPE SGI 8600, HPE Cray EX [AFRL, OH]; Liquid [ARL, MD]

Research Objectives: To understand and predict mechanical, structural, and energetic material properties

Methodology: Monte Carlo for the uniform sampling of atomic configurations in the nested sampling phase diagram calculation method, using the embedded atom method (EAM), Gaussian approximation potentials (GAP), and atomic cluster expansion (ACE) for single- and multispecies interatomic potentials. Atomic energy, force, and stress calculation using density functional theory (DFT) for machine-learning interatomic potential reference data. Resnet architecture neural network for determining free energies from phase diagrams. The software implementing these methods includes VASP for DFT simulations, ASE, libAtoms/QUIP and ACESuite for machine-learning potential development and interfacing between various programs, pymatnext for nested sampling, and the wfl Python package for job workflow management. The Resnet neural network used GPGPUs via the pytorch library.

Results: To develop a machine-learning interatomic potential for Ni-Al bronzes, we used VASP DFT calculations to evaluate well-converged and accurate reference energies for a large number of Cu-Al atomic configurations. The calculations were initiated using the wfl workflow package with a script that ran on a local machine and used ssh to submit jobs and to gather results from the HPC login nodes. The reference calculation results were added to the preliminary fitting database and were refit, improving the accuracy of the resulting GAP and ACE machine-learning interatomic potentials.

Calculations related to solid- and liquid-state phase diagrams were performed using the nested sampling method and a Resnet-architecture neural network. Nested sampling was used to calculate the temperature-dependent canonical partition function based on an empirical potential for Cu-Al, from which all other thermodynamic quantities, such as melting temperatures and stable structures, can be calculated. A neural network with the Resnet architecture was used to determine the underlying free energy function as a function of temperature and composition from a digitized image of the phase diagram, directly solving the inverse problem.

DoD Impact/Significance: Nonmagnetic structural materials such as Ni-Al bronzes, composed mainly of Al and Cu, have a number of useful properties including high strength and toughness, corrosion resistance, and low magnetic signature. Atomistic simulations can be used to predict these properties given a fast and accurate quantitative description of the interatomic interactions, enabling the development of new materials for improved performance. The machine-learning potentials we have developed for the simplified $\text{Cu}_x\text{Al}_{1-x}$ composition provide such a description, enabling simulations of phase stability, phase transformation, deformation, and fracture. When a description of the interatomic interaction is available, the nested sampling method can predict the phase diagram, which includes information on the melting point and the crystal structure as a function of composition and temperature, providing parameters for mesoscopic models that can predict microstructure and processing parameters to optimize performance. When such a potential is not available, other ways of determining the thermodynamic properties are essential to enable the mesoscopic models to make meaningful predictions for different processing conditions. Directly inverting the experimentally measured phase diagram to determine the free energies using a deep-learning Resnet architecture neural network can achieve this with dramatically lower computational cost than inversion by repeated solution of the forward (potential \Rightarrow free energy \Rightarrow phase diagram) problem.

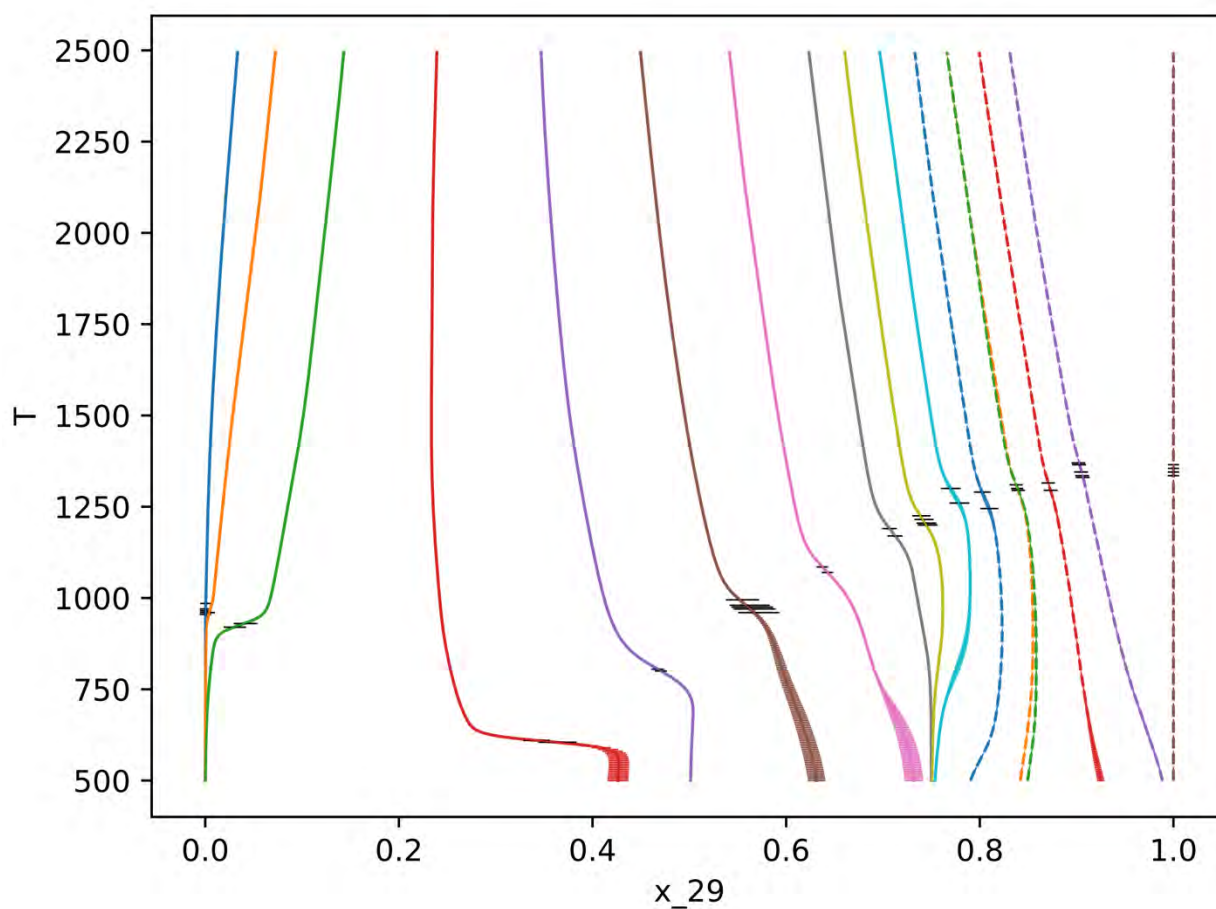


Figure 1. Phase diagram of $\text{Cu}_x\text{Al}_{1-x}$ computed using the nested sampling method and an atomic cluster expansion (ACE) SAS machine learning interatomic potential. Each color vertical line summarizes the results of a single nested sampling run at constant chemical potential, predicting the composition (horizontal axis) as a function of temperature (vertical axis). Horizontal, black lines indicate the temperatures (and compositions) at which phase transitions, in this case, freezing, occur. Areas where adjacent curves diverge from each other, e.g., third from left (green) going to $x = 0$ near 900 K and adjacent red going to $x = 0.45$ near 600 K, indicate unstable, phase separated regions.

Title: Surfaces and Interfaces in Oxides and Semiconductors

Author(s): C.S. Hellberg

Affiliation(s): U.S. Naval Research Laboratory, Washington, DC

CTA: CCM

Computer Resources: HPE SGI 8600 [AFRL, OH]; SGI ICE X, Liquid [ARL, MD]; Cray XC40/50, nvidia v100 [ERDC, MS]

Research Objectives: Determine the atomic reconstruction in twisted moiré van der Waals heterostructures and effects of the reconstruction on the electronic structure.

Methodology: We performed first-principles density function calculations of bilayers of two-dimensional semiconducting transition metal dichalcogenides that are twisted relative to each other. The specific materials are MoSe₂, WSe₂, MoS₂, and WS₂. At certain angles, twisted bilayers form periodic structures that can be modeled with density functional codes; at all other angles, the twisted bilayer is incommensurate. The size of the periodic structures increases with decreasing twist angles; we have performed calculations of supercells containing up to 3786 atoms, which corresponds to a twist angle of 2.28 degrees. The layers are bound to each other via the weak van der Waals interaction. We used the VASP density functional theory (DFT) code at the AFRL, NAVY, ERDC, and ARL HPC centers. It is important to converge the atomic positions fully, as the structural relaxation provides the confining potential within the layers due to the intrinsic piezoelectricity of the materials.

Results: We showed the materials exhibit localized electronic states below critical twist angles. The localized states exhibit flat electronic states in the band structures. In the selenides, flat valence band states emerge at twists below 4 degrees. Flat conduction band states emerge below 3.5 degrees, and a second, higher-energy, flat conduction state emerges at twist smaller than 3.2 degrees. In the sulfides, flat bands form in the valence band below 5-degree twists. There is significant strain in the moiré structures. The electronic band edges vary strongly with strain in the piezoelectric dichalcogenides, and these strains provide the confining potential, causing flat electronic states to form.

DoD Impact/Significance: Twisted dichalcogenide bilayers are candidates for hosting strongly correlated electrons, where the dispersion of the electrons can be tuned by adjusting the angle of the twist. Our results show that at the band edges, conduction-band electrons bind to the vertices of the moiré pattern, while carriers in the valence band bind to the “bulk” regions between the vertices and the domain walls. Due to their tighter confinement, the Coulomb interaction will be stronger between conduction-band electrons, and we expect Mott-insulating states to form in the conduction band at larger angles than in the valence band.

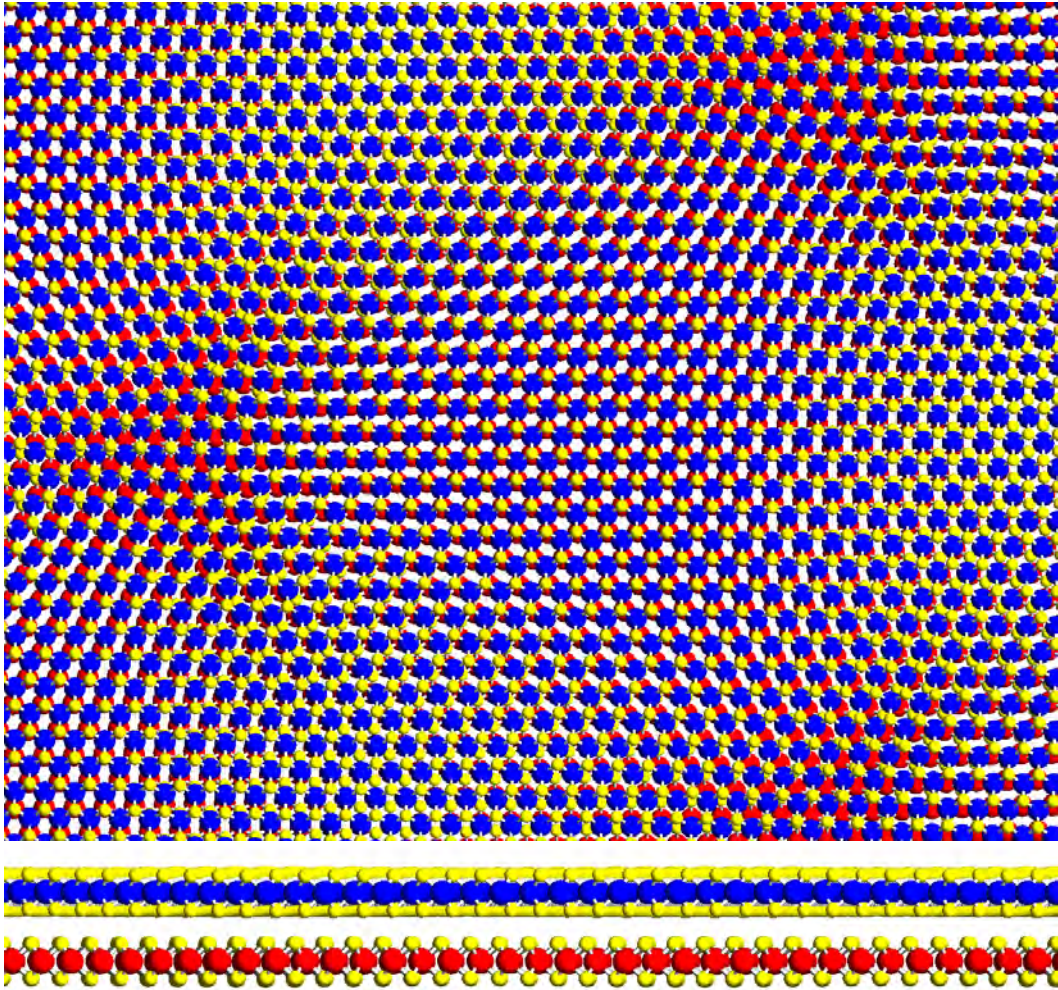


Figure 1. Relaxed atomic structure of MoSe₂/WSe₂ twisted at 2.28 degrees. Shown are views from the top and the side. Mo atoms are blue, W atoms are red, and Se atoms are yellow. The small twist angle creates a moiré interference pattern in the top view. The reconstruction strains the piezoelectric layers, confining electrons in the regions where the red Mo are not visible.

Title: Particle-Dynamics Modeling of Autonomous-Agent Clustering

Author(s): S. Lambrakos, A. Shabaev, E. Ward, and D. Chichka

Affiliation(s): U.S. Naval Research Laboratory, Washington, DC

CTA: CCM

Computer Resources: HPE SGI 8600 [AFRL, OH], [NAVY, MS]; SGI ICE X [ARL, MD]; Cray XC40/50 [ERDC, MS]

Research Objectives: Modeling autonomous-agent clustering using particle dynamics.

Methodology: The general methodology adopted involves molecular dynamics (MD) modeling and simulation of particle clustering as a function of pseudopotential fields. Prototype systems considered are interacting swarms of particles having mutually attractive potentials. The spatiotemporal characteristics of these prototype systems can be quantified and generalized formally to potential-field representation of clustering within particle systems, whose spatiotemporal distributions are characteristic of autonomous-agent clustering. This understanding is important in that the statistical characteristics of particle clustering with near-neighbor particles, associated with various types of particle systems, e.g., molecular or autonomous-vehicle swarms,¹ must be quantified for either prediction or control of particle distributions within these systems. Pseudopotential function representation of interparticle interactions provides a general approach for quantifying spatiotemporal trends of particle clusters, which can be correlated with additional information obtained from laboratory measurements or field observations.

Results: The particle-dynamics modeling and simulation of agent clustering as a function of pseudopotential fields provides foundation for extending established potential-field models, which are used in simulations of molecular physics processes, to modeling and simulation of autonomous-agent clustering, which is significant for realistic control algorithm development that concerns autonomous agents. Shown in Fig. 1 are results of simulating 50 blue particles engaging with 50 red particles. The assigned interaction potential is short-range repulsion between particles of same color, but short-range attraction between blue and red.

DoD Impact/Significance: Results of this study provide foundation for development of potential-field models for autonomous-agent clustering using existing off-the-shelf software technology, i.e., the MD software LAMMPS,^{2,3} as well as existing postprocessing software. A significant aspect of the potential-field framework applied for simulating autonomous-agent clustering is that it adopts the perspective of computational physics according to which a numerical simulation represents another source of “experimental” data. This perspective is significant in that a general procedure may be developed for simulating autonomous-agent clustering that uses particle-dynamics models motivated by measurements and field observations.

¹A. Shabaev, S.G. Lambrakos, D. Chichka, C.A. Howells, “Case-Study Non-Equilibrium Particle-Dynamics Modeling of Swarm-on-Swarm Engagements,” Naval Research Laboratory Memorandum Report, Naval Research Laboratory, Washington, DC, NRL/6360/MR—2022/1, March 16, 2022.

²A. Shabaev, C. A. Roberts, M. R. Papantonakis, R. A. McGill, C. A. Kendziora, R. Furstenberg, Y. Kim, S. G. Lambrakos, “Molecular-dynamics modeling of hydrogen-bond vibrational modes correlated with annealing,” Proc. SPIE 12107, Infrared Technology and Applications XLVIII, 1210725 (27 May 2022); doi: 10.1117/12.2618991

³S. Plimpton, “Fast parallel algorithms for short-range molecular dynamics,” J. Comp. Phys. 117(11), 1–19 (1995).

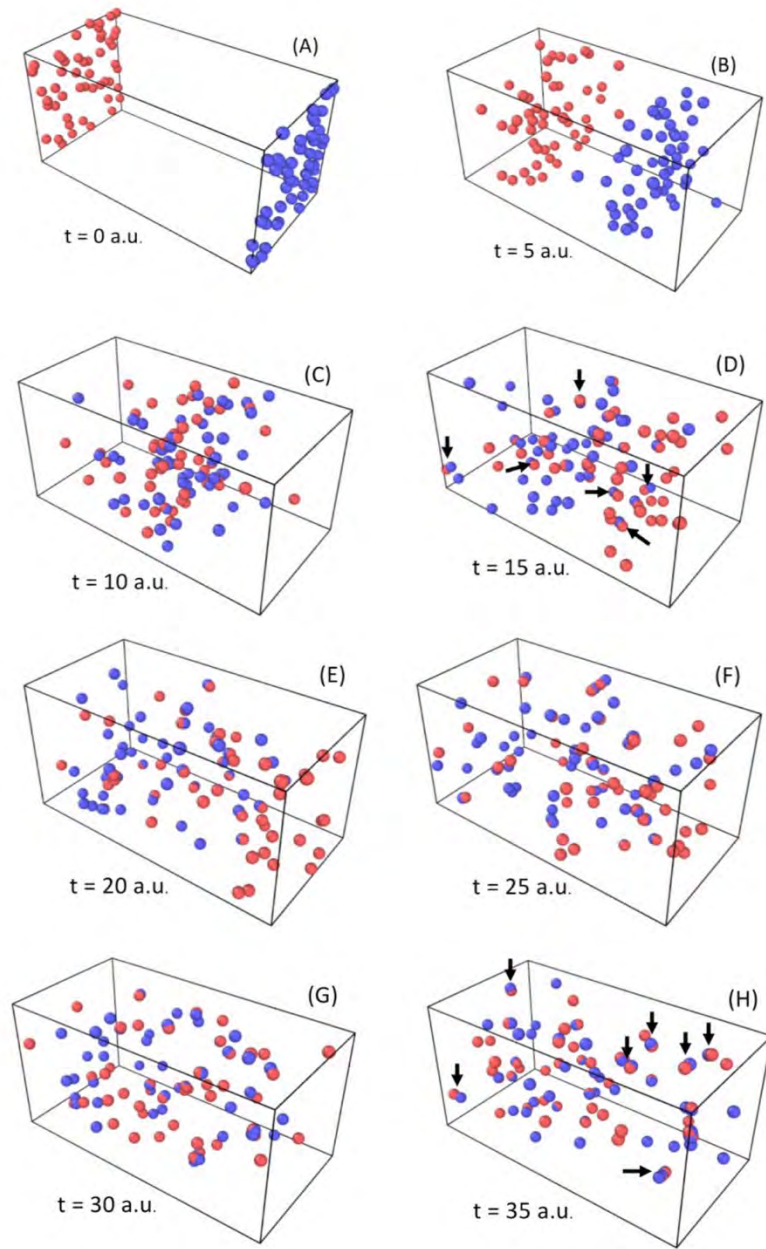


Figure 1. Agent-swarm engagement where 50 blue attract 50 red

Title: Materials Properties of Surfaces and Two-dimensional Systems

Author(s): M. Phillips

Affiliation(s): U.S. Naval Research Laboratory, Washington, DC

CTA: CCM

Computer Resources: HPE SGI 8600 [AFRL, OH]; SGI ICE X [ARL, MD]; Cray XC40/50 [ERDC, MS]

Research Objectives: Map the effects of structural changes in twisted two-dimensional transition metal dichalcogenide (TMD) bilayers on local strain, atomic relaxation, and electronic properties.

Methodology: To carry out this work, we use density functional theory (DFT) implemented in the VASP code. The most interesting twisted two-dimensional (2D) TMD bilayers are those with twist angles close to commensurate stacking orientations (0 or 60 degrees). However, these “low-twist” systems have very large supercells containing thousands of atoms. For example, the 63.15° system contains 1,986 atoms. We are able to relax this and even larger (smaller twist) systems using DoD HPC resources, and this made up the bulk of our computer usage this year. However, we also complement these large calculations with 6-atom simulations of the “aligned” (i.e., 0° or 60° orientations) as reference calculations or because these aligned calculations, with appropriate translations between layers, represent approximate snapshots of local stacking in the full twisted systems (Fig. 1a). These local calculations can also be used for reference or to benchmark calculations and experiments of collaborators.

Results: One of our most exciting results this year was the successful relaxation of a 62.45° twisted MoSe₂/WSe₂ bilayer. This system contains 3,282 atoms. This calculation, along with relaxation data from smaller systems, allows us to build up a picture of twist-angle-dependent properties in this bilayer material, such as shear strain and local twist angle (Fig. 1b, c). Electronic calculations show that at 63.48°, electronic flat bands begin to emerge in the conduction band of these materials. Flat bands are associated with correlated physics such as superconductivity. Accurate atomic relaxation data allows us to probe the relationship between structural and electronic properties. For example, we are using the structural information from DFT to build a model of the displacement fields in these small-twist bilayer (Fig. 1d). The displacement field is related to quantities such as piezoelectricity and flexoelectricity, which may be connected to the emergence of the flat electronic bands in these systems. Additional work this year included a series of 6-atom calculations of WSe₂ bilayers, which are being used to benchmark Monte Carlo simulations of a collaborator, which may be able to model relaxation of twisted TMD bilayers at nonzero temperature and with point defects, conditions that more closely mimic experiments.

DoD Impact/Significance: Twisted 2D bilayer systems are attractive to the DoD because of their potential to act as a new platform for correlated physics such as interaction-driven metal-insulator transitions, ferroelectricity, and superconductivity. Even more importantly, because of the unique geometry of these systems, it should be possible to alter the properties of the material, e.g., from insulator to superconductor, by simply tuning a gate voltage. This functionality makes these materials very attractive for applications in information storage, communication technologies, and next-generation computing. In addition, because of their nanoscale thickness, technologies utilizing these materials should be low-weight and low-power, both attractive properties for technologies utilized in naval and other DoD scenarios.

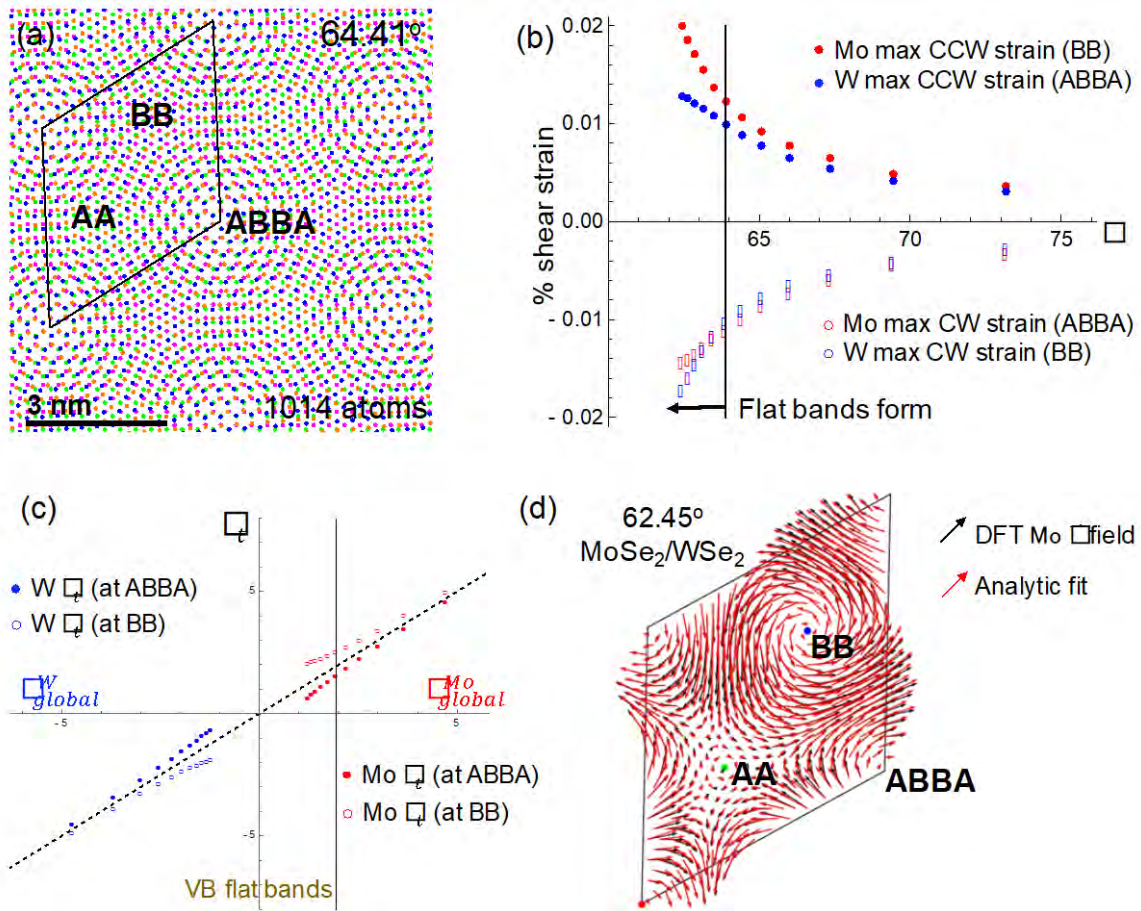


Figure 1. Twisted $\text{MoSe}_2/\text{WSe}_2$ bilayer results and analysis. (a) Unrelaxed moiré pattern of 64.41° $\text{MoSe}_2/\text{WSe}_2$ bilayer. Rhombus is the repeat supercell. Regions marked AA, BB, and ABBA have high-symmetry configurations that can be modeled by a 6-atom calculation. (b) Shear strain as a function of global twist angle for $\text{MoSe}_2/\text{WSe}_2$ bilayers. The relationship between strain in the ABBA and BB regions in opposite layers (Mo/W) changes roughly at the angle where electronic flat bands emerge. Shear strain is computed from DFT results. (c) Deviation of total twist (θ_t) from global twist angle, where $\theta_t = \theta_{\text{global}} + \theta_{\text{local}}$. The dashed line represents expected results in the case of no additional local twist. Local twist is computed from DFT results. (d) The displacement field, u , (the vector difference between relaxed positions and unrelaxed positions) of Mo atoms in a 62.45° $\text{MoSe}_2/\text{WSe}_2$ bilayer. Black arrows represent the DFT results, and red arrows represent the results of a nonlinear analytic fit. It is possible to take derivatives of the analytic fit function to analyze properties like piezoelectricity and flexoelectricity.

Title: First-principles Simulations of Condensed-phase Decomposition of Energetic Materials

Author(s): I.V. Schweigert

Affiliation(s): U.S. Naval Research Laboratory, Washington, DC

CTA: CCM

Computer Resources: HPE SGI 8600 [AFRL, OH]; SGI ICE X [ARL, MD]; HPE Cray EX [NAVY, MS]

Research Objectives: To predict thermal, mechanical, and chemical properties of crystals, polymers, and molecular compounds of interest to DoD.

Methodology: We use density functional theory (DFT) and quantum molecular dynamics (QMD) simulations to predict crystal and molecular properties of various materials. DFT-based structure optimizations with gas-phase or periodic models are used to determine changes in the atomic coordinates and crystal lattice parameters when materials are subjected to elevated pressures. QMD simulations are used to identify possible chemical reactions when materials are subjected to elevated temperatures. Infrared absorption (IR) spectra, nuclear magnetic resonance (NMR) shifts, and X-ray photoelectron spectra (XPS) are simulated to enable comparisons with experiments.

Results: This year, we focused on developing a computational workflow to facilitate DFT simulations in projects that involve a large number of similar molecules or crystals. Our implementation relies on makefiles to track the progress of each individual section of the workflow, similarly to how large software projects track changes in complex source codes. For each section of the workflow, a custom makefile defines standard operations such as generating input files, submitting jobs for execution, checking log files for possible failures, and processing simulation results. On the user's prompt, the workflow checks the date stamps of all input and output files and executes sections of the workflow for which the associated output files do not exist or are outdated. The workflow incorporates custom bash and Python scripts to diagnose common execution errors (either hardware-related failures or physics-related solver errors) and remediate them by adjusting relevant execution and/or simulations parameters. Several open-source software libraries, including the Atomic Simulation Environment (ASE) and Research and Development Toolkit (RDKit), are used for file conversion and structure visualization. We are currently testing the workflow in application to computing ^{13}C NMR shifts for organosulfur compounds (Fig. 1). Using an open-source database of NMR shifts as the reference, we collected experimental NMR shifts for 30 compounds. For each compound, up to 25 molecular conformers were generated using a distance-geometry algorithm in RDKit and optimized using a dispersion-corrected DFT method. Gibbs free energies for each conformer were estimated using the ideal gas, rigid rotor, and harmonic oscillator partition functions based on unscaled vibrational frequencies and moments of inertia. For each compound, all distinct molecular conformers with the free energies within 3 kcal/mol of the lowest-energy conformer were selected for subsequent simulations. Nuclear shielding tensors were computed using different DFT methods and the associated chemical shifts were estimated from the shielding tensors using linear relations recommended in the literature. All these steps were implemented in the workflow, which enabled us to quickly test different DFT approaches to predicting NMR spectra. The best-performing method is currently being used in simulations of molecular analogues of organically modified chalcogenide polymers.

DoD Impact/Significance: The developed computational workflow facilitates atomistic simulations of molecular and crystal properties for various materials of interest to DoD. We are currently extending the workflow to predict crystal properties of high-energy-density molecular crystals and to simulate thermal decomposition reactions of polymers.

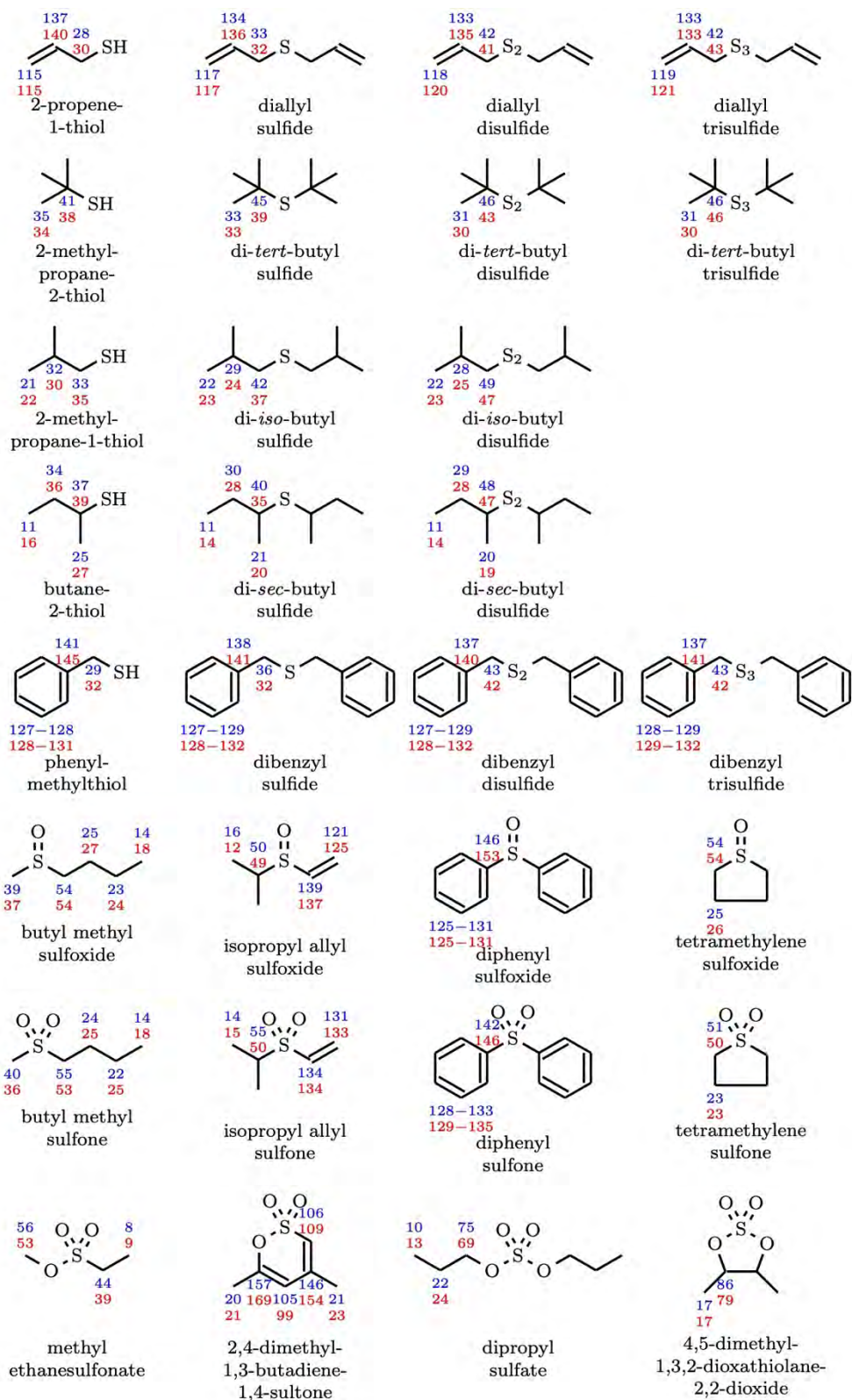


Figure 1. Structures and ^{13}C NMR shifts for molecular compounds studied in this work. Reference experimental values are shown in blue and theoretical predictions are shown in red. All NMR shifts are given in ppm.

Title: Crystal Properties of Explosives from Quantum Molecular Dynamics

Author(s): I.V. Schweigert

Affiliation(s): U.S. Naval Research Laboratory, Washington, DC

CTA: CCM

Computer Resources: HPE SGI 8600 [AFRL, OH]; HPE Cray EX [NAVY, MS]

Research Objectives: To predict crystal lattice parameters of high-energy-density molecular crystals such as HMX using quantum molecular dynamics (QMD) simulations based on density functional tight binding (DFTB).

Methodology: In this Pathfinder project, QMD simulations were used to predict changes in the crystal-lattice parameters of the β (monoclinic) and δ (hexagonal) polymorphs of HMX subjected to elevated temperatures. QMD simulations were performed using a Parrinello-Rahman constant-pressure, constant-temperature (NPT) integrator combined with five replicas of each polymorph for each temperature value. Various QMD settings such as the size of the supercell, QMD time step, trajectory lengths, and ensemble size were tested last year and those that provided reasonable accuracy at a reduced computational cost were using in these simulations. Atomic forces needed to perform QMD simulations were computed using the self-consistent charge (SCC) variant of DFTB that uses a third-order expansion of the Kohn-Sham Hamiltonian (SCC-DFTB3). The “mio” set of the CHNO Slater-Koster parameters was used for the DFTB Hamiltonian and the Universal Forcefield (UFF) parameters for pairwise Lennard-Jones 6-12 potentials were used to describe long-range dispersion. The smooth particle mesh Ewald method with a convergence threshold of 10^{-8} Hartree was used to compute the long-range Coulomb terms. The k -point sampling of the Brillouin zone was limited to the Γ point only. All simulations were done with the CP2K code.

Results: The computed lattice parameters at room temperature are compared to the available experimental data in Table 1. For both polymorphs, the computed values are within 4% of the experimental values, with the largest difference occurring for the c lattice parameter of β -HMX. For other parameters, the relative differences between the computed and experimental values range from 0.5 to 3%. Although no symmetry constraints were imposed in the QMD simulations, the symmetry of each crystal is approximately preserved, with the average angles remaining near their symmetry-prescribed values. The computed temperature-induced variations in the lattice parameters of the β and δ polymorphs are compared to the corresponding experimental values in Fig. 1. For β -HMX, the QMD simulations correctly reproduce the very weak thermal expansion of the crystal lattice in the a and b crystal directions and a much stronger expansion in the c direction observed in the experiments. However, the thermal expansion in the c direction is overestimated by about 1%. For δ -HMX, the QMD simulations correctly reproduce the moderate thermal expansion along the symmetry-equivalent a and b crystal directions but overestimate the weak thermal expansion along the c direction.

DoD Impact/Significance: Unlike classical MD methods, QMD does not require reparameterization of interatomic potentials for new compounds and thus is applicable to various energetic materials of interest to DoD. In this Pathfinder project, we evaluated the accuracy of DFTB-based QMD simulations in application to temperature-dependent crystal lattice parameters of HMX, a high-energy-density molecular crystal commonly used in explosive and propellant formulations.

Table 1. Comparison between the experimental and computed lattice parameters of β -HMX and δ -HMX polymorphs at room temperature.

β -HMX, Z = 2, space group $P2_1/n$						
	Temp.	a (Å)	b (Å)	c (Å)	β (deg)	V(Å ³)
Experiment ^a	30 °C	6.526	11.037	7.364	102.67	517.45
QMD simulations	30 °C	6.425	11.152	7.606	102.83	530.97
Difference		-1.5%	1.0%	3.3%	0.2%	+2.6%
δ -HMX, Z = 6, space group $P6_1$						
	Temp.	a (Å)	b (Å)	c (Å)	γ (deg)	
Experiment ^a	30 °C	7.714	7.714	32.480	120.0	1673.81
QMD simulations	30 °C	7.850	7.855	31.834	119.77	1703.88
Difference		+1.8%	+1.8%	-2.0%	-0.2%	+1.8%

^a Experimental lattice parameters for β -HMX were taken from Deschamps et al. 2011 and for δ -HMX from Xue et al. 2010. The reported experimental values were rounded to three significant digits after the period.

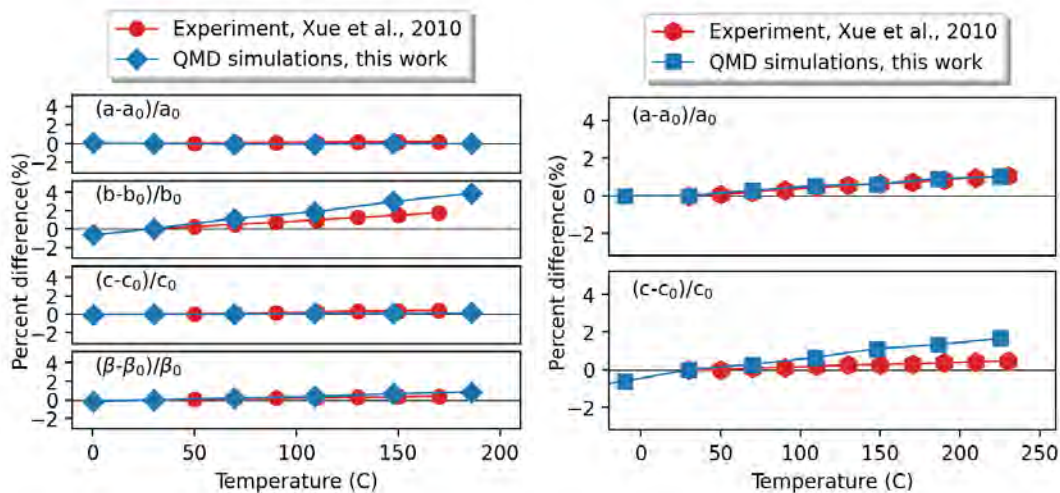


Figure 1. Comparison between the experimental (red) and computed (blue) temperature-dependent crystal lattice parameters of β -HMX (left panel) and δ -HMX (right panel). Shown are the relative differences from the room-temperature values.

Title: Marine Biofilm Metaproteomics
Author(s): W.J. Hervey and G.J. Vora
Affiliation(s): U.S. Naval Research Laboratory, Washington, DC
CTA: CCM

Computer Resources: HPE SGI 8600 [AFRL, OH]; Cray XC40/50 [ERDC, MS]

Research Objectives: To maintain and update a data analysis workflow for large-scale multiomics analytics, namely metagenomics and metaproteomics. Previous HPC Application Software Initiative (HASI) investments in distributed bioinformatics software development have enabled characterization of biological samples from complex environmental matrices, such as marine biofilms. One FY23 research objective was to perform testing and evaluation of metagenomics software tools, specifically GPU- vs. CPU-based versions of the nucleotide base-calling application Guppy (Oxford Nanopore Technologies). Additional resource use during FY23 included exploratory tool evaluation in our bioinformatics workflow, as well as increasing throughput and automation of data extract, transform, and load (ETL) processes for large-scale biological data. Incorporation of new data formats and support for biomanufacturing laboratory devices enables our bioinformatics workflow to remain agile and applicable to research use cases across the Department of Defense.

Methodology: Overall, our experimental workflow spans field, lab, and *in silico* environments, as depicted in Fig. 1. In our metaomics workflow, biological material is split into two portions for biomolecular measurement: DNA is extracted from one portion for metagenomic sequencing, and protein is extracted from the second portion for metaproteome profiling. The metagenomics approach depicted uses the MinION genome sequencer Mk1C device (Oxford Nanopore Technologies) and the nucleotide base-caller Guppy. In FY23, both GPU- and CPU-based versions of Guppy were used in our workflow. The metaproteomics approach depicted is a “shotgun” proteomics profiling via liquid chromatography tandem mass spectrometry (LC-MS/MS) on the Orbitrap MS platform (ThermoFisher Scientific). Multiple software tools for peptide-spectrum matching (PSM) between observed and theoretical tandem mass spectra were used in FY23. Improvements in ETL throughput and automation to our workflow were made during the course of the year.

Results: Our subproject’s data analysis workflow for large-scale multiomics analytics is an integral component of multiple internally and externally funded research programs. These systems range from a single microbial species to complex environmental biofilms. Specific FY23 results included incorporation of GPU-based Guppy into the metagenomics workflow, as offloading nucleotide base-calling and filtering processes to GPUs increased our workflow’s performance. To make the most of FY23 allocations, we continued evaluation of our scripting code base to ensure efficient resource use. Moving into FY24, more efficient allocation use will continue to be a focus in our subproject, particularly as we explore new architectures. In FY23, HPC allocations on this subproject yielded contributions to three peer-reviewed publications, one technical report, and one invited presentation.

DoD Impact/Significance: This HPC subproject has broad significance across both the U.S. Naval Research Enterprise (NRE) and the larger DoD enterprise. Our subproject’s general workflow for metagenomics and metaproteomics is applicable to the Navy Focus of “Sense and Sense-Making” from large data. Further, biotechnology, biomanufacturing, artificial intelligence, and machine learning, continue to be foci across DoD and OUSD Reliance 21 Communities of Interest.

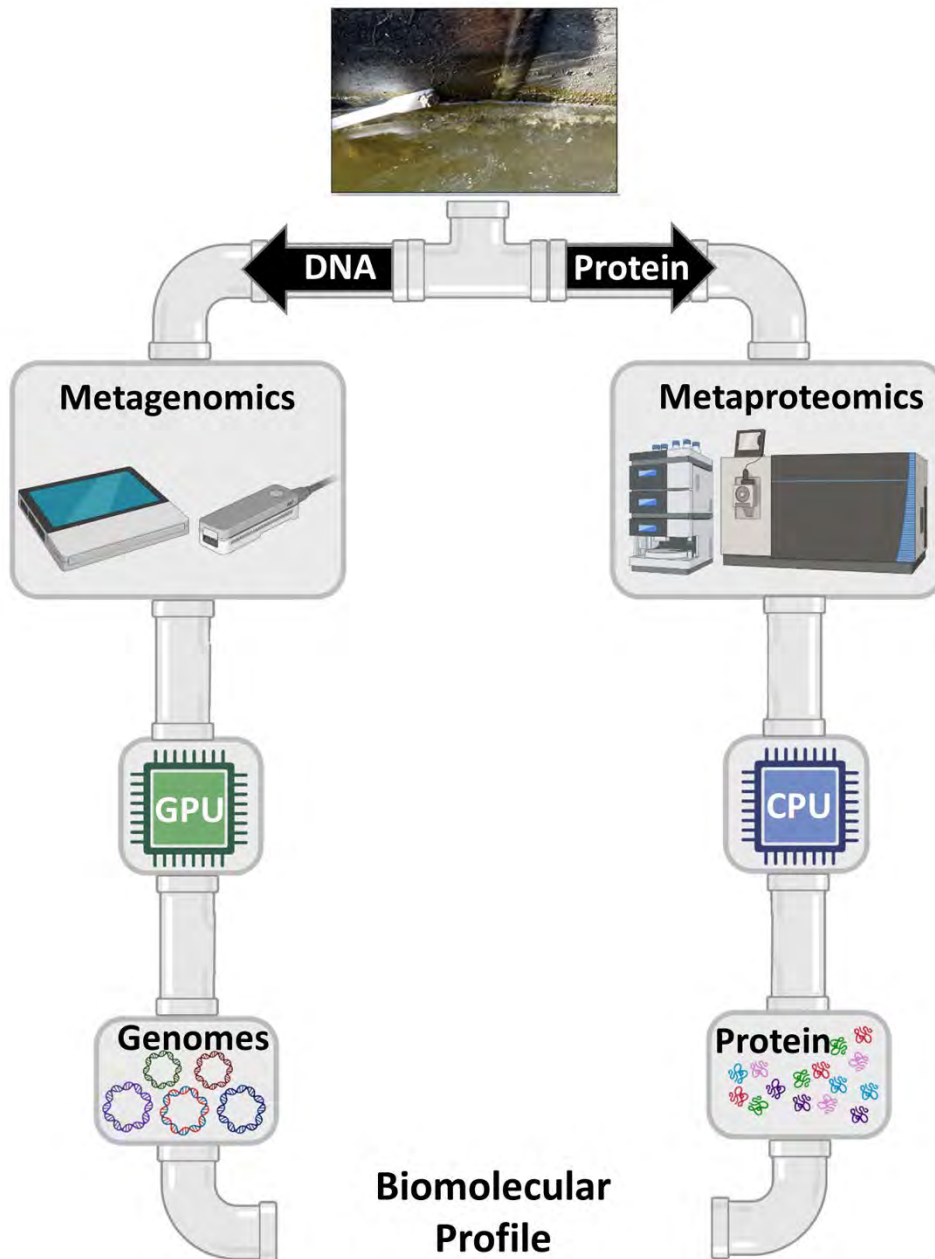


Figure 1. Marine biofilm metaproteomics workflow. Sample material is split into two portions in this workflow: DNA is sequenced by metagenomics (above left) and the protein profile is measured by metaproteomics (above right), as described in Leary et al.¹ *Biofouling* 2014. In metagenomics, GPU resources are used for nucleotide base-calling (Guppy, Oxford Nanopore Technologies) and read filtering. Additional resources are used for assembly of metagenomes. Metaproteomics uses CPU resources to compare observed peptide fragmentation with theoretical peptide fragmentation via peptide-spectrum matching (PSM). Reference protein sequences are predicted from genomes output by the metagenomics workflow. Taken together, this workflow yields a biomolecular profile from each sample from disparate – omics measurements.

¹Leary et al. *Biofouling*, 2014: <https://doi.org/10.1080/08927014.2014.977267>

Title: Synthetic Biology for Military Environments
Author(s): W.J. Hervey and G.J. Vora
Affiliation(s): U.S. Naval Research Laboratory, Washington, DC
CTA: CCM

Computer Resources: HPE SGI 8600 [AFRL, OH]; Cray XC40/50 [ERDC, MS]

Research Objectives: To engineer and deploy synthetic biology tools for biomaterials production. Biotechnology research is largely conducted in model genomic species such as *E. coli* and the yeast *Saccharomyces cerevisiae*. While harnessing these species has shown tremendous promise to date, these species are not directly relevant to military systems of interest, especially marine environments. At NRL, synthetic biology research efforts have focused on microbial chassis native to marine environments, namely *Marinobacter atlanticus* and *Vibrio natriegens*, and the development of novel genetic and genomic tools for synthetic biology. To assist with tool development in novel chassis species, HPCMP allocations are used to help guide the synthetic biology “design, build, test, learn” (DBTL) paradigm. Originally created to enable synthetic biology research on an Applied Research for Advancement of S&T Priorities (ARAP) program, in FY23, this HPCMP subproject continued to be leveraged by multiple DoD Tri-Service labs and the Reliance 21 Biotechnology Community of Interest (Biotech CoI).

Methodology: To guide the DBTL paradigm, this highly multidisciplinary project spans molecular genetics, microbiology, biochemistry, and bioinformatics (among others), as shown in Fig. 1. In the iterative DBTL cycle, the “design” and “build” phases consist of engineering a designer function into DNA, either via a plasmid (shown) or another genetic method. In the “test” phase, performance of the designer function or modification can be evaluated through biochemical, analytical, or multiomics approaches (e.g., genomics, transcriptomics, proteomics, and/or metabolomics). A MinION sequencing device (Oxford Nanopore Technologies) depicted in Fig. 1 could be used to evaluate gene expression. The “learn” phase is the most applicable to this subproject, as it directly uses computing resources for analyzing large-scale biological data. Outcomes of the “learn” phase assist with modification of the hypothesis tested and can sometimes yield novel research hypotheses. Large-scale, molecular-level snapshots acquired from genomic and proteomic measurements have assisted research in both *Marinobacter atlanticus* and *Vibrio natriegens*.

Results: FY23 efforts contributed to publication of peer-reviewed articles featuring research efforts in both *Marinobacter atlanticus*¹ and *Vibrio natriegens*² species. Both efforts leveraged large-scale proteome profile measurements in the iterative “test” phase, as shown in the figure. In addition to these two peer-reviewed publications, FY23 productivity enabled by this subproject included one invited presentation and three conference proceedings.

DoD Impact/Significance: As an enduring product of a previous ARAP in synthetic biology, this collaborative Tri-Service effort has proven essential to performing biotechnology research across multiple service labs. This subproject is also used for exploratory tool development across the Reliance 21 Biotechnology Community of Interest. This subproject is directly applicable to “Sense and Sense-Making” from large data, biotechnology, artificial intelligence, machine learning, biologically inspired materials design, biosensing, synthetic biology, systems biology, and alternative energy sources.

¹ Bird LJ, Leary DH, Hervey WJ IV, Compton JR, Phillips D, Tender LM, Voigt CA, Glaven SM. Marine Biofilm Engineered to Produce Current in Response to Small Molecules. *ACS Synthetic Biology*. 2023, 12, 4, 1007–1020. Published online 16 MAR 2023. URL: <https://pubs.acs.org/doi/full/10.1021/acssynbio.2c00417>
DOI: <https://doi.org/10.1021/acssynbio.2c00417>

² Coppens L, Tschirhart T, Leary DH, Colston SM, Compton JR, Hervey WJ IV, Vora GJ, et al. *Vibrio natriegens* genome-scale modelling reveals insights into halophilic adaptations and resource allocation. *Molecular Systems Biology*, 19:e10523 (2023). Published online 27 FEB 2023. URL: <https://www.embopress.org/doi/full/10.15252/msb.202110523>
DOI: <https://doi.org/10.15252/msb.202110523>

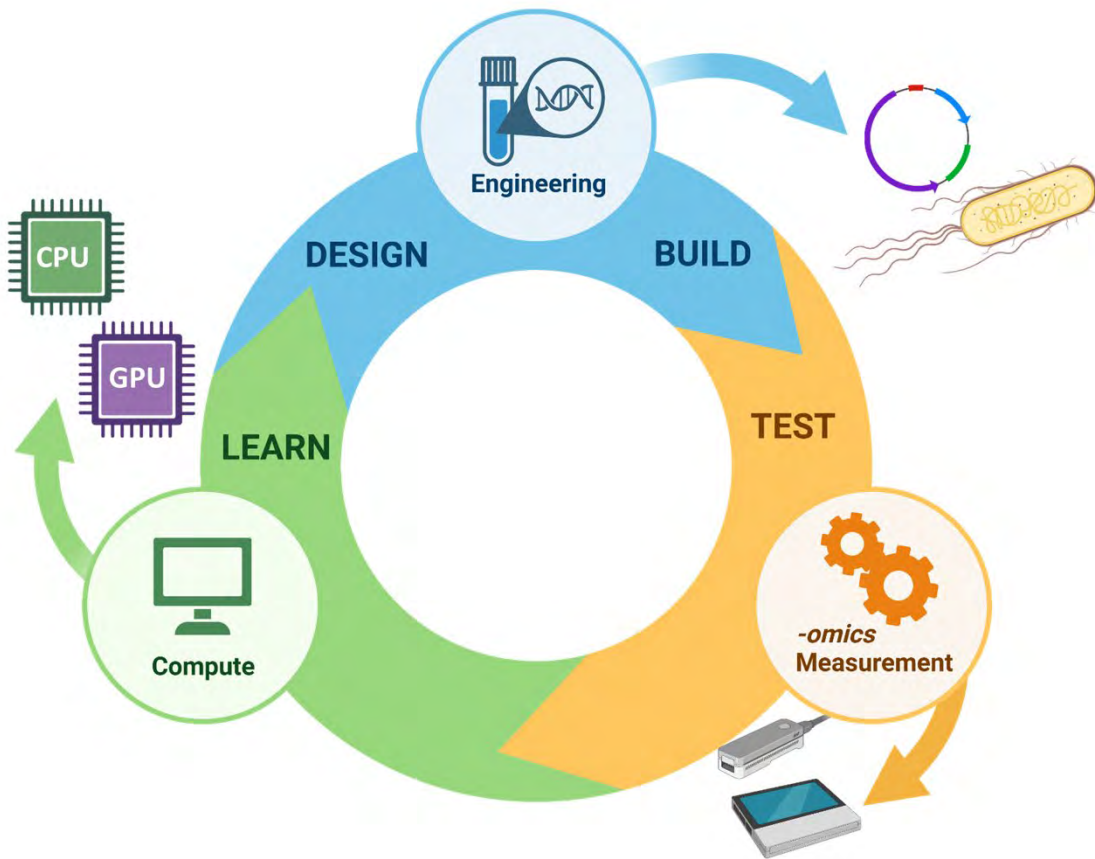


Figure 1. Synthetic biology iterative “design, build, test, learn” (DBTL) cycle. In the design and build phases of the cycle, desired functions are engineered into DNA, often as a plasmid, and are incorporated into a microbial strain of interest. In the test phase, -omics measurements are used to evaluate performance of the desired functions, as well as other biomolecular outcomes. As depicted above, the learn phase is the most compute intensive in our subproject, as allocations are used for analyzing large-scale experiments such as proteome profiles from liquid chromatography tandem mass spectrometry (LC-MS/MS) experiments. Following data analyses, experimental outcomes from the learn phase feed back into the subsequent design phase. Outcomes may include revising the original hypothesis tested and/or yielding novel hypotheses to test in subsequent experiments.

Title: Atomistic Simulations of Navy-relevant Materials

Author(s): D. Fragiadakis

Affiliation(s): U.S. Naval Research Laboratory, Washington, DC

CTA: CCM

Computer Resources: HPE SGI 8600 [AFRL, OH], [NAVY, MS]; SGI ICE X [ARL, MD]; HPE Cray EX [NAVY, MS]

Research Objectives: The objectives of the work conducted were to determine the most suitable intermolecular potential for large-scale molecular dynamics simulations of soda-lime glass under shock conditions and to assess the potential for homogeneous crystallization during shock under the conditions present in laser and plate impact shock experiments.

Methodology: Six intermolecular potentials that have been extensively tested on silicate systems were chosen. Molecular dynamics simulations were conducted with each to determine the structure (partial radial distribution functions), the equation of state, and the transport properties of soda-lime glass. In addition, the equation of state of two silicate crystal phases, stishovite SiO_2 and perovskite CaSiO_3 were also calculated. The shock Hugoniot, as well as the temperatures, wave speeds, and shear moduli at a short time (100 ps) following a shock, were also assessed; the multiscale shock technique (MSST) was employed. For the chosen potential, suitably modified, shock simulations were continued to longer times of up to 300 ns, similar to those encountered during plate impact experiments. The LAMMPS software package was used to conduct the calculations on HPCMP resources, and in-house code was used for data analysis.

Results: Simultaneously giving an accurate description of the structure and dynamics of the open network of ambient pressure glass, the densely close-packed, high-pressure liquid, as well as multiple crystal structures, is a very challenging task for an intermolecular potential, as these are typically parametrized on a limited (either high- or low-pressure, amorphous or crystalline) data set. The potential yielding the best agreement with experiment across these criteria was the one proposed by Teter et al. with a necessary modification of the Na-Na interaction at short distances (< 0.2 nm) by adding a screened nuclear repulsion term to avoid the unphysical formation of Na-Na pairs. The PMMCS potential by Pedone et al. performed nearly as well, with larger deviations from experiment on the shock Hugoniot and crystalline equations of state. The other potentials considered were the SHIK potential by Sundararaman et al. (the concentration-dependent partial charge on the O atom leads to an artificially homogeneous spatial distribution of cations in the ambient pressure glass), the potentials parametrized for high-pressure silicates by Guillot and Sator (which gives a far greater degree of phase separation into cation-rich and poor regions), and Dufils (overly stiff coordination environment around the cations, and unstable stishovite structure below 40 GPa).

Using the Teter potential with our modification, shock simulations were continued to much longer times of up to 300 ns. At short times, a complete loss of shear stiffness, accompanied by a drop in sound speed, is observed above 60 GPa, indicating that above a threshold pressure, the glass transitions into the liquid state in agreement with recent experimental studies. For a narrow range of shock velocities above the glass transition threshold, substantial crystallization into a combination of a CaSiO_3 perovskite structure with Na^+ ions substituting for a fraction of Ca^{2+} , as well as a minority component of stishovite was observed. Further simulations are in progress to assess the effect of crystallinity on the mechanical properties of the shocked glass and the stability of these phases on unloading.

DoD Impact/Significance: The results of this study will enable accurate modeling of high-velocity impact on glass materials.

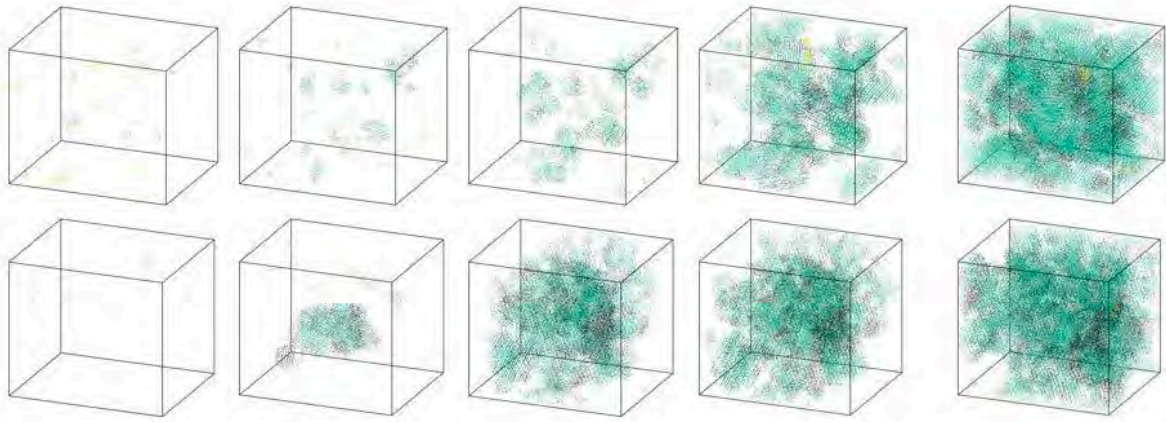


Figure 1. Crystallization of soda-lime glass during shock: shock velocity of 7.2 km/s (top row) and 7.6 km/s (bottom row). Amorphous regions are transparent; black, green, and yellow atoms are in crystalline regions with different local structures.

THIS PAGE INTENTIONALLY LEFT BLANK



Computational Electromagnetics and Acoustics

CEA covers two primary computational disciplines. Computational electromagnetics covers the high-resolution multidimensional solutions of Maxwell's equations. DoD applications include calculating radiofrequency (RF) sensor performance, radar scattering of tactical ground, air, and sea vehicles, the electromagnetic signature of buried munitions, high-power microwave performance, and the interdisciplinary applications in magnetohydrodynamics and laser systems. The computational acoustics area covers the high-resolution multidimensional solutions of the acoustic wave equations in solids and fluids. DoD applications include the modeling of acoustic fields for surveillance and communication, seismic fields for mine detection, and the acoustic shock waves of explosions for antipersonnel weapons.

Title: Small-Slope Approximation (SSA) Rough-Surface Backscattering Analysis

Author(s): J. Alatishe

Affiliation(s): U.S. Naval Research Laboratory, Washington, DC

CTA: CEA

Computer Resources: HPE Cray EX [AFRL, OH]

Research Objectives: To determine and characterize the spatial coherence effects inherent in sea clutter by numerically analyzing the associated response at the antenna port of a monostatic radar. The sea-surface coherence effects are examined with respect to the associated antenna characteristics and the surface properties.

Methodology: The surface model used in the Time Evolving Backscatter Sea-Clutter Simulation (TEBSS) is based on the nonlinear propagation model for deep-water ocean waves called the “Choppy” Wave Model (CWM). The nonlinearities represented in the CWM are related through a process that takes into account the horizontal displacement of the fluid particle path. The nonlinear surface is then expressed as a deformation of the horizontal coordinates of the linear surface. This deformation generates ocean surface waves with narrower crests and broader troughs. Once the response from the surface has been computed, the properties of the simulated sea-clutter responses are characterized. The surface scattering amplitude (SA) characterizes the spatial coherence of the scattered electromagnetic field. The surface scattering approximation for small slopes (SSASS), which approximates the induced field distribution on the sea surface, is employed in the SA. Once the SA has been computed, the response at the antenna port is determined and the coherence effects due to the surface are examined. A Doppler-spatial factor was included in the SA to ensure that the range-Doppler responses have the correct structure in range, Doppler shift, and Doppler spectral width. Numerical integration is used to determine the antenna response from the rough-surface profile. The sea surface was derived using the Elfouhaily ocean wave-number spectrum for wind speeds of 5 to 10 m/s for an upwind direction. With both the SA and the surface model calculated, the response at the antenna port was computed for each antenna aspect angle. The codes used to execute these steps were first written in MATLAB and then were converted into FORTRAN 90. The codes were then parallelized using the message passing interface (MPI) and were run on 1,024 processors (minimum) at the U.S. Naval Research Laboratory (NRL) High-Performance Computing (HPC) facility. Simulations were conducted at X-band (10 GHz).

Results: The simulated received sea-clutter responses were computed for an elevation angle of 85° for both vertical and horizontal polarizations. The simulation generated an 8,192-point frequency response of the sea surface for a given wind speed for an observed time increment. Fast Fourier transform (FFT) convolution was used to generate the complex time-dependent echo, which is the spectral product of the associated sea-surface frequency response and the transmitted waveform. As a result of the previous step, multiple coherent processing intervals (CPIs) were generated for analysis and were compared to experimental data as depicted in the range-time-intensity and range-Doppler plots in Fig. 1. The number of spatial samples of the sea surface was set to 23,103 and 2,047 in the downrange and crossrange dimensions, respectively. The simulation results showed that the range-time and range-Doppler properties were similar to real sea clutter in that the appearance of spiky clutter returns are prevalent, and that the Doppler response has the correct center frequency and spectral width. However, further investigation of the simulated data is still required.

DoD Impact/Significance: Understanding the spatial coherence effects in radar sea clutter provides further insight into the phenomenology of backscattering from the ocean. This will be useful in devising new algorithms for detecting threats over the sea.

Example results:

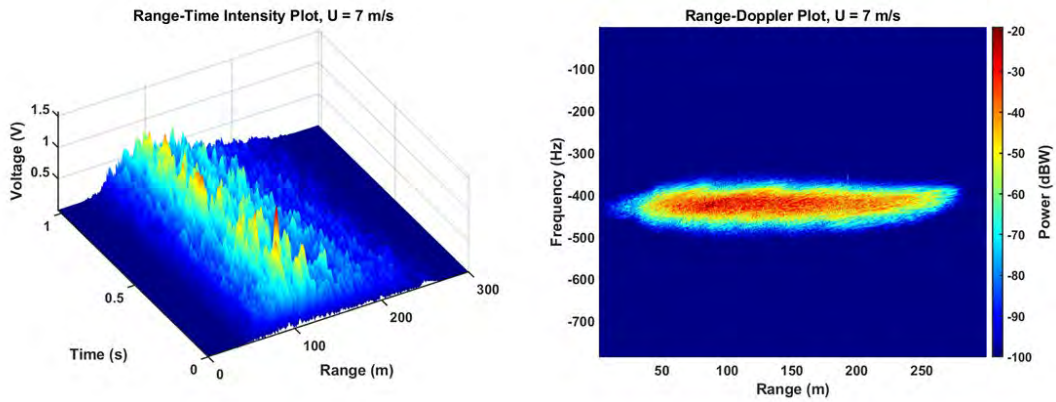


Figure 1. Range-time intensity and range-Doppler plots of X-band simulated sea-clutter returns for VV polarization at 85° elevation. Pulse width is 2.0 ns, pulse repetition interval (PRI) is 500 μ s, and wind speed is 7 m/s toward the radar.

Title: Low Grazing Angle Radar Backscatter

Author(s): J.V. Toporkov, M.A. Sletten, and J.D. Ouellette

Affiliation(s): U.S. Naval Research Laboratory, Washington, DC

CTA: CEA

Computer Resources: HPE Cray EX [AFRL, OH], [NAVY, MS]; Cray XC40/50 [ERDC, MS]

Research Objectives: Coastal, shipborne, and airborne radar systems routinely encounter signal reflections from the sea surface, frequently under low-grazing-angle (LGA) conditions. Such surface signatures are often perceived as clutter that masks a target echo. On the other hand, they can be a source of information about local ocean conditions. Understanding the properties of sea scatter, their dependence on environmental parameters, and how they differ from those of man-made target echoes is key to improving or even enabling performance of such radar systems and applications. This project investigates detailed characteristics of radar returns from the ocean surface under both monostatic and bistatic observation geometries. The task is achieved through simulations that involve both direct numerical solution of the scattering problem and, where appropriate, numerical implementations of approximate scattering models.

Methodology: The approach combines a physics-based model for an evolving ocean surface with computationally efficient evaluation of the scattered electromagnetic field. The most rigorous implementation is limited to the two-dimensional (2D) space but is relevant for commonly occurring three-dimensional (3D) geometries (e.g., oncoming or receding long-crested waves). A wind-driven surface is represented by realizations of a Gaussian random process defined by a certain wave spectrum. Hydrodynamic nonlinearities and associated wave-wave interactions are modeled via Creamer transformation. This affects shape and motion of smaller ripples that have great impact on scattering of decimeter- and centimeter-scale electromagnetic waves. The field scattered by a “time-frozen” scene at a particular frequency is found by iteratively solving a boundary integral equation (BIE) for the induced surface current. This first-principles formulation automatically accounts for many phenomena (multiple scattering, shadowing) that could be problematic for analytical treatment. The 3D code implementation thus far relies on the small slope approximation (SSA) scattering model in lieu of the exact BIE-based solver. The calculations can be run at many frequencies covering a certain band to simulate pulse scattering. The procedure is repeated for every surface profile in the sequence representing temporal evolution. OpenMP parallelism is used.

Results: To assess ways to improve efficiency of sea scattering calculations, we investigated substituting the Creamer transform with a simpler but less rigorous “choppy wave model” (CWM) to capture surface nonlinearities. The 2D space comparisons used the exact BIE scattering solution and focused on backscatter from evolving seas. The CWM was observed to produce Doppler spectra with expected widths while considerably underpredicting Doppler centroids, particularly at LGA. Another research effort addressed feasibility of sensing the long-wave part of the surface wave spectrum by utilizing illumination from an HF skywave radar in conjunction with a satellite-based receiver. To investigate the scattering part of the problem through the full 3D simulations, simplifications were made as shown in Fig. 1. The overall geometry is depicted in Fig. 2a. Ocean scattering is calculated from regularly spaced “resolutions cells” that would result from raw signal processing with a modern synthetic aperture radar-type algorithm, cf. Fig. 2b. As the satellite receiver moves, both the scattering geometry and the shapes of the resolution cells change, which is accounted for in the simulations. The modeled data are used to retrieve the spectrum through the Bragg theory. The result shows good agreement with the input (Fig.3).

DoD Impact/Significance: Increasingly comprehensive and detailed characterization of sea clutter will help in design and performance assessment of the Navy radar systems. This knowledge also supports obtaining more complete and accurate information about environmental conditions in operating areas.

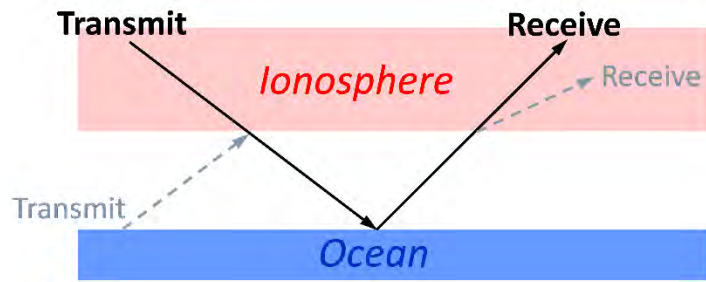


Figure 1. Simplified problem (black rays) that disregards ionospheric reflections and refractions.

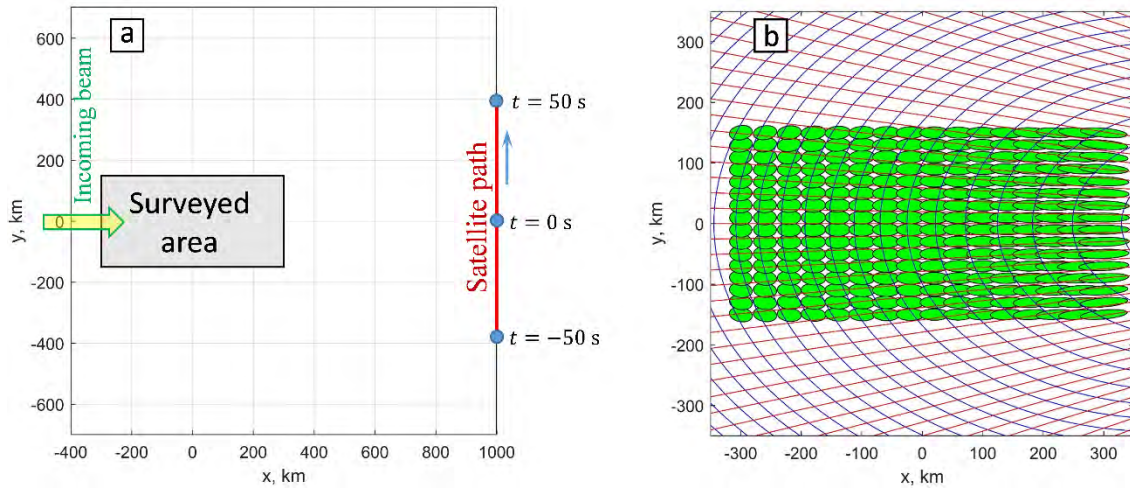


Figure 2. a) Problem setup, top view. b) The surveyed area with resolution elements centered on regularly spaced grid points (isoranges and isodops are shown for reference); the receiver position at $t = 0$ is assumed. The simulations compute bistatic scattering from every such cell.

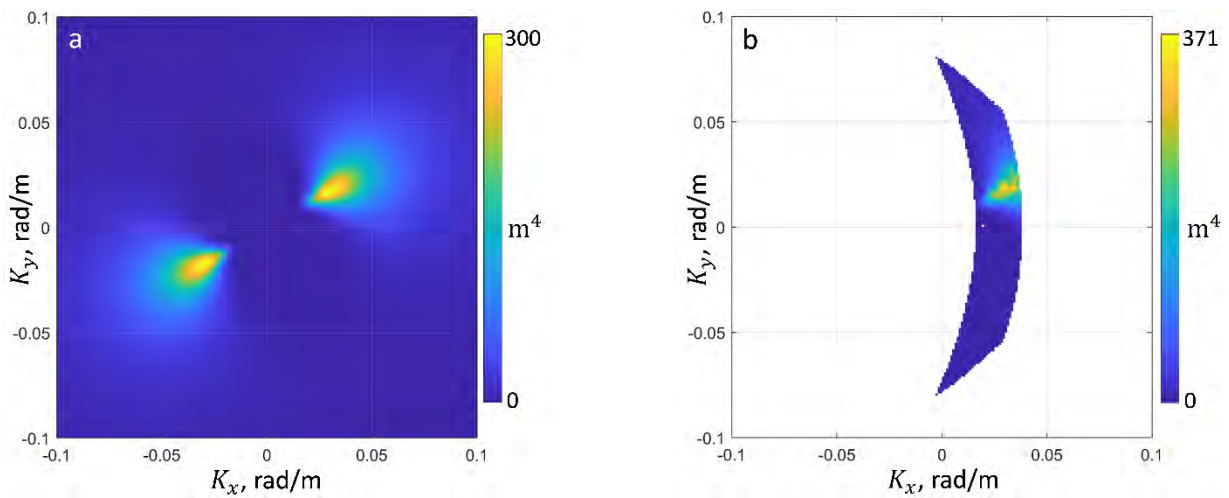


Figure 3. a) Symmetrized version of the directional wave spectrum used to generate the evolving sea surface realization. b) Retrieved spectrum from the simulated data collected over the 100-s satellite traverse (additional K -space averaging with 10^{-3} rad/m \times 10^{-3} rad/m bins is applied).

Title: Interactive Scenario Builder

Author(s): B. Dowd¹ and D. Richie²

Affiliation(s): ¹U.S. Naval Research Laboratory, Washington, DC; ²Brown Deer Scientific, Forest Hill, MD

CTA: CEA

Computer Resources: HPE SGI 8600 [NAVY, MS]

Research Objectives: Many Navy organizations apply NRL's Interactive Scenario Builder (Builder) to compute large-scale critical electromagnetic spectrum products for distribution to fleet users. This is an embarrassingly parallel problem, but Builder only executes on single nodes, limiting the effectiveness of addressing operationally relevant problems of scale. The overall technical objective is to enable the NRL Builder software to execute on an HPC platform so that the Advanced Propagation Model (APM) and Variable Terrain Radiowave Parabolic Equation (VTRPE RF) propagation models are able to utilize the optimizations and MPI parallelization introduced into Builder under FY23 ONR funding and as part of the DoD High Performance Computing Modernization Program (HPCMP) User Productivity Enhancement and Training (PET) program.

Methodology: The overall software design and approach to the parallelization is shown in Fig. 1. The MPI backend is written in C++ while Builder is coded in Java. The backend employs a conventional synchronous data parallel MPI model using a rank-0 manager process and (N-1) worker processes to perform computationally intensive calculations. The work queue manager receives work through callbacks from Builder and schedules the work across MPI processes in a round-robin distribution. Each worker process picks up the work and performs either an APM or a VTRPE calculation and returns the results to the queue. The Builder tool requests results by follow-up callbacks to the management process, which then returns the completed results. The design supports the highly asynchronous model used on the Java side within Builder and couples the tool to a data parallel model. The interfacing can be described as loose coupling because the control flow of Builder is significantly different than the MPI/C++ backend.

Results: Initial benchmarking and stability analysis of Builder MPI has been performed with the VTRPE RF model on the Gaffney HPC. VTRPE demonstrated scaling on up to 64 HPC compute nodes (3072 cores) thus far with a 21× improvement over a single node. This represents parallelization of only the propagation model calculations and does not include the environmental processing backend of Builder, which was a substantial limiting factor within the scaling. A synchronicity issue was encountered at higher core counts and is currently being addressed. Scaling tests with the APM propagation model will be performed in an FY24 6.4 follow-on effort that will also deliver the Builder MPI upgrades to DoD customers.

DoD Impact/Significance: MPI-capable Builder enables leveraging HPC systems to deliver exponentially expanded large-scale electromagnetic products and capabilities for fleet users.

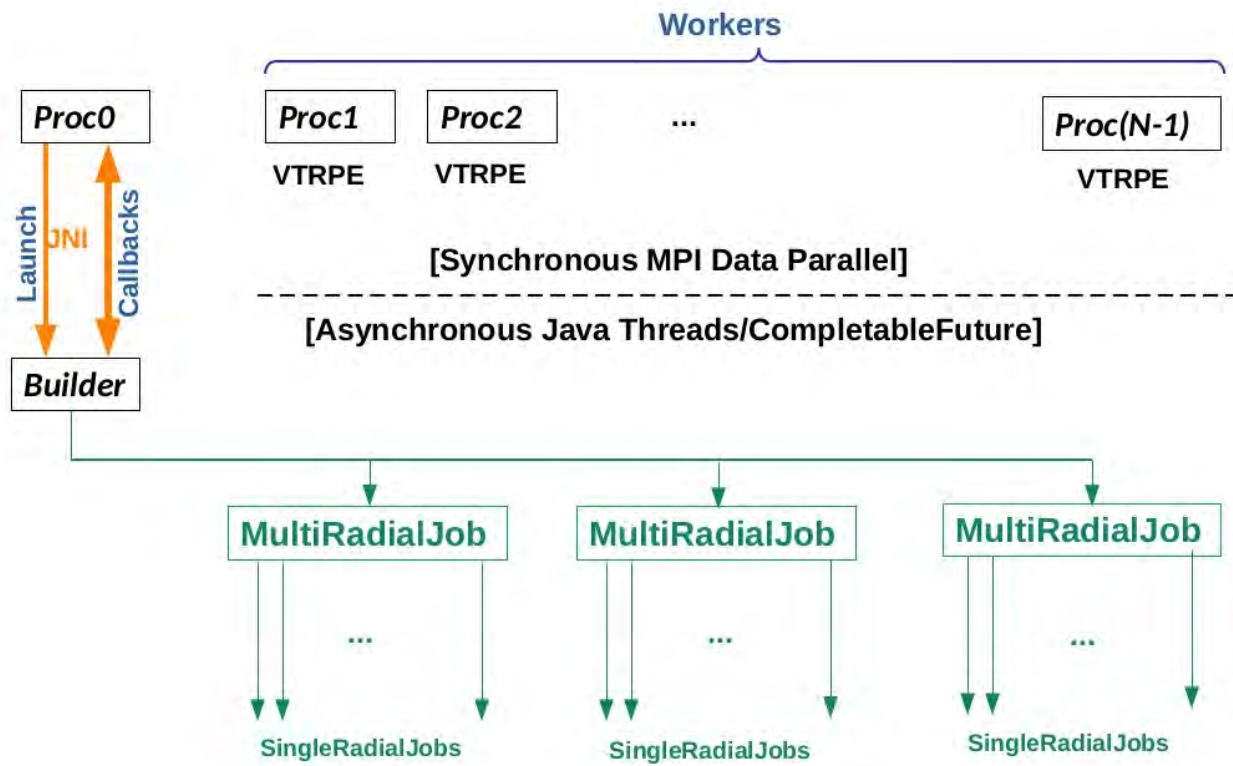


Figure 1. Overall software design and approach for the MPI parallelization of radial calculations in the Interactive Scenario Builder, shown here for the VTRPE model.

Title: Infrared Scattering by Micro-particles

Author(s): R. Furstenberg and A. Shabaev

Affiliation(s): U.S. Naval Research Laboratory, Washington, DC

CTA: CEA

Computer Resources: SGI ICE X [ARL, MD]; Cray XC40/50 [ERDC, MS]; HPE Cray EX [NAVY, MS]

Research Objectives: The objective of this research is to provide insights into spectral features of microparticles, especially those with irregular shapes (i.e., nonspherical), commonly found in solid aerosols and surface contaminants. As the sizes and shapes of these particles vary, the observed signatures differ from their bulk values. This change is most pronounced in the Mie regime, where the wavelength of light is comparable to the size of the particles. Mie theory provides exact solutions for perfect spheres, but those results cannot be widely applied to irregularly shaped particles, often found in solid aerosols and other trace contamination on surfaces. Accurate description of infrared scattering spectra is of importance for the development of detection instrumentation and in other fields such as atmospheric research. The main goal of this research is to develop a predictive tool for spectral signatures of liquid and solid aerosols as a function of size and shape.

Methodology: Our approach to modeling irregularly shaped particles will involve using established electromagnetics codes that are suitable for solving the scattered electromagnetic field. In addition, we have developed a code that generates random particles. For these particles, we calculate the angle-dependent scattering cross sections for a range of optical constants (n and k). Each particle is characterized by the three-dimensional (3D) shape parameters (aspect ratios, convexity, sphericity, etc.) Large datasets are analyzed statistically to ascertain which shape parameters influence the scattering cross sections the most. These parameters can be used to construct a multidimensional lookup table (or a trained neural network) that will be designed to rapidly predict the scattering response (with confidence bands) of an arbitrary ensemble of microparticles. This analysis provides the basis for predictive models.

Results: The modeling of scattering response provides foundation for the analysis of a small number of shape parameters that are responsible for the majority of the observed scattering cross section. This characterization is needed to limit the required dimensionality of the lookup table and, therefore, to allow for the formulation of a reasonably accurate predictive model that can be used both by detection instruments (in the field) or for research purposes (in the lab) in various scientific fields such as atmospheric and environmental science, and for detection of hazardous materials. Figure 1 shows results of calculations for a particle of cubic shape made of dielectric material with zero conductivity. The spectrum of total cross section varies with the direction of incident light. For each frequency, the differential cross section varies with the orientation. The angular distribution of scattered intensity also changes as shown by the stereographic projections of scattered intensity.

DoD Impact/Significance: Better understanding of spectral signatures from microparticles is of great interest to the DoD in general and to the Navy in particular. Protecting the warfighter in contested and hazardous environments as well as the homeland from attacks by monitoring the environment is greatly enhanced from higher sensitivity and lower false-alarm rates made possible when the exact spectral signatures of the hazardous materials are known. An immediate use of our predictive model will be to support relevant DoD agencies that are tasked with mitigation and detection of hazardous aerosols (both liquid and solid) as well as trace contaminants on surfaces. Our predictive models will be used for algorithm training, especially at the beginning of the program, when not enough data is available, but also later to augment the experimental data with synthetic data.

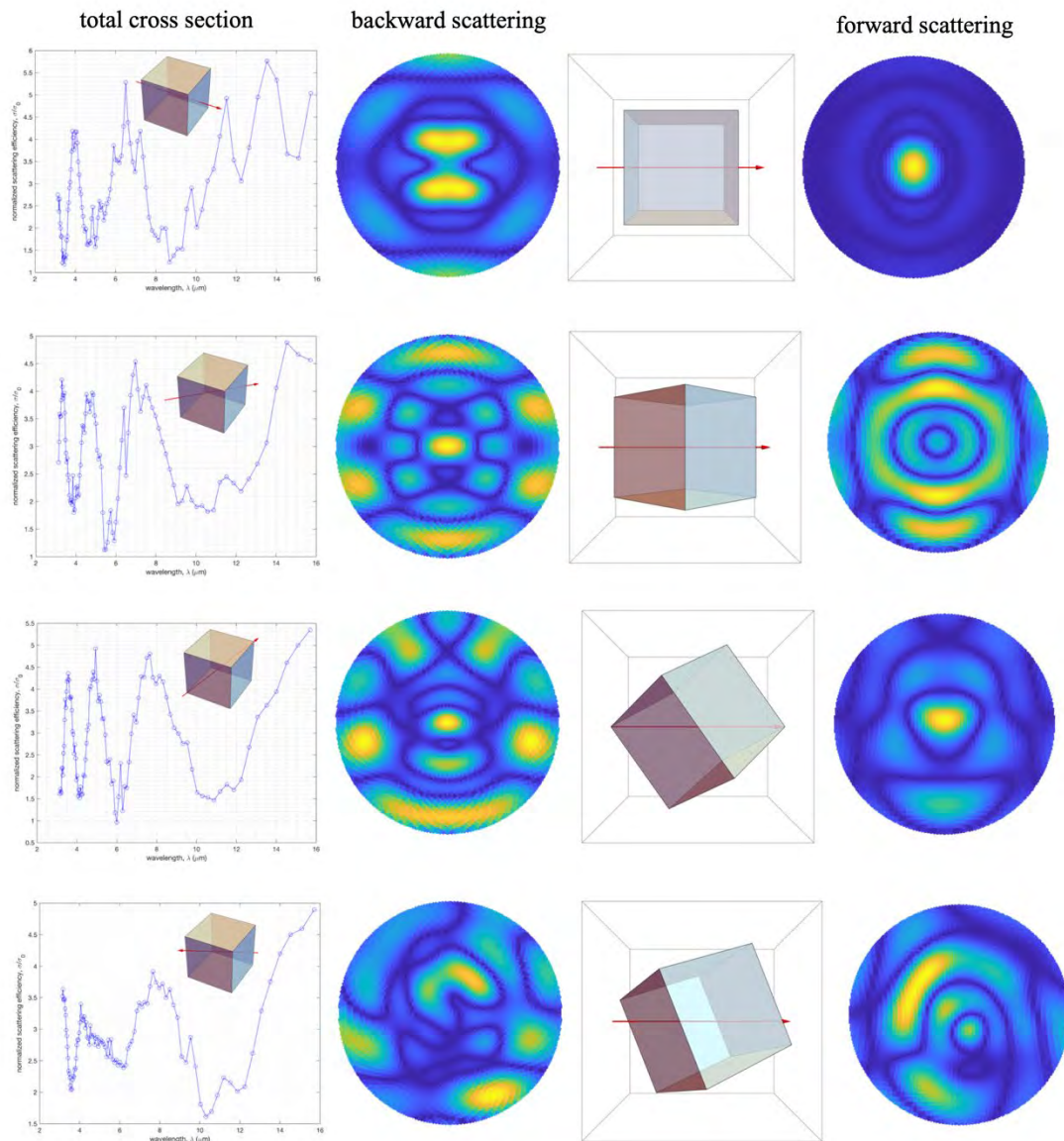


Figure 1. Total scattering cross section (left panels) and angular distribution of intensity for backward and forward scattering ($\lambda = 10.47 \mu\text{m}$) for a particle of cubic shape (size: $10 \mu\text{m}$, refractive index: $n = 2$).

Title: Particle-In-Cell Simulations of Two Cylindrical Reflex Triodes in Parallel
Author(s): I.M. Rittersdorf, B.V. Weber, S.B. Swanekamp, and D.D. Hinshelwood
Affiliation(s): U.S. Naval Research Laboratory, Washington, DC
CTA: CEA

Computer Resources: Cray XC40/50 [ERDC, MS]; HPE Cray EX [NAVY, MS]

Research Objectives: The CRT is a bremsstrahlung diode that is notable for its ability to create low-endpoint X-ray spectra useful for radiation-matter interaction studies. The primary objective of this research is to perform particle-in-cell (PIC) simulations that can predict the X-ray output of multiple cylindrical reflex triodes (CRTs) in either series or parallel.

Methodology: PIC simulations of two CRTs in parallel were performed in a two-dimensional (2D) cylindrical geometry, as shown in Fig. 1, using the code Chicago. The simulation was driven by a voltage waveform as measured on an experiment performed on NRL's Gamble II pulsed-power generator. During the pulse, currents are sufficiently large that the electrons are magnetically insulated from the anode. Electrons travel to the anode tip and scatter through the foil multiple times, creating bremsstrahlung radiation as they do so. PIC simulation lists of scattering electrons are output to be used as inputs for the 2D radiation transport code Cyltran to predict X-ray outputs.

Results: Figure 2 shows a contour plot of current flow near the peak of the voltage and current pulse in the simulation. As expected, the current is magnetically insulated from the anode and instead of flowing directly across the anode-cathode gap, the flow of current is swept down towards the tip of the anode foil (downstream). As the electrons connect with the anode foil, they scatter through because the foil is so thin and create X-rays via bremsstrahlung. The electrons scatter in the foil multiple times, a process known as reflexing, and as they do so, they travel in the negative z-direction (upstream). The current contours in Fig. 2 are asymmetric about the top and bottom of the anode foil, suggesting that there might be some coupling between the two CRTs. Simulation results show that electrons emitted from one CRT can end up in the anode of the other CRT. During the simulation, every time an electron scatters within the anode foil, its position, momentum, and particle weight are recorded as outputs. Those outputs are then used as inputs in Cyltran, a 2D radiation transport code. Figure 3 shows the resultant X-ray dose as a function of radius at a test plane downstream of the source. The blue curve is the Cyltran calculation, and the red points are measurements from the experiment. Figure 3 shows that the simulation and the experiment are in good agreement. There is a 15% underprediction by the code on axis ($r = 0$ cm). The source of this underprediction is not yet understood and is an area of future computational study.

DoD Impact/Significance: The simulations described here show that 2D simulations of two CRTs connected in parallel offer good X-ray output predictive capabilities. This technique can then be used to inform future simulations and experimental studies to increase the X-ray performance of such devices.

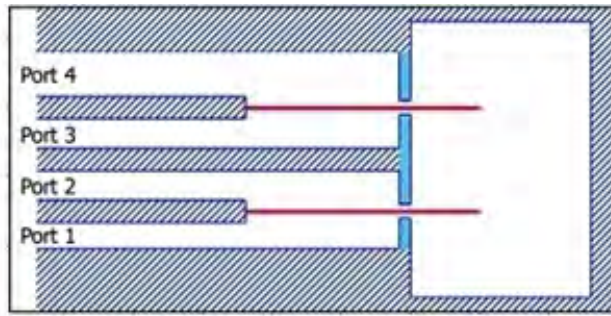


Figure 1. Two-dimensional cylindrical geometry of parallel cylindrical reflex triodes used in particle-in-cell simulations. The blue regions are the cathode plates where an electron emission threshold, $E_{th} = 300 \text{ kV/cm}$, is set. On the tantalum anode foils (shown in red), proton emission is controlled via temperature-threshold-emission criteria. The simulation's drive voltage waves are from the ports on the left.

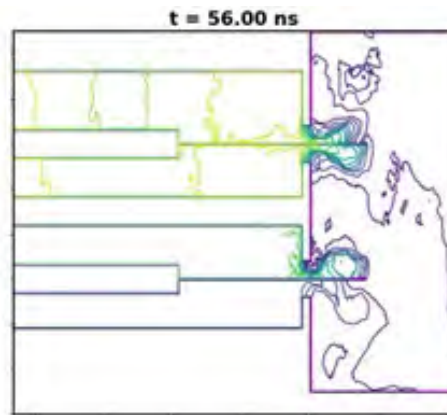


Figure 2. rB_θ contours show the flow of current in the simulation by quantifying the current enclosed inside the contour. The contours are selected so that each region contains 10% of the total current. At time $t = 56 \text{ ns}$, the current can be seen to be magnetically insulated from the anode and connecting at the anode tip.

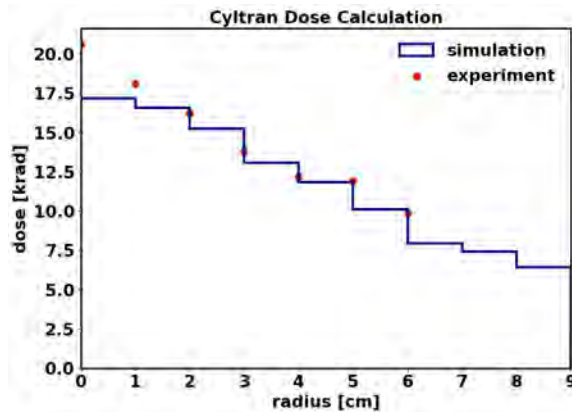


Figure 3. X-ray dose outputs as a function of radius at a test plane downstream of the vacuum chamber. The simulation (blue) shows good agreement with the experiment (red) except for directly on axis, where the simulation underpredicts the experiment by 15%.

Title: 3D Particle-In-Cell Simulations of Electron Beam Plasma: A First Study

Author(s): N.D. Isner,¹ E.R. Kaiser,¹ S.B. Swanekamp,¹ and K.L. Cartwright²

Affiliation(s): ¹U.S. Naval Research Laboratory, Washington, DC; ²Sandia National Laboratories, Albuquerque, NM

CTA: CEA

Computer Resources: Cray XC40/50 [ERDC, MS]; HPE Cray EX [NAVY, MS]

Research Objectives: Intense electron beams are effective in generating plasmas in low- and high-pressure environments. Therefore, electron beam experiments and models are of particular importance when studying radiation sources and effects. The primary objective of this research is to develop the capability to perform particle-in-cell (PIC) simulations of the electron beam plasma system to study the macroscopic quantities of interest and to track relevant plasma component populations (dissociation, charge state, electronic state, vibrational state, and rotational state).

Methodology: PIC simulations are performed to model NRL's Febetron experiment, a small pulsed power device that injects an electron beam into a low-pressure gas cell. Figure 1 shows three-dimensional (3D) models of the vacuum diode and the gas cell that are developed and used in EMPIRE simulations. We analyzed the electric field, the current enclosed contours ($2\pi r B_\theta / \mu_0$), and the plasma electron density at vacuum for a first study. These parameters are all critically dependent on the electron-beam current density and the gas pressure and are inputs that we will vary in the next simulation study.

Results: The plasma-generated parameters of interest are the electric field, the current-enclosed contour, and the electron plasma density. Figure 2 shows that at half the rise time of the experiment, we see the diode increase in electric field strength and electron emission come from the cathode. At electric breakdown, a large induced electric field is created and a rapidly rising beam current accelerates newly created electrons causing an avalanche in the plasma electron density. In the initial rise of the beam pulse, the counter-streaming electrons oppose the beam current and the overall current is reduced. During the fall of the beam pulse, the beam current and the plasma current flow in the same direction and the net current is enhanced. In Figs. 2 and 3, the gas cell showed both an increase in electric field and current enclosed at 80 ns. At vacuum pressure, the formation of a virtual cathode in the current-enclosed contour plot is also visible. After the beam pulse ends, $t = 100$ ns, stored magnetic energy is resistively dissipated through the plasma.

DoD Impact/Significance: The simulations performed demonstrate the 3D modeling capability and the ability to analyze quantities of interest. Currently, the geometry and voltage drive of the simulations are being refined allowing for direct comparisons to results from NRL's experiments. These comparisons will, in turn, be used to inform future model developments. The objective of these validation experiments is to have predictive capability to improve the hardening design of military systems in extreme environments.

²Sandia National Laboratories, SNL is a multimission laboratory managed and operated by National Technology and Engineering Solutions of Sandia, LLC, a wholly owned subsidiary of Honeywell International Inc., for the U.S. Department of Energy's National Nuclear Security Administration under contract DE-NA0003525.

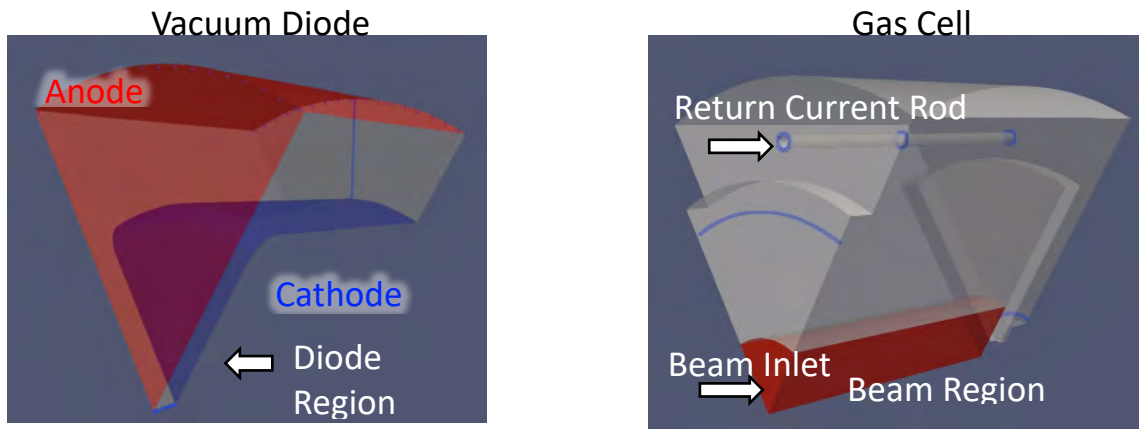


Figure 1. Three-dimensional geometries of the vacuum diode (left) and the gas cell (right) used in the particle-in-cell simulations. In the diode, the blue is the cathode boundary and red is the anode boundary driven with an idealized pulse. In the gas cell, the beam is injected into the lower red region and current is monitored at various points in the region.

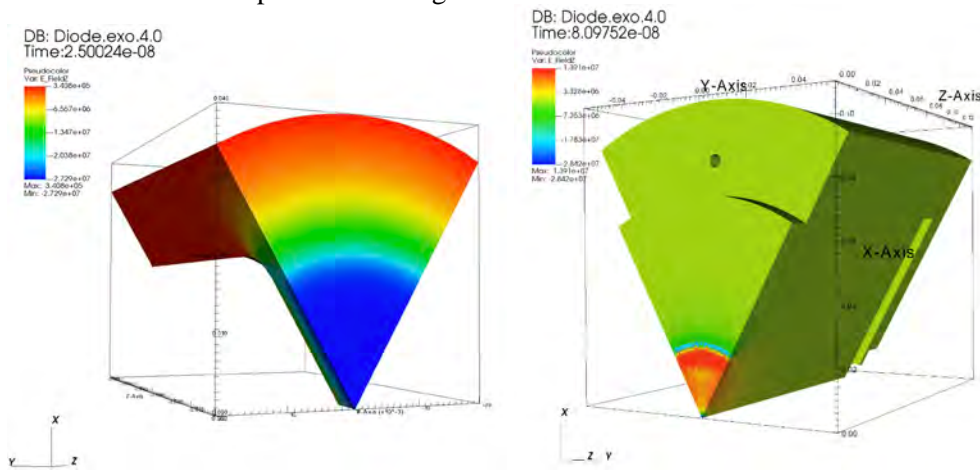


Figure 2. Quantifies the electric field in the diode (left) and the gas cell (right). At $t = 25$ ns, the diode is increasing in electric field strength and shows cathode emission. At $t = 80$ ns, the gas cell at vacuum pressure shows the electron beam injection has increased the electric field strength across the domain.

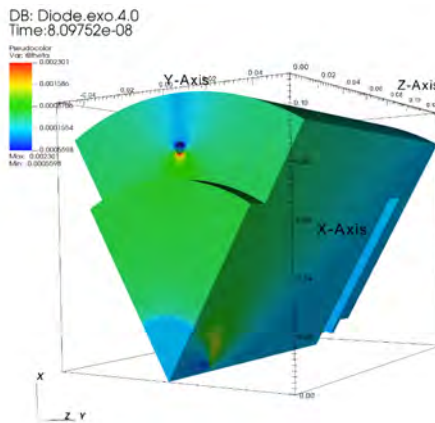


Figure 3. Quantifies the current-enclosed contour in the gas cell at vacuum. At $t = 80$ ns, the electron beam injection has increased current across the domain and a virtual cathode is forming at $z = 0.02$ m.

Title: Simulation of Passively Mode-locked and Frequency Modulated Interband Cascade Laser Frequency Combs

Author(s): I. Vurgaftman,¹ J.R. Meyer,¹ and M. Povolotskyi²

Affiliation(s): ¹U.S. Naval Research Laboratory, Washington DC; ²Jacobs, Hanover MD;

CTA: CEA

Computer Resources: HPE SGI 8600 [AFRL, OH], [NAVY, MS]

Research Objectives: 1) Use the HPC cluster to extend the numerical modeling software for interband cascade laser (ICL) frequency combs. 2) Numerical study of frequency modulated (FM) and amplitude modulated (AM) combs in ICL.

Methodology: The light propagation inside the cavity is modeled in the slowly varying envelope approximation with a single mode cavity being considered. The group velocity dispersion (GVD) of the mode without the active-layer effect is obtained from an external simulator. A stable algorithm based on the fast Fourier transform for the pulse propagation simulation allows treatment of the GVD effects up to an infinite order.

The active-layer effect is included into the light-propagation equation via a dipole polarization term. The polarization is computed by solving the semiconductor Bloch equations for the coupled electric field/electron/hole system. The major difference between the interband system and the intraband system is that in the interband system, the electron transition energy depends on the electron momenta. Therefore, the laser's performance depends on the distribution of electrons and holes over the Brillouin zone. Modeling of a nonequilibrium electron gas distribution over energy is a challenging task. In this research it is assumed that the electron-and-hole-energy relaxation time is constant, so the electrons and holes have gradually thermalized to local Fermi distributions. Previously, we used a model in which electrons and holes were thermalized instantly. A new set of equations has been developed in which the distribution functions are obtained from the particle conservation law, considering the supply current, stimulated radiative recombination, and Auger nonradiative recombination. The local charge neutrality is assumed and the ambipolar diffusion is considered. The model uses as an input the electron-and-hole subband dispersion in the cascade heterostructure, which is computed in 8-band $\mathbf{k} \cdot \mathbf{p}$ approximation.

Results: Two types of the structures have been simulated: a homogeneous cavity structure (Fig. 1a) and a structure in which the cavity has a saturable absorber (Fig. 2a). The homogeneous structure output (Fig. 1b) has a CW output with a periodic modulation. The modulation is due to the spatial hole-burning effect. The output spectrum consists of equidistant lines with an intermodal phase difference from $-\pi$ to π that is a feature of frequency modulated (FM) combs (Fig. 1c, d). For the structure with a saturable absorber, the stabilized output consists of periodically repeated pulses. The output signal is an amplitude modulated (AM) frequency comb with the intermodal phase close to zero (Fig. 2d).

The simulation results show that the numerical model can describe both FM and AM combs. The use of the HPC facility is critical for this work, especially for the FM comb simulation, because the output signal stabilizes after several microseconds (Fig. 1b). In practice, it is required to allocate about 60 wall time hours on two compute nodes (96 CPU cores) to compute the output spectrum. The AM comb simulations require less time because the signal stabilizes faster, so the results can be obtained in 2 hours.

DoD Impact/Significance: We observe that the major factor that limits the spectrum width is not the GVD of the waveguide, as it was previously believed, but the intraband relaxation of electrons and holes. The results show the necessity of further design parameter optimization for ICL combs.

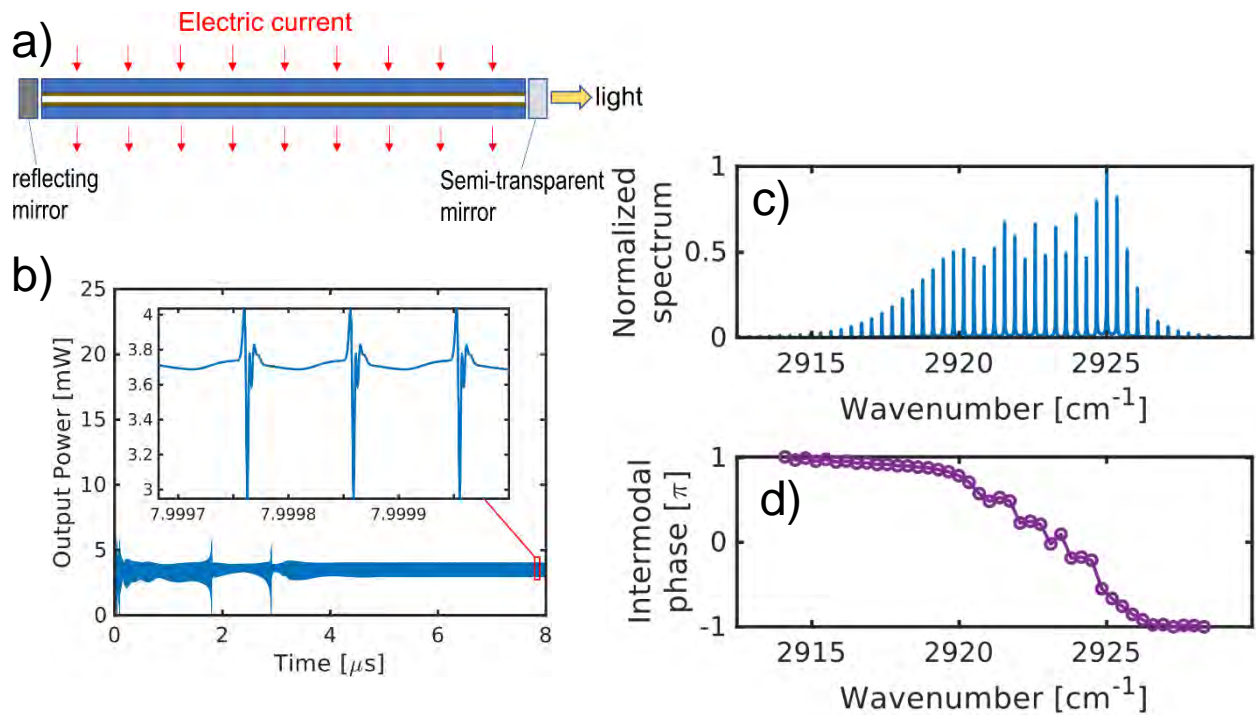


Figure 1. Simulation results for the FM comb. a) Schematic layout of the laser structure. b) Output power vs time. c) Normalized spectrum amplitude of the output signal. d) Intermodal phase of the output signal.

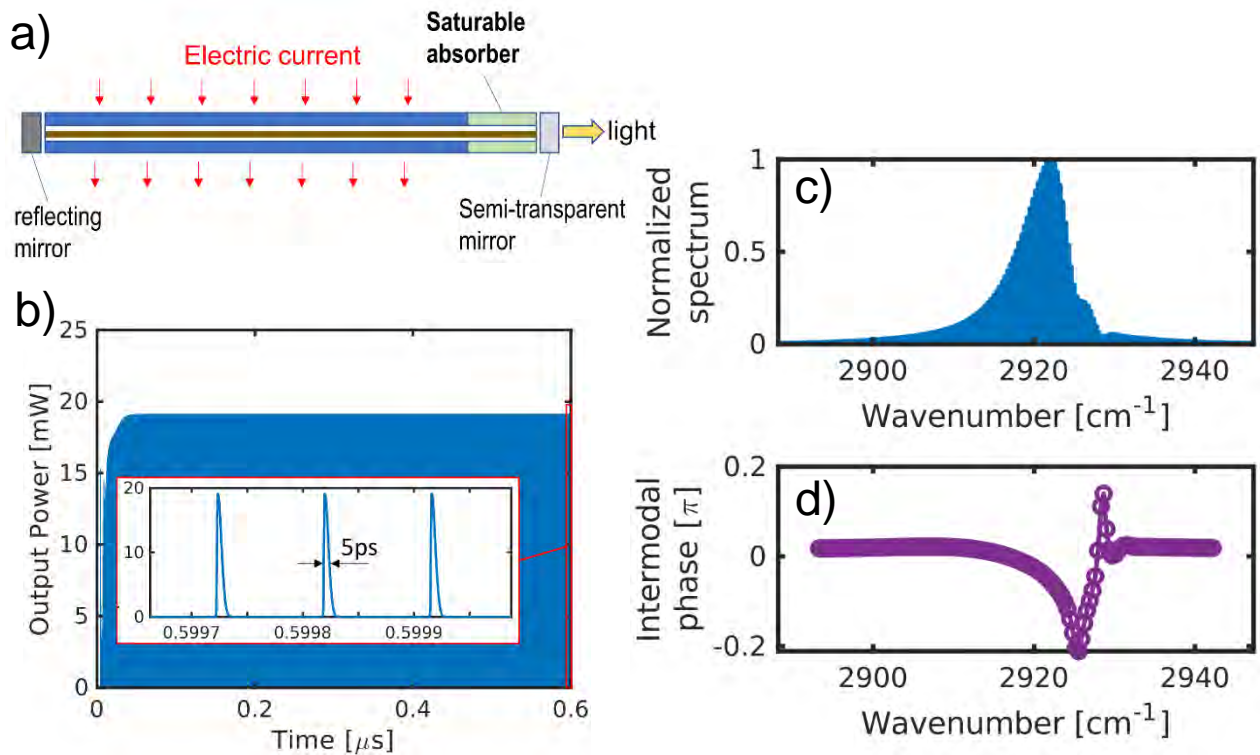


Figure 2. Simulation results for the AM comb. a) Schematic layout of the laser structure. b) Output power vs time. c) Normalized spectrum amplitude of the output signal. d) Intermodal phase of the output signal.

Title: Acoustic Parameter Variability over an Ocean Reanalysis (AVORA)

Author(s): J.P. Fabre

Affiliation(s): U.S. Naval Research Laboratory, Stennis Space Center, MS

CTA: CEA

Computer Resources: HPE SGI 8600 [NAVY, MS]

Research Objectives: Geoacoustic prediction of the seafloor is very important and is beginning to transition to the operational community. Methods of compressing ocean fields are continuing to be developed for easier storage of and transmission to forward platforms. The objectives of this effort are to develop and advance methods that improve understanding of the ocean acoustic environment for operational and fleet applications, to provide recommendations for future Navy products to support operations, and to develop prototype products for testing and evaluation.

Methodology: Investigate the NRL 30 year Ocean Reanalysis and other weather reanalyses to quantify and understand the variability of acoustic properties over various time frames for the purposes of improving battlespace awareness. With the HPC PET team, parallelize, optimize, and investigate geoacoustic predictions made with the global seabed models and compare to measurements. Identify the sensitivity of acoustic propagation and proxy parameters to environmental variability through adjoint modeling. Develop prototype products and make recommendations based on the results for products that could be derived from the described reanalyses and sediment characterizations. Such products will facilitate improved understanding of acoustic system performance and parameter variability in areas of propagation and ambient noise. Develop prototype products and compression techniques and test various ways of storing and accessing large data sets. We include recent advances in machine learning development as part of our analysis, testing, and recommendations and incorporate lessons learned into existing products. If successful, these products could become Navy standard.

Results: We evaluated our dictionary-learning-compression methods against principal-components methods and found them to be less effective, so those techniques will not move forward. We used the transfer queue to cut out (from the global reanalysis) Navy areas of fleet interest and transfer to our local and classified systems to provide input for a number of current and future efforts, including, but not limited to, data assimilation, model evaluation, and reconstruction and analysis. In a similar way, we supported NRL research experiments with timely ocean acoustic fields and prototype capabilities off the US East and West coasts. We further automated evaluation of sound speed differences between forecast increments to inform operations. This year's technical focus was on sediment characterization and compression of ocean fields of various sizes and time spans. The Global Predictive Seabed Model (GPSM) is being implemented on the HPC for use by NAVOCEANO personnel. The figure shows an estimate of marine heat flow from GPSM after Graw et al. (<https://agupubs.onlinelibrary.wiley.com/cms/asset/a532bc89-bf2d-4cb3-959d-f25012534621>).

DoD Impact/Significance: "In Joint Vision 2020, the Department of Defense's strategic plan to ensure battlespace dominance in the 21st century, a key element is information superiority enabled by emerging technologies ..." "An important aspect of information superiority is situational awareness. This implies knowing where you are, where allied and coalition forces are and where enemy forces are. It means understanding the environment, from the sea floor to the top of the atmosphere." [Heart of ForceNet: Sensor Grid, Advanced Command and Control by RADM STEVEN J. TOMASZESKI]. Our efforts directly inform environmental variability as it applies to acoustics.

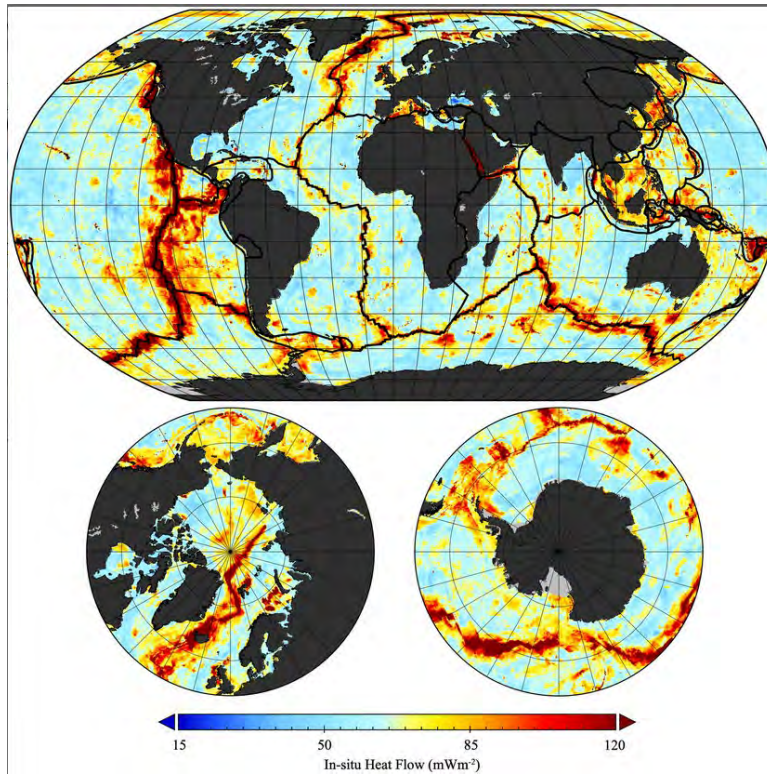


Figure 1. In-situ marine heat flow prediction. Resolution is 100 km². Black lines in top image show tectonic plate boundaries from Graw et al. (<https://agupubs.onlinelibrary.wiley.com/cms/asset/a532bc89-bf2d-4cb3-959d-f25012534621>)

Title: Intense Laser Physics and Advanced Radiation Sources
Author(s): Y.H. Chen, D.F. Gordon, J. Isaacs, and G.M. Petrov
Affiliation(s): U.S. Naval Research Laboratory, Washington, DC
CTA: CEA

Computer Resources: Cray XC40/50 [ERDC, MS]; HPE SGI 8600 [AFRL, MD]

Research Objectives: The primary objectives of this program are to model the propagation of intense, short-pulse lasers in plasmas and other nonlinear media, and to provide computational support for experiments on the NRL MATRIX laser and an intense long-wave IR laser facility at Brookhaven National Laboratory. Current areas of research include nonlinear laser propagation, interaction of short-pulse lasers with materials, novel sources of short-pulse infrared radiation, ultrahigh field physics, and laser-plasma based accelerators.

Methodology: HPC resources are utilized using several codes. turboWAVE is an object-oriented framework that contains modules designed to solve a variety of problems. Both fully explicit and ponderomotive guiding center particle-in-cell (PIC) modules are used to model relativistically intense laser pulses propagating in plasmas. Fluid modules are used to describe hypersonic flow and shock propagation in gas targets, as well as interaction of short laser pulses with metals and dielectrics for studying blow-off plasma generation. Quantum optics modules are used to describe the interaction of the laser pulse with atoms or ions. These modules can be combined, depending on the specific problem. Optimization for the latest computer architectures requires exploiting three levels of hardware parallelism: vector arithmetic units, shared memory threads, and distributed-memory processes. The framework universally supports all of these using a combination of OpenMP directives for vector and loop parallelism and the Message Passing Interface (MPI) for distributed processes. Some modules support general-purpose graphical processing units (GPGPU) via OpenCL.

HELCAAP solves a paraxial wave equation with a large number of source terms representing atmospheric turbulence, dispersion, and various nonlinear processes. HELCAAP simulates the propagation of short and high-energy laser pulses, including adaptive optics. It is often useful to run a large statistical ensemble of initial conditions. Recently, we developed PyCAP, a Python version of HELCAAP that is accelerated using just-in-time compilation, including loop-level parallelism, and takes advantage of the parallel FFTW library.

Results: Using the turboWAVE code, we conducted studies on laser interaction and ablation of metallic materials. Rapid heating and melting at the metal surface by the intense ultrashort laser pulse lead to material removal as well as plasma formation. The turboWAVE code was employed to simulate the ablation process due to its unique capabilities as a fully nonlinear hydrodynamic code with a pressure-sourced electrostatic field solver. Simulation results are shown in Fig. 1. Experimental results on ablation depths for two metals, aluminum and copper, were used to benchmark our simulations. We also investigated propagation and second-harmonic generation (SHG) of a femtosecond laser pulse in the second-order nonlinear medium, using MATLAB code. Realistic laser parameters from the experimental apparatus, including beam radius of curvature, phase mismatch, and residual dispersion from the pulse compressor, are modeled (Fig. 2).

DoD Impact/Significance: Laser propagation in turbulent atmospheres and high-power pulsed sources of long-wavelength radiation are relevant for directed energy. Laser-driven accelerators and radiation sources have potential applications for ultrafast (femtosecond) imaging of chemical and biological systems. High-energy electron beams might be useful as a gamma ray source for detection of special nuclear materials (SNM). High-energy ions might also be useful for SNM detection or for cancer therapy.

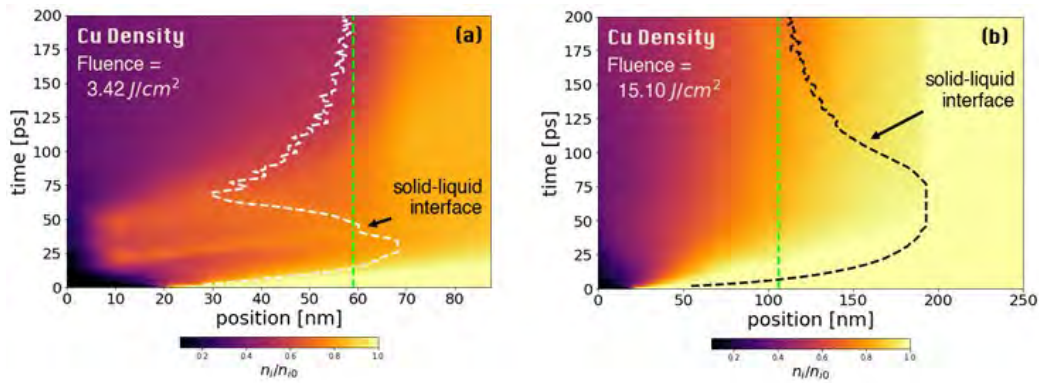


Figure 1. Cu density evolution plotted against the solid-liquid interface of the ablating surface for (a) $F = 3.42 \text{ J/cm}^2$ and (b) $F = 15.10 \text{ J/cm}^2$. In both instances, the surface is initialized at $z = 20 \text{ nm}$. The vertical, lime-green lines represent the depth at which the solid-liquid interface equilibrates. The laser pulse impinges from right to left.

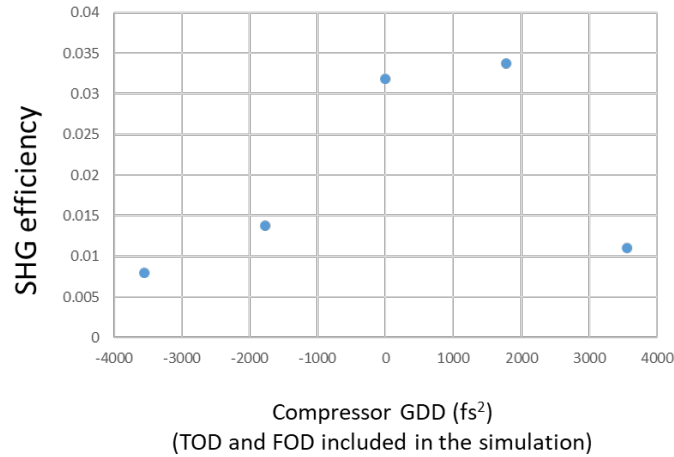


Figure 2. Second harmonic generation (SHG) efficiency of a Ti:sapphire laser pulse with 7 mJ energy in a 0.1-mm-thick BBO crystal, with respect to residual dispersion from the pulse compressor. The rest of the laser parameters are: radius of curvature $R = -1 \text{ m}$, phase mismatch $\Delta k = 100 \text{ rad/mm}$, initial laser pulse duration = 50 fs, with third-order dispersion TOD = $-45,000 \text{ fs}^3$ and fourth-order dispersion FOD = $400,000 \text{ fs}^4$.

Title: Underwater Electrical Impedance Tomography
Author(s): G.R. Gatling and E.M. Tejero
Affiliation(s): U.S. Naval Research Laboratory, Washington, DC
CTA: CEA

Computer Resources: HPE Cray EX [NAVY, MS]

Research Objectives: Use HPC computational resources to generate Jacobians and sensitivity matrices for electrical impedance tomography to facilitate imaging internal impedance structures from boundary measurements of voltage and current. Investigate image reconstruction methods for resolution and stability. Discover novel algorithms to improve inclusion detection, to increase signal-to-noise ratio, and to decrease computation costs.

Methodology: The forward solver is implemented using Python and several open-source tools, including Gmsh for generating arbitrary meshes, scikit-fem, a finite-element assembler, NumPy, which is a library of fast numeric algorithms for python based on LAPACK, and SciPy, which includes a library of sparse matrix routines used to solve the system of equations generated by the FEM. These tools have been built up into an NRL-developed electrical impedance tomography code. In FY23, we extended the research to the impedance of dipoles embedded in a uniform plasma.

Results: The tools developed have been compared to prior theoretical models and data collected in the NRL Space Physics Simulation Chamber. The results of simulations run on Narwhal compare well to both theory and data and are informing decisions regarding the optimal geometry for future plasma impedance probe designs. Shown in Fig. 1 are comparisons of the FEM model to both theory and data.

DoD Impact/Significance: There is a wide-ranging need for noninvasive remote sensing in a number of environments. Applications include biomedical imaging, characterizing fusion plasma, underwater imaging, under-seafloor mine detection, resource prospecting, and a variety of fluid process monitoring applications. Yet modern impedance tomography methods continue to present critical challenges in low signal-to-noise ratio, inherently limited resolution, intense computational costs, and slow reconstructions. Overcoming these challenges will keep the DoD on the frontier of imaging capability.

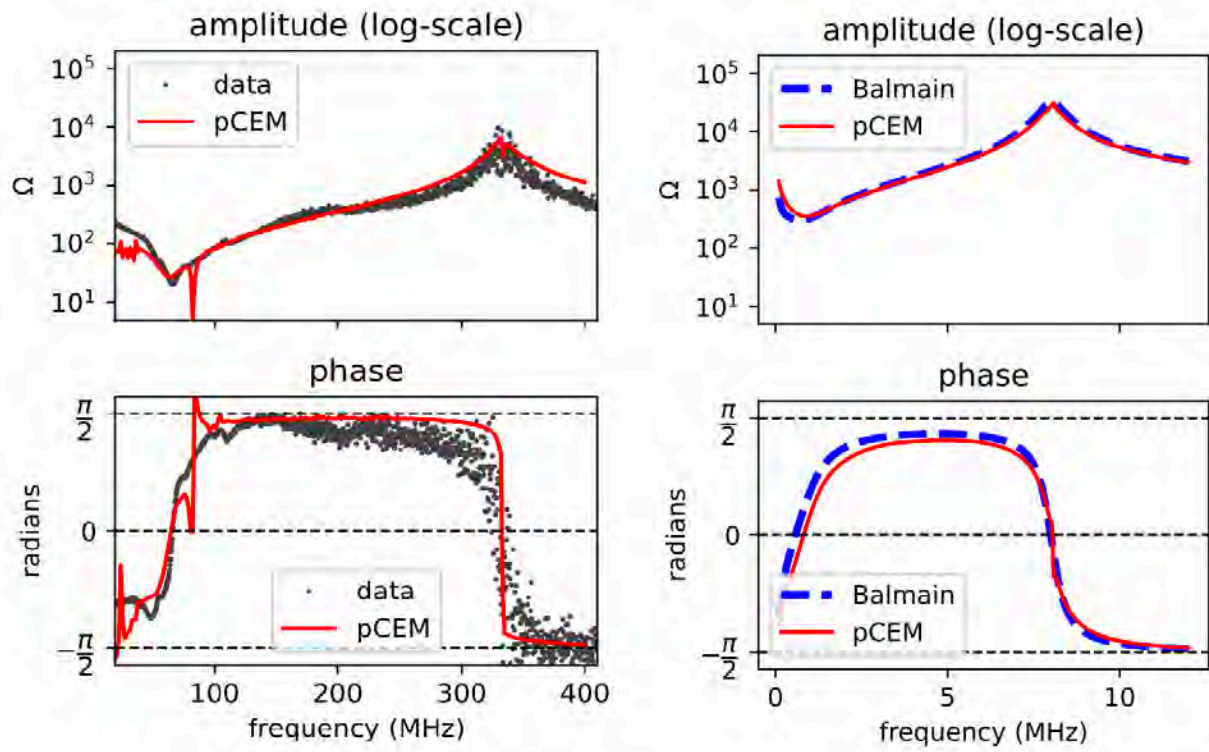


Figure 1. Comparison of the FEM model for a dipole in a plasma (the pCEM) to data from the NRL Space Physics Simulation Chamber (left) and to a simplified analytic theory (right).

THIS PAGE INTENTIONALLY LEFT BLANK



Climate Weather Ocean Modeling

CWO focuses on the accurate numerical simulation of the Earth's atmosphere and oceans on those space and time scales important for both scientific understanding and DoD operational use. This CTA includes the simulation and forecast of atmospheric variability (e.g., temperature, winds, pressure, relative humidity, cloud cover, precipitation, storms, aerosols and trace chemicals, surface fluxes, etc.) and oceanic variability (e.g., temperature, salinity, currents, tides, waves, ice motion and concentration, sediment transport, optical clarity, etc.). Numerical simulations and real-time forecasts are performed from the very top of the atmosphere to the very bottom of the ocean. CWO also includes the development of numerical algorithms and techniques for the assimilation of in situ and remotely sensed observations into numerical prediction systems. CWO has DoD applications on a daily basis for specific warfare areas, mission planning, and execution (air, ground, sea, and space), as well as for flight and sea safety, search and rescue, optimal aircraft and ship routing, and weapon system design. This CTA provides DoD with: 1) real-time, high-resolution weather and oceanographic forecasts leading to incisive decision making and enhanced operational capability in adverse weather and ocean conditions, and 2) realistic simulations of the dynamic oceanic and atmospheric environment to permit effective mission planning, rehearsal and training, and materiel acquisition.

Title: COAMPS-TC[®] Tropical Cyclone Rapid Intensification Prediction
Author(s): J.D. Doyle
Affiliation(s): U.S. Naval Research Laboratory, Monterey, CA
CTA: CWO

Computer Resources: HPE SGI 8600, HPE Cray EX [NAVY, MS]

Research Objectives: The path or track predictions of tropical cyclones (TCs) have steadily improved over the past few decades, while intensity prediction has lagged behind during the same period. This disparity is, in part, attributed to our limited capacity to accurately model the physical processes governing TC structure and intensity and the inherent sensitivity of TC forecasts to initial conditions. The primary aim of this project is to enhance and assess COAMPS-TC[®], a numerical weather-prediction system developed for predicting TCs. This system is designed to support Navy and Department of Defense (DoD) operations, as well as civilian applications. The COAMPS-TC[®] system is currently in operation at the Fleet Numerical Meteorology and Oceanography Center (FNMOC) and has recently undergone significant enhancements for both the deterministic and ensemble prediction systems. Our overall objective is to enhance COAMPS-TC's[®] predictions of TC track, intensity, and wind field.

Methodology: In the past year, advanced versions of the COAMPS-TC[®] deterministic and ensemble systems have been tested. One experiment type facilitates rapid development and testing of COAMPS-TC. Rigorous prototype testing is essential for assessing the system's performance in a statistically significant manner and requires the execution of hundreds of individual cases. This approach is indispensable for scrutinizing every incremental alteration in the development process, such as increased resolution or improved parameterizations. This rapid prototyping is indispensable for the creation and evaluation of the operational version of COAMPS-TC[®] at FNMOC. Another type of COAMPS-TC[®] application pertains to the near-real-time execution of an experimental version of COAMPS-TC[®] with more advanced capabilities compared to the operational version. The real-time testing of this experimental COAMPS-TC[®] "demonstration" system is conducted for numerous TCs across the globe.

Results: A number of different COAMPS-TC[®] configurations were tested over a large quantity of TCs in the Atlantic Ocean and Pacific Ocean basins. New versions of the deterministic and ensemble COAMPS-TC[®] systems have been transitioned to operations at FNMOC in the past two years. As an illustration of the 21-member COAMPS-TC[®] demonstration ensemble system, Fig. 1 shows an ensemble forecast for Hurricane Idalia from 1800 UTC 28 August 2023. The ensemble mean had an excellent forecast of landfall position/timing 42 h in advance (Fig. 1a) and the landfall intensity of 110 kt was well within the ensemble envelope of possibilities (Fig. 1b). COAMPS-TC[®] is one of the top TC prediction models worldwide for track, intensity and storm structure (storm size). This new, advanced version of COAMPS-TC[®], developed on the DSRCs HPE SGI 8600, HPE Cray EX, and Penguin TrueHPC indicates even greater accuracy for improved research and operational tropical cyclone applications.

DoD Impact/Significance: Tropical cyclones continue to pose a substantial threat to U.S. Navy activities. We expect that enhancing the accuracy of tropical cyclone forecasts will yield substantial cost benefits for the Navy. The latest version of COAMPS-TC[®] deterministic and ensemble systems will enable better decision-making regarding sorties and reduce exposure to hazardous weather conditions. The ongoing real-time testing and development of the system using the HPC DSRCs have resulted in substantial enhancements in the predictive capabilities of COAMPS-TC[®]. Furthermore, these advancements facilitate quicker integration into Navy operations at FNMOC. These improvements will play a crucial role in shaping the future of tropical cyclone model development in support of the Navy and the DoD. This is particularly pertinent as computational capabilities increase, enabling higher-resolution forecasts and more accurate representation of physical processes, as demonstrated in this project.

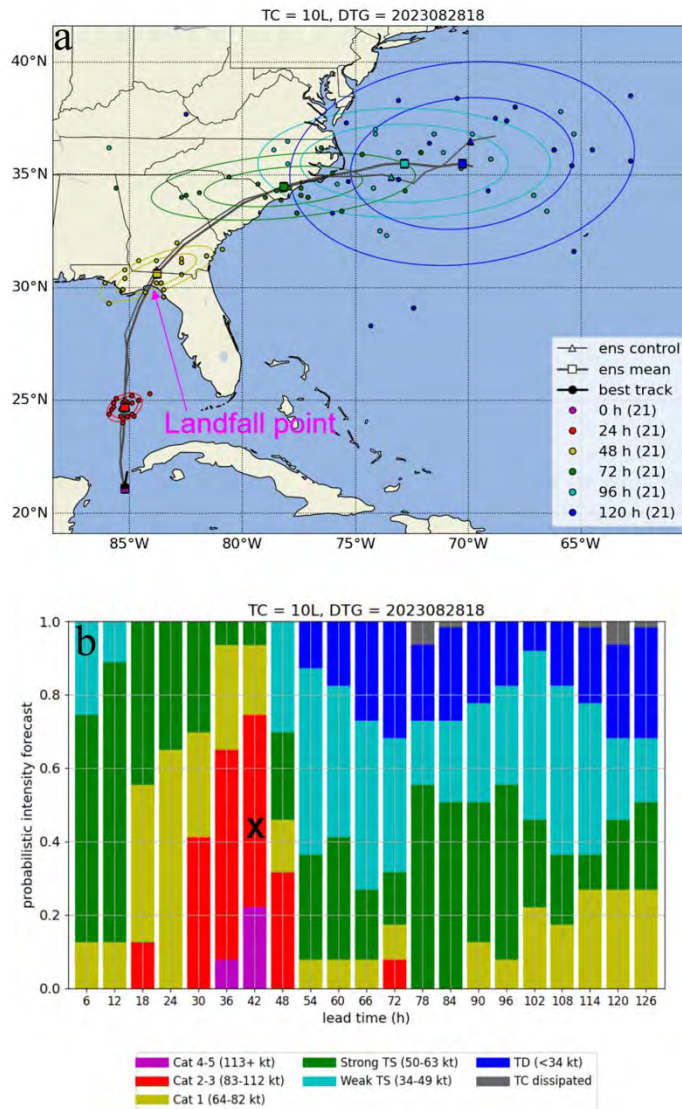


Figure 1. (a) Track and (b) intensity change forecasts from NRL’s experimental 21-member CTCX ensemble for Hurricane Idalia from 1800 UTC 28 Aug 2023. In the track forecast depicted in (a), the ensemble mean (solid line with squares), ensemble control (thin line with triangles), and best track (thick line with filled circles) are shown with shapes indicating the storm’s position in 24-h increments. The ellipses encapsulate the 1/3 and 2/3 distributions of members at various lead times in 24-h increments, with the ellipses’ major and minor axes consistent with the along-track and cross-track variance. In the intensity change forecast shown in (b), the probabilities of various intensity-change categories during successive 24-h periods are indicated, ranging from rapid intensification (≥ 30 kt intensity change in 24 h) to rapid weakening (≤ 30 kt intensity change in 24 h). The landfall point is shown in (a) and the observed intensification rate represented by the “X” in (b).

Title: Performance Study and Potential Optimization Exploration of an Ocean Modeling Code
Author(s): Y. Khine
Affiliation(s): U.S. Naval Research Laboratory, Washington, DC
CTA: CWO

Computer Resources: Cray XC40/50 [ERDC, MS]; HPE Cray EX [NAVY, MS]

Research Objectives: The goal of this project is to study the performance of HYbrid Coordinate Ocean Model (HYCOM) on various DoD HPC platforms using available compilers and profilers. HYCOM is widely used by the US Navy as the ocean component of a global coupled ocean-atmospheric-ice-wave prediction system.

Methodology: In FY23, we investigated the performance of HYCOM code on various DoD HPC systems. It is an open-source code and consists of approximately 50 routines and 10 header files, written in Fortran 90. The code is implemented with MPI and OpenMP. HYCOM is one of the benchmarks of HPCMP. We studied the available benchmark test cases as well as a realistic setup of Gulf of Mexico simulation. The test cases were simulated using different compilers on various HPC platforms. During FY23, we received support from HPCMP PET program on installation and testing of a profiler called HPCToolkit. It was installed and utilized on Narwhal (Navy DSRC) and local HPC systems at NRL, DC using various benchmarks. It is open-source software that can be installed on any HPC system, and it is straightforward to utilize and analyze the profiling results. We also explored other available profilers such as VTune, CrayPat, on DoD HPC systems to study the performance of HYCOM.

Results: Figure 1(a) presents a sample HPC Toolkit results of the Gulf of Mexico 2-day simulation. The grid size is approximately 500×380 . The run was performed on a 128-core node using 32 MPI ranks and 4 OpenMP threads per rank with GNU compiler. The profiling results can be expanded to view the details on top time-consuming routines. We observed insignificant overhead using HPCToolkit on most HPC systems. In Fig. 1(b), the overall run time was over 220 seconds, with about first 10 seconds spent on initialization of the run. The table in Fig. 1(b) summarizes the detail profiling results of the most time-consuming actions. The top two most time-consuming present OpenMP barriers, and it is obvious in the top color chart where gold and aqua colors dominate the top chart. The expanded view at 115 seconds can be seen at the bottom right of Fig. 1(b). Here, we can see large areas of OpenMP occupying the chart and showing load imbalance. We observed similar performance in the Gulf of Mexico test case using other available profilers and also using a 30-day simulation.

DoD Impact/Significance: Because ocean modeling requires a large computational domain, on the scale of kilometers, and a long physical time, over many days, it is important to achieve results in the desired time frame. The performance studies of HYCOM code indicates potential bottlenecks in the code that prevent it from performing efficiently on DoD HPC systems. Accurate ocean forecasts are very important to DoD to achieve successful missions and are also vital in preventing potential natural disasters.

Scope	CPUTIME (sec):Sum (I)	CPUTIME (sec):Sum (E)
Experiment Aggregate Metrics	2.89e+04 100.0%	2.89e+04 100.0%
<thread root>	2.17e+04 75.1%	
<program root>	7.19e+03 24.9%	
<partial call paths>	7.45e-01 0.0%	

Figure 1. (a) Sample profiling results including inclusive and exclusive time of the simulation.

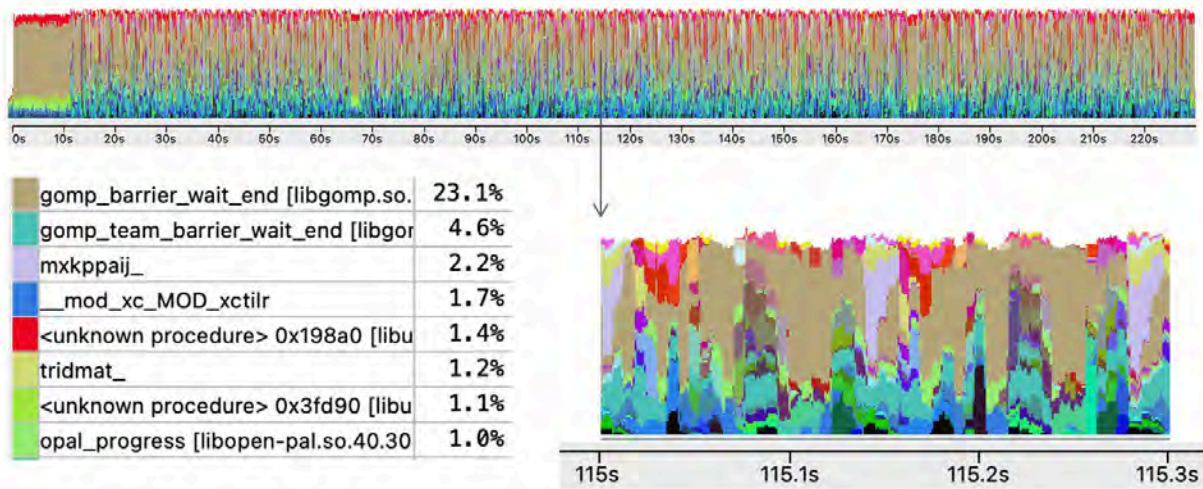


Figure 1. (b) Details of HPC Toolkit profiling results of Gulf of Mexico 2-day simulation.

Title: Coastal Mesoscale Modeling

Author(s): P.M. Finocchio

Affiliation(s): U.S. Naval Research Laboratory, Washington, DC

CTA: CWO

Computer Resources: SGI ICE X, Power 9 [ARL, MD]; Cray XC40/50 [ERDC, MS]; HPE SGI 8600, HPE Cray EX [NAVY, MS]

Research Objectives: The coastal zone is characterized by mesoscale weather phenomena that adversely affect Navy operations. Sharp gradients of wind, temperature, moisture, aerosols, refractivity, and visibility exist in the lowest kilometer of the atmosphere in the coastal zone. Such mesoscale variability also exists in the ocean. Accurate prediction of coastal mesoscale meteorological phenomena requires coupled land-ocean-atmosphere numerical forecast systems that represent dynamics from the synoptic scales to the scales of the largest eddies. The objective of this project is to develop and validate a fully coupled coastal/littoral modeling system that can be used to provide high-resolution (< 5 km) analyses, nowcasts, and short-term (0- to 120-h) forecasts for tactical sized areas of the world. This system is used for basic and applied research leading to improved understanding of Navy-critical atmospheric and oceanic processes.

Methodology: The primary tool being developed, tested, and utilized for research in this project is the Coupled Ocean/Atmosphere Mesoscale Prediction System (COAMPS®). The atmospheric component of COAMPS® is made up of a data-assimilation system, an initialization procedure, and a multinested, nonhydrostatic numerical model. The numerical model includes parameterizations for cloud, precipitation, and radiation processes, as well as for surface and boundary-layer effects. The NRL Coastal Ocean Model (NCOM) is currently used for the simulation of the mesoscale ocean circulation response to the atmospheric forcing in one-way and two-way interactive modes. The Noah Land Surface model is currently used to simulate land surface processes and exchanges with the atmosphere. COAMPS® has also been modified to predict electro-optical quantities of interest for directed-energy applications.

Results: In FY23, HPC resources were used to run very-high-resolution (< 10 m) simulations that revealed a secondary shear instability resulting in the breakdown of Kelvin-Helmholtz (KH) billows (Fig. 1). Understanding the development and breakdown of KH billows is important because these circulations act to deepen the turbulent atmospheric boundary layer. In addition, COAMPS® simulations conducted as part of the FATIMA field campaign highlighted the importance of ocean-atmospheric coupling for the prediction of marine fog. Unlike other operational models, COAMPS® was uniquely capable of predicting fog formation in the Yellow Sea because the interactive ocean model captured tidal mixing along the shelf that brought cool seawater toward the surface (Fig. 2). A number of research projects also resulted in publications in FY23, including projects focused on the development of a new, coast-aware surface flux parameterization, land-atmosphere interaction, observation impact data-assimilation experiments, air-sea interactions in tropical cyclones, and novel machine-learning-based approaches to improve cloud forecasts. Furthermore, the development of the Navy's next-generation global numerical weather prediction system, NEPTUNE, continued in FY23.

DoD Impact/Significance: COAMPS® continues to play a significant role in providing atmospheric forecasts in support of Navy missions involving the deployment of weapons systems, strike warfare, radar propagation, and search and rescue. Research and development performed at HPC DSRCs have led to significant improvements in the predictive skill of COAMPS® that will greatly benefit the operational performance of COAMPS®. The HPC DSRCs will be the primary computing resources in FY24 and beyond for the development of the fully coupled COAMPS® system, including the emerging electromagnetic and electro-optical (EM/EO) and ensemble capabilities for COAMPS®.

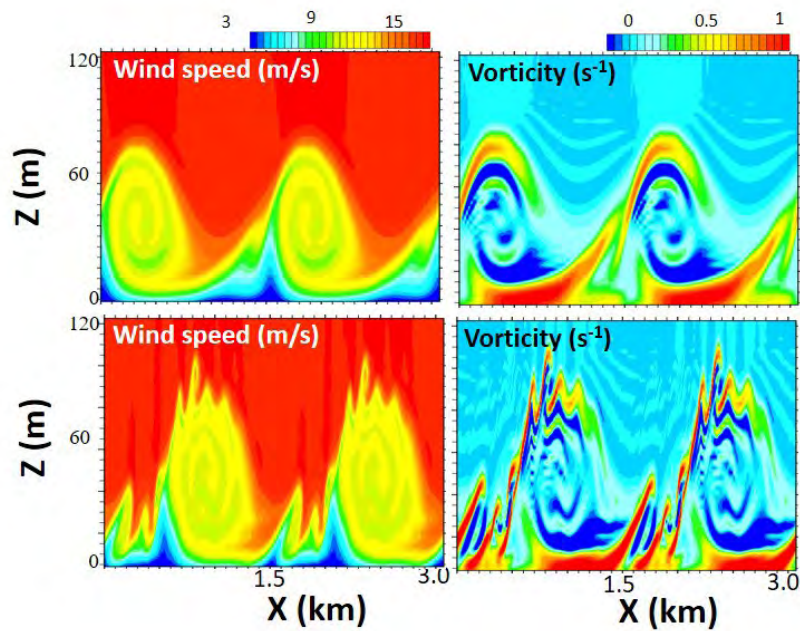


Figure 1. Vertical cross sections of wind speed (left, m/s) and span-wise vorticity (right, s^{-1}) at two different times corresponding mature KHBs (left) and onset of the secondary shear instability (right), respectively (Courtesy: Dr. Qingfang Wang, Code 7533)

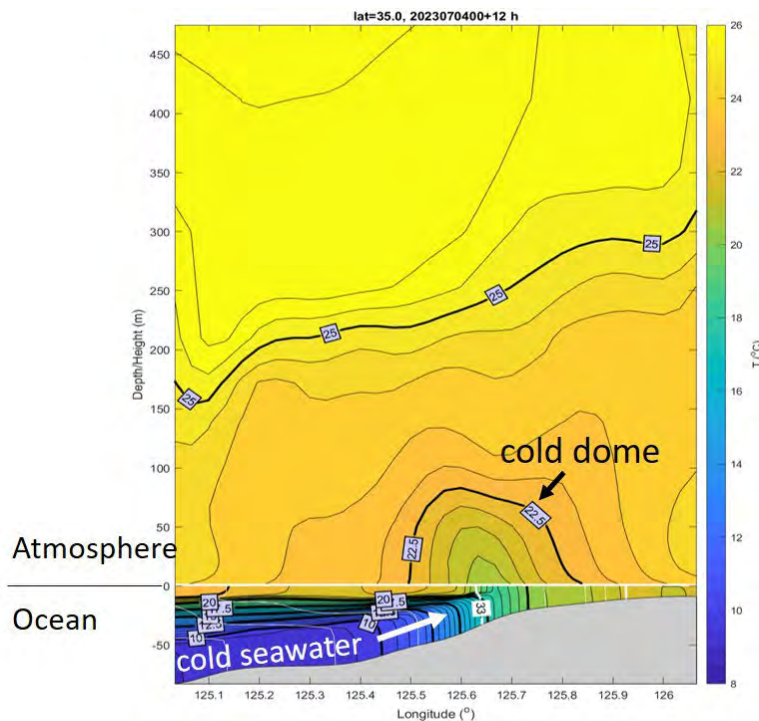


Figure 2. A vertical cross section along a constant latitude (35° N) of the air and water temperature (filled contours and black contours with interval 0.5 K), and salinity (white contours) in the Yellow Sea from a 12-hour coupled atmosphere-ocean COAMPS[®] forecast, valid on 4 July 2023 at 12 UTC. The tidal front pushes deep cold water toward the surface along the sloping shelf, resulting in a cold SST patch and a subsequent cold dome of air, creating favorable conditions for fog occurrence. (Courtesy: Dr. Saša Gaberšek, Code 7533)

Title: Coupled Ocean-Wave-Air-Ice Prediction System

Author(s): R. Allard,¹ T. Campbell,¹ E. Douglass,¹ D. Hebert,¹ T. Jensen,¹ G. Panteleev,¹ M. Phelps,² and T. Smith¹

Affiliation(s): ¹U.S. Naval Research Laboratory, Washington, DC, ²Peraton, Inc., Stennis Space Center, MS

CTA: CWO

Computer Resources: HPE SGI 8600, HPE Cray EX [NAVY, MS]

Research Objectives: Perform research studies with the Coupled Ocean Atmosphere Mesoscale Prediction System (COAMPS[®]) meteorological forecast model, which is six-way coupled with the Navy Coastal Ocean Model (NCOM), WAVEWATCH III[®] (WW3) and SWAN wave models, and the COAMPS[®] atmospheric model. Perform modeling studies with the Community Ice Code (CICE v6), which includes a landfast ice parameterization. Perform storm surge and inundation modeling studies with the Delft3D Flexible Mesh modeling system.

Methodology: For accurate simulation and prediction on regional scales in the tropics, we have used various configurations of NRL's state-of-the-art fully coupled atmosphere-ocean-wave model system COAMPS[®] with very high spatial and temporal resolution. One component under development for the COAMPS[®] model is the generation of spatially varying coefficients for grounding and tensile strength for landfast ice in Arctic regions. These spatially varying parameters will be used in regional COAMPS-CICE and Navy Earth System Prediction Capability (ESPC) V2 ensemble and deterministic forecast systems.

Results: We performed landfast ice (LFI) studies using CICE6 for the Arctic. We divided the Arctic into 10 subregions covering the Beaufort, Chukchi, East Siberian and Laptev seas. Using a conjugate gradient optimization technique, we developed spatially varying LFI parameters based on a series of experiments performed for the periods of October 1, 2015/2017–July 31, 2016/2018. We found the best results for the East Siberian Sea in comparison with USNIC data. In this region, grounding is the dominant factor in the formation of LFI. In regions such as the Laptev Sea, where both grounding and ice arching can contribute to LFI formation, our technique underpredicts the formation of LFI. This may be attributed to our limitation of a maximum water depth of 35 m for grounding and our decision to avoid nonphysical high values for tensile strength, which could have resulted in more LFI. We performed Antarctic LFI testing using differing values of tensile strength (k_t) and grounding k_1 for the period of March 1–December 1, 2019. A regional CICE6 Antarctic domain was set up on a $1/12^\circ$ grid extending from -45°S to the pole. Results showed only minor improvement. We next tried starting the simulation in January 2019 (2 months earlier), but that too showed little improvement. We tested increasing the number of subcycles in the elastic viscous plastic (EVP) solver from 240 to 720. This showed a significant improvement. Additional tests included increasing the number of subcycles from 720 to 1440, but no improvement was shown. Lastly, we initiated testing with grounded icebergs. Using data from the National Ice Center, we incorporated four grounded icebergs into CICE6 by setting the bathymetry at that location to 0; this showed improved results. We set up a 1 km Baltic Sea CICE domain with data assimilation. We used NAVGEM forcing to perform a 2-month test. This will be one of the regions used in validating the fully coupled COAMPS-CICE system. We began processing Sentinel 3A and 3B data and converting freeboard to ice thickness. ESPC snow depth was used in the conversion.

DoD Impact/Significance: The development of a coupled air-ocean-wave prediction system can have a pronounced effect on Navy forecasting by improving ASW performance, tropical cyclone prediction, search and rescue, and mission planning. The relocatable COAMPS-CICE system will provide high-resolution Arctic forecasting of ice thickness, ice drift, and concentration to support navigation. Inclusion of landfast ice in the Navy's global ice prediction systems will yield a more realistic representation of pan-Arctic sea ice.

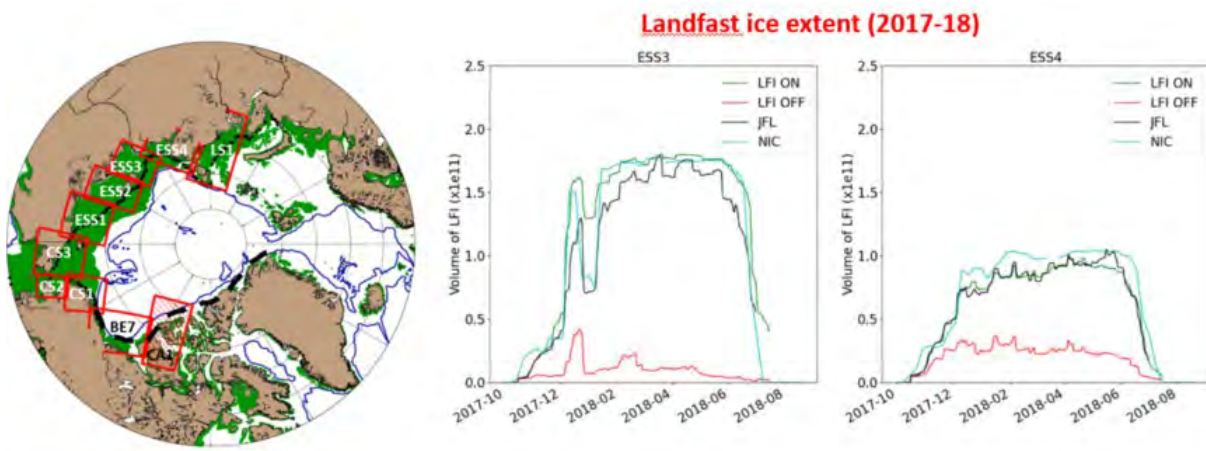


Figure 1. Nine regional CICE Arctic domains shown left, depicting 2 km regions for testing landfast ice parameterization in CICE6. Middle and Right plots depict modeled versus NIC observations for two regions in the East Siberian Sea. Red line denotes model simulation with landfast ice turned off. NIC line showed in cyan; JFL run depicts default settings as recommended by Lemieux et al. (2015, 2016). Optimized solution shown in green.

Title: Dynamics of Coupled Models

Author(s): I. Shulman, A. Thombs, S. Matt, and S. Cayula

Affiliation(s): U.S. Naval Research Laboratory, Stennis Space Center, MS

CTA: CWO

Computer Resources: HPE SGI 8600 [NAVY, MS]

Research Objective: Improve our understanding of coupled bio-optical and physical processes in the coastal zone and the variability and predictability of the coastal ocean's optical properties on time scales of 1–5 days. Investigate the coupled dynamics of ocean bio-optical, physical, and atmospheric models.

Methodology: The approach is based on using nested, coupled physical-bio-optical models of the coastal region together with bio-optical and physical in-situ and remotely sensed observations. Data-assimilation techniques for both physical and bio-optical fields are being used to examine project research issues and objectives. Approach is also based on joint studies of the bioluminescence (BL) potential and inherent optical properties (IOPs) over relevant time and space scales. Dynamical, biochemical, physical, and BL potential models are combined into a methodology for estimating BL potential and nighttime water-leaving radiance (BL_w).

Results: Bioluminescence is light produced by organisms through chemical reaction. In most cases, marine organisms produce mechanically stimulated bioluminescence, which is commonly measured as a bathyphotometer BL potential, defined as mechanically stimulated light measured inside a chambered pump-through bathyphotometer. We have developed a numerical model of a pump-through bathyphotometer (Fig. 1) and have used STAR CCM (2021.2), a computational fluid dynamics solver, for the modeling of the Lagrangian particles flow as an approximation of marine taxa flow. We have investigated a distribution of residence times of particles in the detection chamber of bathyphotometer, as well as statistical distributions of the rate of strain experienced by particles passing through the inlet and the detection chamber. We have found that all particles remain in the detection chamber for at least 0.25 seconds. This suggests that the total first flash of autotrophic dinoflagellates and, for example, heterotrophic dinoflagellates *Protoperdinium* will be measured by the bathyphotometer based on existing literature about their respective flash durations. At the same time, CFD simulations demonstrated that around 90% of particles experienced the rate of strain equals 100 s^{-1} (the well-known threshold for the mechanical stimulation of dinoflagellates *Gonyaulux*) in the inlet of the bathyphotometer, indicating high probability of prestimulation before particles enter the detection chamber. Also, our modeling results have demonstrated a very low sensitivity of particle residence time in the detection chamber to the variations in their sizes, density, or the depth of the instrument deployment.

DoD Impact/Significance: Emerging Navy electro-optical (EO) systems under development and special operations missions require an improved understanding of the ocean optical environment. This is critical for operations and weapon deployment, especially in the coastal and littoral zones. Improved basin-scale-to-mesoscale forecast skill is critical to both military and civilian use of the oceans, particularly on the continental margins.

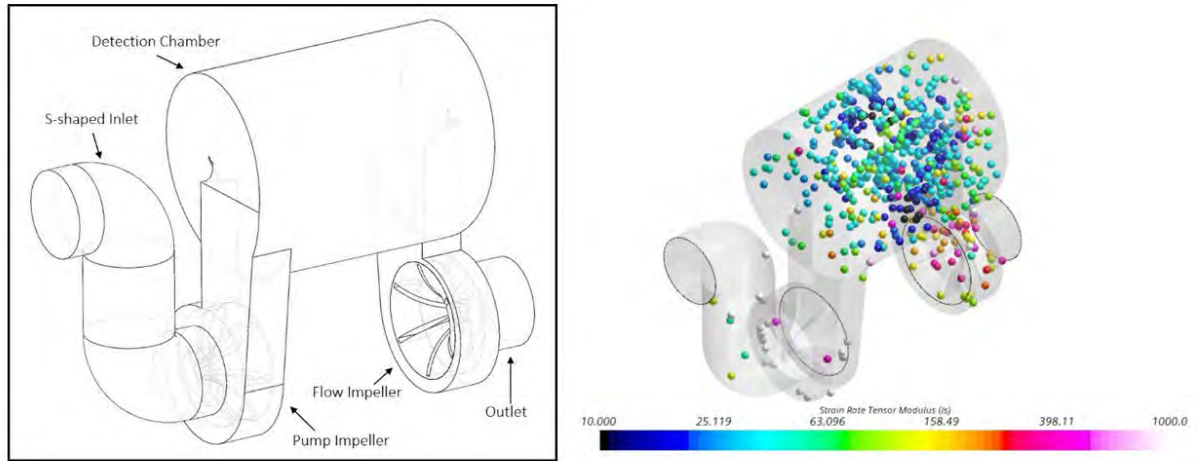


Figure 1. The model of bathyphotometer on the left. The snapshot of the Lagrangian particles distribution in the bathyphotometer. Particles are colored as a function of their experienced instantaneous rate of strain.

Title: Rogue Wave Probability Estimator for WAVEWATCH III®
Author(s): M. Orzech
Affiliation(s): U.S. Naval Research Laboratory, Stennis Space Center, MS
CTA: CWO

Computer Resources: HPE SGI 8600 [NAVY, MS]

Research Objectives: The primary objective of this project is to provide the Navy with software enabling WAVEWATCH III® (WW3) to estimate the relative threat of rogue waves throughout the global ocean. The system that we have created is limited to deep-water wave environments. It employs an empirically based lookup table to determine a rogue threat index (RTI) using several scalar metrics that represent the contributions of selected environmental causal factors. Tabulated values of RTI are based on established theory and extensive analysis of representative sea states. The effort to transition the system began in May 2020. A 20-year WW3 reanalysis with wave-current interaction was completed in FY20, and the rogue threat utility was fully implemented in WW3. The system calibration was completed in FY21, including development of the RTI lookup table. The system was fully validated in FY22, and a VTR was approved and published. Objectives for FY23 included: 1) operational testing of the WW3 v5.16 system in preparation for transition of software to Fleet Numerical Meteorology and Oceanography Center (FNMOC), and 2) implementation of a modified version of the system in WW3 v6.07 in preparation for inclusion in a transition of COAMPS® (planned for either FY24 or FY25). The first objective was significantly delayed due to ongoing staffing issues at FNMOC, while the second objective was completed.

Methodology: In FY23, efforts to transition the WW3 v5.16 rogue threat estimator primarily consisted of intermittent discussions with FNMOC representatives. The initiation of operational testing was repeatedly postponed owing to delays in completing the transition of the WW3-IRI system (within which the rogue threat estimator will eventually operate). It is hoped that this testing will begin by mid-FY24, pending resolution of staffing issues at FNMOC. The rogue wave threat estimator that is currently being transitioned was developed and fully validated within a standalone copy of WW3, version 5.16, the same version that is currently being used for operational forecasts by FNMOC. An additional objective of the transition project is to integrate the rogue threat estimator into a coupled COAMPS-WW3 system. To better align with the next version of COAMPS® that is expected to transition to FNMOC, it was necessary to incorporate the rogue threat code into version 6.07 of WW3. This work was completed in FY23, entailing substantial modification of eight primary Fortran modules along with several additional model input and configuration files. After resolving a variety of compilation issues, the adapted WW3 model was tested (in stand-alone configuration) using several standard test cases from the model's "regtests" directory. Following this, a successful global simulation was completed on gaffney. In FY24, we plan to combine the adapted WW3 code with COAMPS® and to conduct additional tests of the coupled system.

Results: The tests of WW3 v6.07 with the rogue threat estimator have produced qualitatively reasonable results (Fig. 1). Although it was not possible to directly validate the output of the new code with measured data, the WW3 v6.07 system produced RTI estimates for the global domain that were nearly identical to those generated by the same software in the operational version of WW3 v5.16. There is again clear evidence of the impact of wind and current fields on the RTI forecast, and we are continuing to investigate what appear to be anomalously elevated RTI values in some shallower coastal regions.

DoD Impact/Significance: Accurate prediction of environmental hazards is important to tactical and strategic operations in the world's oceans. This configurable WAVEWATCH III® rogue threat utility will enhance the safety of Navy missions and will reduce the potential for damage or loss of Navy assets in rogue wave events.

Global Map of RTI, 1/2/2020, 1200hr (WW3v6.07)

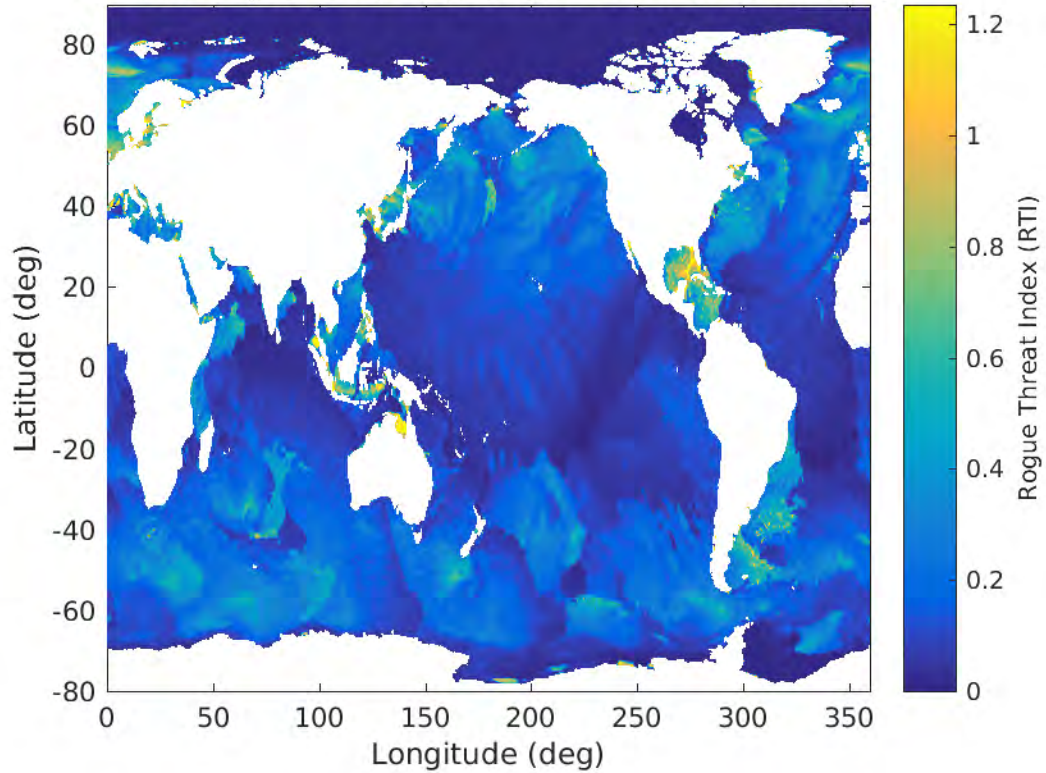


Figure 1. Estimated values of rogue threat index (RTI) for global domain, computed with WAVEWATCH III® v6.07 for three-hour period beginning at 1200 hours on 02 January 2020. Results are nearly identical to those computed with WAVEWATCH v5.16 for the same date and time.

Title: Eddy-Resolving Global/Basin-Scale Ocean Modeling - The Atlantic Ocean's Deep Water Origins
Author(s): R.W. Helber, G. Panteleev, S.R. Smith, and J.F. Shriver
Affiliation(s): U.S. Naval Research Laboratory, Stennis Space Center, MS
CTA: CWO

Computer Resources: HPE SGI 8600, HPE Cray EX [NAVY, MS]

Research Objectives: *NRL 6.1 The Atlantic Ocean's Deep Water Origins:* Understand and quantify kinematics and dynamics governing the evolution of high-northern-latitude-originated water and the circulation feeding the lower limb of the Atlantic Meridional Overturning Circulation. A major goal is to understand the modified ocean dynamics resulting from recent decadal changes in the subsurface hydrographic structure of the Arctic and sub-Arctic seas. The focus is the physical processes governing circulation and water formation, sea-ice retreat, increased fresh water from the Greenland ice sheet, and flow through the Denmark Strait. This project will lead ultimately toward a greater capability to forecast the subsurface ocean structure in Navy-relevant high-latitude oceans that influence sea ice and the moving origins of Atlantic Ocean deep water.

Methodology: The approach is to use the Navy's state-of-the-art numerical ocean modeling capabilities along with the latest in situ observations available through the research community. We investigate, for example, the processes that govern the surface circulation in the Iceland and Irminger Seas resulting from increased freshwater input from the Greenland ice sheet. To accomplish this, we have created regional Navy Coastal Ocean Model (NCOM) simulations with outer 4 km and inner 1 km horizontal resolution nests. The outer nest is a Lambert conformal grid domain covering the Nordic Seas from the Fram Strait to the southern tip of Greenland. We have twin experiments, for both inner and outer nests, with and without freshwater runoff from Greenland. These numerical modeling and tracer release experiments have led to a greater understanding of the evolution of freshwater runoff and its impact on the circulation along the east coast of Greenland.

Results: The NCOM simulations of the Nordic Seas capture the observed current structure along eastern Greenland. Our simulations show a continuous current structure along the eastern Greenland shelf, consistent with prior research, extending along the coast southward toward Cape Farewell at the southern tip of Greenland, where the currents strengthen. From an analysis of the fresh water in the twin simulations, volume-integrated salinity shows that the full domain decreased in salinity by -0.04% while the continental shelf region decreased by -0.26% . The deep ocean, however, decreased only by -0.01% . Calculating the mass of salt in both simulations, with and without fresh water, indicate that most of the fresher water remains on the continental shelf and around Iceland, where a large freshwater runoff exists (Fig. 1).

DoD Impact/Significance: The Navy needs accurate ocean forecasts and because of amplified high-latitude warming, circulation in the tactically relevant Greenland/Iceland/United Kingdom (GIUK) gap is changing. Decreasing sea ice coverage and subsurface hydrographic changes in the seas surrounding the Arctic Ocean are causing the origins of Atlantic Ocean deep water to change. This research accounts for this variability, leading to new forecasting capabilities for high-resolution ocean circulation and sea-ice predictions useful for Navy operations in the GIUK region. This project has led, in part, to the 6.4 project "Ocean Currents for Integrated Operations in Contested Environments."

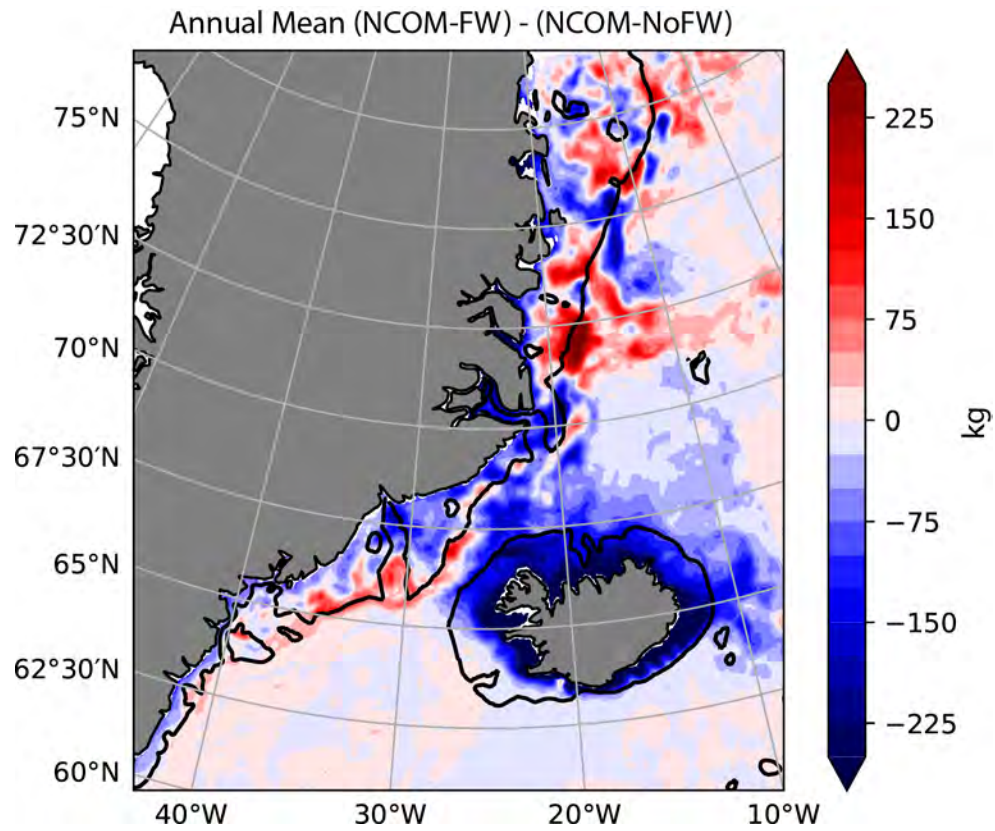


Figure 1. The difference in the mass of salt in kg over the full depth of the ocean, between the NCOM simulations, “with” minus “without” Greenland freshwater runoff, averaged over one simulation year. Blue areas indicate a reduction in salt mass for the simulation with freshwater runoff. The black contour is the 350 m isobath.

Title: Eddy-Resolving Global/Basin-Scale Ocean Modeling - Navy ESPC Participation in NOAA SubX
Author(s): E.J. Metzger
Affiliation(s): U.S. Naval Research Laboratory, Stennis Space Center, MS
CTA: CWO

Computer Resources: HPE SGI 8600, HPE Cray EX [NAVY, MS]

Research Objectives: *Navy ESPC Participation in the NOAA NCEP Subseasonal eXperiment (SubX):* NOAA NCEP SubX is a multimodel subseasonal prediction experiment designed around operational requirements with the goal of improving subseasonal weather forecasts at NOAA's Climate Prediction Center (CPC) (Pegion et al. 2019).

Methodology: Navy Earth System Prediction Capability (ESPC) is one of seven forecast systems that constitute the multimodel ensemble. Using initial conditions from operational NAVGEM 2.1 for the atmosphere and GOFS 3.1 for the ocean and sea ice, a time-lagged ensemble of 45-day ESPC forecasts are generated Saturday, Sunday, Monday, and Tuesday of each week. Atmospheric and ocean output are postprocessed and posted on a password-protected URL for uploading by the CPC. Temperature and precipitation anomalies relative to the long-term model climatology provide subseasonal predictions for each forecast system. The combined multimodel ensemble then provides guidance for CPC forecasters. Pathfinder hours and the associated higher-priority queues were essential for timely submission of the near-real-time Navy ESPC forecasts.

Results: Navy ESPC has been contributing forecasts to NOAA NCEP SubX in near real time since September 2017. The FY23 HPC hours allowed for that to continue. The forecast submission is an automatic process and manual intervention was only required if a system problem caused the metascheduler to lose track of the ensemble. Figure 1 is an example of week 3–4 2 m air temperature anomalies from all the members of the multimodel ensemble. In general, Navy ESPC shows the same subseasonal trends, although there are spatial differences.

DoD Impact/Significance: Navy ESPC participation in the NOAA NCEP SubX project adds an additional forecast system to the multimodel ensemble, thereby increasing model spread that generally leads to better ensemble prediction. CPC uses the forecasts to provide early warning for extreme weather events (heat waves, extreme cold, drought, or flash flooding) that allow for risk reduction and disaster preparedness, potentially preserving life and resources.

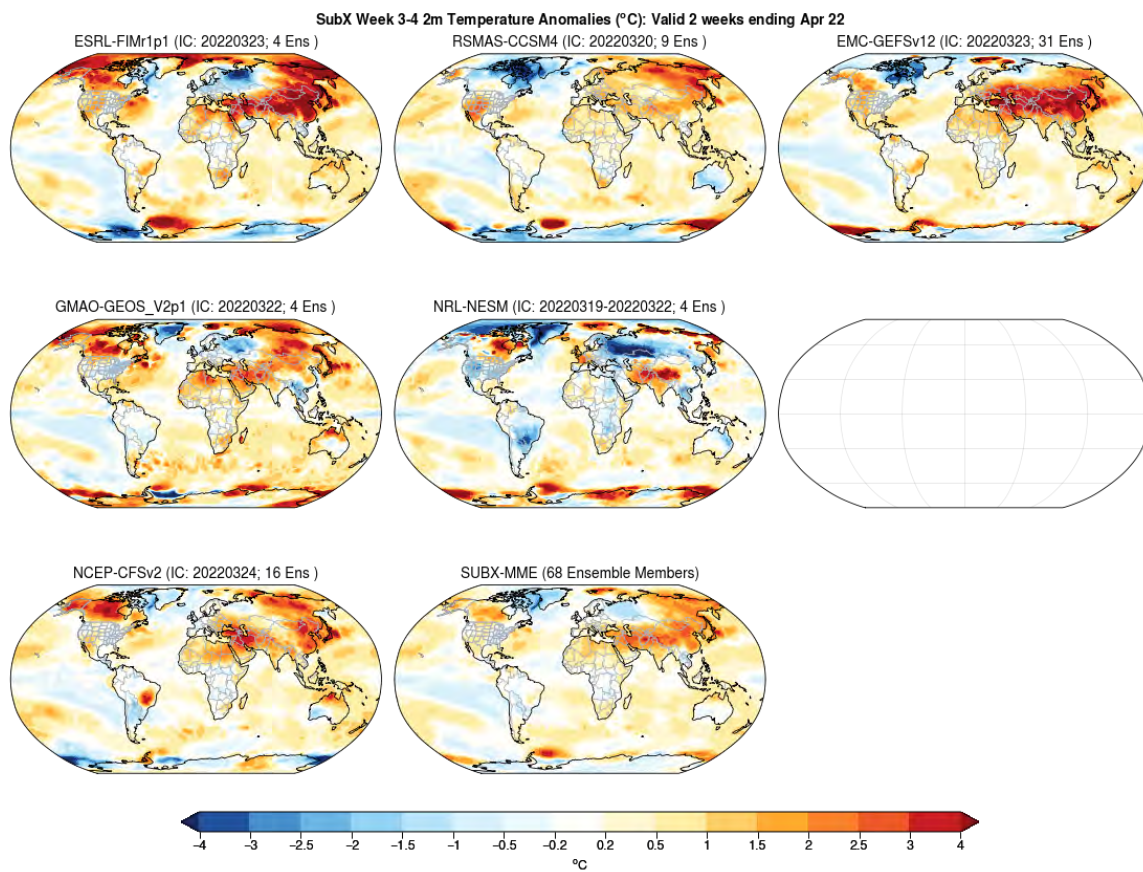


Figure 1. NOAA NCEP SubX Week 3–4 2 m air temperature anomalies (°C), valid for the 2 weeks ending 22 April 2023. The Navy ESPC contribution is the middle row, middle panel. The multimodel ensemble mean is the bottom row, right panel. The other panels are contributions from other groups.

Title: Eddy-Resolving Global/Basin-Scale Ocean Modeling - Winter-mixing Intermittency in the Northern Arabian Sea

Author(s): P.G. Thoppil

Affiliation(s): U.S. Naval Research Laboratory, Stennis Space Center, MS

CTA: CWO

Computer Resources: HPE SGI 8600, HPE Cray EX [NAVY, MS]

Research Objectives: The project aims to identify and isolate the role of mesoscale eddies on the convective formation of water masses and to quantify the physical processes associated with it. The long-term goal of this project is to understand the impact of mesoscale eddies and fronts on the air-sea interaction and how and why such interaction modifies the upper-ocean convection and water mass formation through turbulent heat fluxes.

Methodology: The project utilizes both idealized and realistic simulations using Hybrid Coordinate Ocean Model (HYCOM), complemented by data analysis.

Results: During winter, prevailing northeasterly trade winds bring dry, cool air to the northern Arabian Sea, leading to surface ocean heat loss and convective mixing. The conventional belief is that this mixing injects nutrients into surface waters, exerting dominant control over winter productivity. However, this explanation falls short capturing the significant year-to-year variations in productivity. Here, we introduce an alternate perspective, supported by observational evidence, revealing that widespread winter productivity is triggered by intermittent mixed-layer restratification mediated by atmospheric high-pressure systems. As these weather systems, characterized by clockwise circulation, move south, the southwesterly winds to the west transport warm, humid air into the northern Arabian Sea. This increase in specific humidity reduces latent heat flux, leading to surface heat gain by the ocean. Coupled with abundant sunlight due to clear skies and reduced turbulent mixing from weak winds, this environment extends the residence time of phytoplankton cells in the euphotic layer, fostering the development of a bloom.

DoD Impact/Significance: Ocean convection occurs in regions of surface buoyancy loss in winter and plays an important role in the stratification of water columns. Convective mixing is highly inhomogeneous in regions of mesoscale eddy activity, where propagation of sound speed becomes complex and less predictable. Improved knowledge of the interaction between mesoscale eddies and convective mixing will lead to a better representation of acoustic parameters in ocean models.

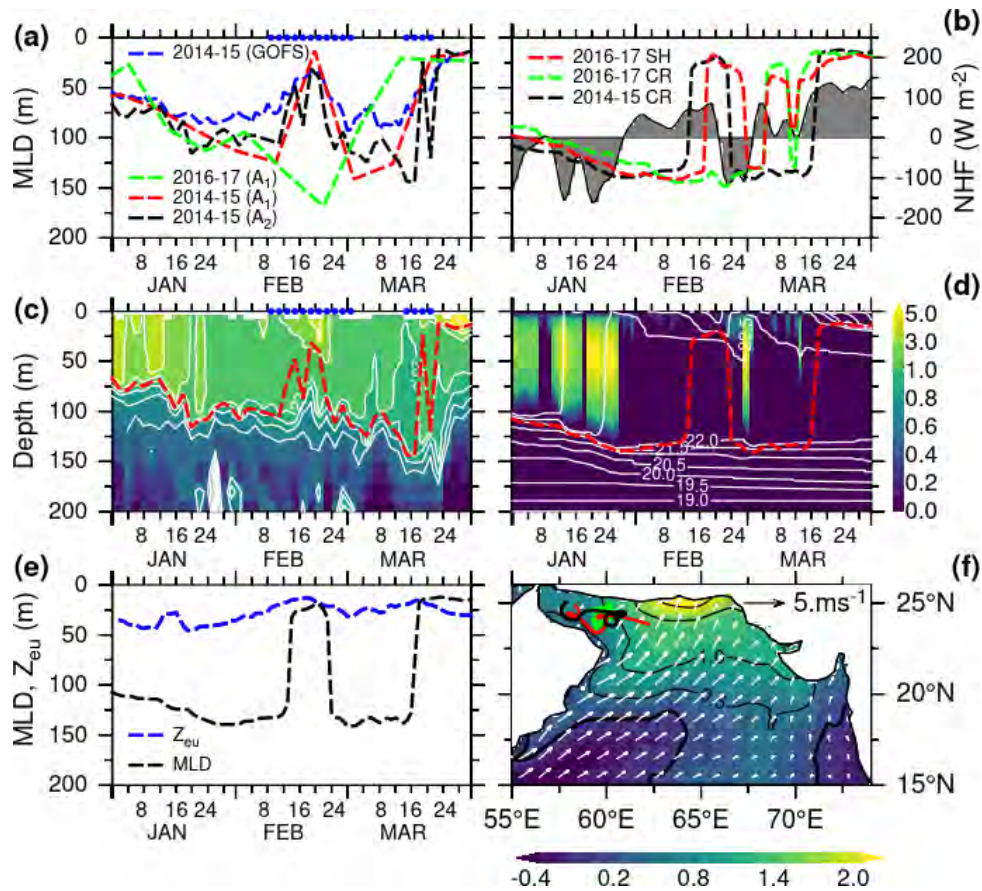


Figure 1. Winter-mixing intermittency and stratification during 2014–2015 winter. (a) Mixed layer depths (MLD, m) from two along-track Argo observations (A_1 and A_2) in the northwestern Arabian Sea including the Gulf of Oman in winter (A_1 : red, A_2 : black) 2014–2015 (A_1 : green) 2016–2017, and (blue) box-averaged MLD from GOFS (58° – 66° E, 18° – 26° N) during 2014–2015. (b) One-dimensional (1D) model MLD at 62° E, 25° N from the control run (CR) during (black) 2014–2015 (green) 2016–2017, and (red) 2016–2017 specific humidity (SH) perturbation experiment. This experiment is designed to isolate the atmospheric forcing that caused 2014–2015 mixed-layer restratification by prescribing specific humidity from 2014–2015 forcing while retaining all other forcing from 2016–2017. One-dimensional (1D) model net heat flux (NHF, W m^{-2}) during 2014–2015 is shaded in gray. (c) Along-track Argo (A_2) temperature profiles ($^\circ\text{C}$, shaded with contours $> 21^\circ\text{C}$) and MLD (red, dashed line). (d) 1D model temperature profiles (contours), MLD (red, dashed line), and temperature diffusivity (shaded, $10^3 \text{ cm}^2 \text{ s}^{-1}$), proxy for turbulent mixing. (e) MODIS-Aqua derived daily euphotic depth centered around 1D model location (61° – 63° E, 24° – 26° N) smoothed using 5-day boxcar filter (blue, dashed line) compared to 1D model MLD (black). (f) February 2015 monthly anomalies of vector wind (m s^{-1}) and anomalies of specific humidity (g kg^{-1} , shaded with contours) from the CFSR. Blue circles in Figs. 1a and 1c mark the periods of mixed-layer restratification induced by atmospheric high-pressure systems.

Title: Eddy-Resolving Global/Basin-Scale Ocean Modeling - Enabling Operations Across Ocean Fronts/Eddies

Author(s): E.J. Metzger and C. Trott

Affiliation(s): U.S. Naval Research Laboratory, Stennis Space Center, MS

CTA: CWO

Computer Resources: HPE SGI 8600, HPE Cray EX [NAVY, MS]

Research Objectives: *6.4 Enabling Operations Across Ocean Fronts/Eddies:* Enable Navy vessels dependent on the acoustic environment to exploit oceanographic fronts and eddies for search-and-avoidance operations. The two main objectives are: 1) advance front and eddy placement accuracy in forecasts for predicting acoustic changes across these oceanographic features by adding new capabilities to the data-assimilation employed by the Global Ocean Forecast System (GOFS)/Earth System Prediction Capability (ESPC) and the regional Coupled Ocean Atmosphere Mesoscale Prediction System (COAMPS®) to improve the accuracy of fronts and eddies, and 2) develop automated frontal detection and eddy-tracking tools and provide assistance to the operational center's subject-matter experts (SMEs) in product generation sent forward to fleet users.

Methodology: This project will a) address shortcomings in front and eddy placement in Navy global and regional ocean-prediction systems by assimilating new data streams (e.g., SWOT altimeter data), and using more advanced multiscale and adaptive sampling data-assimilation techniques, and b) develop automated frontal detection and eddy-tracking software for use by the SMEs at the operational centers.

Results: A significant amount of work this past year was associated with refactoring of the Navy Coupled Ocean Data Assimilation code case ensuring all past advancements are incorporated into the most up-to-date version. Bit-for-bit reproducibility was demonstrated when running either Navy Coupled Ocean Data Assimilation (NCODA) v4.4 or v5.0 prep routines. A process to create the masked area within which a front meanders throughout the year was established. This masked area is written to a file that is read to identify the region in which the front gradient is to be found. The code now reads the file dimensions from the gradient file metadata allowing the flexibility of running on a variety of different file dimensions. If directed in the parameter file, this means an NxN moving window can now be used to reduce the gradient grid size. This decreases the run time and removes the artifact of the fronts tracing back and forth across adjacent pixels when the gradient ridges are broad. Monthly and seasonal eddy climatologies based on GOFS 3.1 reanalysis output are completed for the six Navy-relevant regions. An example of percentage likelihood for anticyclonic eddies is shown in Fig. 1 for the western Pacific Ocean.

DoD Impact/Significance: The advancements to data assimilation in the global ocean-prediction systems will lead to a reduction in error in the location of fronts and eddies, mixed-layer depth and upper ocean temperature. The incorporation of SWOT will take advantage of this new data stream early in the altimeter life cycle. It will also allow better utilization of Navy glider assets by assimilating more profiles on smaller space scales. The automated frontal detection and eddy-tracking tools will assist in product generation of Ocean Feature Analyses and Tactical Oceanographic Features Assessments produced by FNMOC and sent forward to fleet users.

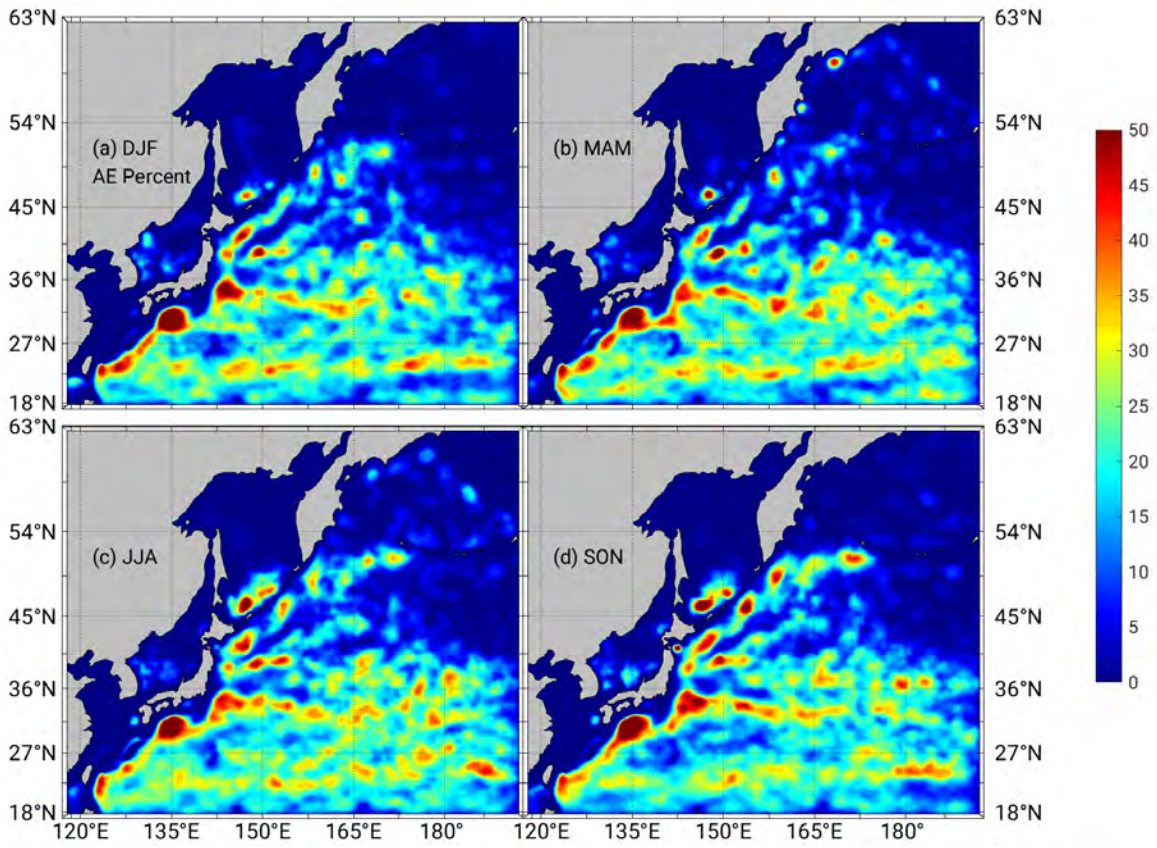


Figure 1. Seasonal percentage likelihood of anticyclonic eddies in the western Pacific Ocean based on 30 years of GOFS 3.1 reanalysis output.

Title: Eddy-Resolving Global/Basin-Scale Ocean Modeling - An Evaluation of the Uncertainty of Internal Tides using HYCOM Ensembles: Implications for Predictability and Future Improvements

Author(s): J.F. Shriver and E.J. Metzger

Affiliation(s): U.S. Naval Research Laboratory, Stennis Space Center, MS

CTA: CWO

Computer Resources: HPE SGI 8600, HPE Cray EX [NAVY, MS]

Research Objectives: To assess how well HYCOM represents internal tides in comparison to observations. To examine this research question, we are using the coupled ocean-atmosphere Navy Earth System Prediction Capability (ESPC)-developed ensemble system with tides to 1) assess the spread of the M_2 phase-locked internal tide and 2) assess where the observations sit in relation to the cloud of possible solutions.

Methodology: Ensemble weather forecasting is used by agencies such as the National Oceanic and Atmospheric Administration (NOAA) and the European Centre for Medium-Range Weather Forecasts (ECMWF) to provide not just forecasts, but also estimates of their uncertainty. At the U.S. Naval Research Laboratory, we are developing a coupled ensemble Navy Global Environmental Model (NAVGEM) - global HYCOM with tides system, which we use in this work to explore the limits of internal tide predictability.

Results: The analysis period we are considering spans September 2020–August 2021. A total of 12 ensemble members were run, and the standard deviation of the of the M_2 internal tide amplitude-weighted phase is shown in Fig. 1a. The largest internal tide spread is found at low latitudes, possibly connected to the connection between internal tide incoherence/tropical current connection. Large areas of more diffuse spread cover most of the world’s oceans, with areas of lowest spread is the southern Indian, southern Pacific, and high-latitude regions. The magnitude of the spread is generally a factor of 10 smaller than the mean amplitude-weighted phase. To better understand the relative impact of this spread, we normalize the internal tide spread (Fig. 1a) by the mean amplitude-weighted phase (Fig. 1b) to obtain the relative spread (Fig. 1c). The relative spread is largest in the tropical Pacific and Northern Hemisphere western boundary currents, coinciding with areas where the mean amplitude-weighted phase is small.

To evaluate where observations sit in relation to the cloud of possible solutions, we compare M_2 internal tide amplitude and phase from each of the 12 ensemble members against those from an altimeter-based tidal analysis, focusing on the western Pacific (Fig. 2). We find that the amplitude along ascending tracks in this region agree qualitatively well with the observations, including matching “wiggles” in the observation curves. We also note similarly good qualitative agreement between the ensemble system and observed phase across this region of interest. In terms of spread, we can have spread in amplitude, phase or a combination of the two. We note larger spread in phase, with areas of spread including east of Japan around 45°N and at low latitudes. Given the likely sources of error, most notably errors in depicting the time-varying medium through which the internal tides propagate (which would affect arrival time), phase is a likely area where we’d see the larger spread.

DoD Impact/Significance: Data-assimilative eddy-resolving models are important components of global ocean and sea ice-prediction systems. Tactical decision aids (TDAs) and mission-planning tools (MPTs) based on these systems provide vital enabling capabilities for the Navy at spatial scales ranging from operational areas to entire theaters and over time horizons ranging from a few hours to many months. An estimate of the spread/uncertainty of the simulated internal tides in global HYCOM would be valuable guidance for those who would use these models as decision-making aids or boundary conditions for regional models.

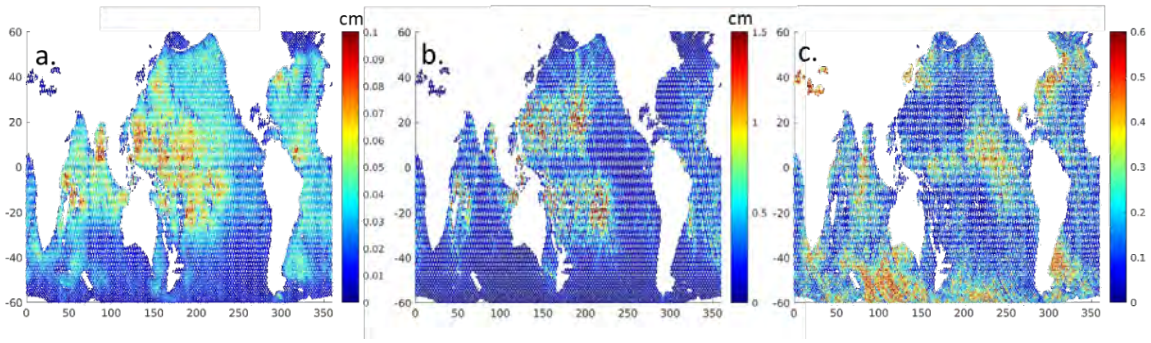


Figure 1. (a) standard deviation of M_2 internal tide amplitude-weighted phase (defined as amplitude \times cos (phase)), (b) mean M_2 internal tide amplitude-weighted phase and (c) the ratio of the mean amplitude-weighted phase spread to its mean (panel (a) / panel (b)), depicting the relative spread of the M_2 internal tide.

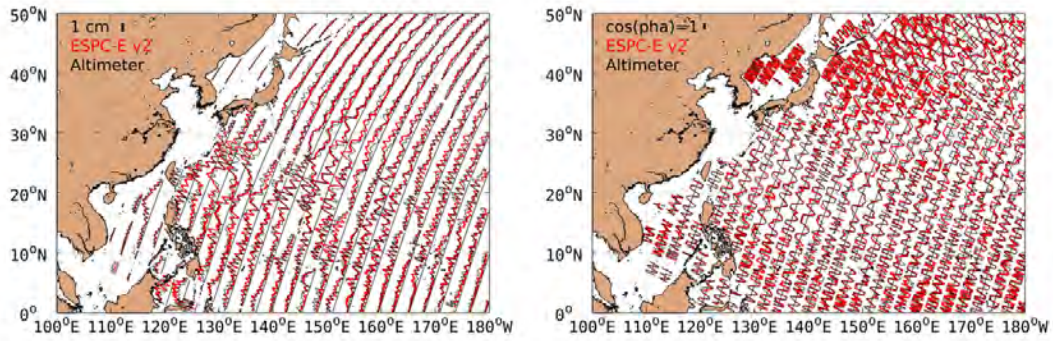


Figure 2. M_2 internal tide amplitude (cm, left) and $\cos(\text{phase})$ (right) along ascending tracks from the ensemble ESPC (ESPC-E) system (black) and an altimeter-based tidal analysis (red) in the western Pacific Ocean. Each of the 12 ensemble members is plotted, so areas where the red lines appear thicker or thinner are indicative of more or less spread, respectively. For amplitude, the line showing the coordinates of the track represents zero amplitude for the tides on that track.

Title: Eddy-Resolving Global/Basin-Scale Ocean Modeling - Accelerating Ocean Forecasts Through Mixed Precision Data Representation

Author(s): C. Rowley,¹ P.G. Thoppil,¹ K. Obenschain,² J. Boris,² Y. Khine,² R. Rosenberg,² G. Patnaik,³ and T. Jensen¹

Affiliation(s): ¹U.S. Naval Research Laboratory, Stennis Space Center, MS; ²U.S. Naval Research Laboratory, Washington, DC; ³Alion Science and Technology Corporation, Hanover, MD

CTA: CWO

Computer Resources: HPE SGI 8600, HPE Cray EX [NAVY, MS]

Research Objectives: Our objective is to reduce the memory-access bandwidth in Navy ocean forecast models through mixed-precision data representation. The goal is to advance speed and skill in current- and next-generation ocean forecast systems. We are working with the HYbrid Coordinate Ocean Model (HYCOM) and the Navy Coastal Ocean Model (NCOM). HYCOM is the global ocean forecast model used in the current and planned operational Global Ocean Forecast System (GOFS) and Earth System Prediction Capability (ESPC) systems, and the resource requirement for HYCOM is a primary limiting factor in the size and forecast range of the ESPC Ensemble Forecast System. NCOM is the regional ocean forecast model used in the Coupled Ocean Atmosphere Mesoscale Prediction System.

Methodology: Our approach is to implement mixed numerical precision in the Navy's operational global and regional forecast ocean models and to assess the impact on physics. We are identifying and isolating the sensitivity of the model calculations to mixed precision by systematically reducing the numerical representation from standard 64-bit to 32-bit (and eventually to 16-bit) floating-point type in model subcomponents. We will apply standard timing and skill metrics to evaluate the sensitivity to precision; western boundary jets, equatorial currents, and high-latitude areas with low stratification will all respond differently to changes in the numerics of horizontal and vertical advection and mixing, so we will initially evaluate the mixed-precision results in regional simulations in a variety of dynamical regimes to identify sensitive model calculations before testing in global configurations. We will test the HYCOM results by implementing similar changes in NCOM. Future CPUs will natively support half-precision data types, so we will implement simple methods to explore using a 16-bit floating-point type in key model components. This may include identifying opportunities for memory bandwidth reduction through alternate strategies (e.g., scaling variables to 16-bit integers in memory and rescaling for computation on the CPU, and using a longer effective time step for slower processes).

Results: In FY23, we developed a stand-alone Gulf of Mexico HYCOM comparable to the ESPC ensemble grid resolution/layer structure using realistic initial, surface, and lateral boundary conditions, and sufficient input data so that the model can be integrated to 30 d (Fig.1). The longer integration allows for more complete profiling of the code with sufficient sampling to accurately characterize the model subcomponent computational resource use. Initial tests at 32-bit resolution using a simplified configuration showed approximately 40% savings relative to the standard 64-bit resolution, with no significant change to the model output (testing with the realistic Gulf of Mexico setup is underway). Profiling the HYCOM code has indicated other avenues to improve HYCOM performance. FY24 plans include an additional HYCOM model configuration and initial testing of the ESPC global ensemble forecast with HYCOM compiled with 32-bit resolution.

DoD Impact/Significance: This work will lead to near-term gains in computational speed in current-generation HYCOM systems, and long-term gains from including reduced precision in next-generation ocean model and data-assimilation system development, enabling ocean forecast models with similar skill at reduced computational cost, enabling potential improved physics: increased vertical and horizontal resolutions, higher-order advection, more complex subgridscale parameterizations, and richer ensembles.

2-day GOM simulation; salinity ~ 0 – 60; temperature ~ 15°C – ~35°C

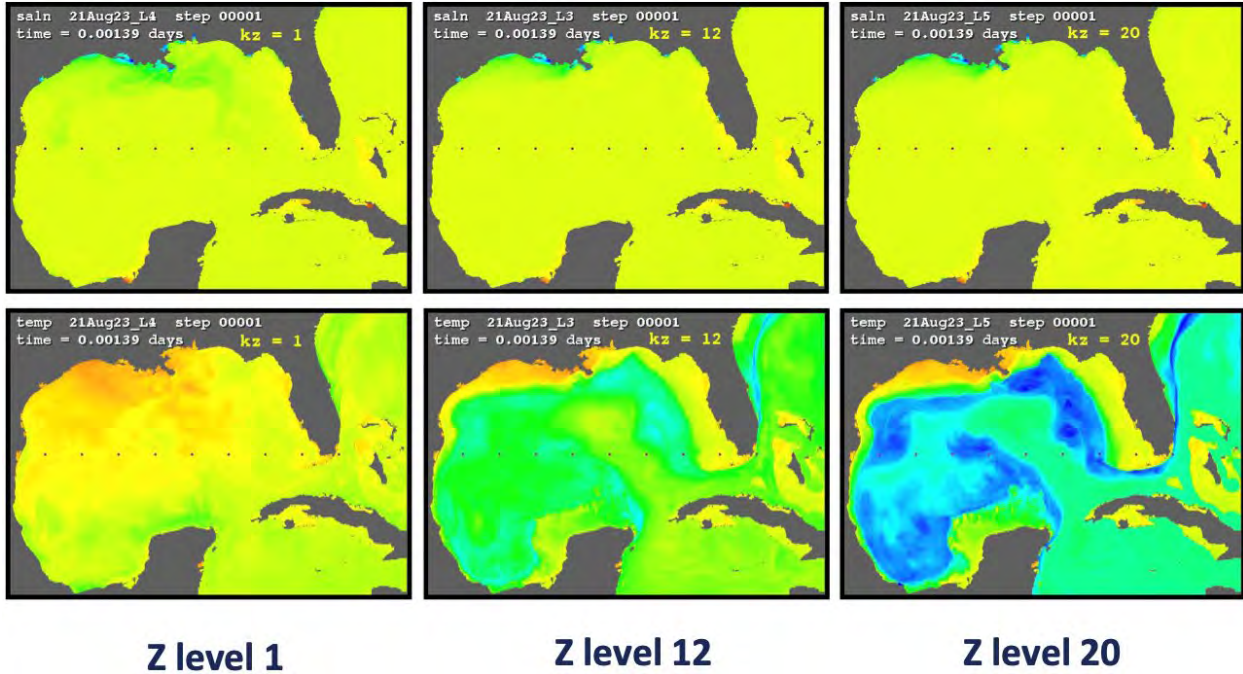


Figure 1. Gulf of Mexico HYCOM salinity (top) and temperature (bottom) at 48 hours, from three HYCOM layers ($k = 1, 12, 20$). The realistic configuration is being used for code profiling and mixed-precision tests.

Title: Eddy-Resolving Global/Basin-Scale Ocean Modeling - Sea Bottom Warfare

Author(s): C.A. Blain,¹ Z. Yu,² T. Jensen,² and T. Campbell²

Affiliation(s): ¹U.S. Naval Research Laboratory, Washington, DC; ²U.S. Naval Research Laboratory, Stennis Space Center, MS

CTA: CWO

Computer Resources: HPE Cray EX, HPE SGI 8600 [NAVY, MS]

Research Objectives: Our Navy must have the capability to sense and understand what is in and what is happening in the deep ocean. The work undertaken addresses this capability gap with its focus on developing a means to simulate and quantify deep ocean currents, particularly in the South China Sea (SCS).

Methodology: To achieve the objective, two components are demonstrated: 1) a robust capability for simulating basin-wide ocean circulation patterns throughout the water column in the SCS, and 2) a regional ocean model (hundreds of meters) simulation capability in the SCS that is appropriately configured to capture dynamics associated with deep flows including those in the bottom boundary layer. A large-eddy-simulation (LES) model is applied in the ocean's deep-bottom-boundary layer to facilitate the determination of deep-ocean-model components, such as algorithms, parameter settings, and configurations, that enable the prediction of ocean currents below 1000 m and their associated bottom-boundary flows.

Results: 1) Two global HYbrid Coordinate Ocean Model (HYCOM) simulations (with focus on the SCS) were integrated from 2016 to 2019 from the same initial state. The only difference between the two simulations is the tidal forcing. Hourly eddy viscosity/diffusivity in June 2019 from the K-Profile Parameterization (KPP, the default turbulence closure of HYCOM) were saved to study the effect of tides on turbulence at Luzon Strait in the SCS (black line in Fig. 1, left). Differences between the monthly mean eddy viscosity in June 2019 from the HYCOM simulation with tides minus the no-tides case (Fig. 1, right) clearly suggests that tides increase eddy viscosity in the ocean interior while mainly suppressing viscosity in the ocean surface boundary layer. 2) To more efficiently and accurately resolve the deep-ocean boundary layer, a generalized vertical coordinate (GVC) system is implemented in the regional ocean model, COAMPS-NCOM. This coordinate system is terrain-following, uses level layers in upper water columns, increases resolution near the surface and the bottom, maintains uniform expansion and contraction of layer thickness with depth, and allows disappearing levels in shallow water. The result is no artificial vertical current jets over the sea mount slope in contrast with the solution based on z-levels. Furthermore, the GVC system can attain the same ocean-bottom-boundary-layer resolution using less overall vertical levels, making it more computationally efficient.

DoD Impact/Significance: Naval warfare is turning to high-endurance, long-range unmanned systems with intelligence, surveillance, and reconnaissance (ISR), electronic warfare (EW), and lethal strike capabilities. These systems will increasingly occupy the deep ocean for transit and loiter operations. Low-cost, high-reliability unmanned underwater vehicle (UUV) operations require long-duration energy management that must account for surrounding dynamic maritime environments. The ocean bottom also hosts an array of critical infrastructure such as fiber-optic cables and pipelines, which may require defending. Advancing the modeling-and-simulation capabilities within the deep ocean at high resolution offers new opportunities to advance this future operational paradigm. Knowing the expected strength, location, and frequency of the deep-ocean and bottom-boundary-layer currents at scales of hundreds of meters enables applications in energy harvesting and CONOPS for swarms of UUVs.

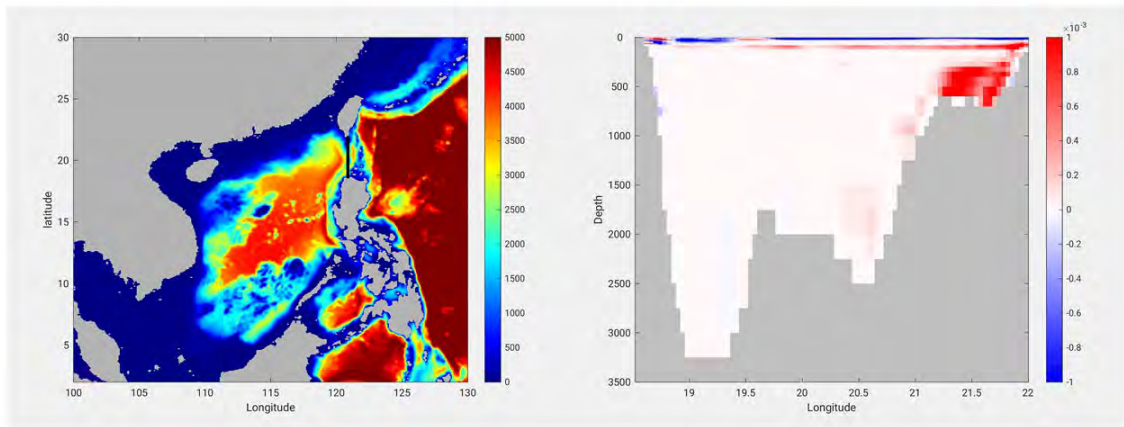


Figure 1. (Left) South China Sea bathymetry with the Luzon transect marked as a black line. (Right) The differences (tides/no tides) of the monthly mean eddy viscosity (m^2/s) in June 2019 along the Luzon Strait transect from global HYCOM simulations in the SCS.

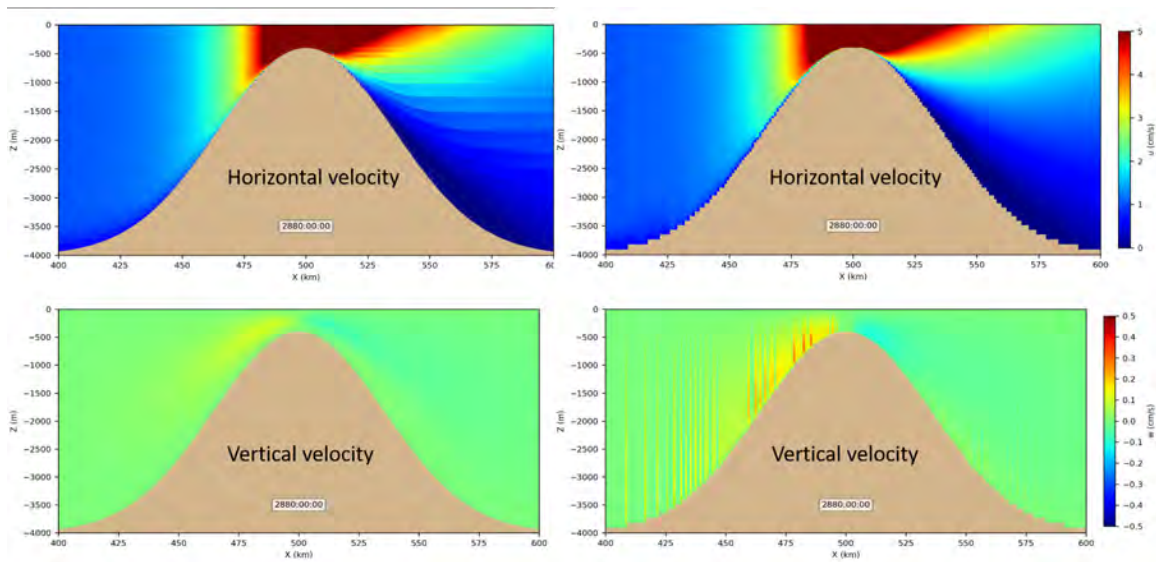


Figure 2. Horizontal (top) and vertical (bottom) velocities resulting from application of a 1 cm/s horizontal current applied over a seamount (whose peak is at 500 m depth) in a model that uses a GVC (left) versus z-level (right) vertical coordinate system. A smooth, realistic vertical velocity in the GVC-based model contrasts with the strong vertical jets produced along the gradient of the seamount when using a z-level vertical coordinate system.

Title: Atmospheric Process Studies
Author(s): T.R. Whitcomb, J. Ridout, and J. McLay
Affiliation(s): U.S. Naval Research Laboratory, Monterey, CA
CTA: CWO

Computer Resources: HPE Cray EX, SGI 8600 [AFRL, OH], [NAVY, MS]; Cray XC40/50 [ERDC, MS]

Research Objectives: We will improve our understanding of the dynamical and physical mechanisms that operate in the atmosphere using numerical-weather-simulation-based investigations and improve the Navy's global weather prediction capability. These objectives are interdependent: advances in understanding underlying processes often lead to improvements in forecast systems, and more skillful forecast systems aid in the project's basic research goals. This project develops and tests systems related to the Navy Global Environmental Model (NAVGEN; the Navy's currently operational global numerical weather prediction system) as well as downstream applications that provide additional forecast skill to end users.

Methodology: We leverage several lines of inquiry to meet the project research objectives including, but not limited to: testing at higher horizontal and vertical resolutions (to improve simulation fidelity), coupled global modeling (to include the impacts of time-varying ocean and upper atmosphere), global atmospheric ensembles (to quantify forecast uncertainty), and postprocessing model output (which applies statistical corrections to raw model output).

Results: We tested the NAVGEN configuration used in the Navy's Earth System Prediction Capability (ESPC) coupled system (a high-altitude version with modified representations of subgridscale processes) in a stand-alone capacity and evaluated for skill. Our goal is that this version will be transitioned to operations as a bridge to the next-generation NEPTUNE (Navy Environmental Prediction system utilizing a Nonhydrostatic Engine) that will become operational over the next few years. The new configuration significantly improved the mean wind speed error at 10 m (i.e., the surface winds) while the control exhibited lower vector wind RMS errors higher in the atmosphere. In the upper troposphere, the new configuration showed superior skill in integrated measures of tropospheric temperature when compared against global radiosondes. Overall, these results support consideration of this new configuration as a near-term upgrade to the current operational forecast system. We look forward to continuing to improve the specification of terrain and surface roughness lengths as well as the treatment of vertical mixing to address weaknesses identified in our analysis.

The NAVGEN ensemble system is crucial for quantifying forecast uncertainty and exploring the fundamental predictability of the atmosphere. We completed validation testing for a new method that uses historical data on observational corrections to forecasts to adjust the ensemble as it runs, demonstrating superior scores versus the current operational capability.

We developed a benchmark calibration for forecasts of total cloud cover based on traditional statistical methods. Based on this new approach, we applied the technique to probability forecasts of total cloud (e.g., the probability of clouds being "broken" or "overcast"). We demonstrated that overall, the calibration system is very effective at improving the probability forecast (see figure).

DoD Impact/Significance: Improved understanding of atmospheric processes and uncertainty mechanisms allow us to better predict future weather conditions, providing decision makers information for environment-affected risk assessment. Using statistical postprocessing techniques allows us to wrest further forecast skill out of existing models, providing a cost-effective mechanism to issue improved guidance. HPCMP resources are critical for numerical weather prediction research and development.

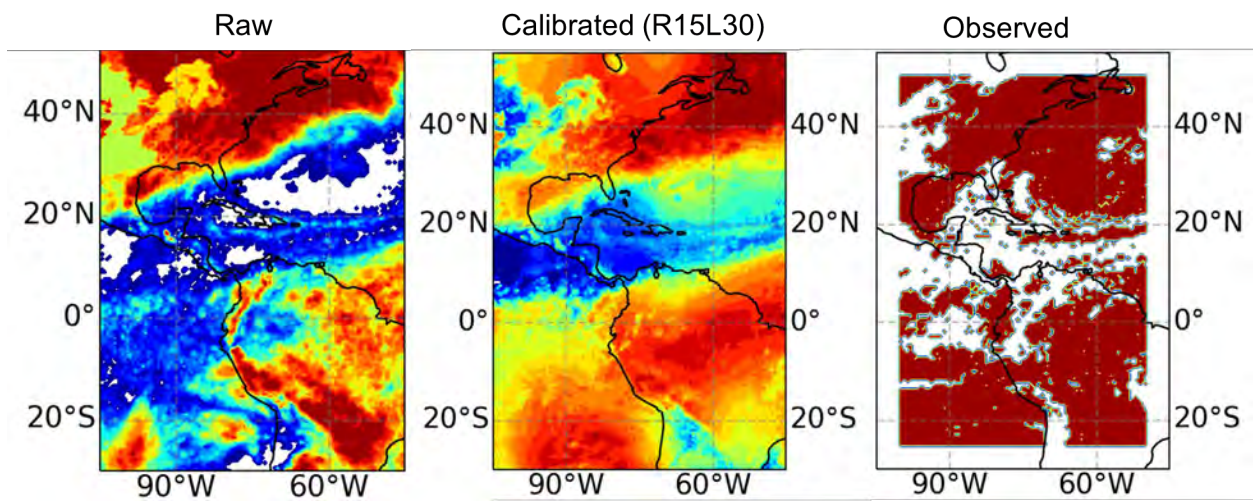


Figure 1. (Left and center) T + 48 h ensemble forecast probability of total cloud cover being in the broken or overcast category, initialized 2017021512 and valid 2023021712. (Right) Observed probability valid 2023021712. The calibrated forecast (center) enhances the probability of broken or overcast conditions across broad swaths of the domain, including the subtropical Atlantic and South Pacific, improving agreement with observations (right).

Title: Multi-scale Characterization and Prediction of the Global Atmosphere from Ground to the Edge of Space using Next-Generation Navy Modeling Systems

Author(s): C.A. Barton, S.D. Eckermann, J.F. Kelly, M.A. Herrera, K.W. Hoppel, D.D. Kuhl, D.R. Allen, J. Ma, and T. Rhodes

Affiliation(s): U.S. Naval Research Laboratory, Washington DC

CTA: CWO

Computer Resources: HPE SGI 8600 [AFRL, OH], [NAVY, MS]; Cray XC40/50 [ERDC, MS]; HPE Cray EX [NAVY, MS]

Research Objectives: To develop and test new, seamless atmospheric specification and prediction capabilities from 0 to 500 km altitude for future Navy Earth System Prediction Capability (ESPC) and ground-to-space numerical weather prediction systems, linking prediction of the ocean, atmosphere, and space over time scales from hours to decades.

Methodology: This project develops and tests key components of state-of-the-art systems required for improved modeling, prediction, and analysis of the extended operational environment for Navy applications, focusing on the atmosphere, the near space, and the geospace. Several model prototypes and operational systems are under development, including: 1) two high-altitude versions of the Navy Global Environmental Model (NAVGEN-HA), based on upward extensions of the Navy's operational global numerical weather prediction (NWP) system into a) the middle atmosphere for seasonal prediction and b) the upper atmosphere for thermospheric prediction and data-assimilation, and 2) two high-altitude extensions of the next-generation Navy NWP model NEPTUNE (Navy Environmental Prediction system Utilizing a Nonhydrostatic Engine) comprising a) a "middle atmosphere" extension (NEPTUNE-MA) for seasonal prediction and b) a ground-to-space prototype extended into the thermosphere.

Results: Major results directly facilitated by HPC resources during FY23 include: 1) completion of long-term NAVGEN-HA meteorological analysis products covering 11 contiguous years with high vertical resolution and middle-atmosphere physics tuning extending into the mesosphere (Fig. 1), 2) study of dynamics and predictability of sudden stratospheric warmings in the NAVGEN-HA coupled forecast/data-assimilation system, 3) linearization of NAVGEN-HA nonorographic gravity wave drag and cloud physics using an ensemble tangent linear model for use during variational data-assimilation, 4) further validation of new wind measurements from meteor radar and satellite observations to improve the NAVGEN-HA reanalysis of the mesosphere and lower thermosphere (Fig. 2), 5) continued development and implementation of the local ensemble transform Kalman filter high-altitude data-assimilation capability in the NAVGEN-HA system to generate initial conditions for high-altitude NEPTUNE R&D and driving of the SAMI ionospheric model, 6) development of ground-to-space NAVGEN and NEPTUNE modeling capabilities using advanced numerical algorithms that enable the dynamical cores to operate at high altitudes, including a complete refactor of middle- and upper-atmospheric physics schemes to comply with the Common Community Physics Package framework used by NEPTUNE.

DoD Impact/Significance: This research addresses Navy/DoD requirements to develop and test new high-altitude atmospheric specification and prediction capabilities leading to 1) a planned Navy Earth System Prediction Capability (ESPC) and 2) a Navy space weather prediction capability. This project performs the R&D needed to install high-altitude (both middle- and upper-atmosphere) specification and forecast capability in next-generation Navy NWP systems, ultimately providing improved near-space specification and prediction to the warfighter over both tactical and strategic time frames. HPC resources for this project provide critical support for the development of novel ground-to-thermosphere NWP models fully coupled to ionospheric models and data-assimilation to address key space-environment prediction goals of the Defense Advanced Research Projects Agency's Space Environment Exploitation (DARPA SEE) program.

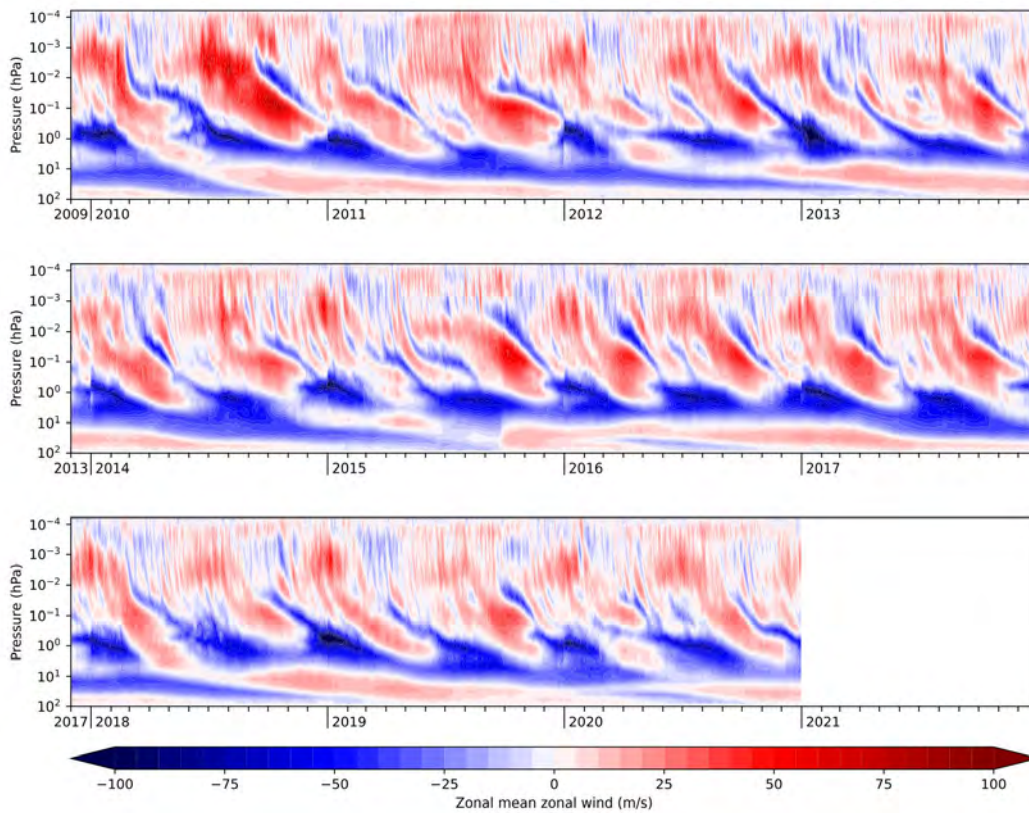


Figure 1. Time series of equatorial zonal-mean zonal wind from the 11- year-long streams constituting the reanalysis generated by the high-altitude version of NAVGEM tuned for middle-atmosphere research.

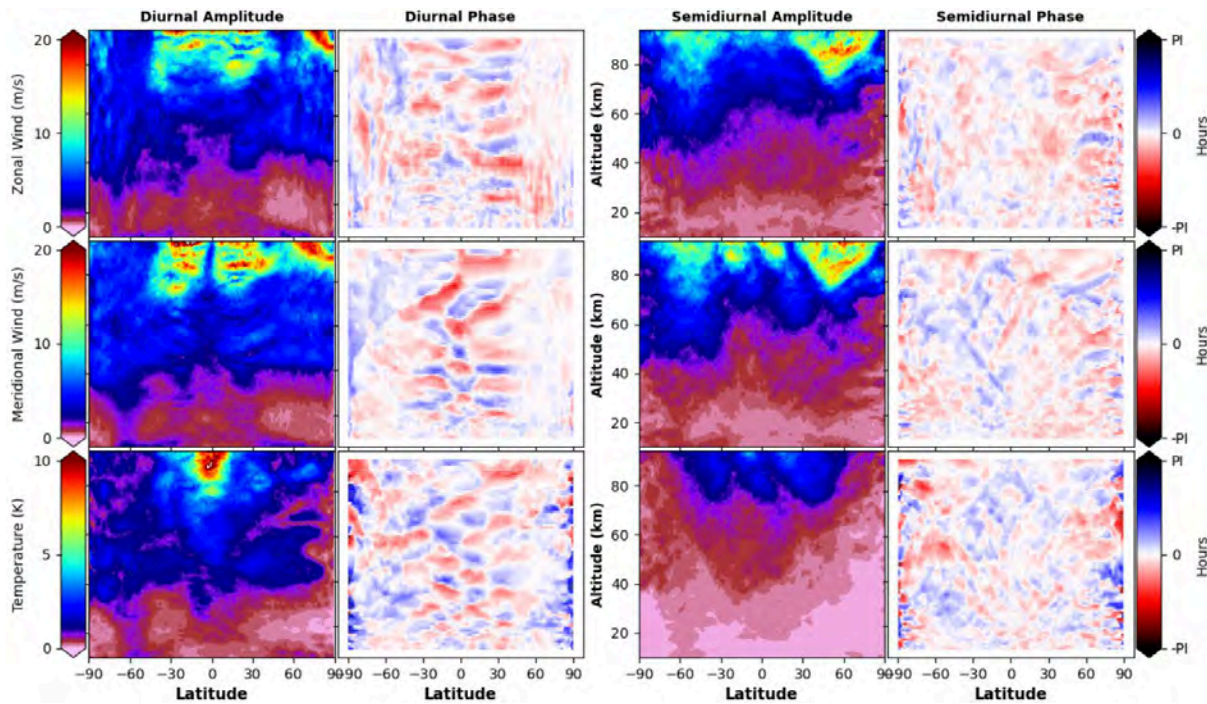


Figure 2. Diurnal (left) and semidiurnal (right) tidal analysis from hourly output of NAVGEM-HA for (from top) zonal wind, meridional wind, and temperature.

Title: Ocean Data Assimilation – Ocean State Estimation and Forecasting using SWOT Observations
Author(s): J.M. D’Addezio, G.A. Jacobs, and S.R. Smith
Affiliation(s): U.S. Naval Research Laboratory, Stennis Space Center, MS
CTA: CWO

Computer Resources: HPE SGI 8600, HPE Cray EX [NAVY, MS]

Research Objectives: In December 2022, NASA launched the Surface Water Ocean Topography (SWOT) satellite. The onboard sensor falls into the category of an “altimeter,” whereby an electromagnetic signal is bounced off the ocean surface, the time to return is measured, and a height is estimated. This measurement of sea surface height (SSH) is an essential parameter for oceanographic studies because it gives an estimate of the integrated heat content of the ocean over depth. These satellite-based altimeters have been used since the early 1990s, but SWOT is different. The prior sensors measured only at the nadir point. SWOT instead measures across a wide swath, giving two-dimensional SSH for the very first time, at very high resolution (~2 km). Because of this, the sensor is expected to radically change the scientific knowledge available to oceanographers on both large- and small-scale phenomena. Specific to Navy applications, the data can be used to correct ocean models, improving both state estimation and prediction. This project utilized HPC resources to demonstrate this improved capability using SWOT.

Methodology: After SWOT launched, NASA conducted a calibration and validation (cal/val) study to evaluate the performance of the new sensor. As a member of this team, NRL used HPC resources to generate real-time ocean forecasts in the region encompassing the primary cal/val site off the coast of California (Fig. 1). To test the SWOT sensor, NASA deployed a number of in-water assets such as moorings and gliders. These “in situ” data were assimilated into the NRL ocean model to correct the initial state and thereby to improve the resulting forecasts. These ocean simulations were also shared with the NASA cal/val team for comparisons with the SWOT data that the NRL team did not yet have access to. Both approaches allowed NRL to gage the performance of the real-time ocean simulations. Near-future work will also directly assimilate the SWOT data to finally demonstrate the extent to which these data improve Navy ocean state estimation and prediction.

Results: The real-time NRL ocean simulations were compared with the in situ data provided by NASA within the California cal/val region. Because SWOT measures SSH, the primary metric of comparison was height above a reference level generated by integrating temperature and salinity from the model and the in situ data. This variable is called “steric height” and is directly comparable to the SSH provided by SWOT. Comparisons of steric height between the model simulations and the cal/val in situ data are shown in Fig. 2. The NRL baseline experiment used assimilation horizontal scales based on relatively large-scale parameters that change as a function of latitude. Even this relatively simple assimilation approach yielded very good correspondence with the in situ steric height (2.4 cm RMS). A second simulation used assimilation horizontal scales that were smaller scale in the presence of high-resolution data, like those at the SWOT cal/val site. This simulation showed improved correspondence with the in situ data (1.6 cm RMS). The results suggest that the NRL models have good prediction skill and have increased capabilities when varying the horizontal scales used in the assimilation.

DoD Impact/Significance: Using HPC resources, we were able to demonstrate NRL model skill by using and comparing with novel observations deployed by the NASA SWOT cal/val team. The results outlined above suggest that the Navy’s ocean model is a good estimator and predictor of the ocean when given the proper data to constrain the solution. These tests are working towards the goal of transitioning SWOT data and improved ocean modeling solutions to Navy operations at the Naval Oceanographic Office (NAVO) and the Fleet Numerical Meteorology and Oceanography Center (FNMOC).

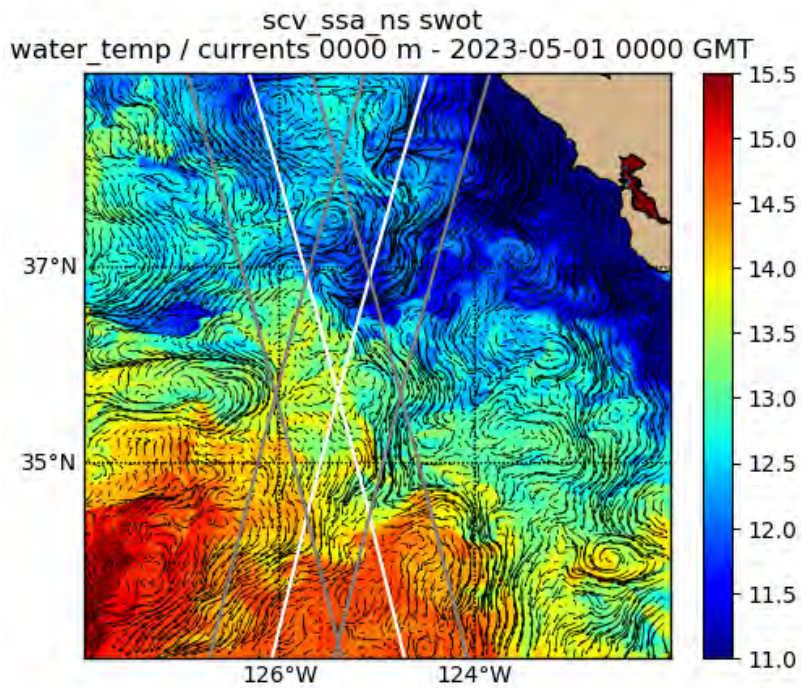


Figure 1. Snapshot of model sea surface temperature (SST) ($^{\circ}\text{C}$) (color) and surface velocity (m s^{-1}) (vectors) from the NRL model domain used during the SWOT cal/val. The gray and white lines denote the SWOT two-dimensional crossover during the cal/val period.

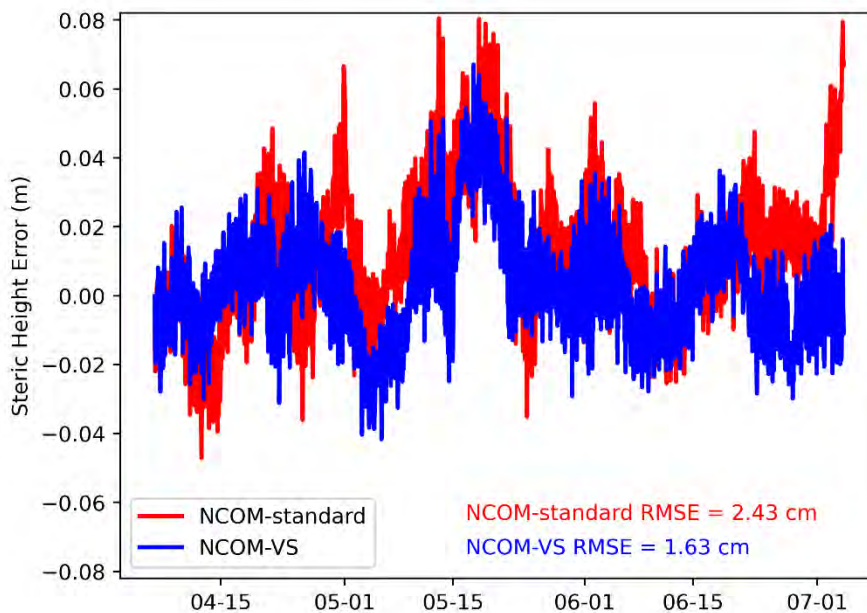


Figure 2. Steric height error (m) when compared with the two NRL ocean simulations created during the SWOT cal/val.

Title: Ocean Data Assimilation - Results of Year-Long NCOM Simulation of the Northeast Atlantic Domain using the 4DVAR Method

Author(s): M. Carrier, H. Ngodock, and S.R. Smith

Affiliation(s): U.S. Naval Research Laboratory, Stennis Space Center, MS

CTA: CWO

Computer Resources: HPE SGI 8600, HPE Cray EX [NAVY, MS]

Research Objectives: In order to assess the overall performance of the four-dimensional variational (4DVAR) analysis system for the Navy Coastal Ocean Model (NCOM) and its performance relative to its 3DVAR counterpart, a yearlong experiment in a Northeast Atlantic domain is configured and run. This experiment, covering from October 2021 through October 2022, allows for examining the performance of the 4DVAR system through seasonal changes and varying observational counts (as special deployments of gliders begin and end). This performance is assessed here from an oceanographic perspective. Due to the yearlong nature of this run, the performance is assessed via average statistics.

Methodology: The model domain for the experiments presented here covers the Northeast Atlantic (NEATL) between Greenland and Iceland, from 48° W to 13° W and 33° to 67.92° N. The model uses a spherical projection with a horizontal resolution of 2 km. In this report, there are two model forecasts used and compared to each other: 1) an NCOM run that uses 4DVAR data-assimilation and 2) an NCOM run that uses 3DVAR data assimilation. The model that uses 3DVAR has been run by the Fleet Numerical Meteorology and Oceanography Center (FNMOC) operationally and is configured with 100 vertical levels (45 sigma levels). The NCOM model with 4DVAR has been run partially in hindcast with real-time run later in the experiment time frame; this model uses 50 vertical levels (25 sigma). The reason for the difference in vertical resolution is due to the computational expense of 4DVAR. Each experiment assimilated SST data from -24 hours to +12 hours around the analysis time, SSH and in situ temperature and salinity data is collected from -120 hours to +12 hours. The method of comparing the observations to the appropriate model background time for the calculation of innovations (i.e., model-observation differences), known as the “first guess at appropriate time” (FGAT), is used in the 3DVAR for the SST data only (all other observations are compared to the model field at the analysis time only, regardless of when the observation is collected). The 4DVAR method employed a 48-hour assimilation window.

Results: Due to the length of this experiment, the simplest route for evaluation is through average statistics and time series plots. For this reason, we examined the oceanographic results of this comparison through daily profile root-mean-square-error (RMSE) plots. Here, we compare the 24-hour forecast from the 3DVAR and 4DVAR analyses to available in situ profiles from gliders and profiling floats. Figure 1 shows the contour RMSE from 0 to 500 m depth beginning on October 1, 2021, and running through October 31, 2022, for the 24-hour forecast of temperature (left plots) and salinity (right plots) from 3DVAR (top plots) and 4DVAR (bottom plots). Right away, some differences stand out. The 24-hour RMSE in temperature from 4DVAR has noticeably lower error between 0 and 200 m around December 2021 and again from August through October of 2022 (by as much as a 1°C in some cases). A similar result is seen in the salinity results, with much lower salinity errors during these same time periods. Interestingly, both models perform very well from February through June of 2022. Overall, however, the 24-hour forecast from the 4DVAR analysis shows remarkably lower error for most of the experimental time frame than that from the 3DVAR analysis.

DoD Impact/Significance: The 4DVAR method of data-assimilation gives the Navy a tactical advantage in terms of 1) using more observations and 2) providing a more accurate analysis that leads to a more accurate ocean forecast. More accurate forecasts, especially in the acoustically significant depths of 0 to 500 m, provides the Navy with greater environmental awareness in the battlespace and also helps to improve the accuracy of acoustic model simulations.

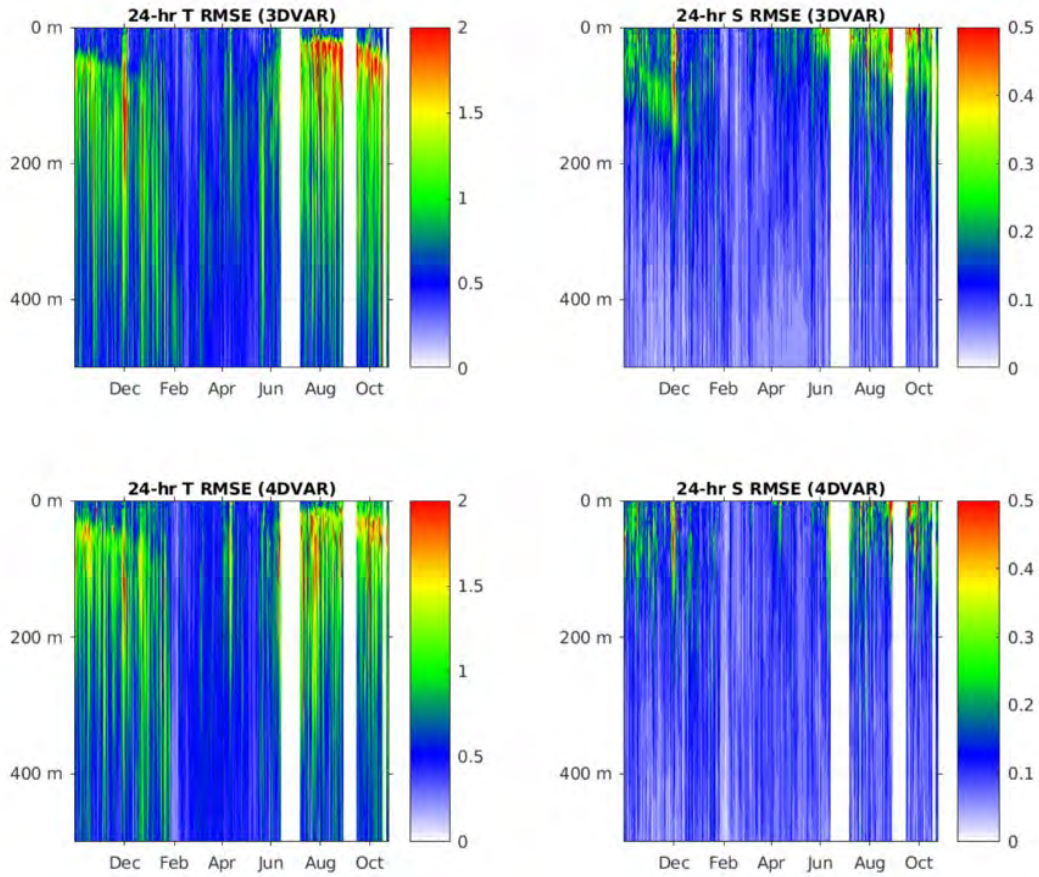


Figure 1. Daily profile RMSE from October 1, 2021 through October 31, 2022 for the 24-hour forecast from 3DVAR (top plots) and 4DVAR (bottom plots) for temperature (left plots) and salinity (right plots). Depth shown on y-axis (0 to 500 m) and analysis day shown on x-axis.

Title: Ocean Data Assimilation - Deterministic and Statistical Predictability of Mid-Frequency Acoustic Ducts

Author(s): J. Osborne,¹ C. Amos,² and G.A. Jacobs¹

Affiliation(s): ¹U.S. Naval Research Laboratory, Stennis Space Center, MS; ² American Society for Engineering Education, Stennis Space Center, MS

CTA: CWO

Computer Resources: HPE SGI 8600, HPE Cray EX [NAVY, MS]

Research Objectives: This project investigates the vertical structure of ocean temperature and salinity and their impact on underwater sound speed in the northeastern Pacific Ocean (Oregon and Washington coasts). Critical sound speed features are local minimums and maximums in sound speed (as a function of depth) that are below the ocean's surface mixed layer and above the deep sound channel as well as the vertical gradient in sound speed. Low-frequency sounds (< 1 kHz) are insensitive to ocean features with small vertical extent and small amplitude, but midfrequency sounds (1–10 kHz) are sensitive to such features. This work quantifies impacts of large, slowly varying “mesoscale” ocean features (length scales of ~100 km or greater, varying on time scales of a several days or longer) and small, rapidly varying “submesoscale” ocean features (length scales of ~10 km and time scales of a few hours to a few days) that impact sound speed in the coastal oceans along coasts of Oregon and Washington (US West Coast). The long-term goal is to deterministically predict ocean features of 50 km length scale and larger for midfrequency sounds.

Methodology: Ocean vertical structure is analyzed from both in situ observations and model results. Observations have been analyzed to identify the depth range at which temperature and salinity variability impact sound speed for midfrequency sounds. Subsequently, a series of nested ocean models have been configured, integrated, and compared with observations to find model configurations that resolve ocean physics for midfrequency acoustic propagation. The nested models use 3 km horizontal resolution/50 vertical levels, 1 km/100 levels, and 250 m/150 level resolution, as higher resolution resolves more small-scale ocean features (e.g., Fig. 1). Observations and models are analyzed for mixed layer depth, thermo-, halo-, and pycnocline depth, temperature inversions (subsurface maximums in temperature), and secondary sound channels (minimums in sound speed below the ocean surface but above the deep sound channel).

Results: In the northeastern Pacific Ocean, temperature inversions are frequently observed between depths of 50 m and 150 m with vertical extent between temperature minimum and maximum often less than 20 m; e.g., an observed inversion has a minimum temperature of 8.57°C at 89 m depth and a maximum temperature of 8.70°C at 101 m depth. We find that coarse resolution models (i.e., 3 km/50 vertical levels) underpredict the presence of temperature inversions, misplace the depths at which inversions occur, and overestimate the vertical thickness of inversions. This has motivated the use of models with increased vertical resolution, particularly in the depth range from the surface to 200 m. Work with increased resolution is ongoing.

DoD Impact/Significance: Inversions are associated with so-called “secondary sound channels.” Secondary sound channels impact the propagation of underwater sound. Understanding underwater sound propagation is important for a number of Navy efforts, most notably antisubmarine warfare, but also acoustic communications. So, ocean models must resolve temperature inversions in order to resolve secondary sound channels. Models with higher resolution, particularly vertical resolution, better resolve temperature inversions and secondary sound channels.

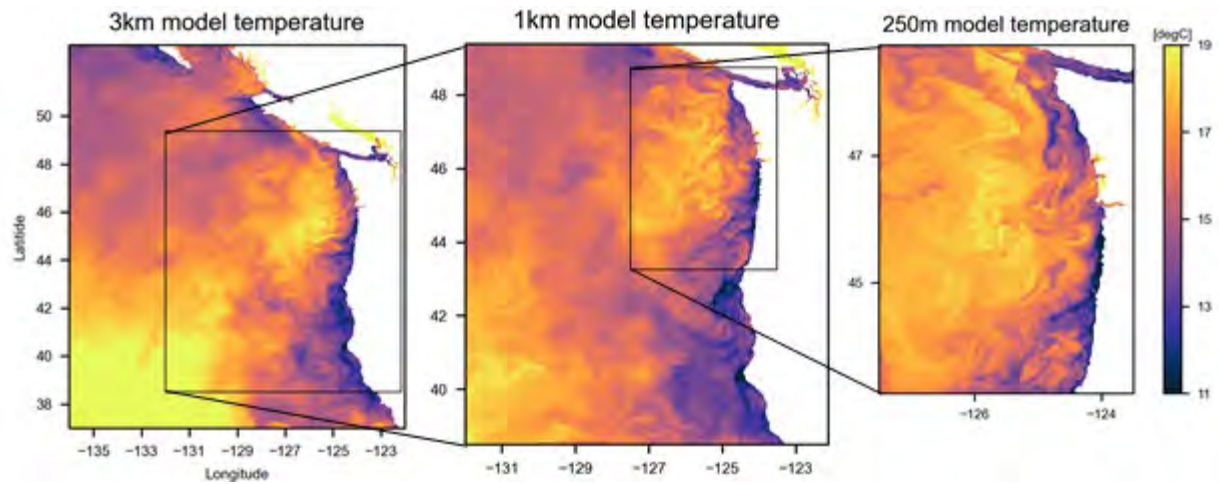


Figure 1. Comparison of sea surface temperature in models with 3 km (left), 1 km (center), and 250 m (right) horizontal resolution. At higher resolution (right), more features with smaller horizontal scale and larger amplitude are apparent. Such features are also found at depth, impacting the underwater propagation of sound, especially at frequencies greater than 1 kHz.

Title: Ocean Data Assimilation – Hybrid NCODA

Author(s): T. Townsend and S.R. Smith

Affiliation(s): U.S. Naval Research Laboratory, Stennis Space Center, MS

CTA: CWO

Computer Resources: HPE SGI 8600, HPE Cray EX [NAVY, MS]

Research Objectives: Develop and implement enhancements to the ocean/ice data-assimilation (DA) system NCODA and the atmospheric data-assimilation system for NEPTUNE (FALCON DA) to be used in the Navy Earth System Prediction Capability version 3 (Navy ESPC v3). Integrate the next-generation DA solvers (NCODA 5 and FALCON DA) into Navy ESPC v3. The analysis state provided by the coupled DA system will provide a consistent starting point for better skill in the coupled km-scale atmosphere/ocean/wave/sea-ice forecasts. In addition to approximating a strongly coupled ocean/atmosphere DA using the block iterative technique with the uncoupled solvers, the ocean/ice analyses will use a hybrid background error covariance that is a combination of static and flow-dependent covariances.

Methodology: Previously developed hybrid NCODA uses a combination of climatological and ensemble-based, flow-dependent forecast error covariances. In addition to the localized ensemble covariances being generated using forecasts from a 16-member ensemble, the ESPC ocean/ice analysis is computed in three overlapping portions of the global domain, one for the cylindrical portion and two others for the Arctic and Antarctic polar cap regions. The plan is to run twin experiments to the global cycling ensemble nowcast/forecast system ESPC V2 (ESPC-E V2) validation test report (VTR) experiment with different linear combinations of the static and flow-dependent background error covariances.

Results: The ESPC system has been formulated with the capability to produce hybrid ice and hybrid ocean analyses. An initial test of NCODA hybrid DA within ESPC used equal weighting of the static and ensemble background error covariances. The resulting sea surface temperature analysis for the cylindrical portion of the global domain is shown in Fig. 1. The corresponding sea ice concentration analyses for the Arctic and Antarctic polar-coordinate regions are shown in Fig. 2. This capability has been merged into the ESPC repository. Attempts to run a twin experiment to ESPC-E V2 are incomplete due to lack of throughput on the Navy DSRC system using the “standard” queue, the only option at the time. Work was begun on completing the setup of a reduced-resolution version of the Navy ESPC to facilitate throughput in order to complete experimentation.

DoD Impact/Significance: Complete testing of hybrid NCODA 3DVAR in ESPC could lead to reduced forecast errors in the next version of Navy ESPC. NAVDAS-AR, the current atmospheric DA component of ESPC, uses hybrid covariances. Adopting the use of hybrid covariances in NCODA, the ocean/ice DA component of ESPC, to improve the ocean/ice solution of the uncoupled portion of the block iterative technique of approximating a strongly coupled ocean/ice/atmosphere DA should produce a consistent initial state for the coupled atmosphere/ocean/wave/sea-ice forecasts, thereby resulting in better forecast skill.

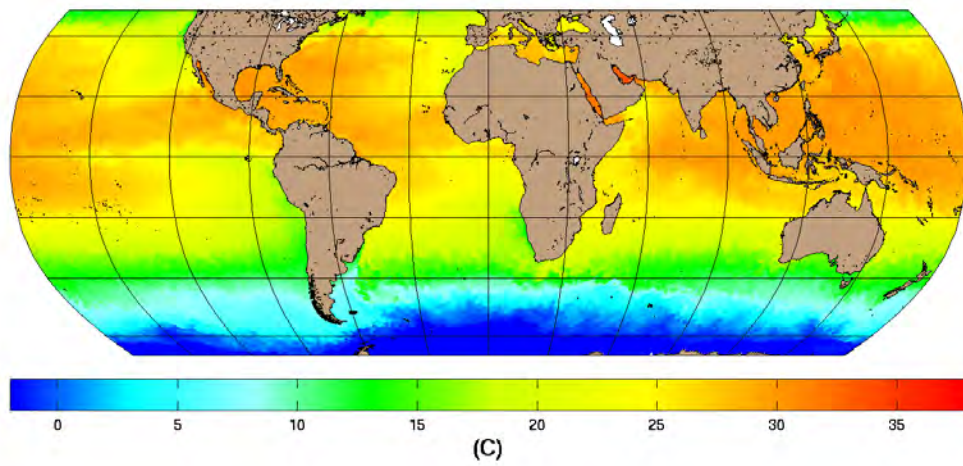


Figure 1. Initial tests of the NCODA coupled hybrid DA have been using $\alpha = 0.5$ (i.e., equal weighting of static and ensemble covariance). The solution is computed in the three overlapping tiles of the global system. A hybrid sea-surface temperature analysis is shown for the cylindrical portion of the domain.

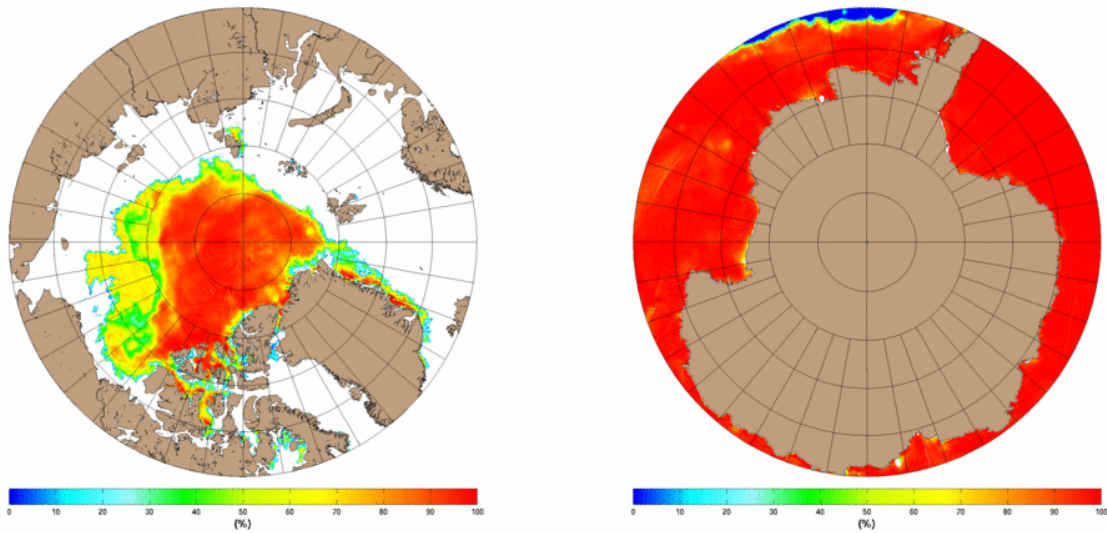


Figure 2. As in Fig. 1, but showing a hybrid sea ice concentration analysis in the Arctic (left) and Antarctic (right) polar-coordinate caps.

Title: Ocean Data Assimilation – Stability of Freshwater Runoff in East Greenland Currents

Author(s): S.R. Smith and R.W. Helber

Affiliation(s): U.S. Naval Research Laboratory, Stennis Space Center, MS

CTA: CWO

Computer Resources: HPE SGI 8600, HPE Cray EX [NAVY, MS]

Research Objectives: High-resolution (1 km) ocean modeling experiments were performed off the eastern Greenland coast using HPC resources. This effort is part of the NRL project, 6.1 The Atlantic Ocean's Deep-Water Origins, which is to understand and quantify kinematics and dynamics governing the evolution of high-northern-latitude-originated water and the circulation feeding the lower limb of the Atlantic Meridional Overturning Circulation. The purpose of the twin model experiments presented here was to determine the impact that fresh water from melting ice has on the water properties and circulation on the eastern Greenland shelf. This will lead ultimately toward a greater capability to forecast the subsurface ocean structure in Navy-relevant high-latitude oceans that influence sea ice and the moving origins of Atlantic Ocean deep water.

Methodology: The approach is to use the Navy's state-of-the-art numerical ocean-modeling capabilities to investigate the processes that govern the circulation along the eastern Greenland shelf resulting from increased freshwater input from the Greenland Ice Sheet. To accomplish this, we created and performed high-resolution regional Navy Coastal Ocean Model (NCOM) simulations from June 1, 2019, to December 31, 2019, with 1-km horizontal resolution and 100 layers. The domain is a Lambert conformal grid centered on the Denmark Strait between Greenland and Iceland and nested within a larger, 4-km-horizontal-resolution domain. Twin experiments were performed on 192 processors on the DSRC. The only difference between these simulations is that one had freshwater runoff from Greenland and Iceland, and the other did not. The freshwater input was estimated based on estimated ice melt observations. An additional tracer field was added to the simulations with peak values at the beginning of the simulations (June 1, 2019) and at locations along the coast with significant ice melt. These numerical-modeling and tracer-release experiments have led to a greater understanding of the evolution of freshwater runoff and its impact on the circulation along the east coast of Greenland.

Results: The NCOM simulations capture the structure of the water currents and properties along eastern Greenland (Fig. 1). This figure compares the two simulations on July 1, 2019, which is one month into the runs from when the tracers were added at dominant ice melt sources along the Greenland and Iceland coasts. The left column of Fig. 1 displays the results of the simulation without the addition of freshwater forcing from ice melting throughout the time period, whereas the right column includes this forcing. The first row of the figure (panels A and B) is the concentration of the tracer field at the surface one month into the assimilation. The remainder of the figure is of salinity on a zoomed-in portion of the region around Scoresby Sound. The middle row (panels C and D) shows the salinity at 10 m depth, and the bottom row is a transect of salinity along the 70.25° latitude. These results show that fresh water extends farther and faster away from the coast when there is runoff.

DoD Impact/Significance: The Navy needs accurate ocean forecasts and because of amplified high-latitude warming, circulation in the tactically relevant Greenland/Iceland/United Kingdom (GIUK) gap is changing. Decreasing sea ice coverage and subsurface hydrographic changes in the seas surrounding the Arctic Ocean are causing the origins of Atlantic Ocean deep water to change. This research accounts for this variability leading to new forecasting capabilities for high-resolution ocean circulation and sea ice predictions useful for Navy operations in the GIUK region. This project has led to the following new NRL project, 6.1 Resolving Northern High Latitude Water-mass Formation Mechanisms.

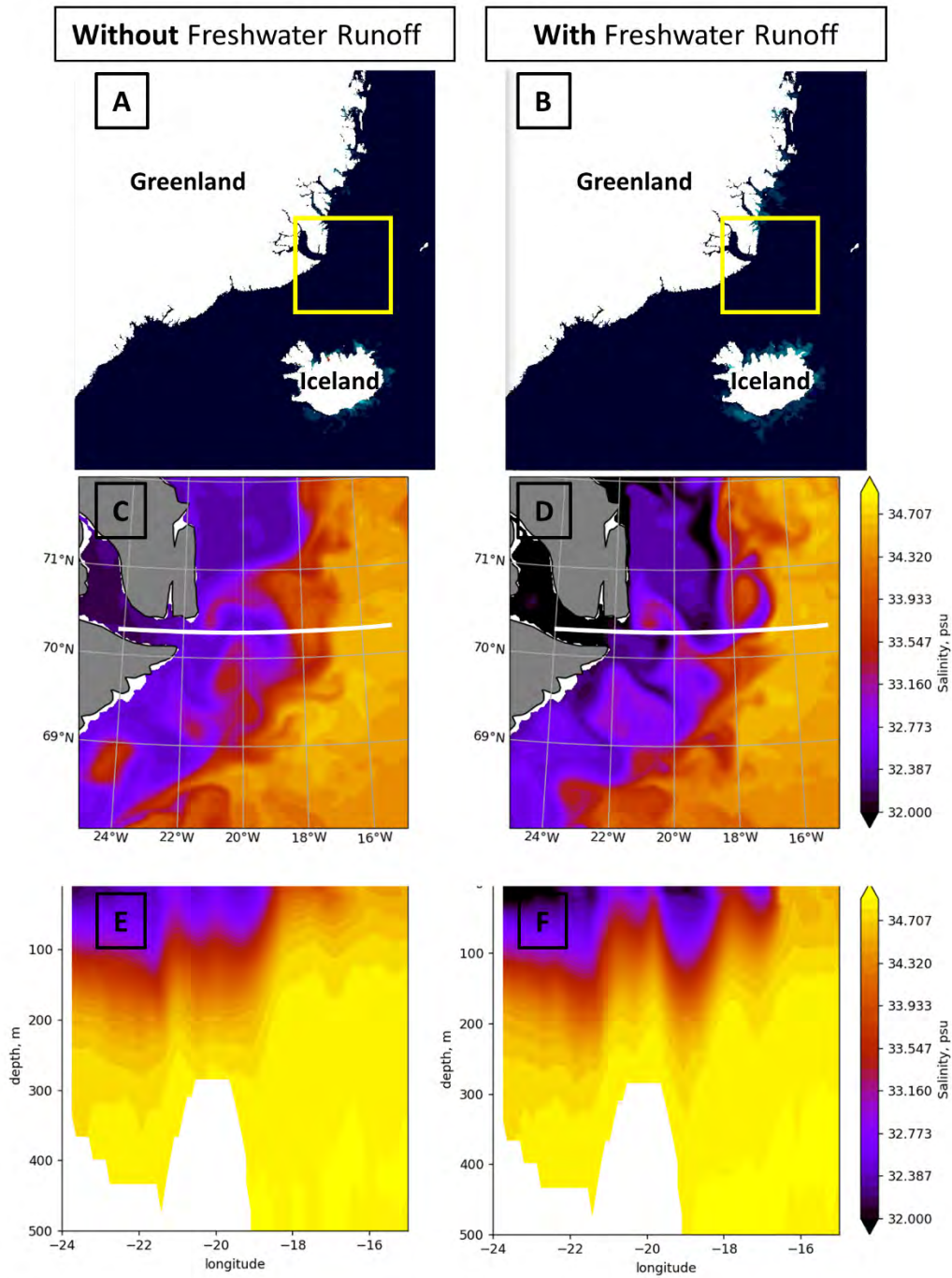


Figure 1. Comparison of two high-resolution model runs, one without freshwater runoff from ice melt (left column) and the other with (right column). A and B show the concentration field at the surface one month after tracers were added along the coast of Greenland. C and D display a zoomed in region of Scoresby Sound (marked by the yellow boxes in panels A and B) of salinity at 10 m depth. E and F are transects of salinity along 70.25° deg latitude (white lines in panels C and D). All of the results are for July 1, 2019, which is one month into the model runs.

Title: Ocean Data Assimilation

Author(s): S.R. Smith,¹ J.M. D’Addezio,¹ C. Amos,³ M. Carrier,¹ C. DeHaan,⁴ S. deRada,¹ R.W. Helber,¹ A. Iversen,⁴ A. Lawrence,⁴ J. May,¹ V. Montiforte,³ H. Ngodock,¹, J. Osborne,¹ M. Phelps,⁴ C. Rowley,¹ W. Stevens,⁵ T. Townsend,¹ and K. Tremblay⁴

Affiliation(s): ¹U.S. Naval Research Laboratory, Stennis Space Center, MS; ² University of New Orleans, Stennis Space Center, MS; ³American Society for Engineering Education, Stennis Space Center, MS; ⁴ Peraton Inc., Stennis Space Center, MS; ⁵ Portland State University, OR

CTA: CWO

Computer Resources: HPE SGI 8600, HPE Cray EX [NAVY, MS]

Research Objectives: The scope of this project is to advance the analysis and prediction capability of the Navy’s environmental modeling and forecasting systems through the improvement of the assimilation software used to merge incoming observations with model forecast fields. Thirteen funded NRL projects used this subproject in FY23 to perform experiments that went toward either using, adding, improving, or validating various capabilities of ocean data assimilation. In this report, we will focus on just one of these efforts: the 6.4 Ocean Currents projects. Other efforts that were conducted in this project, such as those involving surface, water, ocean, topography (SWOT) altimeter data assimilation, four-dimensional variational (4DVAR) assimilation validation, determination of acoustic ducts, and Greenland freshwater runoff and ice assimilation, will be presented in separate reports.

Methodology: The velocity data-assimilation capability has been developed and tested in the Gulf of Mexico. Two papers and a validation test report were submitted detailing this effort. This capability is now being transitioned into the operational systems (COAMPS[®] 2023 and NCODA4.4) and is being validated on the DSRC platforms for a northwestern Atlantic (NATL) Ocean domain where drifters are available. Since NCODA is designed to resolve geostrophic dynamics, the velocity observations that are assimilated need to be processed to just include the geostrophic component. This is accomplished by computing Eulerian velocities using a long time period between successive drifter locations. We use a period of 24 hours here, which is roughly the inertial oscillation period for this region, to filter out much of the small-scale or high-frequency features not resolved by our assimilation system and to focus on the components of velocity more likely to be in geostrophic balance.

Results: In order to validate velocity assimilation, twin experiments are performed on a 1-km horizontal grid with 100 levels within the northwestern Atlantic (NATL) domain (Fig. 1). The first experiment is a control run that has velocity assimilation turned off. This control run was initiated using the Global Ocean Forecasting system on February 1, 2022, and assimilated the normal operational data stream of observations. This experiment has been performed for three months so far (February–April 2022) and will continue through December 2022. The other experiment will be initiated using the control run on March 1, 2022, and will include the assimilation of velocity observations in addition to the standard stream of observations used in the control run. Velocity observations will come from the LANT drifter data set (black dots in Fig. 1) which lasted from March 2022 through February 2023.

DoD Impact/Significance: The assimilation experiments tested under this project went towards improving the Navy’s capability of forecasting the ocean environment, and directly addresses Navy priorities as outlined in the following documents: OPNAV N2N6E FY 2021 RDT&E Priorities Letter 3062, Ser N2N6E/20U119707 (March 26, 2020), and the NRL ocean modeling roadmap developed in consultation with the Navy operational modeling centers Naval Oceanographic Office (NAVOCEANO) and Fleet Numerical Meteorology and Oceanography Center (FNMOC).

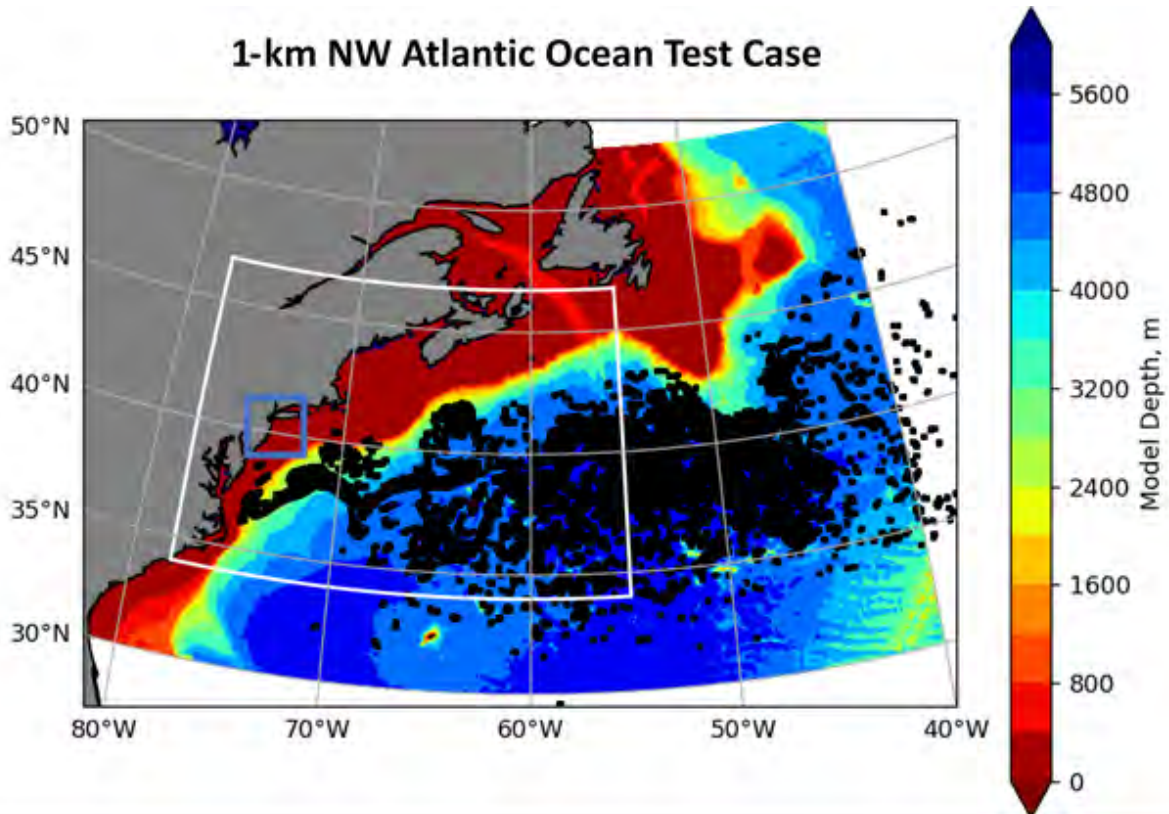


Figure 1. The velocity data-assimilation capability is being validated for a 1km domain in the western Atlantic domain (white box). Velocity derived from drifters (black dots), deployed for the LANT/Ocean of Things field study, and HF radar derived currents (blue box) will be assimilated.

Title: Coupled Ocean-Wave-Air-Ice Prediction System

Author(s): T. Jensen,¹ J. Yu,¹ D. Flagg,² R.W. Helber,¹ G.A. Jacobs,¹ A. Rydbeck,¹ J. Christophersen,² H. Wijesekera,¹ and T. Campbell¹

Affiliation(s): ¹U.S. Naval Research Laboratory, Stennis Space Center, MS; ²U.S. Naval Research Laboratory, Monterey, CA

CTA: CWO

Computer Resources: HPE SGI 8600 [NAVY, MS]

Research Objectives: The weather and oceanic surface and subsurface conditions are affecting Navy operations, and understanding how the atmosphere and ocean interact is crucial for developing better environmental forecast models. At NRL, state-of-the-art numerical models are under constant development for the atmosphere, for the ocean, for surface waves, and for sea ice. In recent years, these models have been coupled to form a comprehensive prediction system. The coupled modeling system Coupled Ocean-Atmosphere Mesoscale Prediction System (COAMPS[®]) is six-way coupled with the Navy Coastal Ocean Model (NCOM), WAVEWATCH III[®] (WW3), and SWAN wave models and is now being used and validated in many regional areas around the globe. The Office of Naval Research (ONR) has several ongoing field experiments in many areas around the world, and an important task is to apply uniquely designed COAMPS[®] modeling systems for each of those areas and to run real-time forecasts as well as hindcasts. Forecasts are used to assist research ships and autonomous platforms such as gliders to provide guidance on where to deploy vessels to get optimal measurements, while hindcasts can assimilate observations and help the quality of model simulations.

Methodology: For accurate simulation and prediction on regional scales in midlatitudes, we have used new configurations of NRL's state-of-the-art fully coupled atmosphere-ocean-wave model system COAMPS[®] with very high spatial and temporal resolution. For the Atlantis Seamounts area, we used a two-nest simulation with very high vertical resolution using 100 layers and up to 600 m resolution in the ocean. Coupling interval for data exchange between the three models is 6 min.

Results: Skin SST parameterizations, Saunders (1967), Saunders with a modification including solar radiation, Soloviev and Schlussel (1994) and Zeng and Beljaars (2005) were added to NCOM last year and were included in the fully coupled COAMPS[®] this year and were tested. The impact of SST, MLD and current was assessed and a journal paper is near completion (Flagg, Yu, and Jensen 2022). A suite of fully coupled COAMPS[®] runs using different SSST parameterizations reveals a significant impact on surface heat fluxes, changes in submesoscale oceanic features and feedback to the atmospheric boundary layer on oceanic mesoscales. The area investigated is that covered by the CASPER-East experiment. In the spring of 2023, COAMPS[®] was used during a pilot experiment for high-resolution modeling for Task Force Ocean (TFO) in areas near the Atlantis Seamounts in the North Atlantic Ocean. We completed a two-month-long coupled COAMPS[®] high-resolution simulation of the Atlantis II Seamounts area (2 atmosphere, 2 ocean nests) and made runs with 100 layers and 600 m resolution in the ocean and produced real-time sections of sound speed, temperature (T), and salinity (S) for an NRL cruise in the area. The high-resolution GEBCO topography data set was implemented and was tested successfully. Additional model calculations were done in the tropical Indian Ocean, a continuation of work in previous years (Christofferson et al. 2023).

DoD Impact/Significance: The development of the relocatable coupled air-ocean-wave prediction system can have a pronounced effect on Navy forecasting by improving ASW performance, tropical cyclone prediction, search and rescue and mission planning.

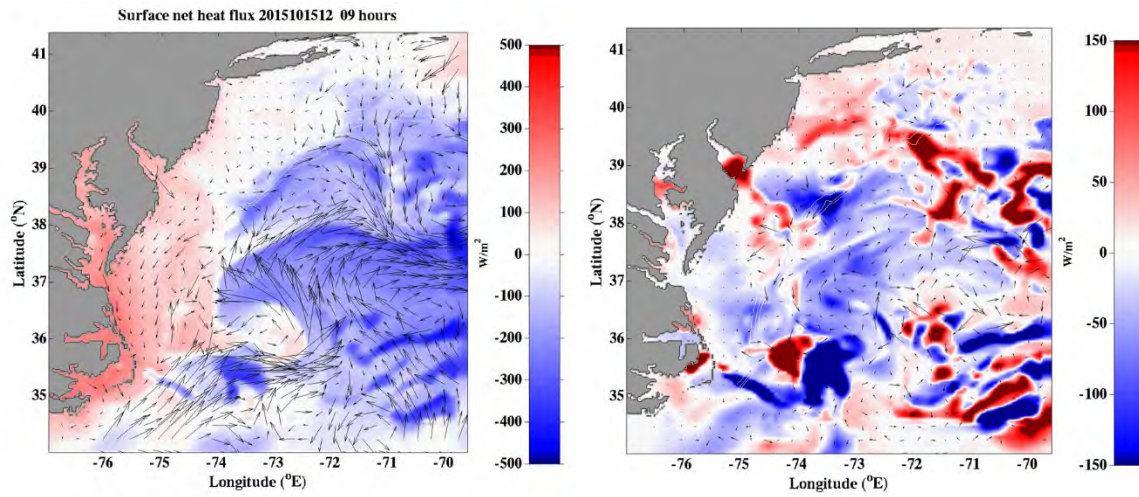


Figure 1. Net surface heat flux on October 25 at 9 pm GMT for a coupled control run using bulk SST (left). Difference in net surface heat flux when skin surface temperature is used (control bulk SST run minus run using Skin SST) (right)

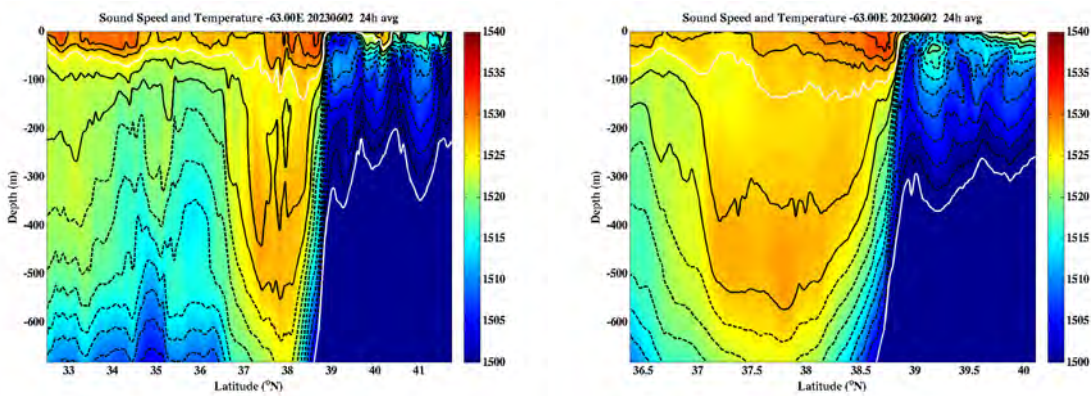


Figure 2. Daily averaged sound speed (color) and temperature (contours) on a 2-km ocean grid (left) along 63°W on June 2, 2023, in the North Atlantic Ocean. The steep gradient near 38.5°N is the position of the North Wall of the Gulf Stream. The right panel shows the solution of the inner nest with 600-m resolution. Note the local minimum in sound speed near 100 m from 37.5°N to 38.5°N, indicating the existence of a sound channel in that area.

Title: Turbulent Mixing in NCOM and HYCOM

Author(s): Y. Fan

Affiliation(s): U.S. Naval Research Laboratory, Stennis Space Center, MS

CTA: CWO

Computer Resources: HPE SGI 8600 [NAVY, MS]

Research Objectives: The goals of this project are to demonstrate the capability and limitation of the Navy Coastal Ocean Model (NCOM) to simulate frontogenesis, and to quantify the combined effect of the dynamical processes on different spatial scales in modulating the upper-ocean density structure.

Methodology: Nineteen NCOM experiments were conducted to study the time evolution of an idealized cold filament. Surface forcing prescriptions in the model experiments are designed with a choice of south-to-north along-filament wind, west-to-east cross-filament wind, or surface cooling. The water side friction velocity is set to be $u_* = 0.01\text{m/s}$. This is corresponding to surface winds of 8.5ms^{-1} . The surface cooling is prescribed as a heat flux of 100Wm^{-2} out of the ocean, which is equivalent to a kinematic surface flux $Q_* = 2.38 \times 10^{-5}\text{Km}^{-1}\text{s}^{-1}$. In all experiments, the forcing (either wind or heat flux) remains uniform across the whole model domain and constant throughout the simulation period. The Coriolis parameter is equal to $7.81 \times 10^{-5}\text{s}^{-1}$, equivalent to 32°N . In each forcing scenario, the effect of different horizontal resolutions is tested using 100-, 50-, and 20-m resolutions. The effect of horizontal mixing by changing the HORCON parameter in the Smagorinsky horizontal mixing scheme, and the effect of surface gravity waves by running experiments with and without the surface wave forcing, are also investigated. The NCOM results are evaluated with large eddy simulation (LES) results from Sullivan and McWilliam (2018, SM18) and Sullivan and McWilliam (2019, SM19) on its capability to realistically represent frontogenesis.

Results: The life cycle of frontal onset, arrest, and decay is analyzed in Fig. 1 through the time evolution of peak vertical vorticity $\langle \zeta \rangle_p = \partial_x \langle v \rangle$, its cross-front location χ_p , and the turbulent kinetic energy (TKE) at the time and location of $\langle \zeta \rangle_p$. The comparison between NCOM results and SM18 suggested that NCOM is able to predict the correct characteristics of filament frontogenesis, but fails to capture the correct dynamics, such as the much weaker TKE produced by NCOM. One of the main reasons for the weak turbulence in NCOM is because the horizontal mixing is parameterized using the Smagorinsky scheme instead of resolved by the model in the LES.

Further analysis of the Smagorinsky horizontal mixing parameterization suggests that its effect on frontogenesis is very small, and the front arrest is controlled by the model's subgrid-scale artificial regularization procedure instead of horizontal shear instability. Consequently, higher resolution is corresponding to stronger frontogenesis in the model. Thus, whether the hydrostatic model can produce realistic magnitude of frontogenesis is purely dependent on the characteristic of the front/filament simulated and model resolution.

Moreover, the comparison of NCOM experiments with and without the surface gravity wave forcing and SM19 (Fig. 2) reveals that the parameterized effect of surface gravity wave forcing through vertical mixing is small on frontogenesis and cannot represent the real physics of wave-front interaction.

DoD Impact/Significance: This study will improve the battlespace environment forecasting accuracy for ocean models with more accurate vertical thermal profiles and better predication of acoustic and optical properties in the upper ocean. Strong scientific foundation and guidelines will be achieved for intelligent ocean forecasts for regional and global tactical planning.

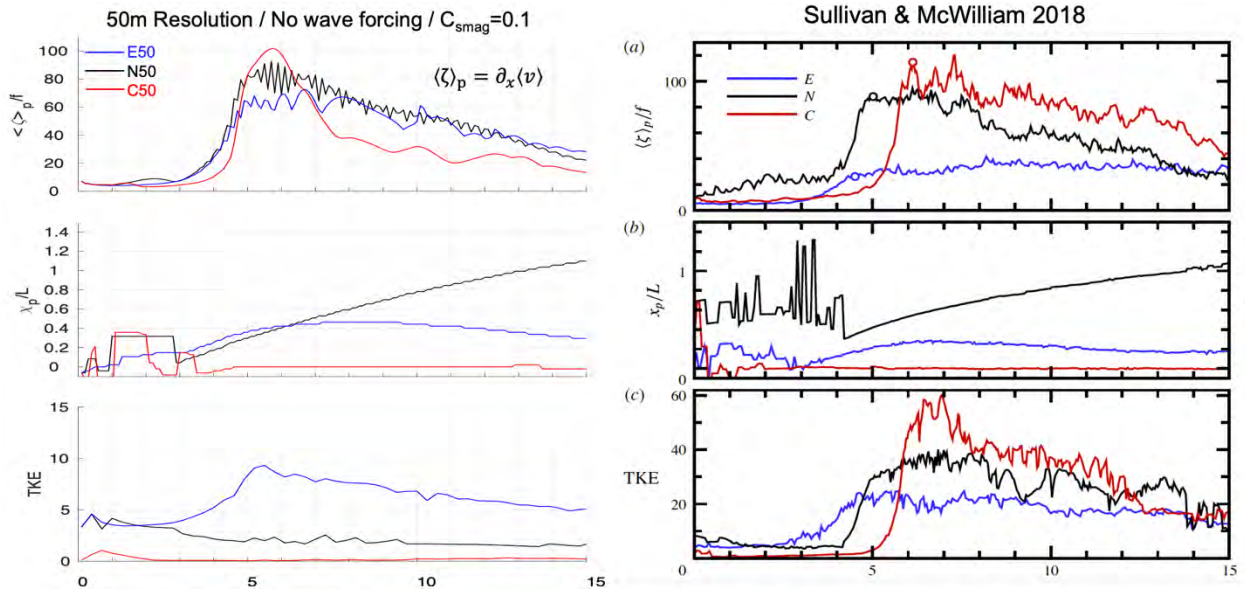


Figure 1. Normalized peak average vertical vorticity $\langle \zeta \rangle_p / f$ (top panels), its cross-front location x_p/L (middle panels), and turbulent kinetic energy TKE (bottom panels) as a function of time for the NCOM 50-m-resolution cases on the left and the LES results in SM18 on the right. In the figure, black, blue, and red are corresponding to the northward wind, the eastward wind, and surface cooling, respectively.

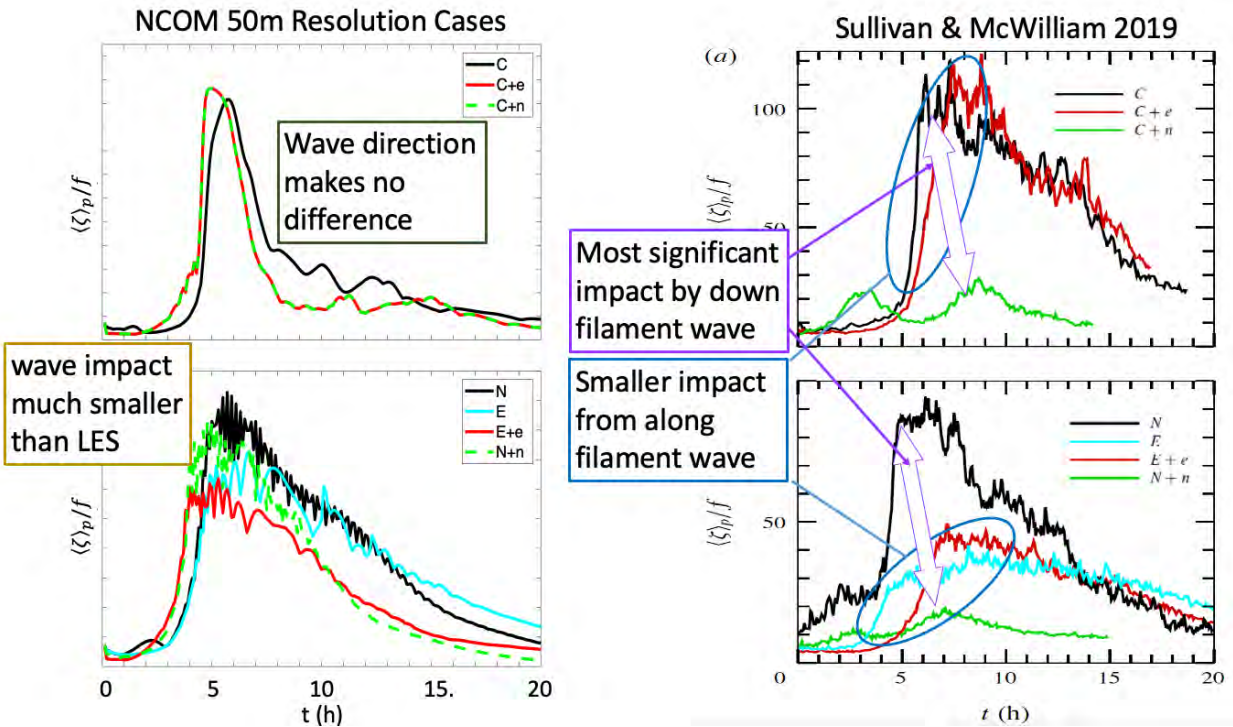


Figure 2. Time variation of average peak vertical vorticity $\langle \zeta \rangle_p / f$ near the water surface for (upper panels) simulations driven by surface cooling and waves (C; C+e; C+n) and (lower panels) simulations driven by winds and waves (N; N+n; E; E+e). The two panels on the left are results from NCOM 50-m-resolution experiments, and the two panels on the right are LES results from SM19.

Title: Improving Tropical Convective Storm Prediction by Bridging the Gap between Large-Scale Moisture and Convective Dynamics

Author(s): Q. Zhao, N. Baker, Y. Jin, and D. Tyndall

Affiliation(s): U.S. Naval Research Laboratory, Monterey, CA

CTA: CWO

Computer Resources: HPE SGI 8600, HPE Cray EX [NAVY, MS]

Research Objectives: This project develops the capability to assimilate previously discarded cloud-affected satellite radiances into the Navy's next-generation numerical weather prediction (NWP) model and studies large- and small-scale interactions of tropical convective systems.

Methodology: The Navy Environmental Prediction System Utilizing a Non-hydrostatic Core (NEPTUNE) is the Navy's next-generation global and regional NWP model. NEPTUNE's data assimilation is facilitated through the Joint Effort for Data-Assimilation Integration (JEDI)-enabled Flexible Assimilation Linking Collaborations to Operations for NEPTUNE (FALCON). This project is adapting FALCON to assimilate both clear- and cloudy-sky radiances (also known as all-sky radiances), which will provide NEPTUNE with additional observation coverage in the tropics. DoD HPC at the DSRC is leveraged to run case studies using the new all-sky assimilation capability, both to evaluate the assimilation implementation and to study the two-way interaction between the large-scale (~1,000 km) atmospheric humidity and the small-scale (10 km–100 km) convective characteristics of individual storms in the tropics. The all-sky radiances are assimilated using an ensemble approach, which is extremely expensive because multiple instances of the NEPTUNE model must be run for each forecast. The evaluation of the technique is done by running NWP simulations using the all-sky radiances and comparing the resulting analyses and forecasts with simulations to observations and simulations that did not assimilate the data. Improvements to the forecasts from use of the observations will indicate whether the technique is working as expected.

Results: Much of the work conducted so far has focused on the development of the initial assimilation capability of the all-sky radiances into NEPTUNE; however, a preliminary test case on convective storms over the Caribbean Sea and the Gulf of Mexico in 2021 has now been run. In this case study, nearly 250,000 all-sky radiances were assimilated over a 6-hour cycling period covering nearly a 10.9 million-square-kilometer domain. The assimilation method itself used 31 CPUs for approximately 60 minutes of wall-clock time on narwhal but requires the input of 31 NEPTUNE forecast members, which required a total of 19,840 CPUs over 30 minutes of wall-clock time. In this particular case study, the radiance assimilation tends to reduce the overpredicted intensity of storms and improves underpredicted storms by enlarging them (Fig. 1); however, it is likely that the assimilation reduces the storm intensity beyond what is supported by observations (Fig. 1). These improvements can be quantified through the equitable threat score (EQTS, Fig. 2), which shows that the radiance assimilation improves the quality of the model's initial condition (EQTS values closer to 1 indicate better accuracy). The majority of the absolute improvement is in brightness temperature bins corresponding to 235 and 240 K; these brightness temperatures mostly correspond with clear regions.

DoD Impact/Significance: The U.S. Navy has significant responsibilities in the tropics, and strong tropical convection imposes a risk to Navy operations through damaging winds, high waves, heavy precipitation, and limited visibility. Rapidly changing weather conditions in these regions due to tropical convective storms present significant challenges to the Navy for mission planning and execution. The scientific understanding from this project will lead to significant tactical advantages for the Navy through the improved prediction of tropical convective storms.

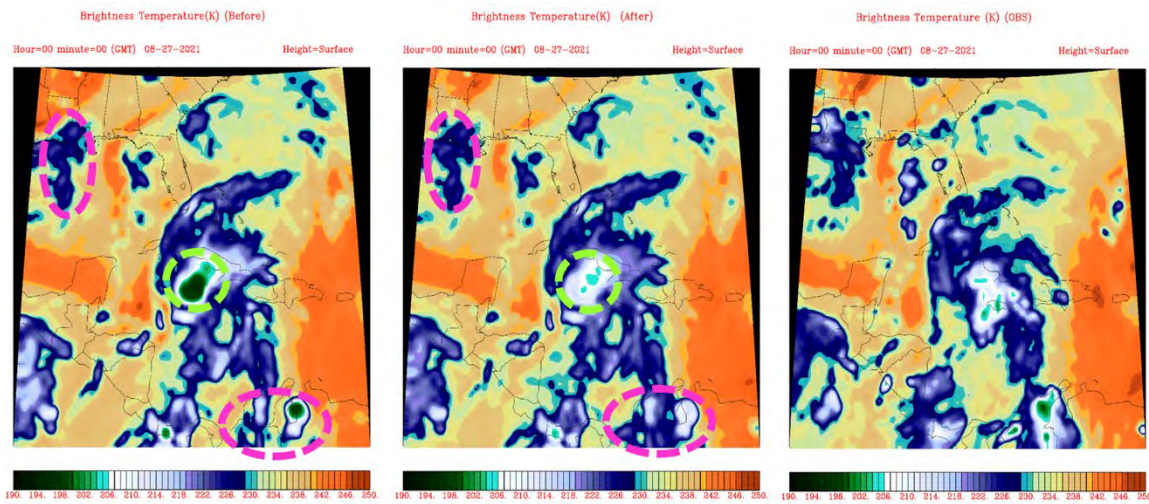


Figure 1. Simulated brightness temperature before all-sky radiance data assimilation (left panel) and after data assimilation (middle panel), along with brightness temperature observations (right panel). The magenta, dashed lines denote storm areas in which the radiance assimilation enlarged the storms that were underpredicted by the model; green, dashed lines denote areas in which the data assimilation reduced the overpredicted storm intensity.

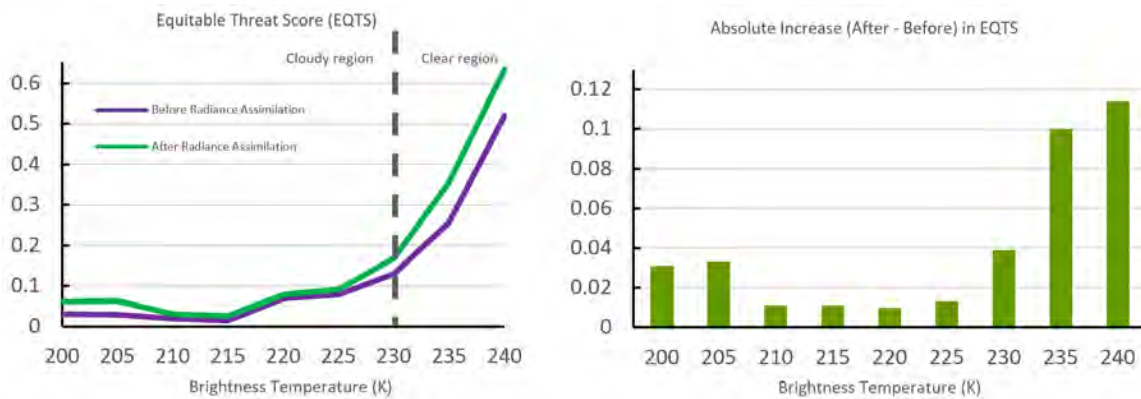


Figure 2. EQTS before and after radiance assimilation, plotted against brightness temperature (left panel) and the absolute difference in improvement in EQTS, binned into brightness temperature categories (right panel).

Title: Bio-Optical Modeling and Forecasting

Author(s): J.K. Jolliff, S. Ladner, and T. Smith

Affiliation(s): U.S. Naval Research Laboratory, Stennis Space Center, MS

CTA: CWO

Computer Resources: HPE SGI 8600 [NAVY, MS]

Research Objectives: The research objectives for FY23 were 1) to continue final testing of the complete end-to-end software and modeling components for the 6.4 “Visible Band Satellite Data to Improve Ocean Model Radiative Transfer” (VISOR) program, and 2) to perform numerical experiments using the Coupled Ocean Atmosphere Mesoscale Prediction System (COAMPS[®]) model in support of the 6.1 program “Integrated Radiometric Indices of Surface Ocean Features (IRIS),” wherein we compare numerical model results with satellite image sequences as part of an integrated physical-bio-optical-remote-sensing analysis.

Methodology: For research objective 1, we have developed a system that starts with satellite processing using the Global Optical Processing System (GOPS) to gather all satellite ocean color data from a growing constellation of satellite platforms. The data are mapped, processed, and composited, and then are sent to the Navy Coupled Ocean Data Assimilation (NCODA) system for assimilation into ocean models. The ocean models then use the information to determine radiant heating rates in the upper ocean due to solar energy attenuation. Without this information, the ocean models must make an uninformed estimate about the solar attenuation length scale in the upper ocean, and this is the default model operational mode. Final testing of the system consists of validating temperature and other ocean state variable predictions using the VISOR systems versus the default model modes. In support of research objective 2, we have set up multiple nested-model configurations for the Gulf of Mexico using the COAMPS[®] framework. Hourly COAMPS[®] results were compared to hourly to daily satellite image sequences for particular scenes where significant changes were evident in the satellite data over the continental shelf, and particularly following the passage of atmospheric fronts. COAMPS[®] results were evaluated with both the atmospheric model output and ocean model output as well as the calculated fluxes of thermal energy between the two planetary boundary layers.

Results: The final testing experiments for the VISOR program confirmed that ocean color satellite data improves model performance of surface temperature predictions, even with the assimilation of satellite SST fields. This is because error in solar shortwave penetration estimation causes a structural problem in the ocean models that cannot be remedied with surface temperature assimilation alone. Air-sea fluxes are also impacted by these differences, leading to divergences in the atmospheric model results. Results from the final testing experiments were presented at the 2023 International Ocean Colour Science meeting. For the 6.1 IRIS program, COAMPS[®] model results were used to examine how hourly and daily satellite ocean color sequences are impacted by changes in water column stability driven by air-sea interactions. Moreover, the numerical hydrodynamic model output was used to drive a sediment submodel that very accurately mimicked patterns seen in the satellite imagery. The integrated analysis showed that the apparent amount of nearshore turbidity was excited then relaxed based upon the COAMPS[®] simulated hydrodynamic stability of the water column (Fig. 1). When the simulated air-sea system was in a state of ocean cooling or warming, the turbidity was enhanced or diminished, respectively.

DoD Impact/Significance: Improving the performance of operational ocean models impacts a wide array of Navy activities that use environmental forecasts for support. The 6.4 VISOR program is in its final year and HPC resources have been vital to its success. COAMPS[®] model executions are also used to support basic research into coastal environmental variability that eventually translates into more applied battlespace environments characterization and prediction.

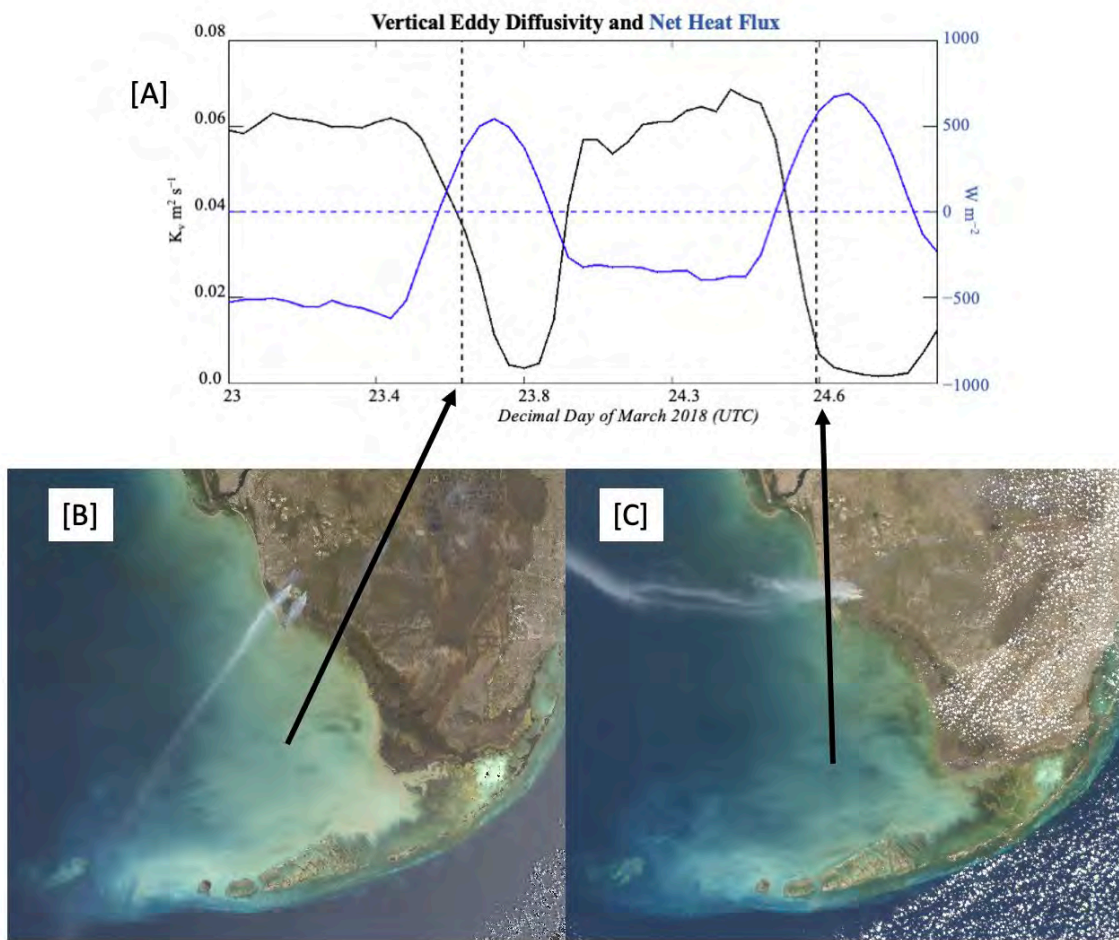


Figure 1. [A] COAMPS[®] results for net heat flux (blue) and vertical eddy diffusivity (black) for a point on the southern West Florida Shelf, [B] satellite true color image from the Ocean Land Colour Imager (OLCI) on the Sentinel 3A satellite (ESA) on 23 March 2018, and the same for [C] 24 March 2018. Diminished turbidity in the color image corresponds to a sharper drop in the vertical eddy diffusivity diurnal pattern on 24 March.

Title: Data Assimilation Studies Project
Author(s): J. Tsu and W.F. Campbell
Affiliation(s): U.S. Naval Research Laboratory, Monterey, CA
CTA: CWO

Computer Resources: Cray XC40/50 [ERDC, MS]; HPE SGI 8600, HPE Cray EX [NAVY, MS]

Research Objectives: Our objective is to improve the quality of numerical weather predictions (NWP) by leveraging vast quantities of observations. Data assimilation (DA) corrects model analyses of the atmosphere, ocean, or surface using a nonhomogenous collection of observations. This project develops, tests, and improves: 1) our 4D-Var assimilation system, which is coupled to the atmospheric global model NAVGEM (Navy Global Environmental Model) and is used by the Navy Earth System Prediction Capability (ESPC), 2) fully ensemble-based data assimilation, now including the ionosphere, 3) hybrid ensemble/4D-Var data assimilation, 4) variational bias correction and its impact on clear-sky microwave assimilation, 5) unified model verification efforts, 6) assimilation of new observations from microsats and NESDIS satellite winds, 7) testing new release of NAVDAS for COAMPS[®] 2.8.13 as well as near-real-time testing of the Ensemble Navy Aerosol Analysis Prediction System, and 8) the 3D-Var assimilation system coupled with the Navy Environmental Prediction System Utilizing the NUMA Core (NEPTUNE). Our goal is to assimilate traditional data (generally in situ, e.g., weather balloons, ship, aircraft, or buoy reports) as well as data from a variety of new sources (often spaceborne) efficiently and effectively to provide the best atmospheric analysis and ultimately to improve numerical weather forecast performance. HPC resources are critical for assimilation studies and next-generation fully coupled atmosphere/land/ocean/sea ice systems.

Methodology: A variety of experimental setups are used to develop and test our global and regional models and data assimilation systems, as well as large datasets of in situ and satellite-based observations for several summer and winter months.

Results: Because DA has a multitude of applications, numerous types of research take place under this project using the Navy's latest global (Hybrid Ensemble NAVGEM, NEPTUNE) and mesoscale (COAMPS[®]) models, along with our global (NAVDAS-AR, hybrid NAVDAS-AR, and coupled hybrid NAVDAS-AR, JEDI) and mesoscale (COAMPS-AR) data-assimilation systems. Results from FY23 research include: 1) assimilation of wind profiles retrieved from the Infrared Atmospheric Sounding Interferometer (IASI), provided by EUMETSAT, in the NAVGEM model demonstrates as beneficial an impact as traditional satellite wind observations retrieved from low-Earth-orbiting (LEO) satellites, 2) discovery of issues with underutilization of water vapor-sensitive observations in NAVGEM radiance assimilation as well as sensor issues with AMSU-A on METOP-B, 3) transition and operational implementation of updated NAVGEM 2.1 at Fleet Numerical Meteorology and Oceanography Center, 4) completed long NAVGEM runs whose output will be used to support broader testing periods for NEPTUNE, 5) development of an all-sky radiance assimilation system for NEPTUNE whose preliminary results show beneficial impacts.

DoD Impact/Significance: The computing platforms provided by HPCMP offer incredible computational resources that make possible the running of experiments involving millions of observations. These resources also provide a common environment for collaboration and the rapid development of NRL's multiple data-assimilation systems. Large common datasets can be stored and accessed by many researchers, greatly facilitating collaboration between NRL scientists at different locations (Monterey, Stennis, and DC) and scientists in academia, government, and other laboratories. The advancements of NEPTUNE, JEDI, NAVDAS-AR, NAVGEM, and COAMPS-AR systems would not have been possible without the HPCMP systems. The core and future of Navy data-assimilation capabilities are being developed mostly, and in many cases solely, by using the resources provided by HPCMP. In summary, the ability to access the HPCMP resources is critical to prepare technology for successful transfer to operations.

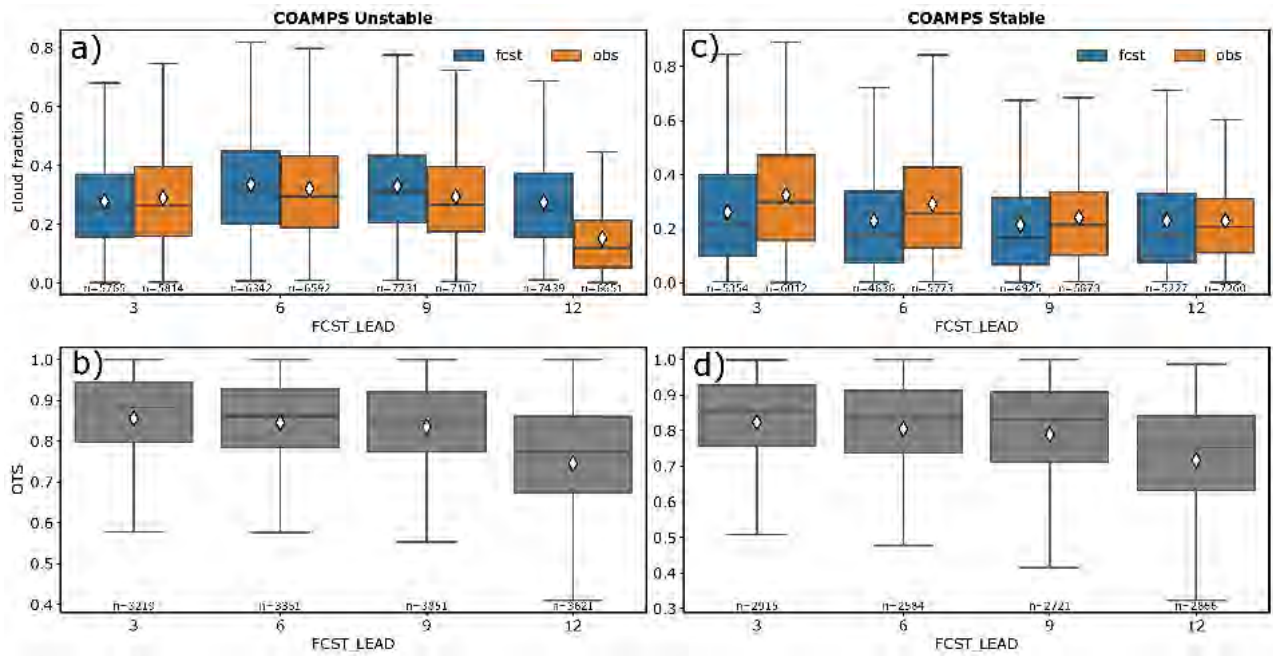
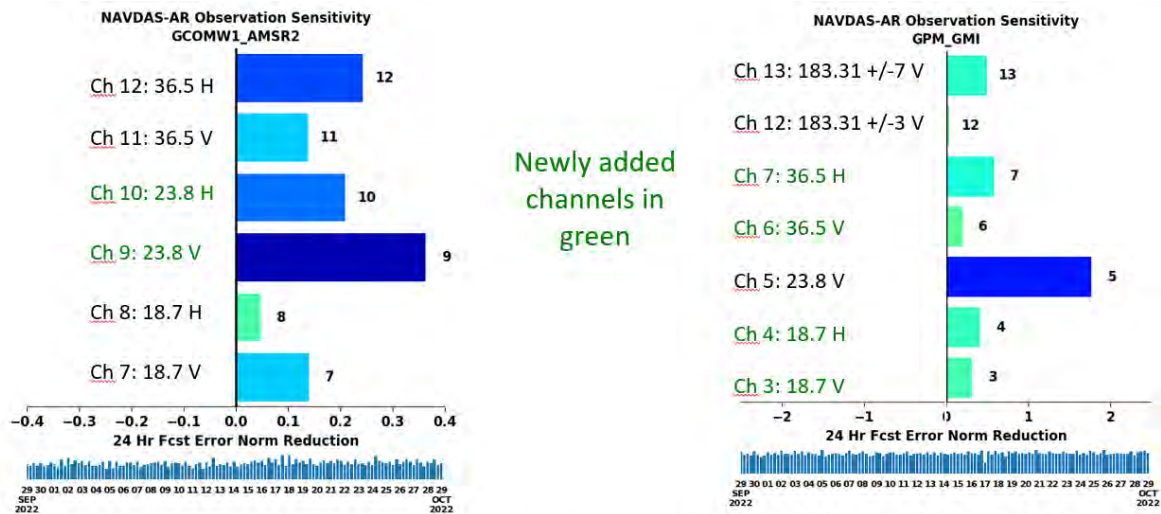


Figure 1. Top: cloud fraction for the forecast and observed fields at lead times of 3, 6, 9, and 12h for COAMPS® stable and unstable clouds (numbers labeled beneath each bar denote the total number of objects for each forecast lead hour). Bottom: the associated object threat score, where the number of matched objects is noted. Overall, COAMPS predicts the stable and unstable clouds well and has decent object threat score (0.8–0.85 for lead times up to 9 h and 0.7–0.75 for lead time of 12 h).



AMSR-2: Window channels only. Conical 55 deg, swath 1450 km, 10 km/scan. Global coverage 1x/day. Integrated water vapor ~ 23 GHz dual polarization. 13:30 asc (Before: Ch 9, 10 only)

GMI: Conical: 53deg, useful swath 850 km ~13.4 km/scan. Near global coverage in 2 days. High latitudes >70deg not covered. (Before: Ch 5, 12, 13 only)

Figure 2. Left: NAVDAS-AR Observation Sensitivity GCOMW1_AMSR2. Right: NAVDAS-AR Observation Sensitivity GPM_GMI.

THIS PAGE INTENTIONALLY LEFT BLANK



Signal Image Processing

SIP covers the extraction of useful information from sensor outputs in real time. DoD applications include surveillance, reconnaissance, intelligence, communications, avionics, smart munitions, and electronic warfare. Sensor types include sonar, radar, visible and infrared images, and signal intelligence (SIGINT) and navigation assets. Typical signal-processing functions include detecting, tracking, classifying, and recognizing targets in the midst of noise and jamming. Image-processing functions include the generation of high-resolution, low-noise imagery, and the compression of imagery for communications and storage. The CTA emphasizes research, evaluation, and testing of the latest signal-processing concepts directed toward these embedded systems. Usually, such processors are aboard deployable military systems and hence require hefty packaging and minimum size, weight, and power. System affordability is expected to improve by an order of magnitude through the development of scalable codes running on flexible HPC systems. This will enable the traditional expensive military-unique “black boxes” required to implement high-speed signal/image processing to be replaced by COTS HPC-based equipment.

Title: Retrieving Surface Soil Moisture from CyGNSS Reflectivity Measurements

Author(s): J.D. Ouellette, E.M. Twarog, L. Li, and S.M. Grossman

Affiliation(s): U.S Naval Research Laboratory, Washington, DC

CTA: SIP

Computer Resources: Cray XC40/50 [ERDC, MS]

Research Objective: Cyclone Global Navigation Satellite System (CyGNSS) is a NASA-funded constellation of microsatellites, each of which receives Global Positioning System (GPS) downlinks and GPS reflections from the Earth's surface in order to derive geophysical and oceanographic parameters. Although CyGNSS's primary objective is to measure ocean surface wind speed (by proxy of surface roughness), it has been shown that CyGNSS measurements are also sensitive to land surface parameters to include surface soil moisture (SSM). This project investigates the derivation of soil dielectric properties and volumetric SSM from CyGNSS. This task is achieved by applying a change detection algorithm to a time series of conditioned CyGNSS reflectivity observations.

Methodology: The approach employs a matrix-based change detection algorithm to derive SSM estimates from CyGNSS reflectivity data. An NRL Karles Fellowship supported development of the original version of this SSM retrieval algorithm, referred to as the time-series ratio (TSR) method. The algorithm relies on ratios between consecutive radar backscatter or reflectivity values within a time series of observations. These ratios, which populate the off-diagonal terms of the TSR matrix equation, theoretically change only with changes in SSM, given that changes in surface roughness and/or vegetation are negligibly small between each repeat pass. The TSR method was originally conceived for use with L-band radar and radiometer data from NASA's Soil Moisture Active/Passive (SMAP) mission. TSR method error performance with SMAP data has since been assessed using in situ data; the TSR method outperformed the official SMAP algorithm and furthermore required no training data and minimal ancillary information. The same algorithm has since been applied to CyGNSS under this project, with significant modifications being necessary for application to this new sensor suite, including reflectivity preconditioning. The preconditioning procedure includes screening for coherence-dominant or low signal-to-noise-ratio reflectivity values, and also includes a newly developed denoising procedure.

Results: Figure 1 shows qualitative algorithm results from CyGNSS/TSR in the form of volumetric soil moisture estimates in the CyGNSS coverage area. Near-concurrent SMAP radiometer-based SSM data was used to cross-validate the CyGNSS SSM retrieval via the modified TSR method. An RMSE of 5.7% was observed during SMAP cross-validation. More detailed error statistics are reported in Fig. 2. Further validation is underway via comparison with upscaled in situ data at the SMAP validation core sites called out in Fig. 2.

DoD Impact/Significance: It is well known that there is a close relationship between SSM and temperature, humidity, and precipitation. Navy forecasting tools use models of soil moisture, derived from precipitation measurements, in order to constrain storm forecasts. A lack of soil moisture data leads to poorly constrained regional weather forecasts with a larger variance in moderate-to-long-term predictions. Furthermore, with the electromagnetic spectrum increasingly congested by wideband communications, the field of microwave remote sensing is beginning to rely more heavily on the use of signals of opportunity to fill data gaps in forecast models. This project addresses the following Science and Technology areas identified by the Navy: Assure Access to Maritime Battlespace, Information Dominance, and Platform Design and Survivability.

CYGNSS SSM (NRL-OSU Algorithm), July 1--7, 2020

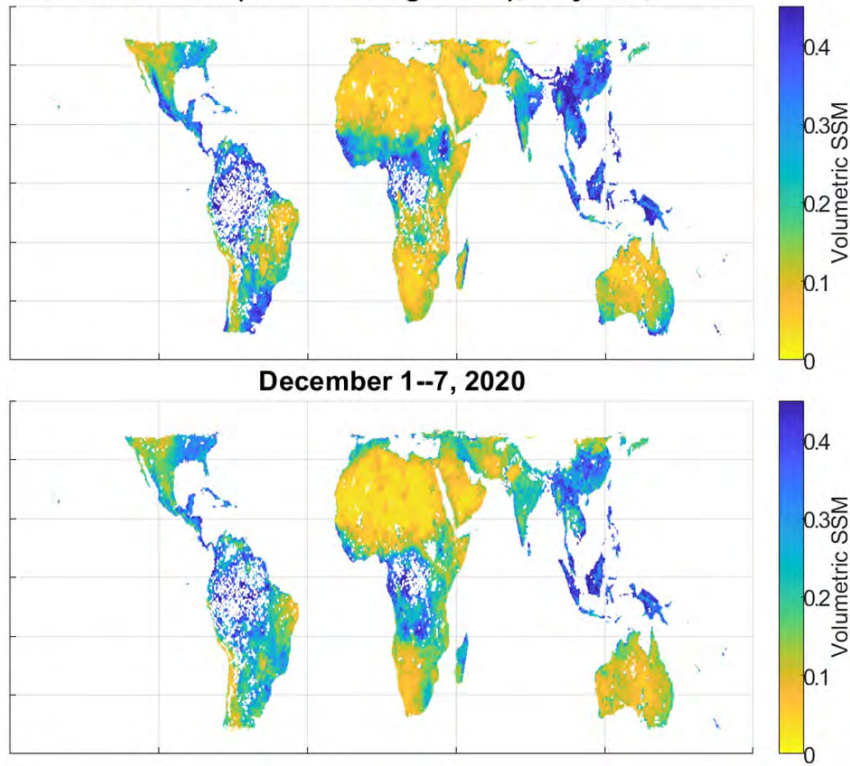


Figure 1. Retrieved volumetric SSM maps using the TSR algorithm with CyGNSS reflectivity inputs. (Top) July 1–7, 2020, (bottom) December 1–7, 2020.

Site-Specific Stats: $p = 4$; OL thresh = 2.5%; SNR thresh = 1 dB; PR thresh = 1.5; ts len = 30 DoY

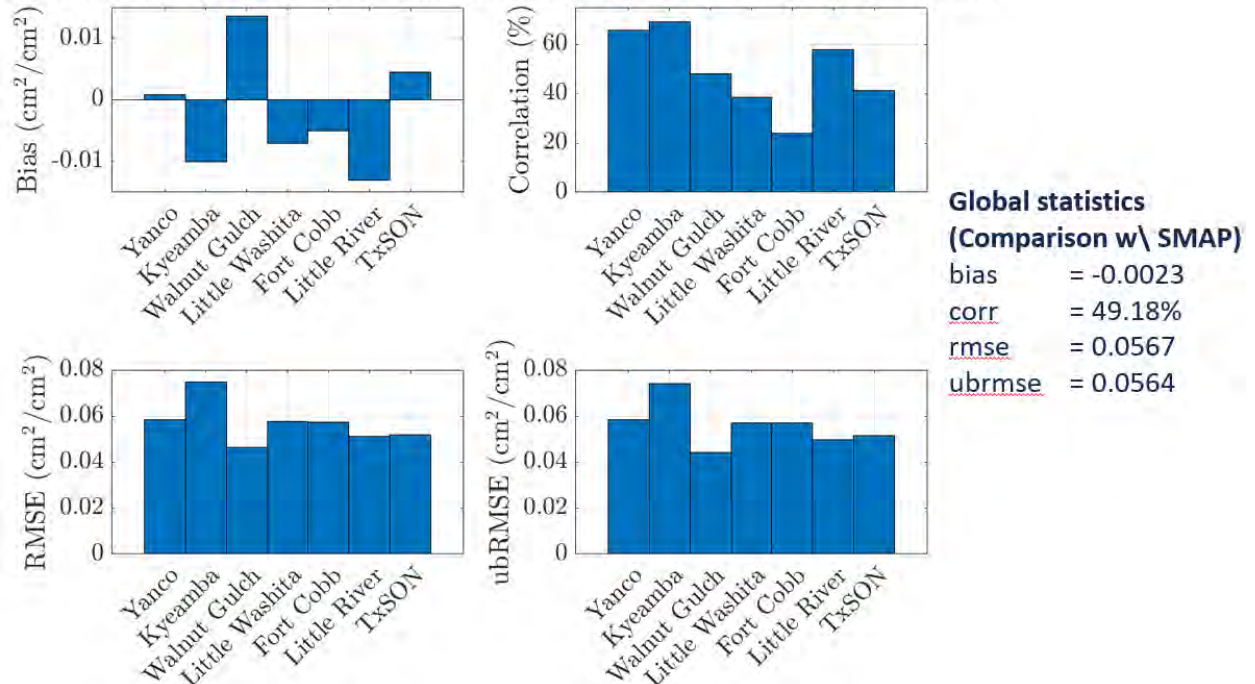


Figure 2. Validation-site-specific and global error statistics computed through cross-validation between CyGNSS/TSR algorithm and the official SMAP level-2 SSM product.

Title: Application of Physics-based Machine Learning to Navy Problems

Author(s): L.N. Smith

Affiliation(s): U.S. Naval Research Laboratory, Washington, DC

CTA: SIP

Computer Resources: HPE Cray EX [AFRL, OH]; Liquid, Power 9 [ARL, MD]

Research Objectives: The primary objective of our Physics-based Acoustic machine Learning for In-Situ Applications (PALIS) project in FY23 was the fast emulation of NRL's acoustics-modeling simulations of transmission loss (TL). Our technical approach made substantial progress.

Methodology: This year's methodology was based on adapting the deep-learning method for computer vision known as image-to-image translation. In our acoustics domain, the input "image" represents undersea physical properties that impact how sound travels in the ocean, which is known as the sound speed profile (SSP). The output "image" is the transmission loss (TL) predicted by the acoustics simulator. Since the TL results also depend on the properties of the sound source, the generated TL depends on these scalar properties in addition to the two-dimensional (2D) SSP. Hence, a new multimodal approach was required.

Results: Significantly, our emulator obtained a speedup of over 100 times compared to the acoustic simulator. In addition, inference with our emulator required only 0.20 seconds per sample for 1,676 samples, with the secondary benefit of essentially no variation in execution time from one run to another (unlike a physics-based acoustics simulator) because the number of floating-point operations is independent of the input.

In addition, our approach (i.e., a variant of image-to-image translation) required a new architecture that was based on architectures used in multi-modal generative models (see Fig. 1). Scalars and/or vectors are fed through dense networks before concatenation to encoded SSPs that are used to compute TLs. In this way, the computation can be modified by other factors that are not measured properties of the environment, such as source frequencies. Evaluation of this model is ongoing but the initial results are promising.

DoD Impact/Significance: Our work demonstrates that applying machine learning to acoustic problems is sound. We are now applying machine-learning methods to solve other challenges in various physics domains in order to enable substantially improved environmental and situational understanding by our fleet. In addition, the understanding gained by the experiments on the HPC GPU servers builds on all the previous understanding gained from previous experiments, and this understanding is crucial for our future progress in the field.

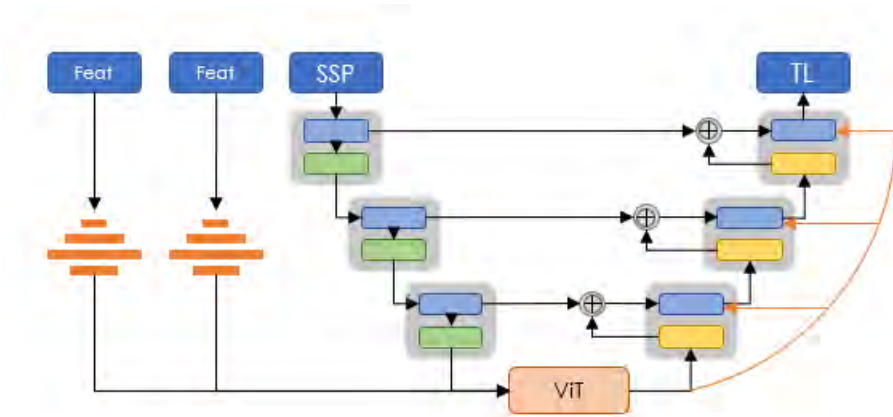


Figure 1. Generalized U-Net (GUN) architecture that was developed to permit multimodal inputs. Scalars and/or vectors are fed through dense networks before concatenation to encoded sound speed profiles (SSPs) that are used to compute transmission losses (TLs). In this way, the computation can be modified by other factors that are not measured properties of the environment, such as source frequencies.

THIS PAGE INTENTIONALLY LEFT BLANK



Space and Astrophysical Science

Space and Astrophysical Sciences (SAS) research and development advance understanding, specification and prediction of the Earth's atmospheric and space domains to exploit the extended operational environment for military advantage and to minimize environmental impacts on military operations. The SAS Computational Technology Area (CTA) embodies the use of mathematics, computational science, and engineering in the analysis, design, identification, modeling, and simulation of the space and near-space environment, and of all objects therein, whether artificial or natural. The SAS CTA encompasses foundational discovery research to study the atmospheres of the Sun and the Earth, including solar activity and its effects on the Earth's atmosphere and ionosphere and near-Earth space, and the unique physics and properties of celestial sources. SAS employs an extensive array of physical and empirical models and analysis tools to integrate observations and theoretical understanding for ever-improving DoD enterprises within, and exploitation of, the extended operational environment. The CTA melds the strengths of a broad range of physical sciences — atomic and molecular physics, materials science, plasma physics, applied optics, radiation survivability, electronic warfare, directed-energy technology, astronautics and space propulsion, orbital mechanics, space situational awareness, and remote sensing — into a structure that helps the DoD multiply force combat effectiveness.

Title: Modeling Propagation of Ionospheric Disturbances Initiated by Magnetospheric Substorms
Author(s): J. Haiducek and J. Helmboldt
Affiliation(s): U.S. Naval Research Laboratory, Washington, DC
CTA: SAS

Computer Resources: HPE SGI 8600 [AFRL, OH], [NAVY, MS]

Research Objectives: This program aims to develop data-assimilation capabilities for space weather applications, particularly focusing on SAMI3 (SAMI3 is Another Model of the Ionosphere), an ionospheric simulation code. Our long-term goal is to assimilate total electron content (TEC) observations from radio interferometers. In the short term, we are utilizing GNSS TEC observations to test the assimilation process. We aim to use the resulting data-assimilation system to better understand transient ionospheric phenomena such as ionospheric irregularities and traveling ionospheric disturbances (TIDs).

Methodology: To support the assimilation of data into SAMI3, we have developed a new parallel data-assimilation tool called LightDA. LightDA is modular software library written in Fortran that provides data-assimilation capabilities in a generic way applicable to any model whose state can be represented as a one-dimensional (1D) array of real numbers. LightDA updates an ensemble of model states to better fit a set of observations. The assimilation is performed using an ensemble Kalman filter. Interfaces to LightDA have been created for SAMI3, and a generic model consisting of a random state vector was created to test LightDA's parallelism.

Results: During FY23, we generalized the parallelism of LightDA, enabling it to support a wider variety of parallelization strategies. This can improve performance by reducing MPI communication when assimilating data from a model that is already parallelized. The more generalized parallelism also enabled experiments to test the performance impact of different parallelization schemes. Previously, LightDA assigned sections of the model state to MPI processes at random, but we found that better efficiency was achieved when assigning an equal-sized contiguous section of the state array to each MPI process. The previous strategy of random assignment may prove more efficient in cases where the observations are spaced very unevenly throughout the model domain, but this remains to be tested. We also conducted tests using LightDA to assimilate synthetic observations (generated by a separate run of SAMI3) into a randomized ensemble of SAMI3 simulations. As shown in Fig.1, the assimilation system achieves an ensemble standard deviation that closely matches the ensemble's root mean squared error relative to the synthetic observations, a demonstration that the system is working as intended.

DoD Impact/Significance: SAMI3 can simulate a variety of ionospheric phenomena that can impact DoD operations by altering radio signals used for radar and communications. The data-assimilation capabilities developed in this program will provide insights into how these ionospheric features develop and will influence the future development of ionospheric forecasting capabilities.

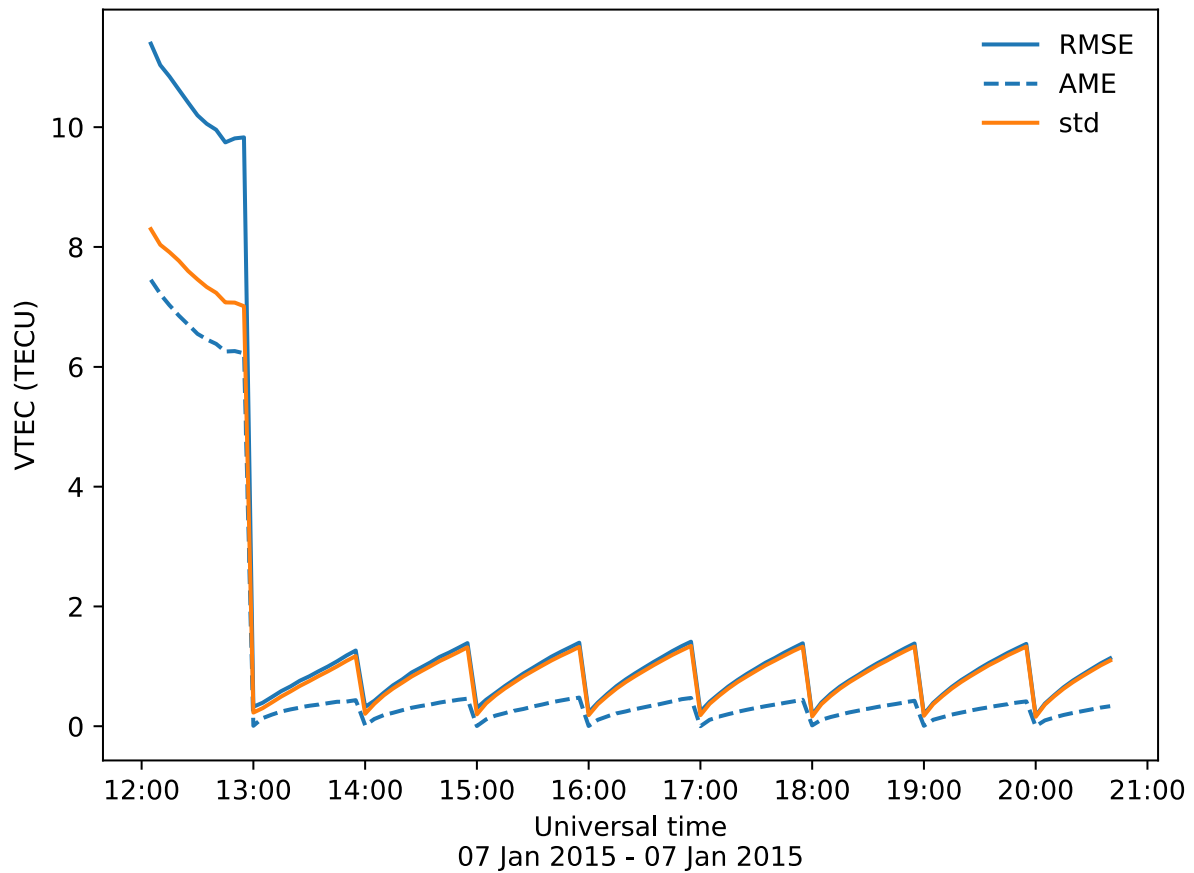


Figure 1. Time series of vertical TEC errors from an ensemble of SAMI3 simulations being updated by LightDA with synthetic TEC observations. The three traces show root mean squared error (RMSE), absolute mean error (AME), and ensemble standard deviation (std). The data-assimilation filter updates the ensemble once per hour of simulation time.

Title: Electromagnetic Pulses from Hypervelocity Impacts on Spacecraft

Author(s): A. Fletcher

Affiliation(s): U.S. Naval Research Laboratory, Washington, DC

CTA: SAS

Computer Resources: SGI ICE X [ARL, MD]

Research Objectives: The objective of this project is to use large-scale simulations to understand electromagnetic pulses (EMPs), electrical anomalies, and other plasma signatures that are associated with hypervelocity impacts (HVIs) on spacecraft and to develop mitigation strategies.

Methodology: Hypervelocity impacts are simulated with two physical models: 1) a continuum mechanics approach for the formation of the crater and plasma, and 2) a kinetic electromagnetic plasma approach for microscale physics and emission of radiation. ALEGRA, a hydrocode from Sandia National Laboratories, is used for the continuum dynamics regime. VPIC, a particle-in-cell from Los Alamos National Laboratory, is used for the kinetic plasma regime. We run simulations to compare to both our theoretical predictions, in particular, the generation of electromagnetic waves and interaction with the spacecraft potential, and to compare to experimental data from Van de Graaff experiments and NASA's Parker Solar Probe.

Results: This year, we focused on simulations related to nonlinear plasma signatures that can be generated by meteoroids and orbital debris moving through space plasma. We matched 1D particle-in-cell (PIC) simulations to a theoretical model based on the forced KdV equation. We showed that for electrostatic solitons, considerably higher grid resolution is necessary to accurately resolve the Debye scale structures due to the small ion Debye length in these cold simulations. We tested different methods of representing the debris source in the simulation. These methods are physically equivalent but numerically different. We showed that a charged point source gives the most consistent results, even in an electromagnetic code. We found that the ion temperature is critical to the generation of solitons; specifically, that any plasmas with T_i near T_e will damp the solitons into nonexistence without including the effects of shear in three dimensions (3D). Higher-dimensional simulations demonstrated the same generation of solitons, except with far lower amplitude due to geometric effects. We did numerous two-dimensional (2D) soliton simulations with a background magnetic field. We showed that when the debris moved parallel to the field, the soliton amplitude is enhanced and focused spatially. For oblique propagation, we showed that the solitons propagate at an angle between the velocity vector and the magnetic field vector, and this intermediate angle is a function of the plasma mass ratio.

DoD Impact/Significance: Protection of critical DoD space assets from this threat is necessary to assure uninterrupted C4ISR capability, which is critical for operational success as envisioned in the Navy's S&T strategic plan for information dominance. Countermeasures against hypervelocity impacts of microprojectiles on DoD space assets depend on the knowledge of the electromagnetic power and frequency spectrum of the impact-associated EMPs and other plasma-based signatures.

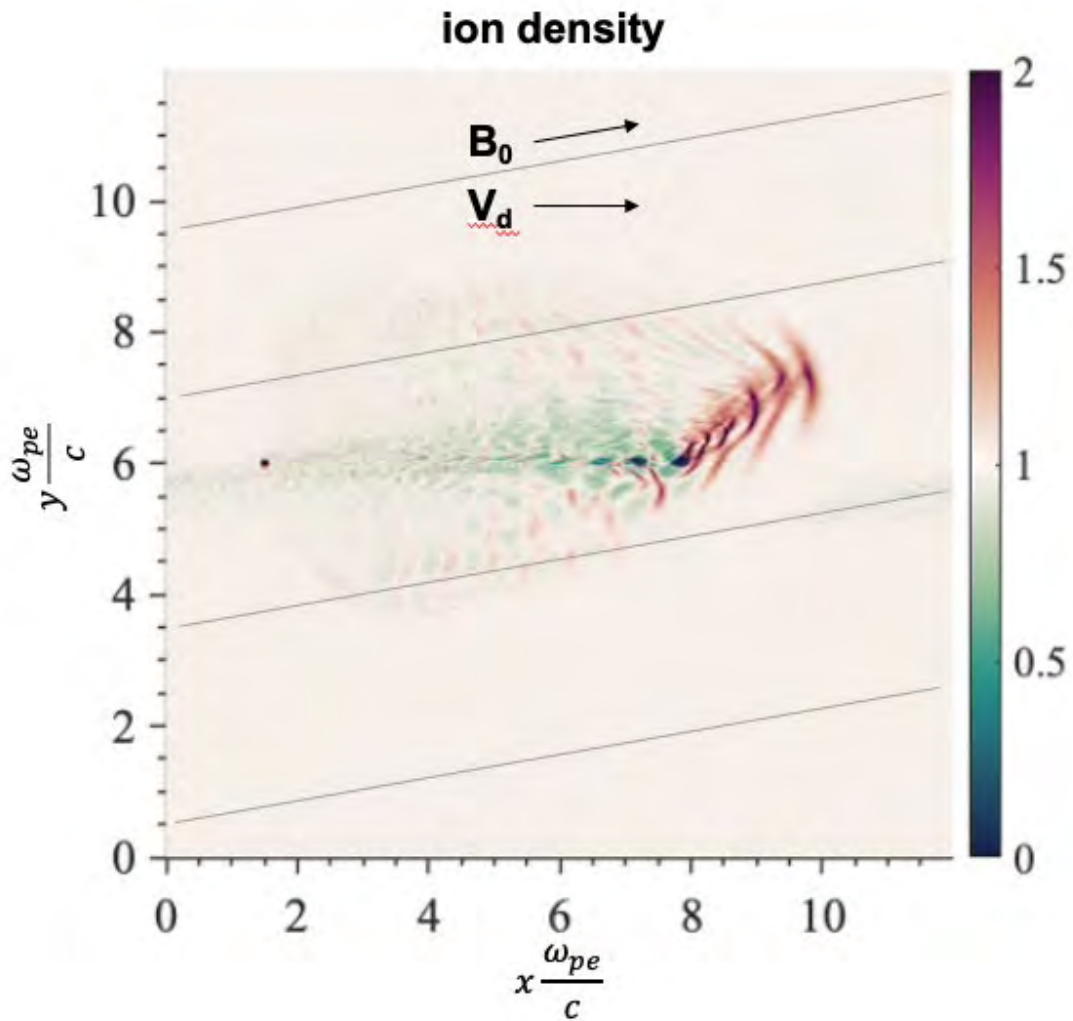


Figure 1. Ion density from a particle-in-cell (PIC) simulation of electrostatic ion acoustic solitons generated by a piece of orbital debris moving at Mach 1.1 in LEO. The debris is moving to the right in the simulation. The debris vector and Earth's magnetic field vector are offset by 10 degrees, causing the precursor solitons to propagate at an intermediate angle.

Title: Global Kinetic Simulations of Space Plasma Waves and Turbulence

Author(s): A. Fletcher

Affiliation(s): U.S. Naval Research Laboratory, Washington, DC

CTA: SAS

Computer Resources: SGI ICE X [ARL, MD]

Research Objectives: The objectives of this project are 1) to support an NRL and DARPA sounding rocket experiment program, SMART (space measurement of a rocket-released turbulence, whose launch has moved from fall 2021 to fall 2024 out of Wake Island) by helping to choose mission parameters and understanding the data from the experiment, and 2) to develop the capability to simulate near-Earth space plasmas on both a global scale while including kinetic effects.

Methodology: We use a combination of four codes: 1) ALEGRA, a continuum dynamics code from Sandia National Laboratories, 2) VPIC, a particle-in-cell (PIC) code from Los Alamos National Laboratories, 3) an NRL-built direct simulation Monte Carlo (DSMC) code, and 4) WICKED, a wave-in-cell (WIC) code developed at NRL. We will determine the density and optical/radar signature of the barium cloud, the amplitude and spectrum of the electrostatic and electromagnetic waves, and the rate of particle precipitation from the radiation belts. WIC, which could simulate the entire process, will need validation via comparable PIC runs. WIC will then be used to simulate as much of the cascade as possible within one simulation.

Results: We finished the series of three-dimensional (3D) simulations of nonlinear scattering in the ion ring instability, which will be published shortly. These simulations included a baseline case, a higher plasma-beta case, and a high-resolution two-dimensional (2D) case with the magnetic field in the plane of the simulation. The final part of the analysis was to show evidence of nonlinear induced scattering being responsible for electromagnetic waves. Using the simulation data, we found several pieces of evidence of nonlinear scattering that match theory and prior experiments at NRL. Crucially, we identified the virtual/quasimodes that facilitate the scattering process and demonstrated that the linear and nonlinear rates match theory. The extremely high-resolution simulations in 2D showed the modes in higher spectral resolution and simulations at different values of plasma beta to show that scaling is consistent with nonlinear scattering instead of three-wave coupling.

DoD Impact/Significance: The SMART experiment and associated simulations will study turbulence in the ionosphere coupling to waves in the magnetosphere. Given the DoD/Navy reliance on spaceborne assets, understanding the space environment is critical to assure uninterrupted C4ISR capability and to maintain information dominance.

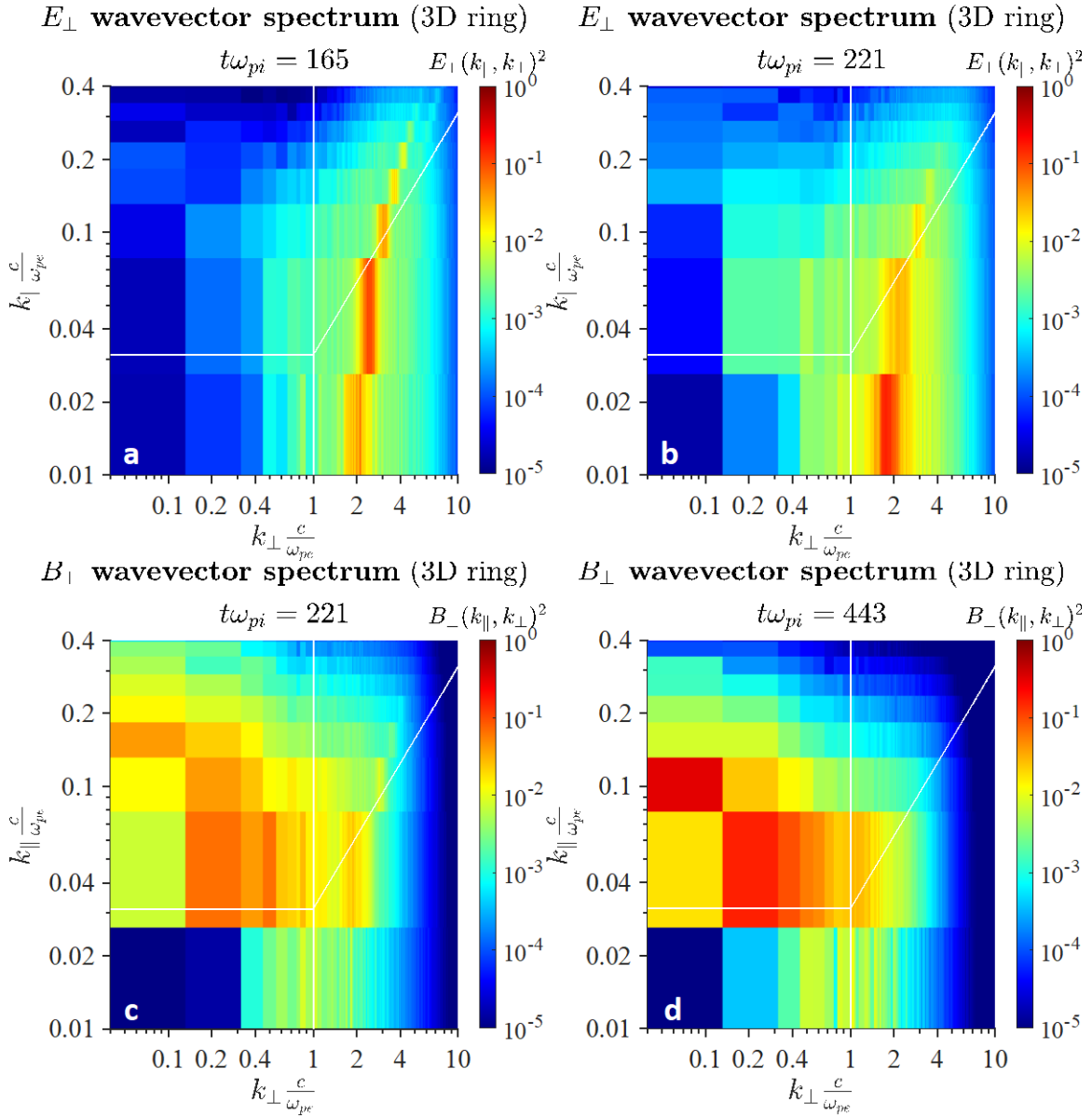


Figure 1. Wavevector spectra from the large-scale 3D particle-in-cell simulations of the ring instability and nonlinear induced scattering into whistler waves. Panel (a) shows the perpendicular electric field from the lower hybrid waves during the initial growth of the instability. Panel (b) shows the condensation of these waves to electrostatic near $k_{\parallel} = 0$. Panel (c) shows the oblique whistler waves excited by the scattering of the waves from panels (a) and (b). These waves are the entire point of the SMART experiment, and these simulations provide further confidence in the physics in the experiment. Panel (d) shows parallel propagating whistler waves at the end of the simulation.

Title: Searches for Millisecond Pulsars and Pulsar Emission Modeling

Author(s): P.S. Ray¹ and J. Deneva²

Affiliation(s): ¹U.S. Naval Research Laboratory, Washington, DC; ²George Mason University, resident at U.S. Naval Research Laboratory, Washington, DC

CTA: SAS

Computer Resources: Cray XC40/50 [ERDC, MS]

Research Objectives: The first goal of this project is to search for millisecond pulsars in ground-based data from the Robert C. Byrd Green Bank Telescope (GBT) in West Virginia. These searches require high-performance computing resources because of the massive parameter spaces that must be searched. The second goal of the project is to model the X-ray emission of pulsars based on data from the NICER X-ray telescope that is currently on the International Space Station.

Methodology: We use custom codes to search for pulsations in our radio data sets. These correct for frequency-dependent delays caused by interstellar dispersion and variable Doppler shifts caused by orbital acceleration in a binary system, then search over a broad range of candidate frequencies using very large Fourier transforms and harmonic summing. We split up the trials over a set of nodes on the cluster. We use another custom code to model pulsar emission. This is an iterative, computationally intensive process involving multithreaded calculations of the Bayesian likelihood of a number of model parameters.

Results: We used Onyx to fit several emission models of PSR J1231-1411. Each model includes known pulsar parameters like the rotation period and pulse shape, and unknown parameters like the pulsar's mass and radius, and the locations and shapes of the hot spots on the pulsar's surface that produce the X-ray emission. In addition to using NICER data in conjunction with data from XMM (the X-ray Multi-Mirror telescope, a spacecraft operated by the European Space Agency) we improved on our previous modeling work by incorporating the SCORPEON background model. Each letter in the model's name stands for a component responsible for a subset of events triggering the NICER detectors that do not originate from pulsars and are not necessarily X-rays. These background components include the South Atlantic Anomaly, cosmic rays, polar and precipitating electrons, non-X-ray particle interactions, and noise events within the NICER detectors.

We also processed GBT data on ten millisecond pulsars discovered in Fermi unidentified sources within the past couple of years. We were able to determine that they are in binary systems with periods ranging from a few hours to a month, and based on the predictive accuracy of the ephemeris we obtained from the GBT data, we were able to detect gamma-ray pulsations from one of the pulsars, J1102+0249. Observations of these pulsars continue with the GBT and we expect to be able to detect gamma-ray pulsations from more of them as our radio-derived ephemerides for them improve as we include the new observations when fitting the pulsar parameters.

DoD Impact/Significance: The main goal is to identify millisecond pulsars that are very stable rotators and therefore useful for detecting gravitational waves with a pulsar timing array (PTA). Among the ~3,300 known pulsars, only 35 fit this criterion and any addition to this set is a significant contribution to the nanohertz gravitational wave detection effort, as it improves the sensitivity of the PTA. The PTA approach to gravitational wave detection is complementary to LIGO and is sensitive to a different range of gravitational wave frequencies. The first PTA detection of the nanohertz gravitational wave background was published in 2023.

The objective of modeling pulsar emission is to obtain fits for as many pulsar mass-radius pairs as possible in order to constrain the equation of state of neutron star matter, an extreme state of matter that cannot be reproduced in a laboratory.

*This work was supported by NASA.

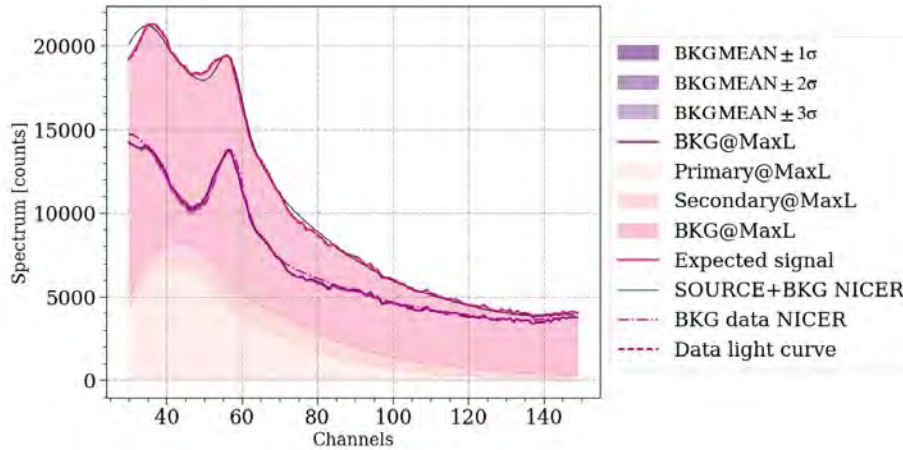


Figure 1. Maximum-likelihood X-ray emission components from an emission-modeling run on PSR J1231-1411 on Onyx using the SCORPEON background model. The plot shows photon counts vs. NICER energy channel sequence numbers. The shaded regions from bottom to top denote emission from the primary and secondary hot spots on the pulsar's surface (pale orange) and the background (pink).

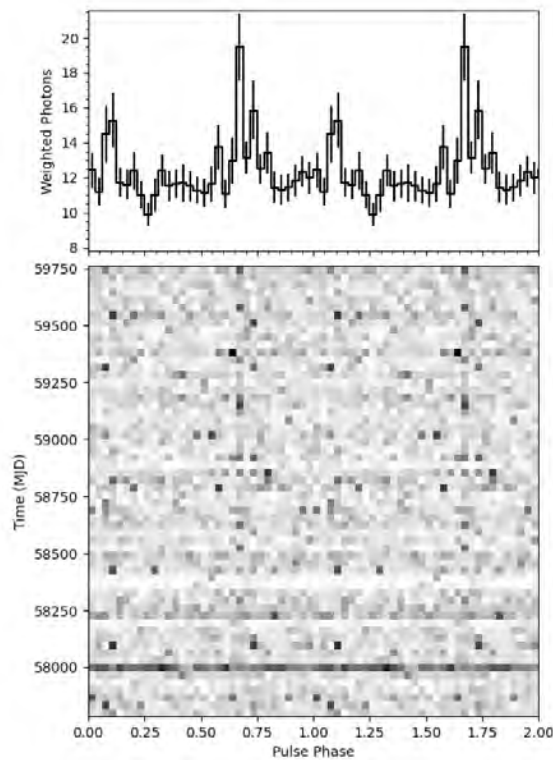


Figure 2. Our discovery of gamma-ray pulsations from PSR J1102+0249, a pulsar in a binary system with an orbital period of 22 days. The top panel shows an averaged (“folded”) pulse profile from Fermi photon data expressed as weighted photon counts vs. pulse phase. Each photon is assigned a probability of originating from the pulsar based on fitting the gamma-ray spectra of other sources as well as the gamma-ray background within a 15-degree radius of the pulsar's position. Each photon is then assigned a pulse phase calculated from a timing model fitted to radio data from the Green Bank Telescope. This timing model includes the pulsar's rotation period, period derivative, position, and orbital parameters. The bottom panel shows weighted photons vs. time and pulse phase.

Title: Particle-in-Cell Simulations of Plasma Waves and Turbulence

Author(s): A.R. Soto-Chavez and J.D. Huba

Affiliation(s): U.S. Naval Research Laboratory, Washington, DC

CTA: SAS

Computer Resources: HPE SGI 8600 [AFRL, OH]; HPE Cray EX [NAVY, MS]

Research Objectives: 1) Support the U.S. NRL and DARPA, SMART sounding rocket experiment program by developing the capability to simulate near-Earth space plasmas on both a kinetic scale and a macroscopic scale in order to predict and assess possible scenarios. 2) Gain deeper understanding of the nonlinear induced scattering process in a turbulent plasma. 3) Also, support the US NRL Space Chamber Experiments by performing nonlinear simulations of plasma-beam instabilities and apply the understanding of turbulence gained from the SMART experiment to the turbulence in the Solar Wind.

Methodology: We used the Tristan-MP code, which is a massively parallel (MP) PIC code that has been tested in HPC systems.

Results: I. This year, we published one important paper on physics of plasmas (accepted September 13, 2023); in which we presented our two-dimensional (2D)-PIC simulations of ion-ring instability leading to the successful excitation and creation of whistler waves with the Tristan-MP PIC code. The whistler waves are the result of the nonlinear scattering of lower-hybrid (LH) waves via the plasma particles. This nonlinear scattering is at the heart of the SMART experiment and something that we needed to test. Of the major results we found were: 1) The confirmation of the generation of whistler waves by the nonlinear scattering mechanism, Fig.1. There we see that in the right panel, the LH wave (E_{ky}) is saturated by the whistler waves (B_{ky}), confirming the scattering mechanism. 2) We also reported, for the first time in a PIC code, the generation of the quasimodes that arise due to the nonlinear scattering process. These quasimodes had been predicted theoretically but had never been seen to come out directly of a PIC simulation. 3) We varied the ion-to-electron mass ratio, with the objective of testing theory, experiment, and other PIC simulations results. In all cases, we find the excitation of the whistler waves.

II. We also performed PIC simulations of whistler wave generation in the Sun's atmosphere. The purpose of this study is to understand the possible generation of whistler waves in the solar wind. For this, we built upon a previous study of LH waves excited in solar flares. Solar flares are one of the most energetic events in the entire solar system. In that study, simulations show the generation of LH waves but not whistlers. However, when we did our simulations using the same setup and parameters as the previous study, we do observe whistler waves generated in the simulations. The generation mechanism is the scattering mechanism above described; see Fig. 2. We are still analyzing in detail the results and implications of this study to the solar wind community. However, we presented some of these early results at the 2023 APS-DPP meeting.

III. We performed PIC simulations of plasma-beam interactions to support the US NRL Space Chamber. This year, we conducted three new simulations, each with different beam energies to study this interaction. We are able to reproduce most of the experiment's features, that is, the creation of electrostatic waves below the electron plasma frequency and also the subpacket structures seen in the experiment; see Fig. 3. We are still analyzing in detail the results and we hope this will be submitted for publication this upcoming year.

DoD Impact/Significance: The SMART experiment and associated simulations will ultimately demonstrate the formation of turbulence and its coupling between the ionosphere and magnetosphere. The production of whistler waves by the sun and their impact on the solar wind particles is an active area of research in the solar wind community. We know that ultimately, the solar wind impacts the Earth's magnetosphere, where most of the DoD and the US Navy's reliance on spaceborne assets is. Furthermore, plasma-beam interactions are very important in understanding the scaping radiation from the sun upper atmosphere. Therefore, understanding both processes in the space environment gives the Department of the Navy new capabilities to predict, prepare for, respond to, and recover from space weather events.

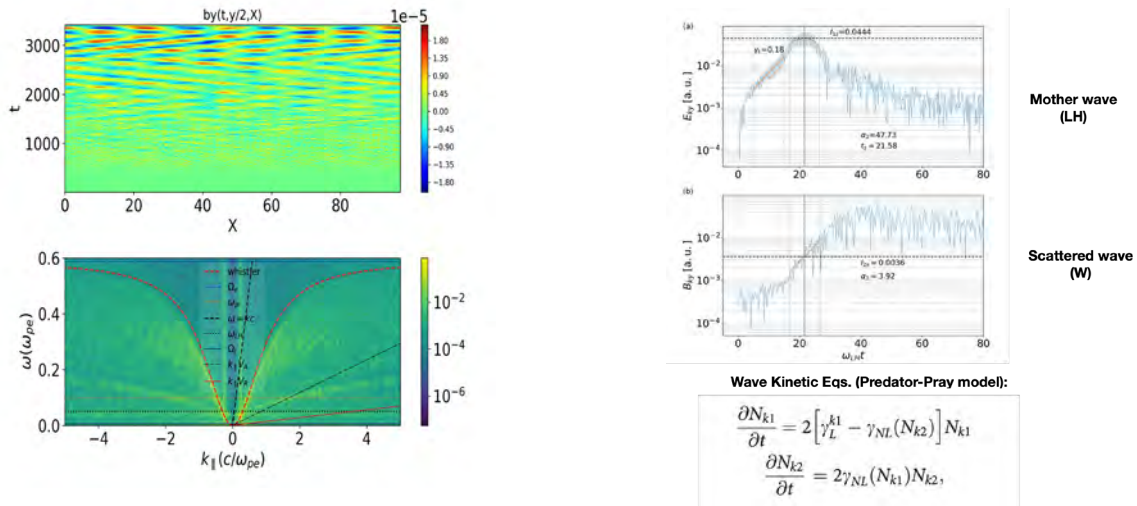


Figure 1. The whistler waves generation snapshot from our 2D PIC simulation. Top left: the B_y magnetic field magnitude (wave fronts) in x - t format. Bottom left: The whistler wave dispersion relation (indicated with the red, dashed line in the bottom). Right: The LH wave, E_y (top), and the whistler wave B_y bottom in k -space (top and bottom, respectively). This confirms the generation of whistler waves

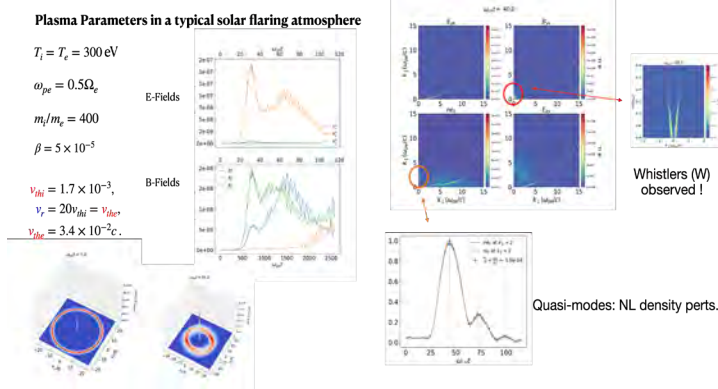


Figure 2. 2D PIC simulations of whistler wave generation in the solar atmosphere. Top left the parameters used. Bottom left, the ion ring velocity distribution injected in the simulation box. Middle: electric (E) and magnetic (B) fields. Right top: the fields and density in k -space showing the dispersion relation for the whistler waves. Bottom right: the quasimodes are seen in the simulations indicating the nonlinear scattering mechanism is present in the simulations.

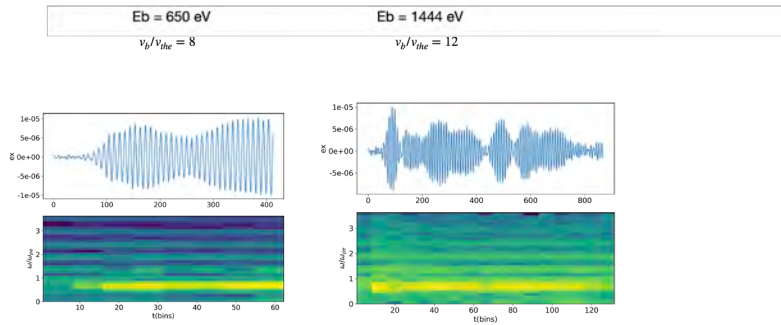


Figure 3. Top: electrostatic nonlinear subpackets created by the interaction of an electron beam and plasma in a 2D geometry, with different beam energies (Eb). Bottom: the frequency spectrogram showing maximum power at frequencies just below the electron plasma frequency.

Title: Thermosphere & Ionosphere Numerical Models and Ensemble Methods

Author(s): D.P. Drob, M. Jones, and J. Emmert

Affiliation(s): U.S. Naval Research Laboratory, Washington, DC

CTA: SAS

Computer Resources: HPE SGI 8600, HPE Cray EX [AFRL, OH]; [NAVY, MS]

Research Objectives: This effort seeks to specify the behavior of the Earth's ionosphere and thermosphere to better understand the impact of the hourly, seasonal, and episodic variations on various DoD Systems. Accurate and efficient large-scale numerical simulations are needed to specify and forecast this region of the space weather environment. The ionosphere and thermosphere are perturbed from below by solar heating-driven tides and internal waves. Simultaneously, ionizing extreme ultraviolet solar radiation from sunspot variations and solar wind fluctuations interacting with Earth's magnetic field result in perturbations from above.

Methodology: Several different global first-principles thermosphere and ionosphere numerical models are utilized. The National Center for Atmospheric Research (NCAR) Thermosphere Ionosphere Mesosphere Electrodynamics - General Circulation Model (TIME-GCM) provides a means to investigate the influence of both forcings from above and below. A whole-atmosphere configuration of the Navy Environmental Prediction System Utilizing a Non-hydrostatic Engine (NEPTUNE) model was coupled to the NRL SAMI3 (Sami is Another Model of the Ionosphere – version 3) ionosphere model to also investigate forcings from below. Version 4 of the SAMI model, with improved model physics and new probabilistic ensemble method forecast capabilities, is also being developed as part of the overall effort.

Results: In FY23, computational resources were utilized to perform a series of observing system simulation experiments (OSSE). In the first study, a 32-member ensemble of multiday SAMI4 forecasts was generated via random-but-known perturbations to the model input drivers and uncertain internal model physics parameters in order to generate a set of "truth runs." The resulting truth runs were then used to generate a corresponding series of synthetic ionospheric observations. These observations were then presented to the SAMI4 ensemble data-assimilation system as actual observations to assess how well the assimilation system could recover the known reference states of the truth runs. Figure 1 shows that the SAMI4 system, configured in this experiment to assimilate the last 6 hours of observations to update the 32-member ensemble forecast every 6-hours, could resolve the "truth run state" over the course of several days.

In the second study, numerical simulations were performed to optimize the design of a space weather-monitoring satellite constellation system comprising multiple satellites in nominal 800 km sun-synchronous orbits at various local time separations making measurement of the Earth's exospheric temperature in the same altitude region. To define the minimum system requirements needed to operationally resolve key thermosphere state parameters to a particular accuracy for global space weather-prediction models, the multidimensional trade space of constellation orbit configurations, the number of hours of measurements, and the required measurement accuracies were examined. Figure 2 shows an example of the trade space needed to resolve the Earth's global average exospheric temperature to better than 10 degrees Kelvin out of typical observed values of 500 to 2,000 degrees Kelvin.

DoD Impact/Significance: The coupled physics-based thermosphere-ionosphere model validation studies performed here address the DoD/Navy's long-term need for environmental prediction of space weather effects for tactical planning purposes, as well as the maximization of DoD space systems performance via adaptation to the variable environment (ref: SECNAVINST 2400.2A).

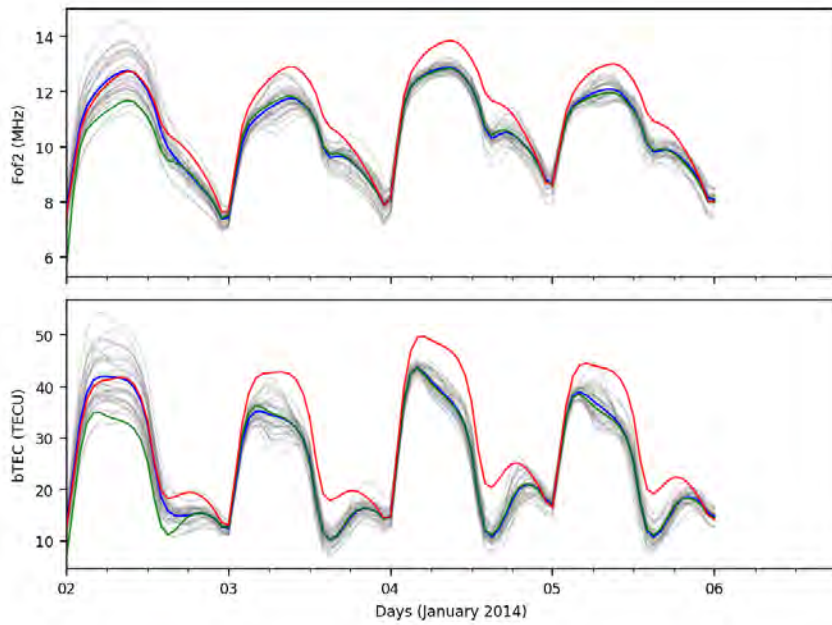


Figure 1. Example results of the time series of two ionospheric parameters at a single station from a multiday global OSSE with the NRL SAMI4 ensemble ionospheric data assimilation/forecast system. The “truth run” used to generate synthetic observations is shown in green. The default unperturbed “free-running” forecasts without data assimilation are shown in red. The ensemble mean state with data assimilation is shown in blue. The probabilistic SAMI4 forecast system ensemble members are given in gray.

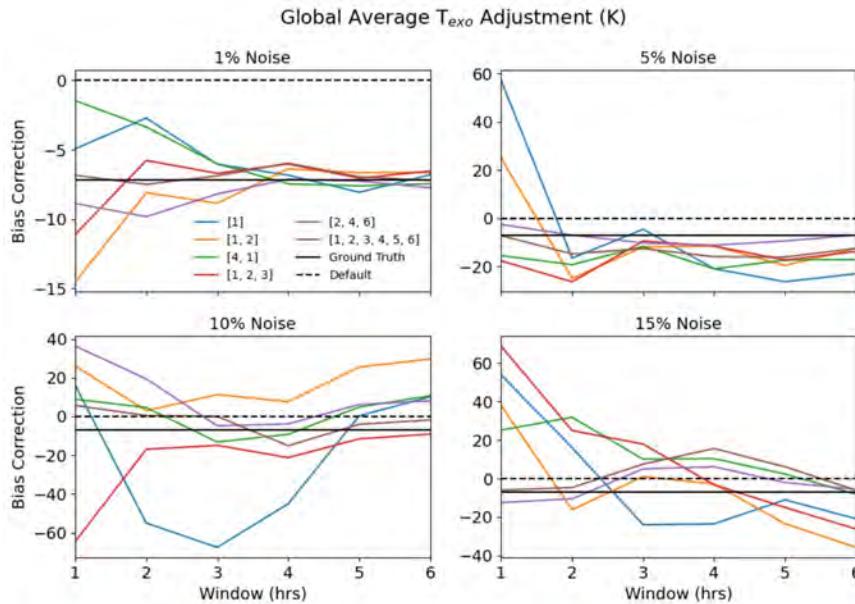


Figure 2. Example OSSE results to investigate the minimum system requirements and optimum orbital configurations of a future space weather-monitoring satellite constellation system, based on available measurement accuracies and number of hours of observations that is needed to resolve the global average exospheric temperature to a particular accuracy.

Title: Navy Ionosphere Model for Operations

Author(s): S.E. McDonald,¹ M.R. Burleigh,¹ C.A. Metzler,¹ J.L. Tate,² D. Hodyss,¹ R. Schaefer,³ G. Romeo³

Affiliation(s): ¹U.S. Naval Research Laboratory, Washington, DC; ²Computational Physics, Inc., Springfield, VA; ³Johns Hopkins University Applied Physics Laboratory, Laurel, MD

CTA: SAS

Computer Resources: HPE SGI 8600, HPE Cray EX [NAVY, MS]; Cray XC40/50 [ERDC, MS]

Research Objectives: The objective of this effort is to develop a physics-based ionosphere model coupled to an ionospheric data assimilation system that provides global and regional electron density specifications and short-term forecasts (0–24 hour). This capability forms the basis of a future Navy operational ionospheric forecasting system, running at multiple resolutions and fully coupled to operational atmospheric forecast models. In FY23, the main objectives were to continue development and testing of incremental releases of the Next-generation Ionosphere Model for Operations (NIMO), and to continue to improve our understanding of the lower atmospheric effects on the ionosphere using SAMI3 coupled to whole atmosphere models, including the Whole Atmosphere Community Climate Model Extended (WACCM-X), the Thermosphere Ionosphere Mesosphere Electrodynamics General Circulation Model (TIME-GCM), and the Navy Environmental Prediction System Utilizing the NUMA Engine (NEPTUNE).

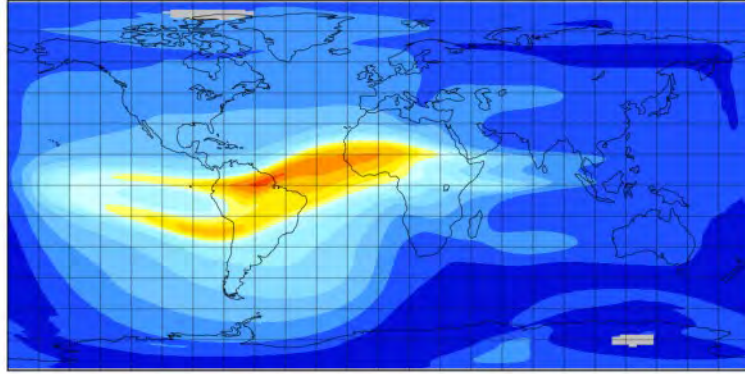
Methodology: NIMO consists of a physics-based ionosphere model, SAMI3, and a 3-dimensional variational (3DVAR) data assimilation system (IDA4D) that can ingest a wide variety of ionospheric datasets. NIMO also includes couplers that use the Earth System Modeling Framework (ESMF) for interpolating between the ionosphere and data assimilation grids. In the context of NIMO, SAMI3 uses an empirical thermosphere, NRLMSIS 2.0. To explore the influence of the lower atmospheric weather on the ionosphere, we have developed and continue to refine a file-based interface to external thermosphere models, including WACCM-X, a whole-atmosphere model that can be nudged with lower-atmospheric data to simulate specific days, and TIME-GCM. In addition, we have developed a NUOPC-based interface to couple SAMI3 with NEPTUNE, a Navy forecast model that allows for modeling atmospheric dynamics seamlessly and accurately from the surface to near the exobase (~500 km altitude) at high space-time resolution. In this coupling configuration, the SAMI3 and NEPTUNE models run concurrently.

Results: In FY23, we have used HPC resources to establish a NIMO production capability that will allow us to complete many months of historical NIMO runs and to test the system. We have continued to improve the file-based coupling of SAMI3 to external thermosphere models using SAMI3/WACCM-X simulations to explore ionospheric instability growth rates and SAMI3/TIME-GCM simulations to assist in understanding nighttime ionospheric depletions associated with sudden stratospheric warmings. We have begun extensive testing of the NUOPC-based SAMI3/NEPTUNE coupling, completing a series of one-way-coupled forecasts in which the SAMI3 ionosphere is driven by the NEPTUNE thermosphere. From these simulations, an example of the peak F2 region electron density (NmF2) is shown in Fig. 1 at 18:00 UT on 12 April 2020 for (top) SAMI3 climatology, (middle) NIMO that includes data ingested from GPS receivers, COSMIC-2 radio occultations, and ionosondes, and (bottom) SAMI3/NEPTUNE.

DoD Impact/Significance: Development of an operational ionospheric forecast model will aid in the numerical forecasting of high-frequency (HF) radio wave propagation through the Earth's atmosphere and ionosphere across the range of conditions relevant to DoD/Navy operations.

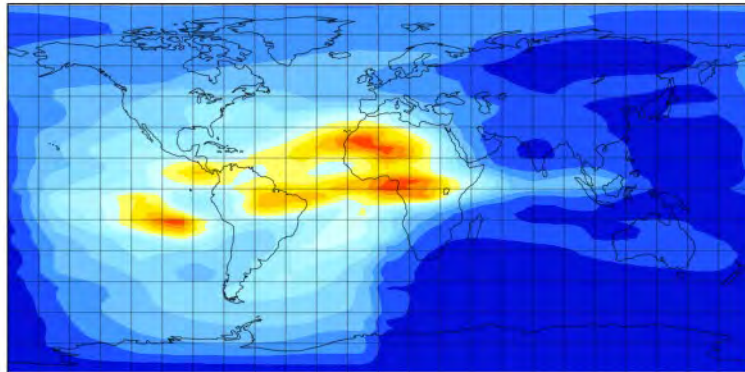
NmF2 12 April 2020 18Z

SAMI3/HWM/MSIS
(climatology)



nmf2

NIMO Analysis



nmf2

SAMI3/NEPTUNE Forecast

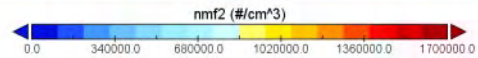
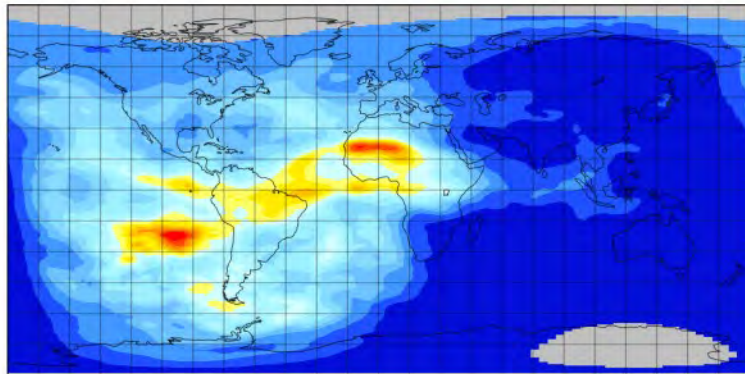


Figure 1. Peak F2 region electron density (NmF2) is shown at 18:00 UT on 12 April 2020 for (top) SAMI3 climatology, (middle) NIMO reanalysis that includes data ingested from GPS receivers, COSMIC-2 radio occultations, and ionosondes, and (bottom) SAMI3 one-way coupled to NEPTUNE with initial conditions provided at 0 Z from high-altitude extension of NAVGEM-LETKF.

THIS PAGE INTENTIONALLY LEFT BLANK

OTH

Other

Work that is not easily categorized as one of the other computational technology areas.

Title: Simulation of High Energy-Radiation Environments

Author(s): J. Finke and W. Duvall

Affiliation(s): U.S. Naval Research Laboratory, Washington, DC

CTA: OTH

Computer Resources: Cray XC40/50 [ERDC, MS]

Research Objectives: 1) Simulate radiation transport for modeling space radiation environments, radiation detection systems, pulsed-power radiation sources, and potential systems for the detection of special nuclear materials and radiological/nuclear materials. 2) Apply an improved model of the extragalactic background light (EBL), computed on HPC machines, to constrain Lorentz invariance violation (LIV), a key prediction of quantum gravity.

Methodology: 1) NRL has created the SoftWare for Optimization of Radiation Detectors (SWORD), a graphic user interface that allows users to quickly and easily simulate radiation in a number of environments. It uses three codes to simulate ionizing radiation transport: Geant4 and Monte Carlo N-Particle (MCNP), both of which use three-dimensional (3D) Monte Carlo techniques to simulate radiation transport, and Denovo, which is a discrete ordinance package. 2) We applied the model of the EBL created by Co-PI Finke to the brightest gamma-ray burst of all time, detected on October 9, 2022 (called GRB 221009A), in order to constrain Lorentz invariance violation, a possible effect of quantum gravity models. The Fermi Large Area Telescope spectrum for this burst was extrapolated to higher energies using the EBL model and was compared with the observed detections of GRB 221009A by the ground-based gamma-ray telescopes LHAASO and Carpet 2 (see Fig. 1 top). The universe at these high energies appears to be more transparent than the model would suggest, unless Lorentz invariance is violated. This can be used to constrain E_{QG} , the energy scale at which LIV is violated.

Results: 1) SWORD on HPC is currently being used to simulate and analyze activation of spacecraft on orbit. This effect requires a lot of simulation because of the high flux of charged particles in space combined with the rarity of the specific interactions and would not be possible without these resources. SWORD on HPC is continuing to be used to help validate the Data Mining Analysis and Modeling Cell's (DMAMC's) library of models. This work was done as part of the DMAMC, a program of the Department of Homeland Security/Countering Weapons of Mass Destruction (DHS/CWMD) Office. HPC is also used to prepare for CWMD exercises, which usually simulate a stolen radiotherapy source that is converted into a radiation dispersal device by combining it with an IED (colloquially referred to as a dirty bomb). HPC is used to propagate a variety of spectra through several different shield thicknesses, allowing a lookup table to be constructed. When an exercise occurs, we can quickly estimate loss to shielding for many common radiotherapy sources. NRL Code 6700 (Plasma Physics) is constructing a new pulsed-power source. SWORD simulations are currently being used to design the shielding required to allow the new machine to safely operate. 2) We put a lower limit on E_{QG} , the energy scale of quantum gravity (see Fig. 1 bottom). This constraint is based on preliminary observations. If it holds up on further analysis, it will be the first evidence for physics beyond the Standard Model of particle physics.

DoD Impact/Significance: 1) Space is becoming increasingly important for the DoD, particularly for the Space Force and the Navy. Large SWORD simulations of this environment will be important to US dominance in space as these charged particles can affect electronics in space. SWORD allows us to quickly and easily perform 3D radiation transport simulations with a number of applications. These allow for the development of spacecraft for sponsors such as NASA and the DoD Space Test Program. It allows for the testing of operational radiation-detection concepts in urban and maritime scenarios that are relevant to sponsors such as DHS/CWMD and the Defense Threat Reduction Agency (DTRA). 2) Understanding LIV and the transparency of the universe is crucial to studying GRBs and other astrophysical objects that accelerate particles. Understanding particle acceleration in these sources can give insight into how particles accelerated elsewhere can impact DoD space assets.

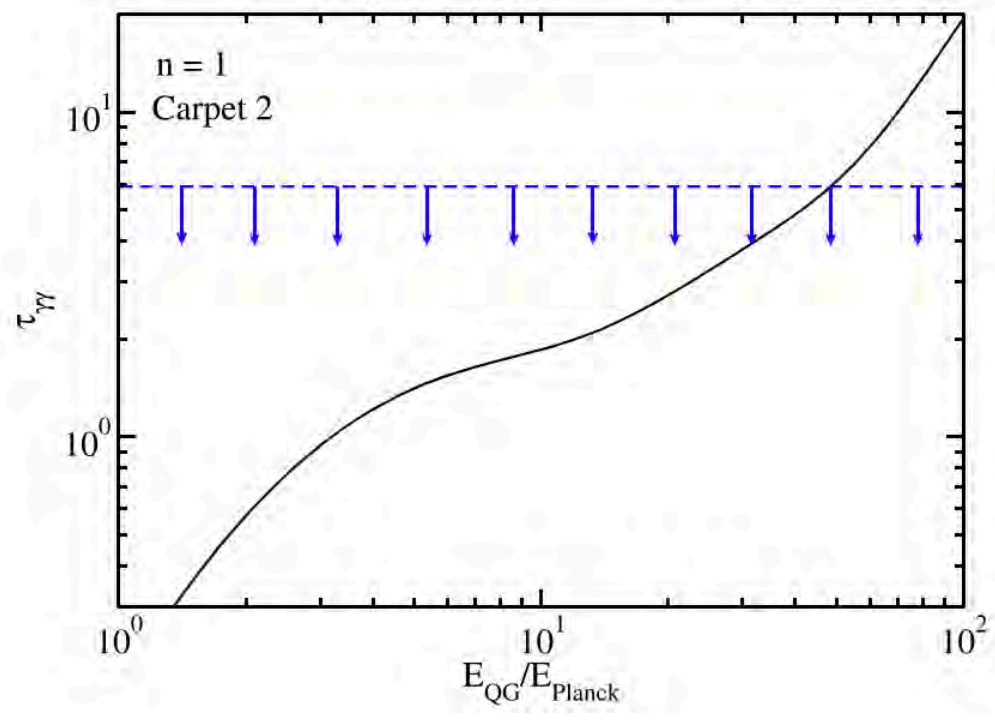
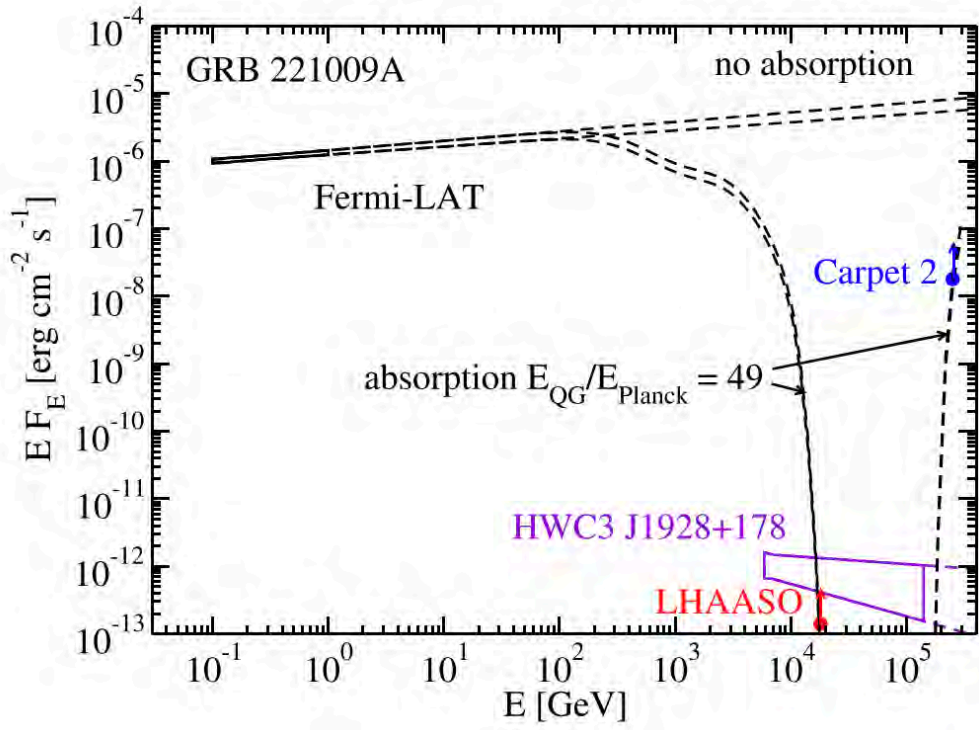


Figure 1. Top: The spectral energy distribution of gamma-ray burst 221009A with the Fermi-LAT spectrum and the LHAASO and Carpet 2 lower limits. The dashed curve indicates the extrapolation of the LAT spectrum to higher energies without $\gamma\gamma$ absorption, and with $\gamma\gamma$ absorption assuming $E_{\text{QG}}/E_{\text{Planck}} = 49$, as indicated. The absorption assuming no LIV is identical to this curve at $E < 3 \times 10^5$ GeV, but does not have the $E > 10^5$ GeV part shown on the plot. Bottom: The γ -ray absorption optical depth for the distance to GRB 221009A and the 251 TeV photon detected by Carpet 2 (solid black curves) as a function of $E_{\text{QG}}/E_{\text{Planck}}$, assuming linear ($n=1$) LIV. The dashed, blue line with arrows shows the $\tau_{\gamma\gamma}$ upper limit from the LAT and Carpet 2 observations.

THIS PAGE INTENTIONALLY LEFT BLANK

Author Index

Adams, I. -----32	Fan, Y. ----- 132
Alatishe, J.-----66	Finke, J.----- 164
Allard, R. -----94	Finocchio, P.M.----- 92
Allen, D.R. ----- 116	Flagg, D.----- 130
Amos, C.----- 122, 128	Fletcher, A.-----150, 152
Ananth, R. -----40	Fragiadakis, D.----- 62
Antillon, E. ----- 4	Furstenberg, R. ----- 72
Arcari, A. ----- 8	
	Gamezo, V.N.----- 24
Baker, N.----- 134	Gatling, G.R.----- 84
Barton, C.A. ----- 116	Goodwin, G.B.----- 14
Bateman, S.-----32	Gordon, D.F. ----- 82
Bernstein, N. -----46	Grossman, S.M.----- 142
Blain, C.A. ----- 112	
Bojko, B.T. -----22	Haiducek, J. ----- 148
Boris, J. ----- 110	Hebert, D. ----- 94
Burleigh, M.R. ----- 160	Helber, R.W. -----100, 126, 128, 130
	Hellberg, C.S. ----- 48
Campbell, T. -----94, 112, 130	Helmboldt, J.----- 148
Campbell, W.F. ----- 138	Herrera, M.A. ----- 116
Carrier, M.----- 120, 128	Hervey, W.J. ----- 58, 60
Cartwright, K.L. -----76	Hess, A.M. ----- 22
Cayula, S.-----96	Hinshelwood, D.D.----- 74
Chen, Y.H. -----82	Hodyss, D.----- 160
Chichka, D.-----50	Hoppel, K.W. ----- 116
Christophersen, J.----- 130	Huba, J.D. ----- 156
Cramer, J.A. -----40	
	Isaacs, J. ----- 82
D'Addezio, J.M. ----- 118, 128	Isner, N.D.----- 76
DeHaan, C. ----- 128	Iversen, A.----- 128
Deneva, J.----- 154	
deRada, S. ----- 128	Jacobs, G.A.-----118, 122, 130
Douglass, E. -----94	Jensen, T. ----- 94, 110, 112, 130
Dowd, B.-----70	Jin, Y. ----- 134
Doyle, J.D. -----88	Johannes, M. ----- 36
Drob, D.P. ----- 158	Johnson, R.F. ----- 18, 22
Duvall, W.----- 164	Jolliff, J.K. ----- 136
	Jones, M. ----- 158
Eckermann, S.D.----- 116	
Edwards, K. -----32	Kaiser, E.R. ----- 76
Emmert, J. ----- 158	Kelly, J.F. ----- 116
	Kessler, D.A.----- 22
Fabre, J.P. ----- 80	Khine, Y. -----16, 90, 110

Author Index

Kuhl, D.D.----- 116	Ray, P.S.----- 154
Kuna, L.P.----- 2, 8	Reinecke, T.L.----- 44
Ladner, S.----- 136	Rhodes, T.----- 116
Lambrakos, S.----- 50	Richie, D.----- 70
Lawrence, A.----- 128	Ridout, J.----- 114
Li, L.----- 142	Rising, C.J.----- 14
Liu, J.----- 26	Rittersdorf, I.M.----- 74
Lyons, J.L.----- 38	Romeo, G.----- 160
Ma, J.----- 116	Rosenberg, R.----- 110
Matt, S.----- 20, 96	Rowley, C.----- 110, 128
May, J.----- 128	Rydbeck, A.----- 130
McCoy, T.----- 8	Saunders, R.N.----- 2
McDonald, S.E.----- 160	Schaefer, R.----- 160
McLay, J.----- 114	Schoenauer, S.----- 32
Metzger, E.J.----- 102, 106, 108	Schweigert, I.V.----- 54, 56
Metzler, C.A.----- 160	Schwer, D.A.----- 28
Meyer, J.R.----- 78	Shabaev, A.----- 50, 72
Michopoulos, J.G.----- 8	Shriver, J.F.----- 100, 108
Montiforte, V.----- 128	Shulman, I.----- 96
Moser, A.E.----- 6	Simeonov, J.----- 32
Mott, D.R.----- 16	Sletten, M.A.----- 68
Ngodock, H.----- 120, 128	Smith, L.N.----- 144
Obenschain, K.----- 110	Smith, S.R.----- 100, 118, 120, 124, 126, 128
Orzech, M.----- 98	Smith, T.----- 94, 136
Osborne, J.----- 122, 128	Soto-Chavez, A.R.----- 156
Ouellette, J.D.----- 68, 142	Stevens, W.----- 128
Pantelev, G.----- 94, 100	Sudol, P.E.----- 40
Patel, T.K.----- 22	Swanekamp, S.B.----- 74, 76
Patnaik, G.----- 110	Swift, M.W.----- 38
Penko, A.----- 32	Tan, X.G.----- 6
Petrov, G.M.----- 82	Tate, J.L.----- 160
Phelps, M.----- 94, 128	Teferra, K.----- 2
Phillip, R.----- 32	Tejero, E.M.----- 84
Phillips, M.----- 52	Thombs, A.----- 96
Poludnenko, A.Y.----- 24	Thoppil, P.G.----- 104, 110
Povolotskyi, M.----- 78	Toporkov, J.V.----- 68
Ramamurti, R.----- 12, 30	Townsend, T.----- 124, 128
	Tremblay, K.----- 128
	Trott, C.----- 106
	Tsu, J.----- 138
	Twarog, E.M.----- 142

Author Index

Tyndall, D. -----	134
Veeramony, J. -----	32
Viswanath, K. -----	30
Vora, G.J. -----	58, 60
Vurgaftman, I. -----	78
Wade, N. -----	8
Ward, E. -----	50
Weber, B.V. -----	74
Welland, I. -----	44
Whitcomb, T.R. -----	114
Wickramaratne, D. -----	42
Wijesekera, H. -----	130
Wimmer, S.A. -----	8
Yu, J. -----	130
Yu, Z. -----	112
Zhao, Q. -----	134

Division/Branch Index

Systems Directorate (Code 5000)

Radar Division (Code 5300)

Surveillance Technology (Code 5340) 66

Information Technology Division (Code 5500)

Navy Center for Applied Research In Artificial Intelligence (Code 5510) 144

Center for Computational Science (Code 5590)..... 110

Optical Sciences Division (Code 5600)

Senior Scientist for Quantum Electronics (Code 5604) 78

Optical Physics (Code 5610) 78

Tactical Electronic Warfare Division (5700)

Electronic Warfare Modeling and Simulation (Code 5770) 70

Materials Science and Component Technology Directorate (Code 6000)

Chief Scientist for Computational Physics and Fluid Dynamics (Code 6003)110

Laboratories for Computational Physics and Fluid Dynamics (Code 6040)12, 16, 18, 22, 24, 26, 28, 30, 90, 110

Chemistry Division (Code 6100)

Materials Chemistry and Dynamics (Code 6120)..... 62

Center for Corrosion Science and Engineering (Code 6130) 8

Navy Technology Center for Safety and Survivability (Code 6180) 40, 54, 56

Materials Science and Technology Division (Code 6300)

Principal Scientist for Materials Innovation (Code 6307) 8

Multifunctional Materials (Code 6350) 2, 6, 8

Materials and Sensors (Code 6360) 50, 72

Center for Materials Physics and Technology (Code 6390)..... 4, 8, 36, 38, 42, 46, 48, 52

Plasma Physics Division (Code 6700)

Charged Particle Physics (Code 6750) 84, 150, 152, 156

Pulsed Power Physics (Code 6770) 74, 76, 156

Beam Physics (Code 6790)..... 82

Electronics Science and Technology Division (Code 6800)

Senior Scientist for Nanoelectronics (Code 6803)..... 44

Electronic Materials (Code 6870)..... 44

Center for Biomolecular Science and Engineering (Code 6900)

Principal Scientist for Biotechnology (Code 6904)..... 58, 60

Laboratory for Bio/Nano Science and Technology (Code 6910)..... 58, 60

Ocean and Atmospheric Science and Technology Directorate (Code 7000)

Acoustics Division (Code 7100)

Acoustics Simulation, Measurements, and Tactics (Code 7180) 80

Remote Sensing Division (Code 7200)

Radio/Infrared/Optical Sensors (Code 7210)..... 148

Remote Sensing Physics (Code 7220) 68, 116, 142, 160

Coastal and Ocean Remote Sensing (Code 7230) 112

Image Science and Applications (Code 7260)..... 68

Ocean Sciences Division (Code 7300)

Ocean Dynamics and Prediction (Code 7320)..... 32, 94, 98, 100,
102, 104, 106, 108, 110, 112, 118, 120, 122, 124, 126, 128, 130, 132, 136

Ocean Sensing and Processing (Code 7330) 20, 96, 128, 130, 136

Seafloor Sciences (Code 7350)..... 32

Marine Meteorology Division (Code 7500)

Senior Scientist for Mesoscale Meteorology (Code 7503)..... 88

Atmospheric Dynamics and Prediction (Code 7530) 92, 114, 130, 134, 138

Space Science Division (Code 7600)

Special Projects Office for High Altitude Numerical Weather Prediction (Code 7604)116

Geospace Science and Technology (Code 7630)..... 116, 158, 160

High-Energy Space Environment (Code 7650) 154, 164

Naval Center for Space Technology (Code 8000)

Space Systems Development Division (Code 8100)

Mission Development (Code 8110) 50

Spacecraft Engineering Division (Code 8200)

Design and Verification (Code 8220) 8, 14

Site Index

DSRCs

AFRL	4, 8, 12, 18, 22, 24, 26, 30, 36, 38, 40, 42, 44, 46, 48, 50, 52, 54, 56, 58, 60, 62, 66, 68, 78, 82, 114, 116, 144, 148, 156, 158
ARL	16, 20, 30, 36, 46, 48, 50, 52, 54, 62, 72, 92, 144, 150, 152
ERDC	2, 4, 24, 26, 30, 32, 38, 42, 44, 48, 50, 52, 58, 60, 68, 72, 74, 76, 82, 90, 92, 114, 116, 138, 142, 154, 160, 164
NAVY	2, 6, 8, 14, 20, 22, 24, 26, 28, 30, 32, 38, 50, 54, 56, 62, 68, 70, 72, 74, 76, 78, 80, 84, 88, 90, 92, 94, 96, 98, 100, 102, 104, 106, 108, 110, 112, 114, 116, 118, 120, 122, 124, 126, 128, 130, 132, 134, 136, 138, 148, 156, 158, 160

THIS PAGE INTENTIONALLY LEFT BLANK